CAROLIN RÖDING Doctoral Dissertation 2022

Hominin fossil remains from the Middle-Late Pleistocene Mediterranean

Virtual anthropological case studies of fragmentary cranial and dental remains

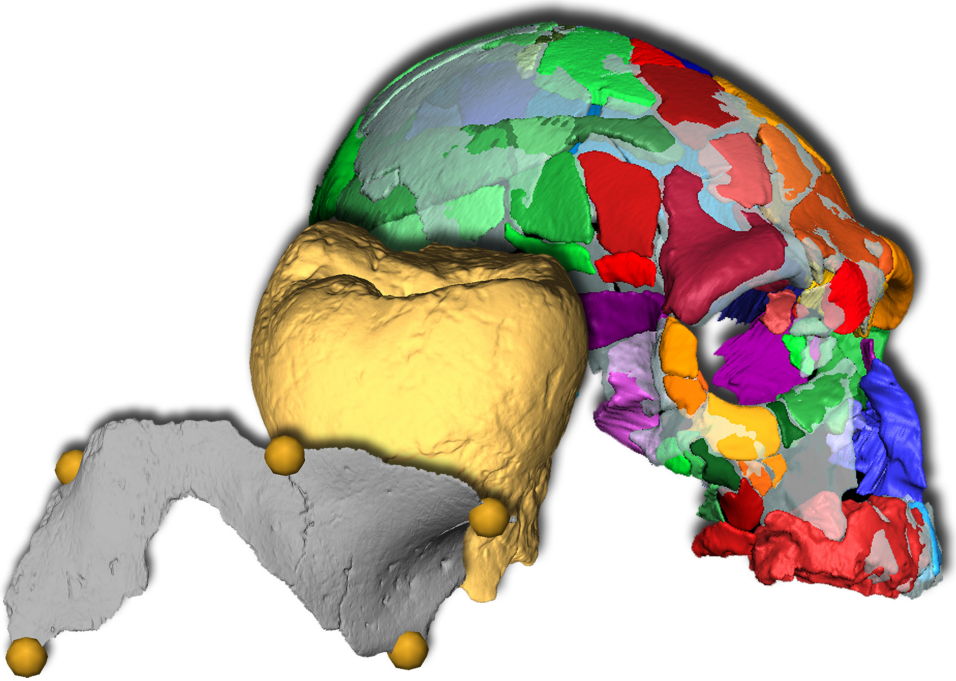

Supervisors
Prof. Dr. Katerina Harvati
Prof. Dr. Joachim Wahl

Reviewers
Prof. Dr. Katerina Harvati
Dr. habil. Philipp Gunz

Hominin fossil remains from the Middle-Late Pleistocene Mediterranean: virtual anthropological case studies of fragmentary cranial and dental remains

Dissertation
der Mathematisch-Naturwissenschaftlichen Fakultät
der Eberhard Karls Universität Tübingen
zur Erlangung des Grades eines
Doktors der Naturwissenschaften
(Dr. rer. nat.)

vorgelegt von
Carolin Röding
aus Witten

Tübingen
2022

Gedruckt mit Genehmigung der Mathematisch-Naturwissenschaftlichen Fakultät der Eberhard Karls Universität Tübingen.

Tag der mündlichen Qualifikation:	04.03.2022
Dekan:	Prof. Dr. Thilo Stehle
1. Berichterstatterin:	Prof. Dr. Katerina Harvati
2. Berichterstatter:	PD Dr. Philipp Gunz

Acknowledgments

I would like to dedicate this first page to all people that were essential for making my PhD project possible and proofed imperative for eventually writing this dissertation. The list of people to thank is long and not everybody can be named here. Nevertheless, I am grateful for each and everyone's help and support!

First of all, I would like to thank Prof. Katerina Harvati (Paleoanthropology, Tübingen University, Germany) for being my first supervisor and giving me the opportunity to be part of the CROSSROADS project. Your support, trust and advice throughout the entire process of this PhD project have proven invaluable.

I am deeply grateful that Prof. Joachim Wahl (Paleoanthropology, Tübingen University, Germany) agreed to be my second supervisor. I really appreciate the time you invested in supporting me and giving me advice after reaching your well-deserved retirement.

In addition, I would like to thank all collaborators, co-authors, as well as people and institutions providing data either in form of CT scans, landmark coordinates, linear measurements or maps. Further, I have to thank all my colleagues and friends that helped in various ways, especially Alexandros Karakostis and Abel Bosman for endless discussions ranging from geometric morphometrics to everybody and his dog; Laura Limmer and Annabelle Lockey for always helping me and accompanying my walks in the Schönbuch; Alessio Maiello for saving me from any computer related issue; Hugo Reyes-Centeno and Melania Ioannidou for their advice; Michael Francken and Hannes Rathmann for letting me roam through the osteological collection on numerous occasions and helping me to compile my recent comparative samples; the CROSSROADS team for

memorable field seasons in Greece; and my incredible former and current office mates!

Although my stay in Leipzig is already more than six years in times past, I am still deeply thankful to Prof. Jean-Jacques Hublin, Dr. Philipp Gunz and Dr. Simon Neubauer (Human Evolution, Max-Planck Institute for Evolutionary Anthropology, Leipzig, Germany) for introducing me to the field of geometric morphometrics. This dissertation in its current form would not have been possible without your support and patience in explaining its fundamentals to me.

Finally, on a personal note, I thank my family and friends outside the university for their support!

Table of Contents

Abstract

Homo sapiens and *Homo neanderthalensis* are the best studied hominin groups. However, many questions remain regarding their evolution, relationships and potential interaction. To reduce existing knowledge gaps three virtual anthropological case studies focused on so far poorly studied fossil materials from understudied Mediterranean regions.

In the first case study, the two partial Middle Pleistocene crania from Apidima were analyzed via metrics, virtual cranial reconstruction and ectocranial landmark-based shape analysis. The results supported previous attributions of Apidima 2 to the Neanderthal lineage and suggested an association of Apidima 1 with the *H. sapiens* lineage. The latter contributed to the scientific debate about the timing and range of early *H. sapiens* dispersals out of Africa and the temporal and spatial possibilities for interaction between *H. sapiens* and Neanderthals.

The second case study was concerned with the taxonomic affiliation of an isolated upper wisdom tooth from the Megalopolis Basin, Greece. Its lack of context and state of preservation limited previous taxonomic attributions. The analyses of dental crown outline shape and form (shape plus size) showed similarities to our Neanderthal sample and thereby, are in agreement with including the molar into the growing Pleistocene Greek hominin fossil record.

The morphological affinities of a Late Pleistocene juvenile maxillary fragment from Mugharet el'Aliya, Morocco, were in focus of the third case study. This individual has previously been assigned to both the modern human and Neanderthal lineage. Analyses of the entire preserved external morphology via the novel surface registration method showed no size-independent affinities

of Mugharet el'Aliya to Neanderthals of comparable age, while linking it with a juvenile early *H. sapiens* individual from Qafzeh. The results contributed to our knowledge about the ontogeny of adult Neanderthal and fossil *H. sapiens* morphology, and the growing evidence connecting cranio-dental morphology from the Levant and the Northwest African Middle Stone Age.

This dissertation employed virtual methods to the study of fragmentary hominin fossil remains and thereby, placed them into to the scientific discussion about fossil *H. sapiens* and Neanderthals, their facial ontogeny and evolution, as well as early *H. sapiens* dispersals out of Africa.

Zusammenfassung

Homo sapiens und *Homo neanderthalensis* sind die am Besten erforschten fossilen menschlichen Gruppen. Viele Fragen bleiben dennoch bezüglich ihrer Evolution, Verwandtschaft und potenzieller Interaktionen offen. In drei Fallstudien wurden daher virtuelle Methoden zur Analyse bisher kaum erforschter Fossilen eingesetzt, um vorhandene Wissenslücken zu verkleinern. Diese bestehen vor allem im östlichen mediterranen Raum, da dieser von der Wissenschaft bisher stark vernachlässigt wurde.

Im Fokus der ersten Fallstudie stehen zwei mittelpleistozäne Schädel aus Apidima, Griechenland. Deren Analyse umfasste lineare Metrik, virtuelle Schädelrekonstruktionen und Landmark-basierte Formanalysen des Ektocraniums. Die Ergebnisse bekräftigten die früheren Zuschreibungen von Apidima 2 zur Linie der Neanderthaler und suggerierten eine Zuordnung von Apidima 1 zur Abstammungslinie des modernen Menschen. Letzteres ist ein bedeutender Beitrag zur wissenschaftlichen Debatte über den Zeitpunkt und die Reichweite der Ausbreitung früher moderner Menschen und über die temporären sowie räumlichen Möglichkeiten zur Interaktion zwischen modernen Menschen und Neanderthalern.

Die zweite Fallstudie befasst sich mit der taxonomischen Zugehörigkeit eines isolierten oberen Weisheitszahnes aus dem Megalopolis Becken in Griechenland. Frühere taxonomische Zuordnungen wurden durch den fehlenden Kontext und den Erhaltungszustand des Zahnes eingeschränkt. Die Analysen der Form und Gestalt (Form plus Größe) des Umrisses der Zahnkrone zeigten Ähnlichkeiten zu unserer Neanderthaler-Stichprobe auf und reihten den Molaren damit in die zunehmende Anzahl menschlicher Fossilien aus dem pleistozänen Griechenland ein.

Im Mittelpunkt der dritten Fallstudie steht die morphologische Zugehörigkeit eines spätpleistozänen juvenilen Oberkieferfragments aus Mugharet el'Aliya, Marokko. In früheren Studien wurde dieses Individuum sowohl als moderner Mensch als auch als Neanderthaler angesprochen. Die innovative Oberflächenregistrierungsmethode ermöglichte erstmals eine Gesamtanalyse der erhaltenen externen Morphologie. Deren Ergebnisse verbinden Mugharet el'Aliya zwar mit einem juvenilen frühen *H. sapiens* Individuum aus Qafzeh, konnten jedoch keine größenunabhängigen Ähnlichkeiten zu Neanderthalern im vergleichbaren Alter aufzeigen. Dies ist einen wichtigen Beitrag zu unserem Wissen über die faziale Ontogenie in Neanderthalern und *H. sapiens* und den sich verdichtenden Hinweisen über Ähnlichkeiten in kranial-dentaler Morphologie zwischen Nordwest Afrika und der Levante in der Mittelsteinzeit.

Diese Dissertation verwendet virtuelle Methoden zur Studie fragmentarischer menschlicher Fossilien und integriert diese in die wissenschaftliche Diskussion über fossile *H. sapiens* und Neanderthaler, deren fazialer Evolution und Ontogenie sowie Ausbreitungen von frühen *H. sapiens* außerhalb von Afrika.

List of Abbreviations

3D	3-dimensional
BL	bucco-lingual
CAC	common allometric component
CS	centroid size
CT	computer tomography
DNA	deoxyribonucleic acid
EDJ	enamel-dentine junction
GMM	geometric morphometrics
GPA	generalized Procrustes superimposition
ICP	iterative closest point
IUP	initial Upper Paleolithic
IZM	inferior zygomatic margin
ka	thousand years
LDA	linear discriminant function analysis
MD	mesio-distal
MIS	marine isotope stage
MSA	Middle Stone Age
PCA	principal component analysis
PD	Procrustes distance
U	Uranium
U-series	Uranium-series
UP	Upper Paleolithic
VA	virtual anthropology

List of Figures

List of Publications for Cumulative Dissertation

Two publications submitted and one in preparation are included in this cumulative dissertation in fulfillment of the requirements. Numbers in parentheses represent the percentage of own contribution to the articles or manuscripts (scientific idea/data generation/analysis and interpretation/paper writing).

Accepted articles

- Study I: Apidima Ectocrania (0/65/30/10)
  Harvati, K., **Röding, C.**, Bosman, A. M., Karakostis, F. A., Grün, R., Stringer, C., Karkanas, P., Thomspon, N. C., Koutoulidis, V., Moulopoulos, L. A., Goroulis, V. G., & Kouloukousssa, M. (2019). Apidima Cave fossils provide earliest evidence of *Homo sapiens* in Eurasia. *Nature*, 571, 500-504. Doi: 10.1038/s41586-019-1376-z.
- Study II: Megalopolis Molar (50/80/100/70)
  Röding, C., Zastrow, J., Scherf, H., Doukas, C., & Harvati, K. (2021). Crown outline analyses of the hominin upper third molar from the Megalopolis basin, Peloponnese, Greece. In: H. Reyes-Centeno & K. Harvati (Eds.), *Ancient Connections in Eurasia* (pp. 16-36). Tübingen: Kerns Verlag. Doi: 10.51315/9783935751377.001.

Manuscripts ready for submission:

- Study III: Mugharet el'Aliya Maxilla (50/100/100/70)
  Röding, C., Stringer, C., Lacruz, R. S., & Harvati, K. (in prep). Mugharet el'Aliya: affinities of an enigmatic North African Aterian maxillary fragment. Manuscript in preparation for submission at the *American Journal of Biological Anthropology*.

1. Introduction

„*Evolution is an obstacle course not a freeway* […]."

Stephen Jay Gould (2007, p. 318)

Discoveries of the past decades have shown that human evolution is not a straight line of groups evolving into each other but rather a complicated network of interactions between groups and populations (e.g., Prüfer et al., 2014; Dannemann & Racimo, 2018; Lipson et al., 2018; Jeong et al., 2019; Lorente-Galdos et al., 2019; Durvasula & Sankararaman, 2020; Hajdinjak et al., 2021). Despite *Homo sapiens* and *Homo neanderthalensis* being the best studied hominin groups, many questions remain regarding their relationships and potential interaction (e.g., Green et al., 2010; Hammer et al., 2011; Harvati & Roksandic, 2016a; Posth et al., 2017; Hublin, 2017; Greenbaum et al., 2019). In addition, the identification of taxonomic affinities of fragmentary fossils remains challenging (cf. e.g., Hershkovitz et al., 2021; Marom & Rak, 2021; May et al., 2021), and consequently the recognition of potential areas of spatial as well as temporal overlap between *H. sapiens* and Neanderthals.

The main aim of this dissertation is to reduce existing gaps in our knowledge about fossil *H. sapiens* and Neanderthals by adding so far poorly studied fossil remains into the broader discussion. In focus are three case studies exploring taxonomic affinities of fragmentary fossils from understudied areas in the broader Mediterranean (Figure 1.1):

- Study I: two partial crania from Apidima cave A, Peloponnese, Greece; found in one block of breccia; dated to the Middle Pleistocene
- Study II: an isolated upper left wisdom tooth from the Megalopolis Basin, Peloponnese, Greece; surface find without secure context
- Study III: a fragmentary juvenile left maxilla from Mugharet el'Aliya, Morocco; dated to the Late Pleistocene

Figure 1.1: Rough geographical locations of the three studied sites: Apidima, Peloponnese, Greece (study I); Megalopolis Basin, Peloponnese, Greece (study II) and Mugharet el'Aliya, Morocco (study III). Cranial remains illustrated as skulls and dental remains as tooth.

1.1 Importance of the broader circum-Mediterranean region

The circum-Mediterranean region plays a pivotal role in modern human origins (Figure 1.2; for discussion see e.g., Shea, 2003; Prüfer et al., 2014; Lazaridis et al., 2016; Kuhlwilm et al., 2016; Vandermeersch & Bar-Yosef, 2019). The so far oldest known *H. sapiens* fossils are from Western Northern Africa (Hublin et al., 2017), while the fossil evidence for the earliest *H. sapiens* outside Africa and the southernmost extent of the Neanderthal geographic range are found in the Eastern Mediterranean (Hershkovitz et al., 2018a; Blinkhorn et al., 2021). Furthermore, some of the earliest Upper Paleolithic (UP) *H. sapiens* in Europe have been recovered from the Italian peninsula (Grotta del Cavallo, Italy) and the Balkans (Bacho Kiro, Bulgaria), the easternmost European Mediterranean peninsula (Figure 1.2; Benazzi et al., 2011a; Hublin et al.,

Figure 1.2: Rough illustration of the geographical range of Neanderthals (sepia) and the geographic locations of mentioned early *H. sapiens* (pre-MIS 5: Jebel Irhoud, Misliya; MIS 5: Skhul, Qafzeh) and Upper Paleolithic *H. sapiens* (Bacho Kiro, Grotta del Cavallo, Peștera cu Oase) fossils in the broader Mediterranean region.

2020). The site of Bacho Kiro yielded also evidence for contact between Neanderthals and *H. sapiens* in the form of recent admixture (Hajdinjak et al., 2021), as did the Peştera cu Oase remains, also from the Balkans (Romania) (Fu et al., 2015; Siska, 2019).

Early *H. sapiens* fossils in the broader Mediterranean region. The timing and exact geographic origin of the emergence of *H. sapiens* and especially of anatomical modernity are a matter of debate (e.g., Endicott, Ho & Stringer, 2010; Bräuer, 2015; Mirazón Lahr, 2016; Henn, Steele & Weaver, 2018; Galway-Witham & Stringer, 2018; Scerri et al., 2018; Kissel & Fuentes, 2021). The majority of researchers accepts an African origin during the late Middle Pleistocene (before Marine Isotope Stage (MIS) 5) (e.g., Rightmire, 2012; Campbell et al., 2014; Reyes-Centeno et al., 2015; Stringer, 2016; Grine, 2016; Nielsen et al., 2017; Bae, Douka & Petraglia, 2017; Schlebusch et al., 2017). The fossils from Jebel Irhoud, Morocco, which date to ca. 300 ka, are the so far oldest known accepted representatives of early *H. sapiens,* although they do not show the full complement of modern human features and retain aspects of archaic morphology (Figure 1.2; Richter et al., 2017; Hublin et al., 2017).

The commonly accepted out-of-Africa dispersal(s) took place during the terminal Middle Pleistocene and Late Pleistocene (MIS 5 – MIS 2) (e.g., Grün et al., 2005; Rightmire, 2009; Gronau et al., 2011; Weaver, 2012; Scozzari et al., 2014; Campbell et al., 2014; Reyes-Centeno et al., 2014; Groucutt et al., 2015; Pagani et al., 2016; Bae, Douka & Petraglia, 2017; Galway-Witham, Cole & Stringer, 2019; Vizzari et al., 2020), although earlier out-of-Africa dispersals of early *H. sapiens* in the Middle Pleistocene have been proposed (e.g. Posth et al., 2017; Hershkovitz et al., 2018a). Fossil evidence for such an early out-of-Africa dispersal comes from the early *H. sapiens* fossils from Misliya cave (Figure 1.2; Hershkovitz et al., 2018a). These

Levantine fossils consist of a fragmentary maxilla and associated dentition (Hershkovitz et al., 2018a). The minimum age of the Misliya fossils is ca. 60 ka, while the most probable age range spans ca. 177-194 ka (Valladas et al., 2013; Sharp & Paces, 2018; Hershkovitz et al., 2018b). Undisputed fossil evidence for early *H. sapiens* outside of Africa dating to ca. 90-120 ka has also been found in the Levant from the sites of Skhul and Qafzeh (Figure 1.2; e.g., Schwarcz et al., 1988; Stringer et al., 1989; Mercier et al., 1993; Grün et al., 2005). These fossils are unique in their demographic constellation by comprising all age groups from infancy to adulthood and are generally considered part of one group showing individual and potentially temporal variation (e.g., Schwartz & Tattersall, 2003; Shea & Bar-Yosef, 2005; Groucutt et al., 2017; Weber et al., 2020). Despite their importance for modern human evolution, the fossils from Skhul and Qafzeh are often considered as part of a 'failed' out of Africa dispersal, with these early groups likely having been replaced by Neanderthal populations in the same region before the final *H. sapiens* out-of-Africa population movement ca. 50 ka (e.g., Shea & Bar-Yosef, 2005; Mellars, 2006a; Shea, 2008; Klein, 2009; Oppenheimer, 2012; Hölzchen et al., 2016; Vizzari et al., 2020). New evidence, especially from South East Asia and Australia, as well as paleogenetic data, have challenged this view and suggest a much greater temporal and geographic duration of this dispersal with importance for the expansion of *H. sapiens* into South East Asia (for discussion see e.g., Reyes-Centeno et al., 2014; Grove et al., 2015; Westaway et al., 2017; Rabett, 2018; Groucutt et al., 2018).

Independent of this dispersal's success in producing long term settlement of *H. sapiens* in the region, the Levant is the southernmost region where archaeological sites of both groups, *H. sapiens* and Neanderthals, can be found (Figure 1.2; e.g., Shea, 2003; Hershkovitz et al., 2018a;

Vandermeersch & Bar-Yosef, 2019). Although Neanderthals are often referred to as a European, their known geographical range extended as far east as Denisova cave, Siberia (Prüfer et al., 2014), and as far south as Shukbah cave, Palestine West Bank (Blinkhorn et al., 2021). Levantine archaeological sites associated with *H. sapiens* fossils cluster in two phases, MIS 5 and MIS 3, which enclose a phase in MIS 4 where *H. sapiens* fossils are absent (for review see e.g., Shea, 2008; Bar-Yosef & Belmaker, 2011; Heydari-Guran et al., 2021). An overlap of several thousand years for sites associated to Neanderthals and *H. sapiens* fossils was proposed for the terminal MIS 5 and the beginning of MIS 3 (e.g., Grün et al., 2005; Hershkovitz et al., 2015; Abadi, Bar-Yosef & Belfer-Cohen, 2020). A scenario of alternating occupations between *H. sapiens* and Neanderthal groups seems more accepted than a continuous *H. sapiens* presence throughout MIS 5-3 (e.g., Mercier et al., 1993; Shea, 2003; Hershkovitz et al., 2015, 2018a; Stringer & Galway-Witham, 2018; Weber et al., 2020). The archeological evidence cannot elucidate the more likely scenario due to the association of not clearly distinguishable lithic assemblages with Levantine Neanderthals and early *H. sapiens* (for discussion see e.g., Shea, 2003; Been et al., 2017; references therein).

Paleogenetic evidence for admixture and out-of-Africa dispersals. More direct evidence for the contact between *H. sapiens* and Neanderthals comes from paleogenetic evidence for admixture. Genetics shows at least two phases of interbreeding between Neanderthals and *H. sapiens* that are traceable at the level of population genetics: an early phase pre-MIS 5 and a later phase around 50-60 ka (e.g., Green et al., 2010; Fu et al., 2014; Prüfer et al., 2014, 2017; Meyer et al., 2016; Kuhlwilm et al., 2016; Posth et al., 2017; Nielsen et al., 2017; Dannemann & Racimo, 2018; Villanea & Schraiber, 2019; Petr et al., 2020). These proposed time ranges for

admixture roughly coincide with a hypothesized early pre-MIS 5 out-of-Africa dispersal and the widely accepted later dispersal wave(s) of modern humans from Africa into Eurasia which led to a widespread continuous modern human presence outside of Africa (cf. Grün et al., 2005; Rightmire, 2009; Gronau et al., 2011; Weaver, 2012; Scozzari et al., 2014; Campbell et al., 2014; Reyes-Centeno et al., 2014; Groucutt et al., 2015; Pagani et al., 2016; Bae, Douka & Petraglia, 2017; Hershkovitz et al., 2018a; Galway-Witham, Cole & Stringer, 2019; Vizzari et al., 2020).

The two phases of interbreeding differ in their detected direction of gene flow. Mitochondrial DNA replacement in Neanderthals was proposed due to discrepancies between divergence times between *H. sapiens* and Neanderthals calculated based on mitochondrial and nuclear DNA (e.g., Fu et al., 2013; Rieux et al., 2014; Prüfer et al., 2014; Mendez et al., 2016). Such genetic estimates for population split times are calculated based on predicted mutation rates (e.g., Posth et al., 2017; Prüfer et al., 2021). Evaluation of Neanderthal mitochondrial genome diversity places this gene flow from *H. sapiens* into Neanderthals before approximately 220 ka (Posth et al., 2017). Similarly, evidence from the Neanderthal Y-chromosome indicates introgression from modern humans into Neanderthals between approximately 370-100 ka (Petr et al., 2020).

In contrast, present day non-African modern humans exhibit ca. 2 % of genes with Neanderthal ancestry, which most likely result from the later phase of interbreeding (e.g., Green et al., 2010; Prüfer et al., 2014; Meyer et al., 2016; Posth et al., 2017; Dannemann & Racimo, 2018). In addition to the large-scale interbreeding phases, individual cases of rather recent admixture between modern humans and Neanderthals are traceable in five completely sequenced genomes from European early UP *H. sapiens* from Bacho Kiro and Peștera cu Oase overlapping in time

with Neanderthals (cf. Fu et al., 2015; Siska, 2019; Hajdinjak et al., 2021). These individuals in combination with further sequenced Eurasian individuals reveal a complex population structure in the early UP Europe with individuals predating ca. 40 ka not contributing significantly to later European modern humans (e.g., Fu et al., 2014, 2015; Prüfer et al., 2021; Hajdinjak et al., 2021; references therein). Thereby, genetic evidence from the European early UP *H. sapiens* is in agreement with the latter phase of large-scale admixture taking place before the UP modern human expansion into Europe (e.g., Fu et al., 2014, 2015; Prüfer et al., 2014, 2021; Lazaridis et al., 2016; Kuhlwilm et al., 2016; Hajdinjak et al., 2021).

The broader circum-Mediterranean region as a possible contact zone. The known Neanderthal range does not include the African continent (cf. Blinkhorn et al., 2021). Therefore, Western Asia and especially the Eastern Mediterranean have been proposed as likely regions for both large-scale interbreeding phases due to their location on a potential dispersal corridor for *H. sapiens* and in a contact zone between human populations (e.g., Osborne et al., 2008; Green et al., 2010; Harvati & Tourloukis, 2013; Prüfer et al., 2014; Lazaridis et al., 2016; Harvati & Roksandic, 2016b; Kuhlwilm et al., 2016; Bae, Douka & Petraglia, 2017).

Further, the norther rim of the Mediterranean has been suggested to comprise three principal European glacial refugia, i.e., the Iberian, Italian, and Balkan peninsulas (e.g., Taberlet et al., 1998; Hewitt, 1999; Tzedakis et al., 2002). During glacial maxima with extending glacial ice sheets many floral and as consequence thereof, faunal species retreated there (e.g., Zagwijn, 1992; Blondel & Ferris, 1995; Davis & Shaw, 2001; Tzedakis et al., 2002; Michaux et al., 2003; Brito, 2005; Gómez & Lunt, 2007; Médail & Diadema, 2009; Harvati & Roksandic, 2016b). Refugia are considered to show a high diversity, at least at

the intraspecific level, which reflects their complex population dynamics of retreats and expansions (e.g., Petit et al., 2003; Blondel et al., 2010; Hewitt, 2011; Thompson, 2020). It is assumed that human populations would follow a comparable pattern (e.g., Dennell, Martinón-Torres & Bermúdez de Castro, 2011; Tourloukis & Harvati, 2018; Roksandic, Radović & Lindal, 2018; Jones, 2021).

Similarly, the Levant and western Asia are thought to have acted as expansion corridors of African fauna during warm phases in the Early and Middle Pleistocene (e.g., Tchernov, 1992a, 1992b). Although the direct link between faunal expansions and human dispersals, sometimes called 'migratory wave hypothesis', is debated (for discussion see e.g., Bar-Yosef & Belmaker, 2011; Carotenuto, et al., 2016), the faunal examples show that African species repeatedly migrated into and survived in the eastern and southeastern Mediterranean (e.g., Belmaker, 2009, 2010; Bellucci et al., 2014).

1.2 A framework for the study of fragmentary fossils

Despite the importance of the circum-Mediterranean regions for human evolution, paleoanthropological research exhibits major gaps especially in Middle and Late Pleistocene of the Northeastern and African parts of the Mediterranean rim (cf. Figure 1.3). Archaeological materials remain unpublished or poorly studied due to diverse reasons. In the case of hominin remains, an important factor is often the combination of the fragmentary nature of the fossil record and methodological limitations at the time of discovery (e.g., Benazzi et al., 2011a; Rmoutilová et al., 2018; Bosman et al., 2019; Jiménez-Arenas et al., 2019; Mori et al., 2020). In addition to new field surveys and excavation campaigns, the review of already excavated and poorly studied materials is important in reducing such research

Figure 1.3: Excerpt from the ROCEEH Out of Africa Database (ROAD; http://www.roceeh.org) showing all so-far recorded archaeological sites dated between 35-320 ka in the broader Mediterranean region as illustration of the unevenly distributed density of sites dated to the Middle and Late Pleistocene (status: 16.12.2021).

gaps (e.g., Higham et al., 2011; Buck & Stringer, 2015; Blinkhorn et al., 2021; Prüfer et al., 2021). Before the late 20th century, reconstruction and analysis of fossils relied on the original preserved fragment(s), with the study of external linear metrics and non-metric traits being the main analytical tools (for review see e.g., Wu & Schepartz, 2009; Henke, 2015). Since the late 20th century advances in landmark-based morphometrics, so called geometric morphometrics (GMM), and virtual anthropology (VA) have vastly extended the analytical possibilities, particularly in cases of fragmentary fossils.

GMM refers to a toolkit of statistical methods for the study of shape and size in two or three dimensions (e.g., Rohlf & Bookstein, 1990; Bookstein, 1991). In GMM, form (shape and size) is captured as a configuration of landmarks, whose shape aspect can be analyzed independent of size after superimposition (e.g., Rohlf & Bookstein, 1990; Slice, 2007; Zelditch, Swiderski & Sheets, 2012). Generalized Procrustes superimposition (GPA) translates landmarks from all individuals within a sample into a common coordinate system while removing

orientation, location, and size (e.g., Zelditch, Swiderski & Sheets, 2012). This step enables the statistical comparative analysis of complex shape which previously was difficult to quantify (e.g., Harvati, 2003; Gunz et al., 2009; Gunz & Harvati, 2011; Freidline et al., 2012).

During the last decades, 3-dimensional (3D) GMM has been further developed and now often includes the analysis of semi-landmarks along curves and surfaces in addition to fixed landmarks, pseudo-landmark approaches, and methods for geometric and statistical reconstruction of missing data (e.g., Gunz et al., 2004; 2009; Gunz, Mitteroecker & Bookstein, 2005, Mitteroecker & Gunz, 2009; Benazzi et al., 2011a, 2011b, 2012; Gunz & Mitteroecker, 2013). As a consequence, GMM is employed extensively in the study of hominin fossils with regard to their taxonomy, ontogenetic variation, behavior, and virtual reconstruction (e.g., Mitteroecker et al., 2004; Zollikofer et al., 2005; Nicholson & Harvati, 2006; Gunz & Harvati, 2007; von Cramon-Taubadel & Lycett, 2008; Neubauer, Gunz & Hublin, 2010; Bastir et al., 2011; Gunz et al., 2012; Freidline et al., 2012; Reyes-Centeno et al., 2015; Di Vincenzo et al., 2017; Karakostis et al., 2018; Mori et al., 2020). 3D GMM is part of the multidisciplinary approach to analyze morphology in a virtual 3D environment of VA by combining knowledge ranging from anthropology and statistics to computer sciences (Weber et al., 2001; Zollikofer & Ponce de León, 2005; Weber & Bookstein, 2011; Weber, 2015). The 3D component requires to digitize fossil remains, either directly or via imaging techniques, i.e., surface scanning or computer tomography (CT). The study of a digital copy thus not only allows for access to internal structures and repeated analyses, but also reduces handling of the precious original fossil and documents its current state of preservation (e.g., Zollikofer & Ponce de León, 2005; Balzeau et al., 2010; Abel, Laurini & Richter, 2012; Weber, 2015).

2. Research Strategy

In order to reduce existing gaps in our knowledge about fossil *H. sapiens* and Neanderthals, this cumulative dissertation presents three case studies of fragmentary fossil remains from the late Middle and Late Pleistocene of two circum-Mediterranean regions (cf. Introduction, Figure 1.1). These fossils either remained poorly described after their initial discovery and/or present a state of preservation that hindered previous attempts to study their morphology in its entirety. The studies presented here place these fossils in a comprehensive, quantitative, comparative framework for the first time by employing cutting edge techniques from the fields of 3D GMM and VA. The following were the main two objectives of all three case studies:

(1) Add so far poorly studied fossil materials from understudied regions to the scientific knowledge about Middle and Late Pleistocene circum-Mediterranean populations.

(2) Apply virtual methods and potentially adapt methods from other fields to the study of fragmentary fossil remains in order to make this understudied source of information more accessible.

2.1. Research Questions

Each of the three case studies contributes to the scope of the wider main objectives while addressing specific research questions. These specific research questions are adjusted to the context of each case study with regard to known geological dating, potential previous taxonomic attribution of the studied materials, and partially geographic location.

Study I: What is the taxonomic attribution of two fossil crania from Apidima, Greece? The first study investigates the taxonomic attribution of two fragmentary crania from the Apidima cave complex, Greece, that were found in close proximity to each other encased in a block of breccia in cave A in the late 1970s (e.g., Pitsios, 1985, 1995, 1999; Kormasopoulou-Kagalou, Protonotariou-Deilaki & Pitsios, 1995). Previous studies were limited to the more complete but taphonomically distorted cranium Apidima 2 (LOA1/S2), while Apidima 1 (LOA1/S1) remained unstudied. Apidima 2 has been considered a *H. heidelbergensis* or early Neanderthal (e.g., Coutselinis, Dritsas & Pitsios, 1991; Manolis, 1996; Pitsios, 1999; Harvati, Panagopoulou & Runnels, 2009; Harvati, Stringer & Karkanas, 2011). Its minimum age was estimated to be ca. 160 ka based on U-series dating (Bartsiokas et al., 2017). Despite the absence of a published study, Apidima 1 and 2 have been assumed to be of the same taxonomic affiliation (e.g., Bartsiokas et al., 2017), due to their close spatial proximity in the breccia. The specific goals of this study were to conduct a virtual reconstruction of the specimens to enable their comparative shape analysis, in order to evaluate their taxonomic affinities.

Study II: What is the taxonomic attribution of an isolated wisdom tooth from the Megalopolis Basin, Greece? An isolated human tooth, an upper left third molar (hereafter Megalopolis molar), was found on the surface in the Megalopolis Basin during survey for a lignite mine (Marinos, 1975; Sickenberg 1976; Harvati, 2016). Since then, the site was destroyed by exploitation of this lignite mine, thus greatly reducing the possibilities for establishing a chronological context for this putative fossil. The Megalopolis molar was recovered together with faunal remains ascribed to the earlier half of the Middle Pleistocene and the Early Pleistocene and was proposed to have a similar age (Sickenberg, 1976). However, the actual

geological age and species attribution of the Megalopolis molar are unknown due to its problematic context as surface find, as well as its poor state of preservation. The main aim of this study was to investigate the status of this specimen based on the morphology of its dental crown outline, and thereby to shed light on its taxonomic affinities.

Study III: What are the affinities of an enigmatic juvenile maxillary fragment from Mugharet el'Aliya, Morocco? In the first half of the 20th century, many North African fossils were attributed to the Neanderthal lineage (e.g., Şenyürek, 1940; McBurney, Trevor & Wells, 1953; Ennouchi, 1962). Such attributions were mainly due to the presence of archaic traits, like high levels of post-canine megadonty and robust jaws, rather than to Neanderthal derived features. (e.g., Ferembach, 1976; Hublin & Tillier, 1981; Smith et al., 2007; Hublin et al., 2012). More recently, derived modern human traits have also been recognized in many of these specimens, and these fossils are now generally considered as representing early *H. sapiens* groups with some similarities to individuals from Qafzeh and Skhul, Israel (e.g., Hublin & Tillier, 1988; Harvati & Hublin, 2012; Hublin et al., 2012; Freidline et al., 2021). The origin of their archaic traits, however, remains unclear. The goal of study III was to investigate the taxonomic and phylogenetic affinities of the enigmatic modern human maxilla from Mugharet el'Aliya and assess its presumably archaic / 'Neanderthal-like' features in the context of size, ontogeny, and fragmentary status.

3. Materials and Methods

Each case study required the use of different methods within the field of VA and GMM in order to address the outlined research questions. Thereby, the respectively used method was determined by the fossil's general state of preservation and the preserved anatomical region. Differences and similarities between the main steps of these approaches are illustrated in Figure 3.1. The individual measurement protocols are summarized below; in-depth discussions are provided within the manuscripts included in this cumulative dissertation.

Study I: Apidima Ectocrania. The archaeological site of Apidima is situated in a coastal cave complex on the Mani peninsula, southern Peloponnese, Greece (cf. Figure 1.1). Cave A yielded two late Middle Pleistocene partial crania encased in a block of breccia, which complicates their analysis due to the combination of their fragmentary status and the obstacles involved in removing the surrounding, extremely hard, breccia matrix (e.g., Pitsios, 1985, 1995, 1999; Coutselinis, Dritsas & Pitsios, 1991; Manolis, 1996; Harvati, Stringer & Karkanas, 2011; Bartsiokas et al., 2017).

To not further damage the originals, our analyses of their taxonomic affinities were performed in a virtual environment. In a first step, the two crania were CT scanned. Density differences and thereby, grey value differences in the CT scans allowed for virtual removal of the majority of breccia matrix from both crania. However, the reproducible segmentation on the endocranium was not possible throughout all cranial areas. Therefore, our virtual reconstructions and analyses focused on the ectocranial morphology of Apidima 1 and 2.

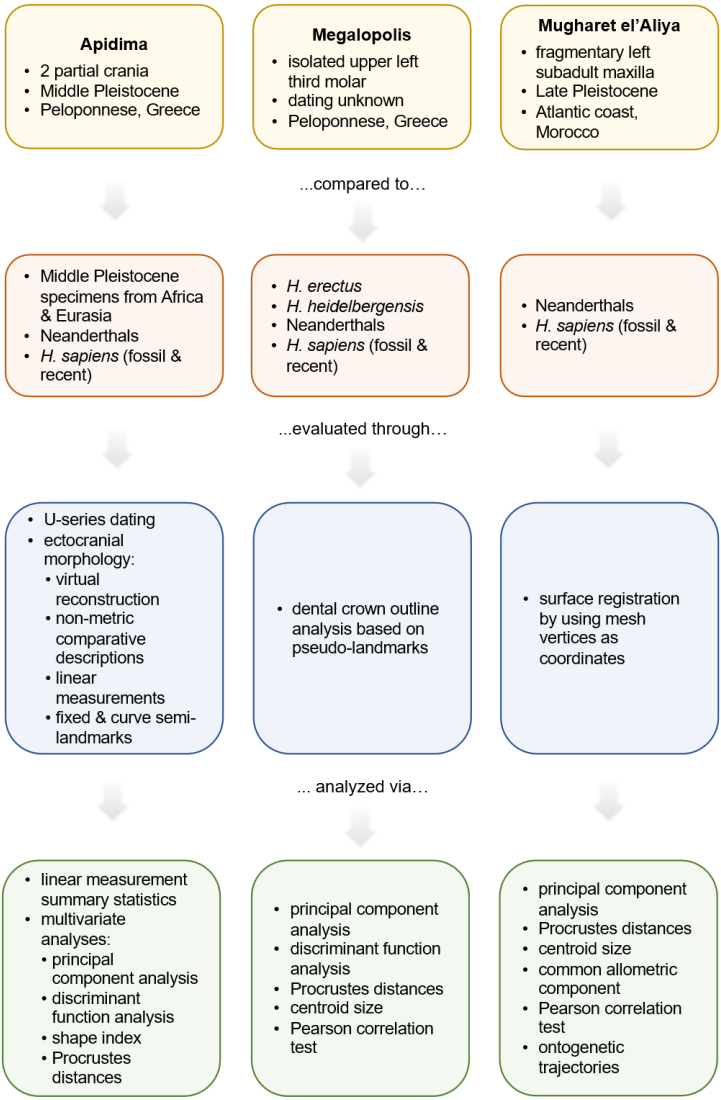

Figure 3.1: Comparison of the general workflows used for the three case studies included in this cumulative dissertation.

The preserved aspects of Apidima 1 include part of the sagittal suture and show no signs of deformation or significant matrix infilling of cracks, which allowed for a reconstruction based on mirroring. The better-preserved left side was mirrored along the midsagittal plane (for discussion see e.g., Zollikofer et al., 1995; Zollikofer, Ponce de Léon & Martin, 1998; Gunz et al., 2009; Wu & Schepartz, 2009; Couette & White, 2010; Grine et al., 2010), resulting in a completely symmetrical reconstruction (cf. Study I: Extended Data Figure 5).

In contrast, Apidima 2 shows taphonomic distortion and matrix infilling of cracks. This requires segmentation of all fragments and their independent movement during reconstruction (cf. Study I: Extended Data Figure 3). In case of more complex reconstruction protocols, multiple reconstructions of the same fossil are prone to show slight shape differences, especially when produced by multiple observers (e.g., Zollikofer et al., 2005; Harvati, Hublin & Gunz, 2010; Spoor et al., 2015). No single reconstruction can be 'absolute', instead a range of reconstructed shapes might be equally biologically plausible (cf. Gunz et al., 2009). Therefore, Apidima 2 was reconstructed by two observers and based on two different protocols, symmetry and smoothness, resulting in four independent reconstructions (cf. Study I: Extended Data Figure 4). Both protocols are well established in a fossil context and exploit the shared feature of approximate bilateral symmetry in vertebrate crania and smooth curvature of the ectocranial surface of most cranial structures, respectively (Figure 3.3; for discussion see e.g., Zollikofer et al., 2005; Ponce de Léon et al., 2008; Gunz et al., 2009; Weber & Bookstein, 2011; Di Vincenzo et al., 2017; Bosman et al., 2019). Independent of the protocol used, the following aspects apply for all four reconstructions. The starting point for the reconstruction was the anterior right part of the neurocranium as it shows a low amount of taphonomic

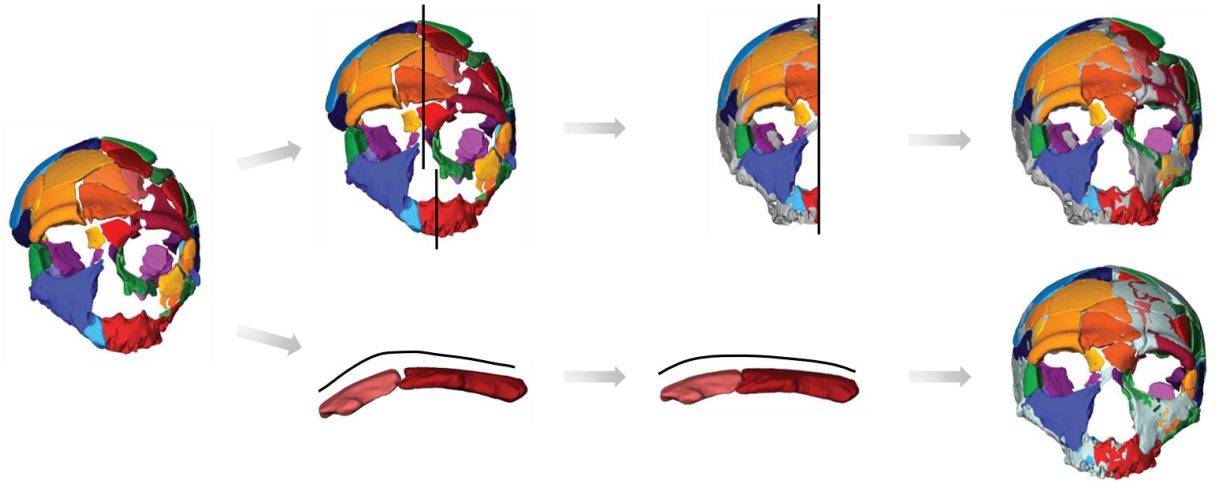

Figure 3.2: Schematic illustration of the reconstruction protocols for Apidima 2. The segmented fragments in their original position (left) represent the starting point of the symmetry and smoothness protocols. The top row illustrates the reconstruction based on symmetry via reconstruction of the right cranial side to align the neurocranial and facial midsagittal planes (vertical black lines), followed by reconstruction of the left cranial side as symmetrical counterpart. The bottom row illustrates the reconstruction based on smoothness via restoring smooth curvature between neighboring fragments throughout the cranium. In both protocols unilateral missing areas were reconstructed via mirroring. Mirrored parts are shown in light grey.

deformation and to a great extent preserves smooth curvature between several fragments. Further, great parts of the more distorted left side were reconstructed using a mirror duplicate of the right side as reference. Due to the taphonomic distortion the position of mirrored fragments had to be partially corrected. In such cases smoothness and/or a biological meaningful position of fragments was prioritized over bilateral symmetry. For missing areas, the mirrored duplicate from their preserved counterpart was used for reconstruction.

In addition, sources for potential bias in the reconstruction process were identified. To account for possible alterations to the edges of fragments cracks were not closed completely. This might lead to slightly exaggerated linear measurements, while no significant influence on size-corrected shape is assumed due to similar expansions in all 3 dimensions. In contrast, shape might be affected by unconscious influences on the reconstruction process due to prior knowledge, expectations, and level of experience (cf. e.g., Weber et al., 2001; Gunz et al., 2009). Prior knowledge and expectations could only be addressed indirectly by two observers without extensive prior knowledge about and involvement in previous analyses of Apidima 2. Additionally, the expectation bias was approached by not relying on reference crania prior to the statistical reconstruction of missing data (see below). The choice of a reference cranium has great influence on the reconstruction outcome (e.g., Weber & Bookstein, 2011; Bosman et al., 2019). Apidima 2 preserves a sufficient amount of cranial anatomy to allow for a reconstruction purely based on its intrinsic information.

The resulting reconstructions of Apidima 1 and 2 were analyzed via summary statistics of traditional metrics based on linear measurements, descriptive observations of their morphological features and size-independent

landmark-based GMM comparative shape analyses (for discussion see e.g., Rohlf & Bookstein, 1990; Bookstein, 1991; Slice, 2007; Zelditch, Swiderski & Sheets, 2012). Shape was captured by landmark-sets incorporating fixed homologous landmarks and semi-landmarks along curves. Each curve was collected as densely spaced points which were resampled to a predetermined number of equidistant points. Missing landmarks along the midsagittal plane were reconstructed by GPA mean substitution (e.g., Neeser, Ackermann & Gain, 2009; Gunz et al., 2009) and lateral landmarks through reflected relabeling or mirroring of the bilateral counterpart (e.g., Mardia, Bookstein & Moreton, 2000; Gunz et al., 2009). During the subsequent GPA, bending energy between landmark configurations was minimized by allowing curve semi-landmarks to slide along a tangent vector to the curve (e.g., Gunz, Mitteroecker & Bookstein, 2005; Mitteroecker & Gunz, 2009; Zelditch, Swiderski & Sheets, 2012; Schlager, 2019). The fixed landmarks were not allowed to slide and thereby, provided the basis for the GPA and framework for semi-landmark sliding. The resulting superimposed and homologous landmark coordinates are called Procrustes coordinates and form the base for all following multivariate analyses.

Multivariate statistics employed to analyze the datasets comprised of fixed and semi-landmarks of the Apidima crania include Principal component analyses (PCA) to evaluate large-scale trends in the data, linear discriminant function analyses (LDA) to explore the most plausible group affiliation of the Apidima crania, Procrustes distances (PD) to examine overall shape differences, and neurocranial shape index to visualize the relative degree of globularisation for Apidima 1 (e.g., Mitteroecker & Gunz, 2009; Harvati, 2009; Abdi & Williams, 2010; Mitteroecker & Bookstein, 2011; Gunz et al., 2019).

Our morphological analyses were supplemented by U-series dating of both crania as well as their surrounding

matrix. The U-series dating was carried out by collaborators and its methodology will not be discussed in this dissertation (for details see Study I: Supplementary Data). Nevertheless, the dating results will be addressed in the discussion section to contextualize the results and conclusions of the morphological analyses.

Study II: Megalopolis molar. The Megalopolis molar is an isolated upper left wisdom tooth without context that lacks most of the dental root and exhibits taphonomic damage on the occlusal surface (cf. Study II: Megalopolis Molar Figure 1). Thereby, its potential analyses are limited to size based on linear measurements, overall shape of the tooth crown, and internal morphology, e.g., at the enamel-dentine junction (EDJ). Previous assessment of the bucco-lingual (BL) and mesio-distal (MD) crown dimensions indicate a relatively small crown size based on the individual measurements (Harvati, 2016). However, dental size alone cannot necessarily be considered as good phylogenetic indicator (e.g., Bernal et al., 2010; cf. Lockey et al., 2022) and the CT scan of the Megalopolis molar shows no clear differentiation between dental tissues, which complicates the analysis of internal structures.

A first attempt at a size-independent analysis was carried out by Harvati (2016) who evaluated the shape index (BL/MD*100) of the Megalopolis molar. This index placed the specimen closer to fossil groups with larger teeth than to recent modern humans but did not offer additional insights on its affinities (Harvati, 2016). A more comprehensive external size-independent framework for the study of fragmentary teeth is provided by the dental outline analysis (see, e.g., Benazzi et al. 2011a, 2011b, 2012). This method is robust against a certain degree of dental wear and absence of the dental root. In previous studies on different tooth types, this method was able to successfully separate Neanderthals and *H. sapiens* as well as populations within *H. sapiens* (e.g., Benazzi et al.,

2011a, 2011b; Harvati et al., 2015). Thereby, dental crown outline analysis provides a possibility to answer questions regarding the Megalopolis molar's taxonomic status.

In absence of homologous fixed landmarks, dental outline analysis relies on pseudo-landmarks which are calculated mathematically. Repeatability is ensured through an orientation system based on the cervical line, where each tooth is oriented in and its centroid translated to a predefined position (cf. Study II: Megalopolis Molar Figure 2; e.g., Benazzi et al., 2009; 2011b, 2012). Radii originating at the tooth centroid are digitized, the coordinates of their interception with the dental outline are size-corrected and treated like fixed landmarks in the subsequent analyses (e.g., Benazzi et al. 2012; Bauer et al. 2018). This method deviates from the typical GMM approach described in study I in that it removes location and orientation before and size after the data collection.

Multivariate statistics employed in the study of the Megalopolis molar include PCA to evaluate large-scale trends in the data, LDA to explore the most plausible group affiliation of this individual, PD to examine overall shape differences, as well as centroid size (CS) and Pearson correlation test to investigate the relationship between shape and size within the dataset (e.g., Lehmann, 1986; Mitteroecker & Gunz, 2009; Harvati, 2009; Abdi & Williams, 2010; Mitteroecker & Bookstein, 2011).

Study III: Mugharet el'Aliya maxilla. Mugharet el'Aliya is a cave site on the Moroccan Atlantic coast at Cap Ashakar (cf. Figure 1.1). Among other fossils, the cave yielded a left maxillary fragment, hereafter Mugharet el'Aliya (cf. Study III: Mugharet el'Aliya Maxilla Figure 1; e.g., Şenyürek, 1940; Minugh-Purvis, 1993). Mugharet el'Aliya most likely dates to the Late Pleistocene between 35-60 ka (for discussion see Study III: Mugharet el'Aliya Maxilla background and previous studies). Linear measurements showed a great absolute size of this

specimen within the range of modern human adults which contrasts with its juvenile dental status (e.g., Şenyürek, 1940; Minugh-Purvis, 1993). This great size and overall robustness initially led to an attribution of Mugharet el'Aliya to the Neanderthal lineage (Şenyürek, 1940).

Mugharet el'Aliya's state of preservation complicates size-independent morphological analyses due to an insufficient number of preserved landmarks for typical GMM approaches. In contrast, the method of surface registration is almost landmark-free while allowing to analyze shape and size independently (cf. Schlager & Rüdell, 2013). A minimum number of fixed landmarks is required in an initial step of registration between a reference mesh and target mesh. Subsequently, a non-rigid iterative closest point (ICP) algorithm coupled with an elastic component based on Gaussian displacement vectors is used to best match the reference onto the target (Moshfeghi, Ranganath & Nawyn, 1994; Schlager & Rüdell, 2013; cf. Study III: Mugharet el'Aliya Maxilla Measurement Protocol). A sample of triangular meshes with the identical number of corresponding vertices is created by deforming the reference to match several target meshes (cf. Study III: Mugharet el'Aliya Maxilla Figure 2). These vertices can be extracted, size-corrected via GPA, and used in the same way as Procrustes coordinates during analyses.

Multivariate statistics employed in the study of Mugharet el'Aliya include PCA to evaluate large-scale trends in the data, PD to examine overall shape differences, CS and Pearson correlation test to investigate the relationship between shape and size within the dataset, as well as the common allometric component (CAC) and dental age group mean shapes to explore ontogenetic shape changes (e.g., Lehmann, 1986; Mitteroecker et al., 2004; Mitteroecker & Gunz, 2009; Harvati, 2009; Neubauer, Gunz & Hublin, 2010; Abdi & Williams, 2010; Mitteroecker & Bookstein, 2011).

4. Key Results and Discussion

This chapter summarizes the main results of each case study included in this dissertation, reviews them in regard to the specific research questions and places them within the broader discussion outlined in the introduction.

Study I: Apidima Ectocrania. The two late Middle Pleistocene crania from Apidima belong to the most important, and intriguing, finds from the southeastern Mediterranean. Study I was the first to place both fossil crania from Apidima in a comprehensive comparative framework. Previous studies did not have access to the original specimens and had to rely on a limited number of published photographs and nine linear measurements from the taphonomically distorted Apidima 2 (e.g., Manolis, 1996; Harvati, Stringer & Karkanas, 2011). On this basis, Apidima 2 has been considered to be a *H. heidelbergensis* or early Neanderthal (e.g., Coutselinis, Dritsas & Pitsios, 1991; Manolis, 1996; Pitsios, 1999; Harvati, Stringer & Karkanas, 2011). Despite the lack of a published description or study of Apidima 1, Apidima 1 and 2 have been assumed to be of the same taxonomic affiliation (e.g., Bartsiokas et al., 2017).

Our results are in agreement with the hypothesis that Apidima 2 most likely belongs to the Neanderthal lineage and suggest a geological age of ca. 170 ka for this individual. Apidima 2 showed the greatest affinities to our Neanderthal sample with regard to its overall features, linear measurements, and facial as well as neurocranial shape in our GMM analyses (cf. Study I: Apidima Ectocrania Description and comparative analyses, Extended Data, Supplementary Data). Solely the facial shape of reconstruction 2 was not classified as Neanderthal but grouped with our Middle Pleistocene European sample, which consists of Aragao 21 (reconstruction described by

Gunz et al., 2009), Petralona and Sima de los Huesos 5. This observation fits with reported similarities in some facial aspects between our Middle Pleistocene European sample and Neanderthals (e.g., Wolpoff, 1980; Hublin, 1996; Harvati & Hublin, 2012; Arsuaga et al., 2014). Therefore, results obtained from all four independent reconstructions as well as their mean shape are in agreement with each other and support a (early) Neanderthal attribution for Apidima 2. In addition to these results, the linear measurements of Apidima 2 are also most consistent with a Neanderthal attribution, as is a suite of Neanderthal derived traits present in this specimen, which include for example inflated infraorbital region, a continuous, thick and rounded supraorbital torus with no break between the glabellar, orbital and lateral regions, and rounded *en bome* cranial profile in posterior view (cf. Study I: Apidima Ectocrania Description and comparative analyses, Figure 1a–c, Extended Data Figures 2, 6, 7c, d). Both the geological age and cranio-facial morphology of Apidima 2 are therefore in agreement with the 'accretion hypothesis' proposed for Neanderthal evolution and the proposed establishment of Neanderthal craniofacial morphology by MIS 7 (cf. Study I: Apidima Ectocrania Description and comparative analyses, Extended Data, Supplementary Data; e.g., Hublin, 2009; Marra et al., 2017). The 'accretion hypothesis' implies a gradual accumulation of morphological traits, which are distinctive for Neanderthals, accompanied by an increase in their frequency (e.g., Hublin, 1998, 2009; Dean et al., 1998).

In contrast, none of our analyses supports the association of Apidima 1 with the Neanderthal lineage. Instead, this specimen showed the greatest affinities to our *H. sapiens* sample with regard to its overall features, linear measurements, and neurocranial shape. Our new dating suggests a geological age of ca. 210 ka for Apidima 1.

Therefore, to our knowledge Apidima 1 is the oldest fossil proposed to represent the *H. sapiens* lineage in Europe. Apidima 1 exhibits a combination of modern human-like features (i.e., the rather rounded posterior cranium) with ancestral ones like the parietal morphology and low occipital scale of the occipital bone (cf. Study I: Apidima Ectocrania Description and comparative analyses, Supplementary Data). However, no Neanderthal derived traits of the posterior cranium were observed on this specimen, despite the well documented early establishment of these features in the fossil record already before MIS 7 (cf. Study I: Apidima Ectocrania Description and comparative analyses, Extended Data, Supplementary Data; e.g., Hublin, 2009). A complete absence of Neanderthal features as in Apidima 1 cannot be explained by factors like ontogenetic age, sexual dimorphism, and intraspecific variation (e.g., Caspari, 2006; Hublin, 2009). This includes a faint occipital depression which differs from the derived Neanderthal combination of features in this anatomical region and is most similar to such features described for some African Middle and Late Pleistocene specimens (cf. Study I: Apidima Ectocrania Description and comparative analyses; Harvati et al., 2020; Harvati, 2022). Earlier Middle Pleistocene European specimens (e.g., Reilingen, Swanscombe, Sima de los Huesos) as well as similarly dated early Neanderthals (e.g., Biache-St-Vaast 1 and Saccopastore) exhibit Neanderthal-like occipital features, including well-developed suprainiac fossae with associated occipital tori, as well as occipital 'bunning' and associated lambdoid flattening (e.g., Vandermeersch, 1978; Arsuaga et al., 1997; Dean et al., 1998; Manzi et al., 2001; Hublin, 2009). Only the Middle Pleistocene individual from Steinheim might appear relatively rounded in the posterior neurocranium in lateral view. However, this specimen is severely taphonomically distorted, making its evaluation difficult in this context

(Prossinger et al., 2003; Balzeau & Rougier, 2010; Buzi et al., 2021).

3D GMM provides a valuable framework for the study of fragmentary fossils (e.g., Zollikofer et al., 2005; Gunz et al., 2009, 2012; Di Vincenzo et al., 2017; Bosman et al., 2019; Mori et al., 2020) and objective analysis of morphological characteristics like curvature. For example, midsagittal curvature of the neurocranium can be captured by curve semi-landmarks and directly compared in a quantitative framework (e.g., Gunz, Mitteroecker & Bookstein, 2005; Gunz et al., 2009; Mitteroecker & Gunz, 2009; Gunz & Mitteroecker, 2013). In case of the shared aspects of morphology, which are limited to the parietal region, Apidima 1 shows a rather rounded and Apidima 2 exhibits a rather flat midsagittal profile (cf. Study I: Apidima Ectocrania Figure 4). Thereby, the four reconstructions of Apidima 2 group with our Neanderthal sample and Apidima 1 in between our Middle Pleistocene African and *H. sapiens* samples. Nevertheless, Apidima 1 is classified as *H. sapiens* with a posterior probability of ca. 92% (cf. Study I: Apidima Ectocrania Extended Data Table 1). Further, when analyzing the entire preserved morphology of Apidima 1, its rather rounded neurocranium falls within fossil and recent *H. sapiens* variation and is classified as *H. sapiens* with posterior probabilities exceeding 93% (cf. Study I: Apidima Ectocrania Figure 3, Extended Data Table 1).

The combination of a laterally rounded midsagittal profile and overall globular neurocranium is a unique feature defining modern humans and its current manifestation is suggested to have evolved only 100 ka (e.g., Lieberman et al., 2002; Stringer, 2016; Neubauer, Hublin & Gunz, 2018; Galway-Witham & Stringer, 2018; Gunz et al., 2019). The crania from Jebel Irhoud, which are commonly accepted as early *H. sapiens*, show a non-globular neurocranium (e.g., Harvati, Hublin & Gunz,

2010; Freidline et al., 2012; Bruner & Pearson, 2012; Hublin et al., 2017; Neubauer, Hublin & Gunz, 2018). In contrast, individuals from Skhul and Qafzeh exhibit globular neurocrania, although not entirely within recent modern human variation, especially in regard to the endocranial shape (e.g., Schwartz & Tattersall, 2003; Trinkaus, 2005; Stringer, 2016; Neubauer, Hublin & Gunz, 2018). The approximately 200 ka, that separate Jebel Irhoud and Skhul/Qafzeh, are characterized by a mix of rather globular (e.g., Herto, Omo 1) and non-globular (e.g., Omo 2, Ngaloba LH18) neurocranial shapes in presumably early *H. sapiens* individuals (for review see Stringer 2016; references therein). Further, overall cranio-facial morphology is characterized by a mix of archaic and derived traits in fossils attributed to early *H. sapiens* (e.g., Vandermeersch, 1981; Hublin et al., 2017; for review see Stringer, 2016; references therein). Our analysis of the Apidima 1 neurocranial shape largely focused on the midsagittal region, with only a few landmarks representing more lateral aspects of its anatomy. Nevertheless, the shape index values of Apidima 1 calculated from our datasets fell within fossil *H. sapiens* variation, showing similarities to individuals from Skhul and Qafzeh, as well as Eliye Springs (cf. Study I: Apidima Ectocrania Figure 3c, Extended Data Figure 8). All of the latter have been shown to differ from the current manifestation of the globular modern human neurocranium (e.g., Schwartz & Tattersall, 2003; Trinkaus, 2005; Stringer, 2016; Neubauer, Hublin & Gunz, 2018). Thereby, the globular midsagittal outline of the neurocranial shape of Apidima 1, combined with the more archaic, ancestral morphology of its parietals, is in agreement with both the association to the early *H. sapiens* lineage and the proposed late evolution of the full set of modern cranio-facial morphology including a fully globular braincase and underlying endocranium (e.g., Neubauer, Hublin & Gunz, 2018; Weber et al., 2020).

Although this dissertation focuses on the morphological aspect of our study, the geological ages of Apidima 1 and 2 should be addressed briefly to highlight the importance of our findings. Uranium-series (U-series) dating is a method of direct dating in which the isotopic ratios in the decay chain of Uranium (U) and Thorium are measured (for discussion see e.g., Grün, 2006; Pickering, 2017). The unstable isotopes decay with a known half-life allowing to calculate the time interval since their uptake. In open systems, i.e., bone, the U concentration increases after burial due to a complex process of U uptake (Pike, Hedges & van Calsteren, 2002). Therefore, U-series dates are generally considered as minimum dates due to potential phases of leaching and / or phases with little or no U uptake (e.g., Pike, Hedges & van Calsteren, 2002; Grün et al., 2014; Bartsiokas et al., 2017). In addition to the actual dating, the ratio between U isotopes can provide information about the U-source, whether it remained constant or may have changed, and whether various material show signals of the same or different U sources (e.g., Grün et al., 2014). In the case of the Apidima crania, samples from bone fragments of both individuals, as well as unidentified bone fragments from the same breccia block and from the surrounding matrix were analyzed (cf. Study I: Supplementary Data). Our results suggest a minimum age of 211±16 ka for Apidima 1 and of 172±11 ka for Apidima 2 combined with differences in the U sources for both crania, consistent also with two clusters of dates obtained from the unidentified bone fragments analyzed. Our minimum age for Apidima 2 is roughly consistent with a previous dating attempt (from the same laboratory and using the same method), which supports our observed isotopic ratios (cf. Bartsiokas et al., 2017). Nonetheless, solidification of the surrounding matrix is placed around 150 ka, which provides the youngest possible date for the enclosed crania. The cranial morphology of Apidima 1 remains intriguing and its importance with regard to the

above discussed points would not change even when placing Apidima 1 around 150 ka.

The next oldest known fossil evidence for *H. sapiens* in Europe postdates Apidima 1 by at least ca. 105 ka and derives from sites like Zlatý kůň, Czech Republic, Grotta del Cavallo, Italy, and Bacho Kiro cave, Bulgaria (cf. Figure 1.2; Benazzi et al., 2011a; Hublin et al., 2020; Prüfer et al., 2021). Fossil remains from these sites have been dated to around 45 ka (Benazzi et al., 2011a; Fewlass et al., 2020; Prüfer et al., 2021). In Bacho Kiro, the human remains are directly associated with initial Upper Paleolithic (IUP) lithics (Hublin et al., 2020). The IUP marks the onset of the UP, which is thought to represent the first widespread population of Europe by modern humans (for discussion see e.g., Mellars, 2006b; Hoffecker, 2009; Benazzi et al., 2015; Hublin, 2015; Stutz, 2020). Earlier out-of-Africa dispersals of *H. sapiens* are often considered as failed and not far-reaching (e.g., Shea & Bar-Yosef, 2005; Mellars, 2006a; Shea, 2008; Klein, 2009; Oppenheimer, 2012; Hölzchen et al., 2016; Vizzari et al., 2020). Nevertheless, paleoanthropological and genetic studies suggest interaction between *H. sapiens* and Neanderthals predating MIS 5 (e.g., Posth et al., 2017; Hershkovitz et al., 2018a; Petr et al., 2020). Mitochondrial and Y-chromosomal DNA suggest gene flow from *H. sapiens* into Neanderthals before ca. 220 ka and between ca. 370-100 ka, respectively (cf. Introduction; Posth et al., 2017; Petr et al., 2020). The known Neanderthal range does not include the African continent (Figure 1.2; cf. Blinkhorn et al., 2021) and thereby, indicates the Eastern Mediterranean and Southwest Asia as most likely places of contact with early *H. sapiens*. Such a pre-MIS 5 dispersal out-of-Africa is supported by the early *H. sapiens* fossils from Misliya cave that date to approximately 177-194 ka (Valladas et al., 2013;

Hershkovitz et al., 2018a) and could also be evidenced by Apidima 1.

Further, the distinctive morphology of the two crania from Apidima combined with their diverging geological ages suggests a complex demographic pattern for southern Greece during the Pleistocene. A similar scenario has been proposed for the Levant (cf. e.g., Mercier et al., 1993; Hershkovitz et al., 2018a; Stringer & Galway-Witham, 2018). Levantine archaeological sites associated with *H. sapiens* can be found most likely in MIS 6, securely in MIS 5 and continuously since MIS 3, while sites associated to Neanderthals cluster in MIS4 with some overlap to the terminal MIS 5 and early MIS 3 (e.g., Grün et al., 2005; Shea, 2008; Bar-Yosef & Belmaker, 2011; Hershkovitz et al., 2015, 2018a; Abadi, Bar-Yosef & Belfer-Cohen, 2020; Heydari-Guran et al., 2021). Similarly, our results suggest a scenario of possible alternating occurrence and replacement of late Middle Pleistocene early modern humans and Neanderthals in southern Greece. The Neanderthal presence in southern Greece is well-documented from archaeological as well as paleoanthropological finds, which seem to cluster in the terminal Middle and Late Pleistocene (e.g., Harvati, Panagopoulou & Karkanas, 2003, Harvati, et al., 2013; Tourloukis et al., 2016).

With this study, we contribute to the growing evidence for multiple out-of-Africa dispersals of early members of the *H. sapiens* lineage, independent of these dispersals' long-term success. Furthermore, our results add to the scientific discourse about potential dispersal routes into Europe as well as the increasingly complex demographic processes that characterized human evolution during the Pleistocene.

Study II: Megalopolis molar. Besides the two crania from Apidima discussed in study I, the Pleistocene Greek hominin fossil record is relatively sparse (for review see e.g., Harvati, Panagopoulou & Runnels, 2009; Harvati, 2016).

Study II attempts to clarify the putative fossil status and potential taxonomic affiliation of the Megalopolis molar, that is assumed to date to the Pleistocene. Clarifying its status by direct or indirect dating methods is complicated by the lack of context as surface find, previous chemical treatment (Xirotiris et al., 1979), and the destructive nature of direct dating (cf. Study I: Supplementary Data; e.g., Grün, 2006; Grün et al., 2014). Nevertheless, our results tentatively support a Pleistocene age of the Megalopolis molar (cf. Study II: Megalopolis Molar Results & Discussion). Dental crown outline analyses and discriminant function analysis favor an association of the Megalopolis molar to the Neanderthal lineage. Its overall shape and size show the greatest affinities to Neanderthals from Krapina cave (Croatia), that are dated to approximately 130 ka (Rink et al., 1995). This finding is inconsistent with a modern intrusion and make such a scenario appear unlikely for the Megalopolis molar.

The combination of the Megalopolis Basin's geology and fauna collected at the same time suggest a Middle Pleistocene geological age for the Megalopolis molar. The Megalopolis molar was part of a faunal collection of surface finds. This fauna has been assigned to the lower half of the Middle and Early Pleistocene (Sickenberg, 1976; cf. Koenigswald & Heinrich, 2007). Further, at the time of discovery many of the collected faunal remains were embedded in blocks of lacustrine sediments (Sickenberg, 1976). Sediments within the Megalopolis Basin are mostly of Middle Pleistocene origin and the fossiliferous lacustrine deposits of the Marathousa member of the Choremi Formation exhibit ages between approximately 800-200 ka and have recently yielded evidence of human presence (cf. Study II: Megalopolis Molar Discussion; e.g., Löhnert & Nowack, 1965; Vinken, 1965; Siavalas et al., 2009; Jacobs et al., 2018; Blackwell et al., 2018; Panagopoulou et al. 2018).

Despite its deduced geological age, the Megalopolis molar is an important addition to the few Greek fossils attributed to the broader Neanderthal lineage. Pleistocene Neanderthal and pre-Neanderthal fossils include the Petralona cranium attributed to *H. heidelbergensis* (e.g., Stringer, 1974, 2012; Grün, 1996) and Neanderthal remains from Lakonis, Kalamakia and Apidima cave A (cf. Study I: Apidima Ectocrania; Harvati, Panagopoulou & Karkanas, 2003, Harvati et al., 2013; Bauer et al., 2018). A direct comparison of the Megalopolis molar with the preserved upper wisdom teeth from Petralona and Kalamakia could clarify its relation to the Neanderthal lineage. However, these individuals could not be included into our comparative sample.

With this study, we are not able to answer all questions regarding the Megalopolis molar due to limitations in the applicable methodology and comparative sample. Nevertheless, it highlights the importance and potential of the Megalopolis Basin. A lignite mine situated within the Megalopolis Basin exposes and provides unique access to a long geological sequence (e.g., Tourloukis & Karkanas, 2012; Tourloukis & Harvati, 2018). In this context, the Megalopolis Basin is well-known for its rich fossil fauna (e.g., Skouphos, 1905; Melentis, 1961; Sickenberg, 1976; Athanassiou et al., 2018; Athanassiou, 2018) and more recently also for archaeological sites dating to the Middle Pleistocene (e.g., Panagopoulou et al., 2015; Thompson et al., 2018; Giusti et al., 2018; Konidaris et al., 2019), underlining its role as potential glacial refugium (e.g., Panagopoulou et al., 2018; Michailidis et al., 2018; Bludau et al., 2021). An early human presence is indicated by for example Marathousa 1, which is dated to 400-500 ka and shows signs of butchery in a stratified context (e.g., Tourloukis et al., 2018; Konidaris et al., 2018; Blackwell et al., 2018; Jacobs et al., 2018). Furthermore, archaeological sites within the Basin exhibit an extraordinary preservation

and thereby have the potential to yield precious paleoanthropological finds.

Study III: Mugharet el'Aliya maxilla. The assessment of the taxonomic affinities of paleoanthropological finds is influenced by the available comparative samples and prevailing evolutionary hypotheses. In the context of the early to mid-20th century, North African fossils – including Jebel Irhoud - were attributed to the Neanderthal lineage (e.g., Şenyürek, 1940; McBurney, Trevor & Wells, 1953; Ennouchi, 1962). These fossils are now generally considered as *H. sapiens* (e.g., Hublin & Tillier, 1988; Harvati & Hublin, 2012; Hublin et al., 2012; Freidline et al., 2021). However, the origin of their archaic and in part 'Neanderthal-like' features remains unclear. Study III investigated the taxonomic and phylogenetic affinities of the enigmatic juvenile maxilla from Mugharet el'Aliya and assessed its morphology in the context of size, ontogeny, and fragmentary status. Our results are in agreement with Mugharet el'Aliya being a Late Pleistocene modern human (cf. Study III: Mugharet el'Aliya Maxilla Results, Discussion). Overall shape, the comparison of ontogenetic age group mean shapes, CAC and the relative position of the zygomatic root show the greatest affinities to our *H. sapiens* sample, especially to the juvenile early *H. sapiens* individual Qafzeh 10. In contrast, a PCA could not differentiate between our samples of fossil subadults.

A major limiting factor to all these analyses is the state of preservation of Mugharet el'Aliya, especially in the infra-orbital region (cf. Study III: Mugharet el'Aliya Maxilla Figure 1). The infra-orbital region of adult Neanderthals is characterized by an 'inflated' morphology lacking a distinct canine fossa, which is typical for adult modern humans (e.g., Trinkaus, 1987; Bermúdez de Castro et al., 1997; Hublin, 1998; Harvati, Hublin & Gunz, 2010; Clement, Hillwon & Aiello, 2012; Harvati, 2015). The absence of a distinct canine fossa in Mugharet el'Aliya was interpreted

as affinity to the Neanderthal lineage (Şenyürek, 1940). Mugharet el'Aliya exhibits considerable damage in this area that precludes a full evaluation of its canine fossa morphology. When comparing only the preserved morphology, the absence of a deep, expanded and distinct canine fossa is shared between Mugharet el'Aliya and several subadult individuals, including some Neanderthals, of comparable dental age to Mugharet el'Aliya. Our results support the hypothesis that the development of the canine fossa extends into late ontogenetic phases, i.e., after the eruption of the first permanent molar (e.g., Minugh-Purvis, 1993; Schuh et al., 2020). Moreover, several subadult modern humans share a slightly receding zygoma with Mugharet el'Aliya, which contrasts with using such a slight manifestation for inferring Neanderthal affinities (cf. Şenyürek, 1940).

The greatest disparities between *H. sapiens*, Mugharet el'Aliya and our Neanderthal sample of comparable dental age are in the curvature of the inferior zygomatic margin (IZM) and the position of the zygomatic root in relation to the dentition (cf. Study III: Mugharet el'Aliya Maxilla Figures 3 PC1, 7; e.g., Trinkaus, 1987; Bermúdez de Castro et al., 1997; Hublin, 1998; Harvati, Hublin & Gunz, 2010; Clement, Hillwon & Aiello, 2012; Harvati, 2015). Mugharet el'Aliya shares an arched IZM with *H. sapiens*, which exhibit this feature throughout ontogeny. In contrast, Neanderthals show an ontogenetic trend from weak curvature at the IZM towards a rather straight IZM. With eruption of the first permanent molar, Neanderthals clearly deviate from the IZM pattern observed in *H. sapiens*. Another feature considered as derived for Neanderthals is a relatively posterior zygomatic root position (e.g., Trinkaus, 1987; Weber & Krenn, 2017). All our samples of early and later *H. sapiens* as well as Neanderthals show a shared ontogenetic trend of a relative posterior shift in the position of the zygomatic root in relation to the dentation

(cf. Study III: Mugharet el'Aliya Maxilla Figures 4 PC1, 7, 8; Supplementary Data Figure S4). However, its expression varies, with adult Neanderthals showing a more posterior zygomatic root position than adult *H. sapiens* and subadult Neanderthals plotting towards the overlap with older age groups. In contrast, some adult *H. sapiens*, Qafzeh 10 and Mugharet el'Aliya show a more anterior zygomatic root position as expected from the modern human sample (Study III: Mugharet el'Aliya Maxilla Figure 4 PC1; Minugh-Purvis, 1993).

This shared tendency as well as very similar overall shapes between Mugharet el'Aliya and Qafzeh 10 add to the evidence connecting fossils attributed to the Northwest African Middle Stone Age (MSA) to early *H. sapiens* sites in the Levant (ca. Study III: Mugharet el'Aliya Maxilla Figures 4, 6, Discussion, Supplementary Data Table S2; e.g., Ferembach, 1976; Hublin & Tillier, 1981, 1988, Hublin et al., 2012, 2017; Harvati & Hublin, 2012; Freidline et al., 2021). Similarities between the Northwest African MSA and the earliest undisputed out of Africa dispersal of *H. sapiens* exceed fossil morphology and include aspects of their lithic assemblages. Levantine Middle Paleolithic assemblages from MIS 5 show characteristics described as Mousterian or belonging to the centripetal Levallois method (for discussion see e.g., Shea & Bar-Yosef, 2005; Prévost & Zaidner, 2020; references therein). Such characteristics seem to be shared between African MSA and Levantine sites yielding early *H. sapiens* fossils (e.g., Shea & Bar-Yosef, 2005; Tryon, Roach & Logan, 2008; Richter et al., 2017; Prévost & Zaidner, 2020). The relevance of such morphological and archaeological similarities and their implications on possible connections across populations from the MSA Moroccan Atlantic Coast to the Middle Paleolithic Levant, remain an important area of future research.

One aspect of our results not only connects Mugharet el'Aliya with fossil *H. sapiens* but also with Neanderthals. All fossil subadults exhibit a greater maxillary size than recent *H. sapiens* of comparable age (cf. Study III: Mugharet el'Aliya Maxilla Figure 3, Supplementary Data Tables S3, S4). Reduction in jaw and facial size are frequent in recent *H. sapiens* due to potential absence of wisdom teeth (Oeschger et al., 2020). In contrast, great mesio-distal extension of the post-canine dentition is associated with a relative size increase of the corresponding jaw. Early *H. sapiens* from the Northwest African MSA and the Levant are characterized by megadonty relative to recent modern humans (e.g., Hershkovitz et al., 2011; Hublin et al., 2012). Therefore, a lack of subadult *H. sapiens* fossils in the metric analysis of Mugharet el'Aliya led to its great absolute size playing a crucial role in the previous attribution to the Neanderthal lineage (Şenyürek, 1940).

Examples like Mugharet el'Aliya highlight the need for approaches that allow size-independent analyses as well as evaluation of the relationship between shape and size. Landmark-based GMM is used widely for size-independent studies of hominin fossils in the context of various research questions (cf. Introduction, e.g., Mitteroecker et al., 2004; Zollikofer et al., 2005; Nicholson & Harvati, 2006; von Cramon-Taubadel & Lycett, 2008; Neubauer, Gunz & Hublin, 2010; Gunz et al., 2012; Reyes-Centeno et al., 2015; Di Vincenzo et al., 2017; Karakostis et al., 2018). However, landmark-based GMM reaches its limits in fragmentary remains with insufficiently preserved landmarks. The optimal number of landmarks to capture an object's shape is determined by the its complexity and the diagnostic value of the available landmarks. Especially in cases of complex objects with only a few available landmarks of little diagnostic value, the captured shape aspects might not be biologically meaningful. The method

of surface registration as implemented in study III requires only a minimum number of landmarks (cf. Materials and Methods, Study III: Mugharet el'Aliya Maxilla; Schlager & Rüdell, 2013). These landmarks are discarded after an initial step of surface registration and not part of the analyzed dataset, which significantly reduces the method's observer error (cf. Study III: Mugharet el'Aliya Maxilla Error calculations, Supplementary Data Figures S1, S2). Therefore, GMM based on surface registration has the potential to be a robust approach for the study of fragmentary specimens, which are common in the fossil record. It offers an opportunity to investigate the entire preserved morphology of specimens that were impossible to analyze quantitatively up to now.

A core element of the surface registration method is the ICP algorithm, that is used increasingly in the field of paleoanthropology (e.g., Pomidor, Makedonska & Slice, 2016; Hassett & Lewis-Bale, 2017; Beaudet & Bruner, 2017; Haile-Selassie et al., 2019). Although not yet used as extensively as landmark-based GMM possible applications range from pairwise comparison of morphological variation (Beaudet & Bruner, 2017; White & Campione, 2021), to enhancement of the alignment between mirrored and original regions during fossil reconstruction (Haile-Selassie et al., 2019), to quantifying overall shape difference in a comparable way as PD (Pomidor, Makedonska & Slice, 2016; Hassett & Lewis-Bale, 2017), and complete shape analyses (cf. Study III: Mugharet el'Aliya Maxilla, Schlager & Rüdell, 2013). Further, the here implemented protocol could be used for transferring surface semi landmarks from a reference to a target sample by reducing the number of matched vertices and retaining the landmarks used in the initial registration in the subsequent analyses.

This study is an important contribution to the increasing use of ICP algorithms in the attempt to employ size-independent shape analyses relying on no landmarks

or only a minimum number thereof. This allowed the placement of Mugharet el'Aliya's entire external morphology in a comprehensive comparative framework for the first time. Further, our results add valuable insights to both the growing evidence connecting cranio-dental morphology from Northwest African MSA and the Levant, and knowledge about the ontogeny of morphological traits which are frequently used to characterize Neanderthals and modern humans.

5. Future Directions and Concluding Remarks

This dissertation aimed to reduce existing gaps in our knowledge about fossil *H. sapiens* and Neanderthals by applying virtual methods to so far poorly studied fossil materials from understudied circum-Mediterranean regions. Thereby, study I confirmed Apidima 2 as one of the few, and the most complete, Neanderthal fossil from Greece, and our analysis of Apidima 1 suggested a more widespread early *H. sapiens* dispersal reaching southeastern Europe contrary to previous beliefs (cf. e.g., Davies, 2001; Mellars, 2006b; Hoffecker, 2009; Benazzi, 2011a; Higham et al., 2011; Hublin, 2012; Trinkaus, Constantin & Zilhão, 2013; Nigst et al., 2014; Bosch et al., 2015; Harvati, 2015; Hershkovitz et al., 2018a). The taxonomic affiliation of Apidima 1 to *H. sapiens* has been questioned by some (e.g., De Lumley et al., 2020; Rosas & Bastir, 2020; but see Harvati 2022) and may be further elucidated by analyzing internal morphologies, i.e., the bony labyrinth of the inner ear and endocast. Both have been shown to be able to differentiate between samples of later *Homo* (e.g., Spoor et al., 2003; Bouchneb & Crevecoeur, 2009; Uhl et al., 2016; Neubauer, Hublin & Gunz, 2018; Bruner, Oghihara & Tanabe, 2018; Gunz et al., 2019). Although the available CT scan of Apidima 1 excludes a reliable segmentation of internal structures, it indicates their successful segmentation in a new planned scan with slightly adjusted scan parameters. Planned new fieldwork at Apidima will contribute to our understanding of the cave site, its chronology and site formation and perhaps increase our fossil human sample from the site, thereby further help to clarify the dating and affinities of Apidima 1.

In case of the Megalopolis molar, the analyses of internal structures, i.e., EDJ, have great potential for clarifying its relationship with pre-Neanderthals and Neanderthals. The EDJ preserves phylogenetic signals even in cases of slight to moderate dental wear and taphonomic alteration of the outer enamel (e.g., Skinner et al., 2008; Bailey, Skinner & Hublin, 2011; Zanolli & Mazurier, 2013; Hublin et al., 2017). To achieve such an analysis, adaptation of specific filters and protocols for contrast enhancement in the underlying CT scan would be required (cf. Abel, Laurini & Richter, 2012). Nevertheless, study II links the Megalopolis molar to the Neanderthal lineage and supports its inclusion into the growing Pleistocene Greek fossil record.

The results of study III showed that the previously suggested Neanderthal affinities of the North African juvenile maxilla from Mugharet el'Aliya are the result of its great absolute size and ontogenetic status. The comparative analysis contributed to our knowledge about the ontogeny of facial morphology in Neanderthals and modern humans. Further, study III highlights the potential of adapting methods not routinely used in paleoanthropology to the study of fragmentary fossil remains. Combining the here employed surface registration protocol with a data reduction technique based on the Arothron R package (Profico et al., 2021) and reconstruction of missing data via statistical shape models (e.g., Semper-Hogg et al., 2017) offers the opportunity of an almost landmark-free approach to analyze shape in an equivalent way to typical landmark-based GMM.

To conclude, the three case studies included in this dissertation are an important contribution to the scientific discourse about the evolution and ontogeny of modern human morphology, early *H. sapiens* dispersals out of Africa as well as temporal and spatial possibilities for the interaction between fossil *H. sapiens* and Neanderthals.

These aspects continue to be important areas of paleoanthropological research as many open questions and gaps in our knowledge remain. Although, additional fieldwork is important in closing these gaps, the careful reconstruction and analysis of existing so far understudied hominin fossils have great potential to significantly contribute to our knowledge about human evolution.

6. References

Abadi, I., Bar-Yosef, O., & Belfer-Cohen, A. (2020). Kebara V—a contribution for the study of the middle-upper paleolithic transition in the Levant. P*aleoAnthropology*, 2020:1, 1-28. Doi: 10.4207/PA.2020.ART139.

Abdi, H., & Williams, L. J. (2010). Principal component analysis. *Wiley Interdisciplinary Reviews: Computational Statistics*, *2* (4), 433-459. Doi: 10.1002/wics.101.

Abel, R. L., Laurini, C. R., & Richter, M. (2012). A palaeobiologist's guide to 'virtual' micro-CT preparation. *Palaeontologia Electronica*, 15 (2), 1-16.

Arsuaga, J. L., Martınez, I., Gracia, A., & Lorenzo, C. (1997). The Sima de los Huesos crania (Sierra de Atapuerca, Spain). A comparative study. *Journal of Human Evolution*, *33* (2-3), 219-281. Doi: 10.1006/jhev.1997.0133.

Arsuaga, J. L., Martínez, I., Arnold, L. J., Aranburu, A., Gracia-Téllez, A., Sharp, W. D., Quam, R. M., Flaguères, C., Pantoja-Pérez, A., Bischoff, J., Poza-Rey, E., Parés, J. M., Caretero, J. M., Demuro, M., Lorenzo, C., Sala, N., Matinoón-Torres, M., García, N., Alcázar de Velasco, A., Cuenca-Bescós, G., Gómez-Olivencia, A., Moreno, D., Pablos, A., Schen, C.-C., Rodríguez, L., Ortega, A. I., García, R., Bonmatí, A., Bermúdes de Castro, J. M., & Carbonell, E. (2014). Neandertal roots: Cranial and chronological evidence from Sima de los Huesos. *Science*, *344* (6190), 1358-1363. Doi: 10.1126/science.1253958.

Athanassiou, A. (2018). Pleistocene vertebrates from the Kyparíssia lignite mine, Megalopolis Basin, S. Greece: Rodentia, Carnivora, Proboscidea, Perissodactyla, Ruminantia. *Quaternary International*, 497, 198-221. Doi: 10.1016/j.quaint.2018.06.042.

Athanassiou, A., Michailidis, D., Vlachos, E., Tourloukis, V., Thompson, N., & Harvati, K. (2018). Pleistocene vertebrates from the Kyparíssia lignite mine, Megalopolis Basin, S. Greece: Testudines, Aves, Suiformes. *Quaternary International*, 497, 178–197. Doi: 10.1016/j.quaint.2018.06.030.

Bae, C. J., Douka, K., & Petraglia, M. D. (2017). On the origin of modern humans: Asian perspectives. *Science*, 358, 1269. Doi: 10.1126/science.aai9067.

Bailey, S. E., Skinner, M. M., & Hublin, J. J. (2011). What lies beneath? An evaluation of lower molar trigonid crest patterns based on both dentine and enamel expression. *American Journal of Physical Anthropology*, 145 (4), 505-518. Doi: 10.1002/ajpa.21468.

Balzeau, A., & Rougier, H. (2010). Is the suprainiac fossa a Neandertal autapomorphy? A complementary external and internal investigation. *Journal of Human Evolution*, 58, 1–22. Doi: 10.1016/j.jhevol.2009.05.016.

Balzeau, A., Crevecoeur, I., Rougier, H., Froment, A., Gilissen, E., Grimaud-Hervé, D., Mennecier, P., & Semal, P. (2010). Applications of imaging methodologies to paleoanthropology: Beneficial results relating to the preservation, management and development of collections. *Comptes Rendus Palevol*, 9 (6), 265-275. Doi: 10.1016/j.crpv.2010.07.006.

Bartsiokas, A., Arsuaga, J. L., Aubert, M. & Grün, R. (2017). U-series dating and classification of the Apidima 2 hominin from Mani Peninsula, Southern Greece. *Journal of Human Evolution*, 109, 22–29. Doi: 10.1016/j.jhevol.2017.04.008.

Bar-Yosef, O., & Belmaker, M. (2011). Early and Middle Pleistocene faunal and hominins dispersals through Southwestern Asia. *Quaternary Science Reviews*, *30* (11-12), 1318-1337. Doi: 10.1016/j.quascirev.2010.02.016.

Bastir, M., Rosas, A., Gunz, P., Peña-Melian, A., Manzi, G., Harvati, K., Kruszynski, R., Stringer, C., & Hublin, J. J. (2011). Evolution of the base of the brain in highly encephalized human species. *Nature Communications*, 2 (1), 1-8. Doi: 10.1038/ncomms1593.

Bauer, C. C., Benazzi, S., Darlas, A., & Harvati, K. (2018). Geometric morphometric analysis and internal structure measurements of the Neanderthal lower fourth premolars from Kalamakia, Greece. *Quaternary International*, *497*, 14-21. Doi: 10.1016/j.quaint.2018.01.035.

Beaudet, A., & Bruner, E. (2017). A frontal lobe surface analysis in three archaic African human fossils: OH 9, Buia, and Bodo. *Comptes Rendus Palevol*, 16 (5-6), 499-507. Doi: 10.1016/j.crpv.2016.12.002.

Been, E., Hovers, E., Ekshtain, R., Malinski-Buller, A., Agha, N., Barash, A., Bar-Yosef Mayer, D. E., Benazzi, S., Hublin, J.-J., Levin, L., Greenbaum, N., Mitki, N., Oxilia, G., Porat, N., Roskin, J., Soudack, M., Yeshurun, R., Shahack-Gross, R., Nir, N., Stahlschmidt, M. C., Rak, Y., & Barzilai, O. (2017). The first Neanderthal remains from an open-air Middle Palaeolithic site in the Levant. *Scientific Reports*, 7 (1), 1-8. Doi: 10.1038/s41598-017-03025-z.

Bellucci, L., Bona, F., Corrado, P., Magri, D., Mazzini, I., Parenti, F., Scardia, G., & Sardella, R. (2014). Evidence of late Gelasian dispersal of African fauna at Coste San Giacomo (Anagni Basin, central Italy): Early Pleistocene environments and the background of early human occupation in Europe. *Quaternary*

Science Reviews, *96*, 72-85. Doi: 10.1016/j.quascirev.2013.10.011.

Belmaker, M. (2009). Hominin adaptability and patterns of faunal turnover in the Lower-Middle Pleistocene transition in the Levant. In: M. Camps & P. R. Chauhan (Eds.), *A Sourcebook of Paleolithic Transitions: Methods, Theories and Interpretations* (pp. 211-227). Springer: New York. Doi: 10.1007/978-0-387-76487-0_12.

Belmaker, M. (2010). The presence of a large cercopithecine (cf. *Theropithecus* sp.) in the 'Ubeidiya Formation (Early Pleistocene, Israel). *Journal of Human Evolution*, 58, 79-89. Doi: 10.1016/j.jhevol.2009.08.004.

Benazzi, S., Fantini, M., De Crescenzio, F., Persiani, F., & Gruppioni, G. (2009). Improving the spatial orientation of human teeth using a virtual 3D approach. *Journal of Human Evolution,* 56, 286–293. Doi: 10.1016/j.jhevol.2008.07.006.

Benazzi, S., Douka, K., Fornai, C., Bauer, C. C., Kullmer, O., Svoboda, J., Pap, I., Mallegni, F., Bayle, P., Coquerelle, M., Condemi, S., Ronchitelli, A., Harvati, K., & Weber, G. W. (2011a). Early dispersal of modern humans in Europe and implications for Neanderthal behaviour. *Nature*, *479* (7374), 525-528. Doi: 10.1038/nature10617.

Benazzi, S., Coquerelle, M., Fiorenza, L., Bookstein, F., Katina, S., & Kullmer, O. (2011b). Comparison of dental measurement systems for taxonomic assignment of first molars. *American Journal of Physical Anthropology*, 144, 342–54. Doi: 10.1002/ajpa.21409.

Benazzi, S., Fornai, C., Buti, L., Toussaint, M., Mallegni, F., Ricci, S., Gruppioni, G., Weber, G. W., Condemi, G. W., & Ronchitelli, A. (2012). Cervical and crown outline analysis of worn Neanderthal and modern human lower second deciduous molars. *American Journal of Physical Anthropology*, 149, 537–546. Doi: 10.1002/ajpa.22155.

Benazzi, S., Slon, V., Talamo, S., Negrino, F., Peresani, M., Bailey, S. E., Sawyer, S., Panetta, D., Vicino, G., Starnini, E., Mannino, M. A., Salvadori, P. A., Meyer, M., Pääbo, S., & Hublin, J.-J. (2015). The makers of the Protoaurignacian and implications for Neandertal extinction. *Science*, 348, 793-796. Doi: 10.1126/science.aaa2773.

Bermúdez de Castro, J., Arsuaga, J. L., Carbonell, E., Rosas, A., Martınez, I., & Mosquera, M. (1997). A hominid from the Lower Pleistocene of Atapuerca, Spain: possible ancestor to Neandertals and modern humans. *Science*, 276 (5317), 1392-1395. Doi: 10.1126/science.276.5317.1392.

Bernal, V., Perez, S. I., Gonzalez, P. N., & Diniz-Filho, J. A. F. (2010). Ecological and evolutionary factors in dental morphological diversification among modern human populations from southern South America. *Proceedings of the Royal Society B*, 277, 1107-1112. Doi: 10.1098/rspb.2009.1823.

Blackwell, B. A., Sakhrani, N., Singh, I. K., Gopalkrishna, K. K., Tourloukis, V., Panagopoulou, E., Karkanas, P., Blickstein, J. I. B., Skinner, A. R., Florentin, J. A., & Harvati, K. (2018). ESR Dating Ungulate Teeth and Molluscs from the Paleolithic Site Marathousa 1, Megalopolis Basin, Greece. *Quaternary*, 1, 22. Doi: 10.3390/quat1030022.

Blinkhorn, J., Zanolli, C., Compton, T., Groucutt, H. S., Scerri, E. M., Crété, L., Stringer, C., Petraglia, M. D., & Blockley, S. (2021). Nubian Levallois technology associated with southernmost Neanderthals. *Scientific Reports*, *11* (1), 1-13. Doi: 10.1038/s41598-021-82257-6.

Blondel, J., & Ferris, R. (1995). *Biogéographie: Approche Écologique et Évolutive*. Paris: Editions Masson.

Blondel, J., Aronson, J., Bodiou, J. Y., & Boeuf, G. (2010). *The Mediterranean region: biological diversity in space and time* (2nd ed.). New York, NY: Oxford University Press.

Bludau, I. J. E., Papadopoulou, P., Iliopoulos, G., Weiss, M., Schnabel, E., Thompson, N., Tourloukis, V., Zachow, C., Kyrikou, S., Konidaris, G. E., Karkanas, P., Panagopoulou, E., Harvati, K., & Junginger, A. (2021). Lake-level changes and their paleo-climatic implications at the MIS12 Lower Paleolithic (Middle Pleistocene) site Marathousa 1, Greece. *Frontiers in Earth Science*, 9, 668445. Doi: 10.3389/feart.2021.668445.

Bookstein, F. L. (1991). *Morphometric Tools for Landmark Data: Geometry and Biology*. New York: Cambridge University Press.

Bosch, M. D., Mannino, M. A., Prendergast, A. L., O'Connell, T. C., Demarchi, B., Taylor, S. M., Niven, L., van der Plicht, J., & Hublin, J.-J. (2015). New chronology for Ksâr 'Akil (Lebanon) supports Levantine route of modern human dispersal into Europe. *Proceedings of the National Academy of Sciences*, *112* (25), 7683-7688. Doi: 10.1073/pnas.1501529112.

Bosman, A. M., Buck, L. T., Reyes-Centeno, H., Mirazón Lahr, M., Stringer, C., & Harvati, K. (2019). The Kabua 1 cranium: Virtual anatomical reconstructions. In: Y. Sahle, H. Reyes-Centeno, & C. Bentz (Eds.), *Modern Human Origins and Dispersal* (pp. 137-170). Tübingen: Kerns Verlag.

Bouchneb, L., & Crevecoeur, I. (2009). The inner ear of Nazlet Khater 2 (Upper Paleolithic, Egypt). *Journal of Human Evolution*, *56* (3), 257-262. Doi: 10.1016/j.jhevol.2008.12.003.

Bräuer, G. (2015). Origin of Modern Humans. In: W. Henke & I. Tattersall (Eds.), *Handbook of Paleoanthropology* (pp. 2299-2330). Heidelberg: Springer. Doi: 10.1007/978-3-642-39979-4_57.

Brito, P. H. (2005). The influence of Pleistocene glacial refugia on tawny owl genetic diversity and phylogeography in western Europe. *Molecular Ecology*, *14* (10), 3077-3094. Doi: 10.1111/j.1365-294X.2005.02663.x.

Bruner, E., & Pearson, O. (2012). Neurocranial evolution in modern humans: the case of Jebel Irhoud 1. *Anthropological Science*, 120927. Doi: 10.1537/ase.120927

Bruner, E., Ogihara, N., & Tanabe, H. C. (2018). *Digital Endocasts*. Tokyo: Springer Japan. Doi: 10.1007/978-4-431-56582-6.

Buck, L. T., & Stringer, C. B. (2015). A rich locality in South Kensington: the fossil hominin collection of the Natural History Museum, London. *Geological Journal*, 50 (3), 321-337. Doi: 10.1002/gj.2657.

Buzi, C., Profico, A., Di Vincenzo, F., Harvati, K., Melchionna, M., Raia, P., & Manzi, G. (2021). Retrodeformation of the Steinheim cranium: Insights into the evolution of Neanderthals. *Symmetry*, *13* (9), 1611. Doi: 10.3390/sym13091611.

Campbell, M. C., Hirbo, J. B., Townsend, J. P., & Tishkoff, S. A. (2014). The peopling of the African continent and the diaspora into the new world. *Current Opinion in Genetics and Development*, 29, 120-132. Doi: 10.1016/j.gde.2014.09.003.

Carotenuto, F., Tsikaridze, N., Rook, L., Lordkipanidze, D., Longo, L., Condemi, S., & Raia, P. (2016). Venturing out safely: The biogeography of Homo erectus dispersal out of Africa. *Journal of Human Evolution*, *95*, 1-12. Doi: 10.1016/j.jhevol.2016.02.005.

Caspari, R. (2006). The Krapina occipital bones. *Periodicum biologorum*, 108 (3), 299–307.

Clement, A. F., Hillwon, S. W., & Aiello, L. C. (2012). Tooth wear, Neanderthal facial morphology and the anterior dental loading hypothesis. *Journal of Human Evolution*, 62 (3), 367-376. Doi: 10.1016/j.jhevol.2011.11.014.

Couette, S., & White, J. (2010). 3D geometric morphometrics and missing-data. Can extant taxa give clues for the analysis of fossil primates?. *Comptes Rendus Palevol*, *9* (6-7), 423-433. Doi: 10.1016/j.crpv.2010.07.002.

Coutselinis, A., Dritsas, C. & Pitsios, T. K. (1991). Expertise médico-légale du crane pléistocène LAO1/S2 (Apidima II), Apidima, Laconie, Grèce. *L'Anthropologie*, 95, 401–408.

Dannemann, M., & Racimo, F. (2018). Something old, something borrowed: admixture and adaptation in human evolution. *Current Opinion in Genetics & Development*, 53, 1-8. Doi: 10.1016/j.gde.2018.05.009.

Davies, W. (2001). A very model of a modern human industry: New perspectives on the origins and spread of the Aurignacian in Europe. *Proceedings of the Prehistoric Society*, 67, 195–217. Doi: 10.1017/S0079497X00001663.

Davis, M. B., & Shaw, R. G. (2001). Range shifts and adaptive responses to Quaternary climate change. *Science*, *292* (5517), 673-679. Doi: 10.1126/science.292.5517.673.

Dean, D., Hublin, J.-J., Holloway, R., & Ziegler, R. (1998). On the phylogenetic position of the pre-Neandertal specimen from Reilingen, Germany. *Journal of Human Evolution*, 34, 485–508. Doi: 10.1006/jhev.1998.0214.

De Lumley, M. A., Guipert, G., de Lumley, H., Protopapa, N., & Pitsios, T. (2020). Apidima 1 and Apidima 2: Two anteneandertal skulls in the Peloponnese, Greece. *L'Anthropologie*, *124* (1), 102743. Doi: 10.1016/j.anthro.2019.102743.

Dennell, R. W., Martinón-Torres, M. & Bermúdez de Castro, J. M. (2011). Hominin variability, climatic instability and population demography in Middle Pleistocene Europe. *Quatenary Science Rev*iew, 30, 1511–1524. Doi: 10.1016/j.quascirev.2009.11.027.

Di Vincenzo, F., Profico, A., Bernardini, F., Cerroni, V., Dreossi, D., Schlager, S., Zaio, P., Benazzi, S., Biddittu, I., Rubini, M., Tuniz, C., & Manzi, G. (2017). Digital reconstruction of the Ceprano calvarium (Italy), and implications for its interpretation. *Scientific Reports*, *7* (1), 1-11. Doi: 10.1038/s41598-017-14437-2.

Durvasula, A., & Sankararaman, S. (2020). Recovering signals of ghost archaic introgression in African populations. *Science Advances*, 6 (7), eaax5097. Doi: 10.1126/sciadv.aax5097.

Endicott, P., Ho, S. Y. W., & Stringer, C. B. (2010). Using genetic evidence to evaluate four palaeoanthropological hypotheses for the timing of Neanderthal and modern human origins. *Journal of Human Evolution*, 59 (1), 87-95. Doi: 10.1016/j.jhevol.2010.04.005.

Ennouchi E. (1962). Un neandertalien: l'homme du Jebel Irhoud (Maroc) *L'Anthropologie*, 66: 279–299.

Ferembach, D. (1976). Les restes humains de la Grotte de Dar-es-Soltane II (Maroc). Campagne 1975. *Bulletines et Mémoires de*

la Société d'Anthropologie de Paris, XIII, 183-193. Doi: 10.3406/bmsap.1976.1849.

Fewlass, H., Talamo, S., Wacker, L., Kromer, B., Tuna, T., Fagault, Y., Bard, E., McPherron, S. P., Aldeias, V., Maria, R., Martisius, N. L., Paskulin, L., Rezek, Z., Sinet-Mathiot, V., Sirakova, S., Smith, G., M., Spasov, R., Welker, F., Sirakov, N., Tsanova, T., & Hublin, J.-J. (2020). A 14C chronology for the Middle to Upper Palaeolithic transition at Bacho Kiro cave, Bulgaria. *Nature Ecology & Evolution*, *4* (6), 794-801. Doi: 10.1038/s41559-020-1136-3.

Freidline, S. E., Gunz, P., Harvati, K., & Hublin, J.-J. (2012). Middle Pleistocene human facial morphology in an evolutionary and developmental context. *Journal of Human Evolution*, 63 (5), 723-740. Doi: 10.1016/j.jhevol.2012.08.002.

Freidline, S. E., Schuh, A., Gunz, P., Alichane, H., Oujaa, A., El Hajaroui, M., & Hublin, J.-J. (2021). The undescribed juvenile maxilla from Grotte des Contrebandiers, Morocco – a study on Aterian facial growth. *PaleoAnthropology*, 2021:1, p. 180.

Fu, Q., Mittnik, A., Johnson, P. L., Bos, K., Lari, M., Bollongino, R., Sun, C., Giemsch, L., Schmitz, R., Burger, J., Ronchitelli, A. M., Martini, F., Cremonesi, R. G., Svoboda, J., Bauer, P., Caramelli, D., Castellano, S., Reich, D., Pääbo, S., & Krause, J. (2013). A revised timescale for human evolution based on ancient mitochondrial genomes. *Current Biology*, *23* (7), 553-559. Doi: 10.1016/j.cub.2013.02.044.

Fu, Q., Li, H., Moorjani, P., Jay, F., Slepchenko, S. M., Bondarev, A. A., Johnson, P. L. F., Aximu-Petri, A., Prüfer, K., de Filippo, C., Meyer, M., Zwyns, N., Salazar-García, D. C., Kuzmin, Y. V., Keates, S. G., Kosintsev, P. A., Razhev, D. I., Richards, M. P., Peristov, N. V., Lachmann, M., Douka, K., Higham, T. F. G., Slatkin, M., Hublin, J.-J., Riech, D., Kelso, J., Viola, T. B., & Pääbo, S. (2014). Genome sequence of a 45,000-year-old modern human from western Siberia. *Nature*, 514, 445–449. Doi: 10.1038/nature1381.

Fu, Q., Hajdinjak, M., Moldovan, O. T, Constantin, S., Mallick, S., Skoglund, P., Patterson, N., Rohland, N., Lazaridis, I., Nickel, B., Viola, B., Prüfer, K., Meyer, M., Kelso, J., Reich, D., & Pääbo, S. (2015). An early modern human from Romania with a recent Neanderthal ancestor. *Nature*, 524, 216–219. Doi: 10.1038/nature14558.

Galway-Witham, J., & Stringer, C. (2018). How did Homo sapiens evolve?. *Science*, *360* (6395), 1296- 1298. Doi: 10.1126/science.aat6659.

Galway-Witham, J., Cole, J., & Stringer, C. (2019). Aspects of human physical and behavioural evolution during the last 1

million years. *Journal of Quaternary Science*, 34 (6), 355-378. Doi: 10.1002/jqs.3137.

Giusti, D., Tourloukis, V., Konidaris, G. E., Thompson, N., Karkanas, P., Panagopoulou, E., & Harvati, K. (2018). Beyond maps: Patterns of formation processes at the Middle Pleistocene open-air site of Marathousa 1, Megalopolis Basin, Greece. *Quaternary International*, 497, 137–153. Doi: 10.1016/j.quaint.2018.01.041.

Gómez, A., & Lunt, D. H. (2007). Refugia within refugia: Patterns of phylogeographic concordance in the Iberian Peninsula. In: S. Weiss & N. Ferrand (Eds.), *Phylogeography of southern European Refugia* (pp. 155–188). Dodrecht: Springer. Doi: 10.1007/1-4020-4904-8_5.

Gould, S. J. (2007). *Eight little piggies: Reflections in natural history* (revised ed.; 1st ed. 1993). London (UK): Vintage.

Green, R. E., Krause, J., Briggs, A. W., Maricic, T., Stenzel, U., Kircher, M., Patterson, N., Li, H., Zhai, W., Fritz, M. H., Hansen, N. F., Durand, E. Y., Malaspinas, A.-S., Jensen, J. D., Marques-Bonet, T., Alkan, C., Prüfer, K., Meyer, M., Burbano, H. A., Good, J. M., Schultz, R., Aximu-Petri, A., Butthof, A., Höber, B., Höffner, B., Siegemund, M., Weihmann, A., Nusbaum, C., Lander, E. S., Russ, C., Novod, N., Affourtit, J., Egholm, M., Verna, C., Rudan, P., Brajkovic, D., Kucan, Ž., Gušic, I., Doronichev, V. B., Golovanova, L. V., Lalueza-Fox, C., de la Rasilla, M., Fortea, J., Rosas, A., Schmitz, R. W., Johnson, P. L. F., Eichler, E. E., Falush, D., Birney, E., Mullikin, J. C., Slatkin, M., Nielsen, R., Kelso, J., Lachmann, M., Reich, D., & Pääbo, S. (2010). A draft sequence of the Neandertal genome. *Science*, 328, 710–722. Doi: 10.1126/science.1188021.

Greenbaum, G., Friesem, D. E., Hovers, E., Feldman, M. W., & Kolodny, O. (2019). Was inter-population connectivity of Neanderthals and modern humans the driver of the Upper Paleolithic transition rather than its product?. *Quaternary Science Reviews*, *217*, 316-329. Doi: 10.1016/j.quascirev.2018.12.011.

Grine, F. E., Gunz, P., Betti-Nash, L., Neubauer, S., & Morris, A. G. (2010). Reconstruction of the late Pleistocene human skull from Hofmeyr, South Africa. *Journal of Human Evolution*, 59 (1), 1-15. Doi: 10.1016/j.jhevol.2010.02.007.

Grine, F. E. (2016). The Late Quaternary Hominins of Africa: The Skeletal Evidence from MIS 6-2. In: S. C. Jones & B. A. Stewart (Eds.), *Africa from MIS 6-2: Population Dynamics and Paleoenvironments* (pp. 323-381). Dordrecht: Springer. Doi: 10.1007/978-94-017-7520-5_17.

Gronau, I., Hubisz, M. J., Gulko, B., Danko, C. G., & Siepel, A. (2011). Bayesian inference of ancient human demography from individual genome sequences. *Nature Genetics*, 43, 1031-1034. Doi: 10.1038/ng.937.

Groucutt, H. S., Petraglia, M. D., Bailey, G., Scerri, E. M. L., Parton, A., Clark-Balzan, L., Jennings, R. P., Lewis, L., Blinkhorn, J., Drake, N. A., Breeze, P. S., Inglis, R. H., Devès, M. H., Meredith-Williams, M., Boivin, N., Thomas, M. G., & Scally, A. (2015). Rethinking the dispersal of Homo sapiens out of Africa. *Evolutionary Anthropology: Issues, News, and Reviews*, 24 (4), 149-164. Doi: 10.1002/evan.21455.

Groucutt, H. S., Scerri, E. M. L., Stringer, C., & Petraglia, M. D. (2017). Skhul lithic technology and the dispersal of Homo sapiens into Southwest Asia. *Quaternary International*, 515, 30-52. Doi: 10.1016/j.quaint.2017.12.027.

Groucutt, H. S., Grün, R., Zalmout, I. A. S., Drake, N. A., Armitage, S. J., Candy, I., Clark-Wilson, R., Louys, J., Breeze, P. S., Duval, M., Buck, L. T., Kivell, T. L., Pomeroy, E., Stephens, N. B., Stock, J. T., Stewart, M., Price, G. J., Kinsley, L., Sung, W. W., Alsharekh, A., Al-Omari, A., Zahir, M., Memesh, A. M., Abdulshakoor, A. J., Al-Masari, A. M., Bahameem, A. A., Al Murayyi, K. M. S., Zahrani, B., Scerri, E. L. M., & Petraglia, M. D. (2018). *Homo sapiens* in Arabia by 85,000 years ago. *Nature Ecology & Evolution*, 2, 800–809. Doi: 10.1038/s41559-018-0518-2.

Grove, M., Lamb, H., Roberts, H., Davies, S., Marshall, M., Bates, R., & Huws, D. (2015). Climatic variability, plasticity, and dispersal: A case study from Lake Tana, Ethiopia. *Journal of Human Evolution*, *87*, 32-47. Doi: 10.1016/j.jhevol.2015.07.007.

Grün, R. (1996). A re-analysis of electron spin resonance dating results associated with the Petralona hominid. *Journal of Human Evolution*, *30* (3), 227-241. Doi: 10.1006/jhev.1996.0020.

Grün, R., Stringer, C., McDermott, F., Nathan, R., Porat, N., Robertson, S., Taylor, L., Mortimer, G., Eggins, S., & McCulloch, M. (2005). U-series and ESR analyses of bones and teeth relating to the human burials from Skhul. *Journal of Human Evolution*, 49 (3), 316–334. Doi: 10.1016/j.jhevol.2005.04.006.

Grün, R. (2006). Direct dating of human fossils. *American Journal of Physical Anthropology*, *131* (S43), 2-48. Doi: 10.1002/ajpa.20516.

Grün, R., Eggins, S., Kinsley, L., Moseley, H., & Sambridge, M. (2014). Laser ablation U-series analysis of fossil bones and

teeth. *Palaeogeography, Palaeoclimatology, Palaeoecology*, *416*, 150-167. Doi: 10.1016/j.palaeo.2014.07.023.

Gunz, P., Mitteroecker, P., Bookstein, F., & Weber, G. (2004). Computer aided reconstruction of human crania. In: K. Fischer-Ausserer, W. Börner & M. Goriany (Eds.), *Enter the Past: The E-way into the Four Dimensions of Cultural Heritage* (pp. 92-95). Oxford: BAR Publishing. Doi: 10.15496/publikation-3648.

Gunz, P., Mitteroecker, P., & Bookstein, F. (2005). Semilandmarks in Three Dimensions. In: D. E. Slice (Eds.), *Modern Morphometrics in Physical Anthropology* (pp. 73-98). Boston: Springer.

Gunz, P., & Harvati, K. (2007). The Neanderthal "chignon": variation, integration, and homology. *Journal of Human Evolution*, 52 (3), 262-274. Doi: 10.1016/j.jhevol.2006.08.010.

Gunz, P., Mitteroecker, P., Neubauer, S., Weber, G. W., & Bookstein, F. L. (2009). Principles for the virtual reconstruction of hominin crania. *Journal of Human Evolution*, *57* (1), 48-62. Doi: 10.1016/j.jhevol.2009.04.004.

Gunz, P., & Harvati, K. (2011). Integration and Homology of "Chignon" and "Hemibun" Morphology. In: S. Condemi & G. C. Weniger (Eds.), *Continuity and Discontinuity in the Peopling of Europe* (pp. 193-202). Springer, Dordrecht. Doi: 10.1007/978-94-007-0492-3_17.

Gunz, P., Neubauer, S., Golovanova, L., Doronichev, V., Maureille, B., & Hublin, J.-J. (2012). A uniquely modern human pattern of endocranial development. Insights from a new cranial reconstruction of the Neandertal newborn from Mezmaiskaya. *Journal of Human Evolution*, *62* (2), 300-313. Doi: 10.1016/j.jhevol.2011.11.013.

Gunz, P., & Mitteroecker, P. (2013). Semilandmarks: a method for quantifying curves and surfaces. *Hystrix, the Italian Journal of Mammalogy*, *24* (1), 103-109. Doi: 10.4404/hystrix-24.1-6292.

Gunz, P., Tilot, A. K., Wittfeld, K., Teumer, A., Shapland, C. Y., Van Erp, T. G., Dannemann, M., Vernot, B., Neubauer, S., Guadalupe, T., Fernández, G., Brunner, H. G., Enard, W., Fallon, J., Hosten, N., Völker, U., Profico, A., Di Vincenzo, F., Manzi, G., Kelso, J., St. Pourcain, B., Hublin, J.-J., Franke, B., Pääbo, S., Macciardi, F., Grabe, H. J., & Fisher, S. E. (2019). Neandertal introgression sheds light on modern human endocranial globularity. *Current Biology*, *29* (1), 120-127. Doi: 10.1016/j.cub.2018.10.065.

Haile-Selassie, Y., Melillo, S. M., Vazzana, A., Benazzi, S., & Ryan, T. M. (2019). A 3.8-million-year-old hominin cranium from

Woranso-Mille, Ethiopia. *Nature*, 573, 214–219. Doi: 10.1038/s41586-019-1513-8.

Hajdinjak, M., Mafessoni, F., Skov, L., Vernot, B., Hübner, A., Fu, Q., Essel, E., Nagel, S., Nickel, B., Richter, J., Moldovan, O. T., Constantin, S., Endarova, E., Zahariev, N., Spasov, R., Welker, F., Smith, G. M., Sinet-Mathiot, V., Paskulin, L., Fewlass, H., Talamo, S., Rezek, Z., Sirakova, S., Sirakov, N., McPherron, S. P., Tsanova, T., Hublin, J.-J., Peter, B. M., Meyer, M., Skoglund, P., Kelso, J., & Pääbo, S. (2021). Initial Upper Palaeolithic humans in Europe had recent Neanderthal ancestry. *Nature*, *592* (7853), 253-257. Doi: 10.1038/s41586-021-03335-3.

Hammer, M. F., Woerner, A. E., Mendez, F. L., Watkins, J. C., & Wall, J. D. (2011). Genetic evidence for archaic admixture in Africa. *Proceedings of the National Academy of Sciences*, 108 (37), 15123-15128. Doi: 10.1073/pnas.1109300108.

Harvati, K. (2003). The Neanderthal taxonomic position: models of intra-and inter-specific craniofacial variation. *Journal of Human Evolution*, 44 (1), 107-132. Doi: 10.1016/S0047-2484(02)00208-7.

Harvati, K., Panagopoulou, E., & Karkanas, P. (2003). First Neanderthal remains from Greece: the evidence from Lakonis. *Journal of Human Evolution*, 45, 465–473. Doi: 10.1016/j.jhevol.2003.09.005.

Harvati, K. (2009). Into Eurasia: a geometric morphometric re-assessment of the Upper Cave (Zhoukoudian) specimens. *Journal of Human Evolution*, *57* (6), 751-762. Doi: 10.1016/j.jhevol.2009.07.008.

Harvati, K., Panagopoulou, E., & Runnels, C. (2009). The paleoanthropology of Greece. *Evolutionary Anthropology: Issues, News, and Reviews*, 18 (4), 131-143. Doi: 10.1002/evan.20219.

Harvati, K., Hublin, J.-J., & Gunz, P. (2010). Evolution of middle-late Pleistocene human cranio-facial form: a 3-D approach. *Journal of Human Evolution*, 59 (5), 445-464. Doi: 10.1016/j.jhevol.2010.06.005.

Harvati, K., Stringer, C. & Karkanas, P. (2011). Multivariate analysis and classification of the Apidima 2 cranium from Mani, Southern Greece. *Journal of Human Evolution*, 60, 246–250. Doi: 10.1016/j.jhevol.2010.09.008.

Harvati, K., & Hublin, J.-J. (2012). Morphological continuity of the face in the Late Middle and Late Pleistocene Hominins from Northwestern Africa: a 3D geometric morphometric analysis. In: J.-J. Hublin, & S. P. McPherron (Eds.), *Modern Origins: A North African Perspective* (pp. 179-188). Vertebrate

Paleobiology and Paleoanthropology. Berlin, Germany: Springer. Doi: 10.1007/978-94-007-2929-2_12.

Harvati, K., & Tourloukis, V. (2013). Human evolution in the Southern Balkans. *Evolutionary Anthropology*, 22 (2), 43-45. Doi: 10.1002/evan.21342.

Harvati, K., Darlas, A., Bailey, S. E., Rein, T. R., El Zaatari, S., Fiorenza, L., Kullmer, O., & Psathi, E. (2013). New Neanderthal remains from Mani peninsula, Southern Greece: the Kalamakia Middle Paleolithic cave site. *Journal of Human Evolution*, 64, 486–499. Doi: 10.1016/j.jhevol.2013.02.002.

Harvati, K. (2015). Neanderthals and Their Contemporaries. In: W. Henke & I. Tattersall (Eds.), *Handbook of Paleoanthropolog* (pp. 2243-2280). Berlin, Germany: Springer. Doi: 10.1007/978-3-642-39979-4_56

Harvati, K., Bauer, C. C., Grine, F. E., Benazzi, S., Ackermann, R. R., van Niekerk, K. L., & Henshilwood, C. S. (2015). A human deciduous molar from the Middle Stone Age (Howiesons Poort) of Klipdrift Shelter, South Africa. *Journal of Human Evolution*, 82, 190-196. Doi: 10.1016/j.jhevol.2015.03.001.

Harvati, K. (2016). Paleoanthropology in Greece: recent findings and interpretations. In: K. Harvati & M. Roksandic (Eds.), *Paleoanthropology of the Balkans and Anatolia: Human Evolution and its Context* (pp. 3-14). Dordrecht: Springer Netherlands. Doi: 10.1007/978-94-024-0874-4_1.

Harvati, K., & Roksandic, M. (2016a). The Human Fossil Record from Romania: Early Upper Paleolithic European Mandibles and Neanderthal Admixture. In: K. Harvati & M. Roksandic (Eds.), *Paleoanthropology of the Balkans and Anatolia: Human Evolution and its Context* (pp. 51-68). Dordrecht: Springer Netherlands. Doi: 10.1007/978-94-024-0874-4_4.

Harvati, K., & Roksandic, M. (2016b). *Paleoanthropology of the Balkans and Anatolia: Human Evolution and its Context*. Dordrecht: Springer Netherlands.

Harvati, K., Röding, C., Bosman, A. M., Karakostis, F. A., Grün, R., Stringer, C., Karkanas, P., Thompson, N. C., Koutoulidis, V., Moulopoulos, L. A., Gorgoulis, V., & Kouloukoussa, M. (2020). New 3-D geometric morphometric and dating analyses of the Apidima fossil crania support early dispersal of Homo sapiens out of Africa. *American Journal of Physical Anthropology*, 171 (S69), 116.

Harvati, K. (2022)**.** The hominin fossil record from Greece. In: E. Vlachos (Eds.), *The Fossil Vertebrates of Greece Vol. 1 – Basal vertebrates, basal tetrapods, afrotherians, glires, and primates* (pp. 669-688). Cham: Springer – Nature Publishing Group. Doi: 10.1007/978-3-030-68398-6_19.

Hassett, B. R., & Lewis-Bale, T. (2017). Comparison of 3D Landmark and 3D Dense Cloud Approaches to Hominin Mandible Morphometrics using Structure-Form-Motion. *Archaeometry*, 59 (1), 191-203. Doi: 10.1111/arcm.12229.

Henke W. (2015) Historical Overview of Paleoanthropological Research. In: W. Henke & I. Tattersall (Eds.), *Handbook of Paleoanthropology* (pp. 3-95). Berlin, Heidelberg: Springer. Doi. 10.1007/978-3-642-39979-4_1.

Henn, B. M., Steele, T. E., & Weaver, T. D. (2018). Clarifying distinct models of modern human origins in Africa. *Current Opinion in Genetics & Development*, 53, 148-156. Doi: 10.1016/j.gde.2018.10.003.

Hershkovitz, I., Smith, P., Sarig, R., Quam, R., Rodríguez, L., García, R., Arsuaga, J. L., Barkai, R., & Gopher, A. (2011). Middle pleistocene dental remains from Qesem Cave (Israel). *American Journal of Physical Anthropology*, *144* (4), 575-592. Doi: 10.1002/ajpa.21446.

Hershkovitz I, Marder O, Ayalon A, Bar-Matthews M, Yasur G, Boaretto E, Caracuta, V., Alex, B., Frumkin, A., Goder-Goldberger, M., Gunz, P., Holloway, R. L., Latimer, B., Lavi, R., Matthews, A., Slon, V., Bar-Yosef Mayer, D., Berna, F., Bar-Oz, G., Yeshurun, R., May, H., Hans, M. G., Wever, G. W., & Barzilai, O. (2015). Levantine cranium from Manot Cave (Israel) foreshadows the first European modern humans. *Nature*, 520 (7546), 216–9. Doi: 10.1038/nature14134.

Hershkovitz, I., Weber, G. W., Quam, R., Duval, M., Grün, R., Kinsley, L., Ayalon, A., Bar-Matthews, M., Valladas, H., Mercier, N., Arsuaga, J. L., Martinón-Torres, M., Bermúdez de Castro, J. M., Fornai, C., Martín-Francés, L., Sarig, R., May, H., Krenn, V. A., Slon, V., Rodriguez, L., Garcia, R., Lorenzo, C., Carretero, J. M., Frumkin, A., Shahack-Gross, R., Bar-Yosef Mayer, D. E., Cui, Y., Wu, X., Peled, N., Groman-Yaroslavski, I., Weissbrod, L., Yeshurun, R., Tsatskin, A., Zaidner, Y., & Weinstein-Evron, M. (2018a). The earliest modern humans outside Africa. *Science*, 359, 456-459. Doi: 10.1126/science.aap8369.

Hershkovitz, I., Duval, M., Grün, R., Mercier, N., Valladas, H., Ayalon, A., Bar-Matthews, M., Weber, G. W., Quam, R., Zaidner, Y., & Weinstien-Evron, M. (2018b). Response to Comment on „The earliest modernn humans outside Africa“. *Science*, 362 (6413), eaat8964. Doi: 10.1126/science.aat8964.

Hershkovitz, I., May, H., Sarig, R., Pokhojaev, A., Grimaud-Hervé, D., Bruner, E., Fornai, C., Quam, R., Arsuaga, J. L., Krenn, V. A., Matinón-Torres, M., Bermúdez de Castro, J. M., Martín-Francés, L., Slon, V., Albessard-Ball, L., Vialet, A., Schüler, T.,

Manzi, G., Profico, A., Di Vincenzo, F., Weber, G. W., & Zaidner, Y. (2021). A Middle Pleistocene Homo from Nesher Ramla, Israel. *Science*, 372 (6549), 1424-1428. Doi: 10.1126/science.abh3169.

Hewitt, G. M. (1999). Post-glacial re-colonization of European biota. *Biological Journal of the Linnean Society*, 68 (1-2), 87-112. Doi: 10.1111/j.1095-8312.1999.tb01160.x.

Hewitt, G. M. (2011). Mediterranean peninsulas – the evolution of hotspots. In: F. E. Zachos & J. C. Habel (Eds.), *Biodiversity Hotspots* (pp. 123-147). Amsterdam: Springer. Doi: 10.1007/978-3-642-20992-5_7.

Heydari-Guran, S., Benazzi, S., Talamo, S., Ghasidian, E., Hariri, N., Oxilia, G., Asiabani, S., Azizi, F., Naderi, R., Safaierad, R., Hublin, J.-J., Foley, R. A., & Mirazón Lahr, M. (2021). The discovery of an in situ Neanderthal remain in the Bawa Yawan Rockshelter, West-Central Zagros Mountains, Kermanshah. *PloS one*, *16* (8), e0253708. Doi: 10.1371/journal.pone.0253708.

Higham, T., Compton, T., Stringer, C., Jacobi, R., Shapiro, B., Trinkaus, E., Chandler, B., Gröning, F., Collins, C., Hillson, S., O'Higgins, P., FitzGerald, C., & Fagan, M. (2011). The earliest evidence for anatomically modern humans in northwestern Europe. *Nature*, *479* (7374), 521-524. Doi: 10.1038/nature10484.

Hoffecker, J. F. (2009). The spread of modern humans in Europe. *Proceedings of the National Academy of Sciences*, 106 (38), 16040–16045. Doi: 10.1073/pnas.0903446106.

Hölzchen, E., Hertler, C., Timm, I., & Lorig, F. (2016). Evaluation of Out of Africa hypotheses by means of agent-based modeling. *Quaternary International*, *413*, 78-90. Doi: 10.1016/j.quaint.2015.11.022.

Hublin, J.-J., & Tillier, A. M. (1981). The Mousterian juvenile mandible from Irhoud (Morocco): a phylogenetic interpretation. In: C. B. Stringer (Eds.), *Aspects of Human Evolution* (pp. 167–185). London, UK: Taylor and Francis.

Hublin, J.-J., & Tillier, A.-M. (1988). Les enfants moustériens de Jebel Irhoud (Maroc), comparaison avec les Néandertaliens juveniles d'Europe. *Bulletins es Mémoires de la Société d'anthropologie de Paris*, 5 (4), 237-246. Doi: 10.3406/bmsap.1988.1680.

Hublin, J.-J. (1996). The first Europeans. *Archaeology*, 49, 36-44.

Hublin, J.-J. (1998). Climatic changes, paleogeography and the evolution of Neanderthals. In: T. Akazawa, K. Aoki & O. Bar-Yosef (Eds.), *Neanderthals and Modern Humans in Western*

Asia (pp. 295-310). Boston, MA: Springer. Doi: 10.1007/0-306-47153-1_18.

Hublin, J.-J. (2009). The origin of Neandertals. *Proceedings of the National Academy of Sciences*, 106, 16022–16027. Doi: 10.1073/pnas.0904119106.

Hublin, J.-J. (2012). The earliest modern human colonization of Europe. *Proceedings of the National Academy of Sciences*, 109 (34),13471–13472. Doi: 10.1073/pnas.1211082109.

Hublin, J.-J., Verna, C., Bailey, S., Smith, T., Olejniczak, A., Sbihi-Alaoui, F. Z., & Zouak, M. (2012). Dental Evidence from the Aterian Human Populations of Morocco. In: J.-J. Hublin, & S. P. McPherron (Eds.), *Modern Origins: A North African Perspective* (pp. 189-204). Vertebrate Paleobiology and Paleoanthropology. Berlin, Germany: Springer. Doi: 10.1007/978-94-007-2929-2_13.

Hublin, J.-J. (2015). The modern human colonization of western Eurasia: When and where?. *Quaternary Science Reviews*, 118, 194–210. Doi: 10.1016/j.quascirev.2014.08.011.

Hublin, J.-J. (2017). The last Neanderthal. *Proceedings of the National Academy of Sciences*, *114* (40), 10520-10522. Doi: 10.1073/pnas.1714533114.

Hublin, J.-J., Ben-Ncer, A., Bailey, S. E., Freidline, S. E., Neubauer, S., Skinner, M. M., Bergmann, I., Le Cabec, A., Benazzi, S., Harvati, K., & Gunz, P. (2017). New fossils from Jebel Irhoud, Morocco, and the pan-African origin of Homo sapiens. *Nature*, 546, 289-292. Doi: 10.1038/nature22336.

Hublin, J.-J., Sirakov, N., Aldeias, V., Bailey, S., Bard, E., Delvigne, V., Endarova, E., Fagault, Y., Fewlass, H., Hajdinjak, M., Kromer, B., Krumov, I., Marreiros, J., Martisius, N. L., Paskulin, L., Sinet.Mathiot, V., Meyer, M., Pääbo, S., Popov, V., Rezek, Z., Sirakova, S., Skinner, M. M., Smith, G. M., Spasov, R., Talamo, S., Tuna, T., Wacker, L., Welker, F., Wilcke, A., Zahariev, N., McPherron, S. P., & Tsanova, T. (2020). Initial Upper Palaeolithic *Homo sapiens* from Bacho Kiro Cave, Bulgaria. *Nature*, 581, 299–302. Doi: 10.1038/s41586-020-2259-z.

Jacobs, Z., Li, B., Karkanas, P., Tourloukis, V., Thompson, N., Panagopoulou, E., & Harvati, K. (2018). Optical dating of K-feldspar grains from Middle Pleistocene lacustrine sediment at Marathousa 1 (Greece). *Quaternary International*, 497, 170–177. Doi: 10.1016/j.quaint.2018.06.029.

Jeong, C., Balanovsky, O., Lukianova, E., Kahbatkyzy, N., Flegontov, P., Zaporozhchenko, V., Immel, A., Wang, C.-C., Ixan, O., Khussainova, E., Bekmanov, B., Zaibert, V., Lavryashina, M., Pocheshkova, E., Yusupov, Y., Agdzhoyan, A.,

Koshel, S., Bukin, A., Nymadawa, P., Turdikulova, S., Dalimova, D., Churnosov, M., Skhalyakho, R., Daragan, D., Bogunov, Y., Bogunova, A., Shtrunov, A., Dubova, N., Zhabagin, M., Yepiskoposyan, L., Churakov, C., Pislegin, N., Damba, L., Saroyants, L., Dibirova, K., Atramentova, L., Utevska, O., Idrisov, E., Kamenshchikova, E., Evseeva, I., Metspalu, M., Outram, A. K., Robbeets, M., Djansugurova, L., Balanovska, E., Schiffels, S., Haak, W., Reich, D., & Krause, J. (2019.) The genetic history of admixture across inner Eurasia. *Nature Ecology & Evolution*, 3 (6), 966–976. Doi: 10.1038/s41559-019-0878-2.

Jiménez-Arenas, J. M., Bienvenu, T., Toro-Moyano, I., de León, M. S. P., & Zollikofer, C. P. (2019). Virtual reconstruction and re-evaluation of the Neanderthal frontal bone from Carigüela Cave (Granada, Spain). *Quaternary Science Reviews*, 217, 89-97. Doi: 10.1016/j.quascirev.2019.03.014.

Jones, E. L. (2021). What is a refugium? Questions for the Middle–Upper Palaeolithic transition in peninsular southern Europe. *Journal of Quaternary Science*, early view online record. Doi: 10.1002/jqs.327.

Karakostis, F. A., Hotz, G., Tourloukis, V., & Harvati, K. (2018). Evidence for precision grasping in Neandertal daily activities. *Science Advances*, 4 (9), eaat2369. Doi: 10.1126/sciadv.aat2369.

Kissel, M., & Fuentes, A. (2021). The ripples of modernity: How we can extend paleoanthropology with the extended evolutionary synthesis. *Evolutionary Anthropology: Issues, News, and Reviews*, 30 (1), 84-98. Doi: 10.1002/evan.21883.

Klein, R. G. (2009). *The Human Career: Human Biological and Cultural Origins*. Chicago: University of Chicago Press.

Koenigswald, W. V., & Heinrich, W. D. (2007). Biostratigraphische Begriffe aus der Säugetierpaläontologie für das Pliozän und Pleistozän Deutschlands. *Eiszeitalter und Gegenwart Quaternary Science Journal*, 56, 96–115.

Konidaris, G. E., Athanassiou, A., Tourloukis, V., Thompson, N., Giusti, D., Panagopoulou, E., & Harvati, K. (2018). The skeleton of a straight-tusked elephant (Palaeoloxodon antiquus) and other large mammals from the Middle Pleistocene butchering locality Marathousa 1 (Megalopolis Basin, Greece): Preliminary results. *Quaternary International*, 497, 65–84. Doi: 10.1016/j.quaint.2017.12.001.

Konidaris, G. E., Tourloukis, V., Athanassiou, A., Giusti, D., Thompson, N., Panagopoulou, E., Karkanas, P., & Harvati, K. (2019). Marathousa 2: A new Middle Pleistocene locality in

Megalopolis Basin (Greece) with evidence of human modifications on faunal remains. *PESHE*, 8, 82.

Kormasopoulou-Kagalou, L., Protonotariou-Deilaki, E., & Pitsios, T. K. (1995). Paleolithic skull burials at the cave of Apidima. *Acta Anthropologica,* 1, 119–124.

Kuhlwilm, M., Gronau, I., Hubisz, M. J., de Filippo, C., Prado-Martinez, J., Kircher, M., Fu, Q., Burbano, H. A., Lalueza-Fox, C., de la Rasilla, M., Rosas, A., Rudan, P., Brajkovic, D., Kucan, Ž., Gušic, I., Marques-Bonet, T., Andrés, A. M., Viola, B., Pääbo, S., Meyer, M., Siepel, A., & Castellano, S. (2016). Ancient gene flow from early modern humans into Eastern Neanderthals. *Nature*, 530, 429–433. Doi: 10.1038/nature16544.

Lazaridis, I., Nadel, D., Rollefson G., Merrett, D. C., Rohland, N., Mallick, S., Fernandes, D., Novak, M., Gamarra, B., Sirak, K., Connell, S., Stewardson, K., Harney, E., Fu, Q., Gonzalez-Fortes, G., Jones, E. R., Roodenberg, S. A., Mizrahi, A.-S., Meiklejohn, C., Gerritsen, F., Bejenaru, L., Blüher, M., Campbell, A., Cavalleri, G., Comas, D., Froguel, P., Gilbert, E., Kerr, S. M., Kovacs, P., Krause, J., McGettigan, D., Merrigan, M., Merriwether, D. A., O'Reilly, S., Richards, M. B., Semino, O., Shamoon-Pour, M., Stefanescu, G., Stumvoll, M., Tönjey, A., Torroni, A., Wilson, J. F., Yengo, L., Hovhannisyan, N. A., Patterson, N., Pinhasi, R., & Reich, D. (2016). Genomic insights into the origin of farming in the ancient Near East. *Nature*, 536, 419-424. Doi: 10.1038/nature19310.

Lehmann, E. L. (1986). *Testing Statistical Hypotheses* (2nd ed.). New Jersey: Wiley-Blackwell.

Lieberman, D. E., McBratney, B. M., & Krovitz, G. (2002). The evolution and development of cranial form in Homo sapiens. *Proceedings of the National Academy of Sciences*, 99 (3), 1134-1139. Doi: 10.1073/pnas.022440799.

Lipson, M., Cheronet, O., Mallick, S., Rohland, N., Oxenham, M., Pietrusewsky, M., Pryce, T. O., Willis, A., Matsumura, H., Buckley, H., Domett, K., Nguyen, G. H., Trinh, H. H., Kyaw, A. A., Win, T. T., Pradier, B., Broomandkhoshbacht, N., Candilio, F., Changmai, P., Fernandes, D., Ferry, M., Gamarra, B., Harney, E., Kampuansai, J., Kutanan, W., Michel, M., Novak, M., Oppenheimer, J., Sirak, K., Stewardson, K., Zhang, Z., Flegontov, P., Pinhasi, R., & Reich, D. (2018). Ancient genomes document multiple waves of migration in Southeast Asian prehistory. *Science*, 361 (6397), 92–95. Doi: 10.1126/science.aat3188.

Lockey, A.-L., Karakostis, A. F., Harvati, K., & El Zaatari, S. (2022). *A comprehensive analysis of dental metric variation in Eurasian hominins*. Manuscript in preparation.

Löhnert, E., & Nowack, H. (1965). Die Braunkohlenlagerstätte von Khoremi im Becken von Megalopolis/Peloponnes. *Geologisches Jahrbuch*, 82, 847–868.

Lorente-Galdos, B., Lao, O., Serra-Vidal, G., Santpere, g., Kuderna, L. F. K., Arauna, L. R., Fadhlaoudi-Zid, K., Pimenoff, V. N., Soodyall, H., Zalloua, P., Marques-Bonet, T., & Comas, D. (2019). Whole-genome sequence analysis of a Pan African set of samples reveals archaic gene flow from an extinct basal population of modern humans into sub-Saharan populations. *Genome Biology*, 20 (1), 77. Doi: 10.1186/s13059-019-1684-5.

Manolis, S. K. (1996). The Hellenic late Pleistocene fossils. *Anthropologie,* 34 (2), 89-97.

Manzi, G., Bruner, E., Caprasecca, S., Gualdi, G., & Passarello, P. (2001). CT-scanning and virtual reproduction of the Saccopastore Neandertal crania. *Rivista di Antropologia*, *79*, 61-72.

Mardia, K. V., Bookstein, F. L., & Moreton, I. J. (2000). Statistical Assessment of Bilateral Symmetry of Shapes. *Biometrika*, 87 (2), 285-300. Doi: 10.1093/biomet/87.2.285.

Marinos, G. (1975). Über einen menschlichen Zahn unter den Säugetier-Resten biharischen Alters von Megalopolis. *Annales Géologiques des Pays Helléniques*, 27, 64–65.

Marom, A., & Rak, Y. (2021). Comment on "A Middle Pleistocene Homo from Nesher Ramla, Israel". *Science*, 374 (6572), eabl4336. Doi: 10.1126/science.abl4336.

Marra, F., Ceruleo, P., Pandolfi, L., Petronio, C., Rolfo, M. F., & Salari, L. (2017). The aggradational successions of the Aniene River Valley in Rome: age constraints to early Neanderthal presence in Europe. *PloS one*, 12 (1), e0170434. Doi: 10.1371/journal.pone.0170434.

May, H., Sarig, R., Pokhojaev, A., Fornai, C., Martinón-Torres, M., Bermúdez de Castro, J. M., Weber, G. W., Zaidner, Y., & Hershkovitz, I. (2021). Response to Comment on "A Middle Pleistocene Homo from Nesher Ramla, Israel". *Science*, 374 (6572), eabl5789. Doi: 10.1126/science.abl5789.

McBurney, C. B. M., Trevor, J. C., & Wells, L. H. (1953). The Haua Fteah Fossil Jaw. *The Journal of the Royal Anthropological Institute of Great Britain and Ireland*, 83 (1), 71-85.

Médail, F., & Diadema, K. (2009). Glacial refugia influence plant diversity patterns in the Mediterranean Basin. *Journal of*

Biogeography, 36 (7), 1333-1345. Doi: 10.1111/j.1365-2699.2008.02051.x.

Melentis, J. K. (1961). Die Dentition der Pleistozänen Proboscidier des Beckens von Megalopolis im Peloponnes (Griechenland). *Annales Géologiques des Pays Helléniques*, 12, 153–262.

Mellars, P. (2006a). Why did modern human populations disperse from Africa ca. 60,000 years ago? A new model. *Proceedings of the National Academy of Sciences*, 103, 9381–9386. Doi: 10.1073/pnas.0510792103.

Mellars P (2006b) Archeology and the dispersal of modern humans in Europe: Deconstructing the "Aurignacian". *Evolutionary Anthropology; Issues, News and Reviews*, 15 (5), 167–182. Doi: 10.1002/evan.20103.

Mendez, F. L., Poznik, G. D., Castellano, S., & Bustamante, C. D. (2016). The divergence of Neandertal and modern human Y chromosomes. *The American Journal of Human Genetics*, *98* (4), 728-734. Doi: 10.1016/j.ajhg.2016.02.023.

Mercier, N., Valladas, H., Bar-Yosef, O., Vandermeersch, B., Stringer, C., & Joron, J.-L. (1993). Thermoluminescence date for the Mousterian burial site of Es-Skhul, Mt. Carmel. *Journal of Archaeological Sciences*, 20, 169–174. Doi: 10.1006/jasc.1993.1012.

Meyer, M., Arsuaga, J.-L., de Filippo, C., Nagel, S., Aximu-Petri, A., Nickel, B., Martínez, I., Gracia, A., Bermúdez de Castro, J. M., Carbonell, E., Viola, B., Kelso, J., Prüfer, K., & Pääbo, S. (2016). Nuclear DNA sequences from the Middle Pleistocene Sima de los Huesos hominins. *Nature*, 531, 504–507. Doi:10.1038/nature17405.

Michailidis, D., Konidaris, G. E., Athanassiou, A., Panagopoulou, E., & Harvati, K. (2018). The ornithological remains from Marathousa 1 (middle Pleistocene; Megalopolis basin, Greece). *Quaternary International*, 497, 85-94. Doi: 10.1016/j.quaint.2018.06.045.

Michaux, J. R., Magnanou, E., Paradis, E., Nieberding, C., & Libois, R. (2003). Mitochondrial phylogeography of the wood mouse (*Apodemus sylvaticus*) in the western Palaearctic region. *Molecular Ecology*, 12, 685–697. Doi: 10.1046/j.1365-294X.2003.01752.x.

Minugh-Purvis, N. (1993). Reexamination of the Immature Hominid Maxilla from Tangier, Morocco. American *Journal of Physical Anthropology*, 92 (4), 449-461. Doi: 10.1002/ajpa.1330920404.

Mirazón Lahr, M. (2016). The shaping of human diversity: filters, boundaries and transitions. *Philosophical Transactions of the*

Royal Society of London. Series B: Biological Sciences, 371 (1698), 20150241. Doi: 10.1098/rstb.2015.0241.

Mitteroecker, P., Gunz, P., Bernhard, M., Schaefer, K., & Bookstein, F. L. (2004). Comparison of cranial ontogenetic trajectories among great apes and humans. *Journal of Human Evolution*, 46 (6), 679-698. Doi: 10.1016/j.jhevol.2004.03.006.

Mitteroecker, P., & Gunz, P. (2009). Advances in Geometric Morphometrics. *Evolutionary Biology*, 36 (2), 235-247. Doi: 10.1007/s11692-009-9055-x.

Mitteroecker, P., & Bookstein, F. (2011). Linear discrimination, ordination, and the visualization of selection gradients in modern morphometrics. *Evolutionary Biology*, 38 (1), 100-114. Doi: 10.1007/s11692-011-9109-8.

Mori, T., Profico, A., Reyes-Centeno, H., & Harvati, K. (2020). Frontal bone virtual reconstruction and geometric morphometric analysis of the mid-Pleistocene hominin KNM-OG 45500 (Olorgesailie, Kenya). *Journal of Anthropological Sciences*, *98*, 49-72. Doi: 10.4436/jass.98022.

Moshfeghi, M., Ranganath, S., & Nawyn, K. (1994). Three-Dimensional Elastic Matching of Volumes. *IEEE Transactions on Image Processing*, 3 (2), 128-138. Doi: 10.1109/83.277895.

Neeser, R., Ackermann, R. R., & Gain, J. (2009). Comparing the accuracy and precision of three techniques used for estimating missing landmarks when reconstructing fossil hominin crania. *American Journal of Physical Anthropology*, 140 (1), 1-18. Doi: 10.1002/ajpa.21023.

Neubauer, S., Gunz, P., & Hublin, J.-J. (2010). Endocranial Shape Changes During Growth in Chimpanzees and Humans: a Morphometric Analysis of Unique and Shared Aspects. *Journal of Human Evolution*, 59, 555-566. Doi: 10.1016/j.jhevol.2010.06.011.

Neubauer, S., Hublin, J. J., & Gunz, P. (2018). The evolution of modern human brain shape. *Science advances*, *4* (1), eaao5961. Doi: 10.1126/sciadv.aao5961.

Nicholson, E., & Harvati, K. (2006). Quantitative analysis of human mandibular shape using three-dimensional geometric morphometrics. *American Journal of Physical Anthropology, 131* (3), 368-383. Doi: 10.1002/ajpa.20425.

Nielsen, R., Akey, J. M., Jakobsson, M., Pritchard, J. K., Tishkoff, S., & Willerslev, E. (2017). Tracing the peopling of the world through genomics. *Nature*, 541, 302.-310. Doi: 10.1038/nature21347.

Nigst, P. R., Haesaerts, P., Damblon, F., Frank-Fellner, C., Mallol, C., Viola, B., Götzinger, M., Niven, L., Trnka, G., & Hublin, J.-

J. (2014). Early modern human settlement of Europe north of the Alps occurred 43,500 years ago in a cold steppe-type environment. *Proceedings of the National Academy of Sciences*, 111 (40), 14394-14399. Doi: 10.1073/pnas.1412201111.

Oeschger, E. S., Kanavakis, G., Halazonetis, D. J., & Gkantidis, N. (2020). Number of teeth is associated with facial size in humans. *Scientific Reports*, 10, 1820. Doi: 10.1038/s41598-020-58565-8.

Oppenheimer, S. (2012). A single southern exit of modern humans from Africa: before or after Toba?. *Quaternary International*, 258, 88-99. Doi: 10.1016/j.quaint.2011.07.049.

Osborne, A. H., Vance, D., Rohling, E. J., Barton, N., Rogerson M., & Fello, N. (2008). A humid corridor across the Sahara for the migration of early modern humans out of Africa 120,000 years ago. *Proceedings of the National Academy of Sciences*, 105 (43), 16444-16447. Doi: 10.1073/pnas.0804472105.

Pagani, L., Lawson, D. J., Jagoda, E., Mörseburg, A., Eriksson, A., Mitt, M., Clemente, F., Hudjashov, G., DeGiorgio, M., Saag, L., Wall, J. D., Cardona, A., Mägi, R., Wilson Sayres, M. A., Kaewert, S., Inchley, C., Scheib, C. L., Järve, M., Karmin, M., Jacobs, G. S., Antao, T., Iliescu, F. M., Kushniarevich, A., Ayub, Q., Tyler-Smith, C., Xue, Y., Yunusbayev, B., Tambets, K., Mallick, C. B., Saag, L., Pocheshkhova, E., Andriadze, G., Muller, C., Westaway, M. C., Lambert, D. M., Zoraqi, G., Turdikulova, S., Dalimova, D., Sabitov, Z., Sultana, G. N. N., Lachance, J., Tishkoff, S., Momynaliev, K., Isakova, J., Damba, L. D., Gubina, M., Nymadawa, P., Evseeva, I., Atramentova, L., Utevska, O., Ricaut, F.-X., Brucato, N., Sudoyo, H., Letellier, T., Cox, M. P., Barashkov, N. A., Škaro, V., Mulahasanovic′, L., Primorac, D., Sahakyan, H., Mormina, M., Eichstaedt, C. A., Lichman, D. V., Abdullah, S., Chaubey, G., Wee, J. T. S., Mihailov, E., Karunas, A., Litvinov, S., Khusainova, R., Ekomasova, N., Akhmetova, V., Khidiyatova, I., Marjanović, D., Yepiskoposyan, L., Behar, D. M., Balanovska, E., Metspalu, A., Derenko, M., Malyarchuk, B., Voevoda, M., Fedorova, S. A., Osipova, L. P., Lahr, M. M., Gerbault, P., Leavesley, M., Migliano, A. B., Petraglia, M., Balanovsky, O., Khusnutdinova, E. K., Metspalu, E., Thomas, M. G., Manica, A., Nielsen, R., Villems, R., Willerslev, E., Kivisild, T., & Metspalu, M. (2016). Genomic analyses inform on migration events during the peopling of Eurasia. *Nature*, 538, 238–242. Doi: 10.1038/nature19792

Panagopoulou, E., Tourloukis, V., Thompson, N., Athanassiou, A., Tsartsidou, G., Konidaris, G. E., Giusti, D., Karkanas, P., & Harvati, K. (2015). Marathousa 1: A new Middle Pleistocene

archaeological site from Greece. *Antiquity*, 89, Project Gallery. Doi: 10.15496/publikation-5878.

Panagopoulou, E., Tourloukis, V., Thompson, N., Konidaris, G., Athanassiou, A., Giusti, D., Tsartsidou, G., Karkanas, P., & Harvati, K. (2018). The lower palaeolithic site of Marathousa 1, Megalopolis, Greece: overview of the evidence. *Quaternary International*, 497, 33-46. Doi: 10.1016/j.quaint.2018.06.031.

Petit, R. J., Aguinagalde, I., de Beaulieu, J. L., Bittkau, C., Brewer, S., Cheddadi, R., Ennos, R., Fineschi, S., Grivet, D., Lascoux, M., Mohanty, A., Müller-Strack, G., Demesure-Musch, B., Palmé, A., Martín, H. P., Rendell, S., & Vendramin, G. G. (2003). Glacial refugia: hotspots but not melting pots of genetic diversity. *Science*, 300 (5625), 1563-1565. Doi: 10.1126/science.1083264.

Petr, M., Hajdinjak, M., Fu, Q., Essel, E., Rougier, H., Crevecoeur, I., Semal, P., Golovanova, L. V., Doronichev, V. B., Lalueza-Fox, C., de la Rasilla, M., Rosas, A., Shunkov, M. V., Kozlikin, M. B., Derevianko, A. P., Vernot, B., Meyer, M., & Kelso, J. (2020). The evolutionary history of Neanderthal and Denisovan Y chromosomes. *Science*, 369 (6511), 1653-1656. Doi: 10.1126/science.abb6460.

Pickering, R. (2017) U-Series Dating. In: A. S. Gilbert (Eds.), *Encyclopedia of Geoarchaeology. Encyclopedia of Earth Sciences Series* (pp. 992-1000). Springer, Dordrecht. Doi: 10.1007/978-1-4020-4409-0_50.

Pike, A. W. G., Hedges, R. E. M., & van Calsteren, P. (2002). U-series dating of bone using the diffusion-adsorption model. *Geochimica et Cosmochimica Acta*, *66* (24), 4273-4286. Doi: 10.1016/S0016-7037(02)00997-3.

Pitsios, T. K. (1985). Παλαιοανθρωπολογικές έρευνες στη θέση «Απήδημα» της Μέσα Μάνης. *Αρχαιολογία*, 15, 26–33.

Pitsios, T. K. (1995). Paleoanthropological Research at the cave site of Apidima, Laconia, Greece. *Acta Anthropologica*, 1, 1–180.

Pitsios, T. K. (1999). Paleoanthropological research at the cave site of Apidima and the surrounding region (South Peloponnese, Greece). *Anthropologischer Anz*eiger, 57 (1), 1–11.

Pomidor, B. J., & Makedonska, J., & Slice, D. E. (2016). A landmark-free method for three-dimensional shape analysis. *PloS one*, 11 (3): e0150368. Doi: 10.1371/journal.pone.0150368.

Ponce de León, M. S., Golovanova, L., Doronichev, V., Romanova, G., Akazawa, T., Kondo, O., Ishida, H., & Zollikofer, C. P. E. (2008). Neanderthal brain size at birth provides insights into the evolution of human life history. *Proceedings of the National*

Academy of Sciences, *105* (37), 13764-13768. Doi: 10.1073/pnas.0803917105.

Posth, C., Wißling, C., Kitagawa, K., Pagani, L., von Holstein, L., Racimo, F., Wehrberger, K., Conard, N. J., Kind, C. J., Bocherens, H., & Krause, J. (2017). Deeply divergent archaic mitochondrial genome provides lower time boundary for African gene flow into Neanderthals. *Nature Communications*, 8, 16046. Doi: 10.1038/ncomms16046.

Prévost, M., & Zaidner, Y. (2020). New insights into early MIS 5 lithic technological behavior in the Levant: Nesher Ramla, Israel as a case study. *PloS one*, 15 (4), e0231109. Doi: 10.1371/journal.pone.0231109.

Profico, A., Buzi, C., B., Castiglione, S., Melchionna, M., Piras, P., Veneziano, A., & Raia, P. (2021). Arothron: An R package for geometric morphometric methods and virtual anthropology applications. *American Journal of Physical Anthropology*, 176 (1), 144-151. Doi: 10.1002/ajpa.24340.

Prossinger, H., Seidler, H., Wicke, L., Weaver, D., Recheis, W., Stringer, C., & Müller, G. (2003). Electronic removal of encrustations inside the Steinheim cranium reveals paranasal sinus features and deformations, and provides a revised endocranial volume estimate. *The Anatomical Record,* 273B, 132–142. Doi: 10.1002/ar.b.10022.

Prüfer, K., Racimo, F., Patterson, N., Jay, F., Sankararaman, S., Sawyer, S., Heinze, A., Renaud, G., Sudmant, P. H., de Filippo, C., Li, H., Mallick, S., Dannemann, M., Fu, Q., Kircher, M., Kuhlwilm, M., Lachmann, M., Meyer, M., Ongyerth, M., Siebauer, M., Theunert, C., Tandon, A., Moorjani, P., Pickrell, J., Mullikin, J. C., Vohr, S. H., Green, R. E., Hellmann, I., Johnson, P. L. F., Blanche, H., Cann, H., Kitzman, J. O., Shendure, J., Eichler, E. E., Lein, E. S., Bakken, T., Golovanova, L. V., Doronichev, V. B., Shunkov, M. V., Derevianko, A. P., Viola, B., Slatkin, M., Reich, D., Kelso, J., & Pääbo, S. (2014). The complete genome sequence of a Neanderthal from the Altai Mountains. *Nature*, 505, 43-49. Doi: 10.1038/nature12886.

Prüfer, K., de Filippo, C., Grote, S., Mafessoni, F., Korlevic, P., Hajdinjak, M., Vernot, B., Skov, L., Hsieh, P., Peyrégne, S., Reher, D., Hopfe, C., Nagel, S., Maricic, R., Fu, Q., Theunert, C., Rogers, R., Skoglund, P., Chintalapati, M., Dannemann, M., Nelson, B. J., Key, F. M., Rudan, P., Kucan, Z., Gusic, I., Golovanova, L. V., Doronichev, V. B., Patterson, N., Reich, D., Eichler, E. E., Slatkin, M., Schierup, M. H., Andrés, A. M., Meyer, M., & Pääbo, S. (2017). A high-coverage Neandertal genome from Vindija Cave in Croatia. *Science*, 358, 655–658. Doi: 10.1126/science.aao1887.

Prüfer, K., Posth, C., Yu, H., Stoessel, A., Spyrou, M. A., Deviese, T., Mattonai, M., Ribechini, E., Higham, T., Velemínský, P., Brůžek, J., & Krause, J. (2021). A genome sequence from a modern human skull over 45,000 years old from Zlatý kůň in Czechia. *Nature Ecology & Evolution*, *5* (6), 820-825. Doi: 10.1038/s41559-021-01443-x.

Rabett, R. J. (2018). The success of failed Homo sapiens dispersals out of Africa and into Asia. *Nature Ecology & Evolution*, *2* (2), 212-219. Doi: 10.1038/s41559-017-0436-8.

Richter, D., Grün, R., Joannes-Boyau, R., Steele, T. E., Amani, F., Rué, M., Fernandes, P., Raynal, J.-P., Geraads, D., Ben-Ncer, A., Hublin, J.-J., & McPharron, S. (2017). The age of the hominin fossils from Jebel Irhoud, Morocco, and the origins of the Middle Stone Age. *Nature*, 546, 293-296. Doi: 10.1038/nature22335.

Rieux, A., Eriksson, A., Li, M., Sobkowiak, B., Weinert, L. A., Warmuth, V., Ruiz-Linares, A., Manica, A., & Balloux, F. (2014). Improved calibration of the human mitochondrial clock using ancient genomes. *Molecular Biology and Evolution*, *31* (10), 2780-2792. Doi: 10.1093/molbev/msu222.

Rightmire, G. P. (2009). Middle and later Pleistocene hominins in Africa and Southwest Asia. *Proceedings of the National Academy of Sciences,* 106 (38), 16046-16050. Doi: 10.1073/pnas.0903930106.

Rightmire, G. P. (2012). The evolution of cranial form in mid-Pleistocene Homo. *South African Journal of Science*, 108, 68-77. Doi: 10.4102/sajs. v108i3/4.719.

Rink, W. J., Schwarcz, H. P., Smith, F. H., & Radovčić, J. (1995). ESR dates for Krapina hominids. *Nature*, 378, 24. Doi: 10.1038/378024a0.

Reyes-Centeno, H., Ghirotto, S., Détroit, F., Grimaud-Hervé, D., Barbujani, G., & Harvati, K. (2014). Genomic and cranial phenotype data support multiple modern human dispersals from Africa and a southern route into Asia. *Proceedings of the National Academy of Sciences,* 111, 7248– 7253. Doi: 10.1073/pnas.1323666111.

Reyes-Centeno, H., Hubbe, M., Hanihara, T., Stringer, C. B., & Harvati, K. (2015). Testing modern human out-of-Africa dispersal models and implications for modern human origins. *Journal of Human Evolution*, 87, 95-106. Doi: 10.1016/j.jhevol.2015.06.008.

Rmoutilová, R., Guyomarc'h, P., Velemínský, P., Šefčáková, A., Samsel, M., Santos, F., Maureille, B., & Brůžek, J. (2018). Virtual reconstruction of the Upper Palaeolithic skull from Zlatý kůň, Czech Republic: sex assessment and morphological

affinity. *PloS one*, *13* (8), e0201431. Doi: 10.1371/journal.pone.0201431.

Rohlf, F. J., & Bookstein, F. L. (1990). *Proceedings of the Michigan morphometrics workshop*. Ann Arbor, MI: The University of Michigan Museum of Zoology.

Roksandic, M., Radović, P. & Lindal, J. (2018). Revising the hypodigm of *Homo heidelbergensis*: a view from the Eastern Mediterranean. *Quaternary International*, 466, 66–81. Doi: 10.1016/j.quaint.2017.10.013.

Rosas, A., & Bastir, M. (2020). An assessment of the late Middle Pleistocene occipital from Apidima 1 skull (Greece). *L'Anthropologie*, *124* (1), 102745. Doi: 10.1016/j.anthro.2020.102745.

Scerri, E. M., Thomas, M. G., Manica, A., Gunz, P., Stock, J. T., Stringer, C., Grove, M., Groucutt, H. S., Timmermann, A., Rightmire, G. P., d'Errico, F., Tryon, C. A., Drake, N. A., Brooks, A. S., Dennell, R. W., Durbin, R., Henn, B. M., Lee-Thorp, J., deMenocal, P., Petraglia, M. D., Thompson, J. C., Scally, A., & Chikhi, L. (2018). Did our species evolve in subdivided populations across Africa, and why does it matter?. *Trends in Ecology & Evolution*, 33 (8), 582-594. Doi: 10.1016/j.tree.2018.05.005.

Schlager, S., & Rüdell, A. (2013). Shape analysis of the human zygomatic bone – surface registration. *American Journal of Physical Anthropology*, 150, 243. doi:10.1002/ajpa.22247 (Poster: https://www.researchgate.net/profile/Stefan-Schlager/publication/260135091_Zygomatic_Surface_Registration_AAPA_2013/links/0f31752fb6cc76c40e000000/Zygomatic-Surface-Registration-AAPA-2013.pdf).

Schlager, S. (2019). 3D data analysis using R: 3D data processing, shape analysis, and surface manipulations in R. In: *3D Data Acquisition for Bioarchaeology, Forensic Anthropology, and Archaeology* (pp. 131-159). London: Academic Press. Doi: 10.1016/B978-0-12-815309-3.00007-3.

Schlebusch, C. M., Malmström, H., Günther, T., Sjödin, P., Coutinho, A., Edlund, H., Munters, A. R., Vicente, M., Steyn, M., Soodyall, H., Lombard, M., & Jakobsson, M. (2017). Southern African ancient genomes estimate modern human divergence to 350,000 to 260,000 years ago. *Science*, 358 (6363), 652-655. Doi: 10.1126/science.aao6266.

Schuh, A., Gunz, P., Villa, C., Kupczik, K., Hublin, J.-J., & Freidline, S. E. (2020). Intraspecific variability in human maxillary bone modeling patterns during ontogeny. *American*

Journal of Physical Anthropology, 173, 655-670. Doi: 10.1002/ajpa.24153.

Schwarcz, H. P., Grün, R., Vandermeersch, B., Bar-Yosef, O., Valladas, H., & Tchernov, E. (1988). ESR dates for the hominid burial site of Qafzeh in Israel. *Journal of Human Evolution*, 17, 733–737. Doi: 10.1016/0047-2484(88)90063-2.

Schwartz, J. H., & Tattersall, I. (2003). *The Human Fossil Record: Craniodental morphology of genus Homo (Africa & Asia).* Hoboken (NJ): WILEY-LISS. Doi: 10.1002/0471722715.

Scozzari, R., Massaia, A., Trombetta, B., Bellusci, G., Myres, N. M., Novelletto, A., & Cruciani, F. (2014). An unbiased resource of novel SNP markers provides a new chronology for the human Y chromosome and reveals a deep phylogenetic structure in Africa. *Genome Research*, 24 (3), 535-544. Doi: 10.1101/gr.160788.113.

Semper-Hogg, W., Fuessinger, M. A., Schwarz, S., Ellis, E., Cornelius, C.-P., Probst, F., Metzger, M. C., & Schalger, S. (2017). Virtual reconstruction of midface defects using statistical shape models. *Journal of Cranio-Maxillo-Facial Surgery*, 45 (4), 461-466. Doi: 10.1016/j.jcms.2016.12.020.

Şenyürek, M. S. (1940). Fossil Man in Tangier. In: *Papers of the Peabody Museum of American Archaeology and Ethnology*, Vol. 16, No. 3. Cambridge, Massachusetts: Harvard University Press.

Sharp, W. D., & Paces, J. B. (2018). Comment on "The earliest modern humans outside Africa". *Science,* 362 (6413), eaat6598. Doi: 10.1126/science.aat6598.

Shea, J. J. (2003). The middle paleolithic of the east Mediterranean Levant. *Journal of World Prehistory*, *17* (4), 313-394. Doi: 10.1023/B:JOWO.0000020194.01496.fe.

Shea, J. J., & Bar-Yosef, O. (2005). Who were the Skhul/Qafzeh people? An archaeological perspective on Eurasia's oldest modern humans. *Journal of the Israel Prehistoric Society*, 35, 451-468.

Shea, J. J. (2008). Transitions or turnovers? Climatically-forced extinctions of Homo sapiens and Neanderthals in the east Mediterranean Levant. *Quaternary Science Reviews*, 27, 2253–2270. Doi: 10.1016/j.quascirev.2008.08.015.

Siavalas, G., Linou, M., Chatziapostolou, A., Kalaitzidis, S., Papaefthymiou, H., & Christanis, K. (2009). Palaeoenvironment of Seam I in the Marathousa lignite mine, Megalopolis Basin (Southern Greece). *International Journal of Coal Geology*, 78, 233–248. Doi: 10.1016/j.coal.2009.03.003.

Sickenberg, O. (1976). Eine Säugetierfauna des tieferen Bihariums aus dem Becken von Megalopolis (Peloponnes, Griechenland). *Annales Géologiques des Pays Helléniques*, 27, 25–63.

Siska, V. (2019). *Human population history and its interplay with natural selection*. Ph.D. Dissertation, University of Cambridge. Doi: 10.17863/CAM.31536.

Skinner, M. M., Gunz, P., Wood, B. A., & Hublin, J. J. (2008). Enamel-dentine junction (EDJ) morphology distinguishes the lower molars of Australopithecus africanus and Paranthropus robustus. *Journal of Human Evolution*, 55 (6), 979-988. Doi: 10.1016/j.jhevol.2008.08.013.

Skouphos, T. G. (1905). Über die palaeontologischen Ausgrabungen in Griechenland in Beziehung auf das Vorhandensein des Menschen. In: *Comptes Rendus du Congrès International d'Archéologie* (pp. 231–236). Athènes.

Slice, D. E. (2007). Geometric morphometrics. *Annual Review of Anthropology, 36*, 261-281. Doi: 10.1146/annurev.anthro.34.081804.120613.

Smith, T. M., Tafforeau, P., Reid, D. J., Grün, R., Eggins, S., Boutakiout, M., & Hublin, J.-J. (2007). Earliest evidence of modern human life history in North African early Homo sapiens. *Proceedings of the National Academy of Sciences*, 104 (15), 6128-6133. Doi: 10.1073pnas.0700747104.

Spoor, F., Hublin, J.-J., Braun, M., & Zonneveld, F. (2003). The bony labyrinth of Neanderthals. *Journal of Human Evolution*, *44* (2), 141-165. Doi: 10.1016/S0047-2484(02)00166-5.

Spoor, F., Gunz, P., Neubauer, S., Stelzer, S., Scott, N., Kwekason, A., & Dean, M. C. (2015). Reconstructed Homo habilis type OH 7 suggests deep-rooted species diversity in early Homo. *Nature*, *519* (7541), 83-86. Doi: 10.1038/nature14224.

Stringer, C. B. (1974). A multivariate study of the Petralona skull. *Journal of Human Evolution*, *3* (5), 397-404. Doi: 10.1016/0047-2484(74)90202-4.

Stringer, C., Grün, R., Schwarcz, H. P., & Goldberg, P. (1989). ESR dates for the hominid burial site of Es Skhul in Israel. *Nature*, 338, 756–758. Doi: 10.1038/338756a0.

Stringer, C. (2012). The status of Homo heidelbergensis (Schoetensack 1908). *Evolutionary Anthropology: Issues, News, and Reviews*, *21* (3), 101-107. Doi: 10.1002/evan.21311.

Stringer, C. (2016). The origin and evolution of Homo sapiens. *Philosophical Transactions of the Royal Society B: Biological Sciences*, 371 (1698), 20150237. Doi: 10.1098/rstb.2015.0237.

Stringer, C., & Galway-Witham, J. (2018). When did modern humans leave Africa?. *Science*, 359 (6374), 389-390. Doi: 10.1126/science.aas8954.

Stutz, A. J. (2020). The Middle-Upper Paleolithic transition: A long-term biocultural effect of anatomically modern human dispersal. In: H. Groucutt (Eds.), *Culture History and Convergent Evolution* (pp. 157-186). Cham: Springer. Doi: 10.1007/978-3-030-46126-3_9.

Taberlet, P., Fumagalli, L., Wust-Saucy, A.-G., & Cossons, J.-F. (1998). Comparative phylogeography and postglacial colonization routes in Europe. *Molecular Evolution*, 7, pp. 453-464. Doi: 10.1046/j.1365-294x.1998.00289.x.

Tchernov, E. (1992a). The Afro-Arabian component in the Levantine mammalian fauna - a short biogeographical review. *Israel Journal of Zoology*, 38: 155–192. Doi: 10.1080/00212210.1992.10688668.

Tchernov, E. (1992b). Biochronology, paleoecology and dispersal events of hominids in the southern Levant. In: T. Akazawa, K. Aoki, & T. Kimura (Eds.), *The Evolution and Dispersal of Modern Humans in Asia* (pp. 149-188). Tokyo: Hokusen-sha.

Thompson, N., Tourloukis, V., Panagopoulou, E., & Harvati, K. (2018). In search of Pleistocene remains at the gates of Europe: Directed surface survey of the Megalopolis Basin (Greece). *Quaternary International*, 497, 22–32. Doi: 10.1016/j.quaint.2018.03.036.

Thompson, J. D. (2020). *Plant evolution in the Mediterranean: Insights* for Conversation (2nd ed.). New York, NY: Oxford University Press.

Tourloukis, V., & Karkanas, P. (2012). The Middle Pleistocene archaeological record of Greece and the role of the Aegean in hominin dispersals: new data and interpretations. *Quaternary Science Reviews*, *43*, 1-15. Doi: 10.1016/j.quascirev.2012.04.004.

Tourloukis, V., Thompson, N., Garefalakis, C., Karkanas, P., Konidaris, G. E., Panagopoulou, E., & Harvati, K. (2016). New Middle Paleolithic sites from the Mani peninsula, Southern Greece. *Journal of Field Archaeology*, 41, 68–83. Doi: 10.1080/00934690.2015.1125223.

Tourloukis, V., & Harvati, K. (2018). The Palaeolithic record of Greece: a synthesis of the evidence and a research agenda for the future. *Quaternary International*, 466, 48–65. Doi: 10.1016/j.quaint.2017.04.020.

Tourloukis, V., Thompson, N., Panagopoulou, E., Giusti, D., Konidaris, G. E., Karkanas, P., & Harvati, K. (2018). Lithic

artifacts and bone tools from the Lower Palaeolithic Site Marathousa 1, Megalopolis, Greece: Preliminary results. *Quaternary International*, 497, 47–64. Doi: 10.1016/j.quaint.2018.05.043.

Trinkaus, E. (1987). The Neandertal face: evolutionary and functional perspectives on a recent hominid face. *Journal of Human Evolution*, 16 (5), 429-443. Doi: 10.1016/0047-2484(87)90071-6.

Trinkaus, E. (2005). Early modern humans. *Annual Review of Anthropology*, 34, 207-230. Doi: 10.1146/annurev.anthro.34.030905.154913.

Trinkaus, E., Constantin, S., & Zilhão, J. (2013). *Life and death at the Peştera cu Oase: A setting for modern human emergence in Europe*. Oxford, UK: Oxford University Press.

Tryon, C. A., Roach, N. T., & Logan, M. A. V. (2008). The Middle Stone Age of the northern Kenyan Rift: age and context of new archaeological sites from the Kapedo Tuffs. *Journal of Human Evolution*, 55(4), 652-664. Doi: 10.1016/j.jhevol.2008.03.008.

Tzedakis, P. C., Lawson, I. T., Frogley, M.R., Hewitt, G.M., & Preece, R. C. (2002). Buffered tree population changes in a Quaternary refugium: evolutionary implications. *Science*, 297, 2044–2047. Doi: 10.1126/science.1073083.

Uhl, A., Reyes-Centeno, H., Grigorescu, D., Kranioti, E. F., & Harvati, K. (2016). Inner ear morphology of the Cioclovina early modern European calvaria from Romania. *American Journal of Physical Anthropology*, 160 (1), 62-70. Doi: 10.1002/ajpa.22938.

Valladas, H., Mercier, N., Hershkovitz, I., Zaidner, Y., Tsatskin, A., Yeshurun, R., Vialettes, L., Joron, J.-L., Reyss, J.-L., Weinstein-Evron, M. (2013). Dating the Lower to Middle Paleolithic transition in the Levant: A view from Misliya Cave, Mount Carmel, Israel. *Journal of Human Ev*olution, 65, 585–593. Doi: 10.1016/j.jhevol.2013.07.005.

Vandermeersch, B. (1978). Étude préliminaire du crâne humain du gisement paléolithique de Biache-Saint-Vaast (Pas-de-Calais). *Quaternaire*, *15* (1), 65-67.

Vandermeersch, B. (1981). *Les Hommes fossiles de Qafzeh (Israel)*. Centre National de la Recherche Scientifique, CNRS, Paris.

Vandermeersch, B., & Bar-Yosef, O. (2019). The paleolithic burials at Qafzeh cave, Israel. *PALEO. Revue d'archéologie préhistorique*, 30 (1), 256-275. Doi: 10.4000/paleo.4848.

Villanea, F. A., & Schraiber, J. G. (2019). Multiple episodes of interbreeding between Neanderthal and modern humans.

Nature Ecology & Evolution, *3* (1), 39-44. Doi: 10.1038/s41559-018-0735-8.

Vinken, R. (1965). Stratigraphie und Tektonik des Beckens von Megalopolis (Peloponnes, Griechenland). *Geologisches Jahrbuch*, 83, 97-148.

Vizzari, M. T., Benazzo, A., Barbujani, G., & Ghirotto, S. (2020). A Revised Model of Anatomically Modern Human Expansions Out of Africa through a Machine Learning Approximate Bayesian Computation Approach. *Genes*, *11* (12), 1510. Doi: 10.3390/genes11121510.

von Cramon-Taubadel, N., & Lycett, S. J. (2008). Brief communication: human cranial variation fits iterative founder effect model with African origin. *American Journal of Physical Anthropology*, *136* (1), 108-113. Doi: 10.1002/ajpa.20775.

Weaver, T. D. (2012). Did a discrete event 200,000–100,000 years ago produce modern humans?. *Journal of Human Evolution*, 63 (1), 121-126. Doi: 10.1016/j.jhevol.2012.04.003.

Weber, G. W., Schäfer, K., Prossinger, H., Gunz, P., Mitteröcker, P., & Seidler, H. (2001). Virtual anthropology: the digital evolution in anthropological sciences. *Journal of Physiological Anthropology and Applied Human Science*, *20* (2), 69-80. Doi: 10.2114/jpa.20.69.

Weber, G. W., & Bookstein, F. L. (2011). *Virtual anthropology: a guide to a new interdisciplinary field*. Wien, London: Springer.

Weber, G. W. (2015). Virtual anthropology. *American Journal of Physical Anthropology*, *156*, 22-42. Doi: 10.1002/ajpa.22658.

Weber, G. W., & Krenn, V. A. (2017). Zygomatic root position in recent and fossil hominids. *The Anatomical Record*, 300 (1), 160-170. Doi: 10.1002/ar.23490.

Weber, G. W., Hershkovitz, I., Gunz, P., Neubauer, S., Ayalon, A., Latimer, B., Bar-Matthews, M., Yasur, G., & May, H. (2020). Before the massive modern human dispersal into Eurasia: A 55,000-year-old partial cranium from Manot Cave, Israel. *Quaternary International*, *551*, 29-39. Doi: 10.1016/j.quaint.2019.10.009.

Westaway, K. E., Louys, J., Due Awe, R., Morwood, J., Price, G. J., Zhao, J. X., Aubert, M., Joannes-Boyau, R., Smith, T. M., Skinner, M. M., Compton, T., Bailey, R. M., van den Bergh, G. D., de Vos, J., Pike, A. W. G., Stringer, C., Samptomo, E. W., Rizal, Y., Zaim, J., Santoso, W. D., Trihascaryo, A., Kinsley, L., & Sulistyanto, B. (2017). An early modern human presence in Sumatra 73,000-63,000 years ago. *Nature*, 548, 322-325. Doi: 10.1038/nature23452.

White, M. A., & Campione, N. E. (2021). A three-dimensional approach to visualize pairwise morphological variation and its application to fragmentary palaeontological specimens. *PeerJ*, 9, e10545. Doi: 10.7717/peerj.10545.

Wolpoff, M. H. (1980). Cranial remains of middle Pleistocene European hominids. *Journal of Human Evolution*, *9* (5), 339-358. Doi: 10.1016/0047-2484(80)90047-0.

Wu, X., & Schepartz, L. A. (2009). Application of computed tomography in paleoanthropological research. *Progress in Natural Science*, *19* (8), 913-921. Doi: 10.1016/j.pnsc.2008.10.009.

Xirotiris, N., Henke, W., & Symeonidis, N. (1979). Der M^3 von Megalopolis – ein Beitrag zu seiner Morphologischen Kennzeichnung. *Zeitschrift für Morphologie und Anthropologie*, 70, 117–122.

Zagwijn, W. H. (1992). Migration of vegetation during the Quaternary in Europe. *Courier Forschungsinstitut Senckenberg*, 153, 9–20.

Zanolli, C., & Mazurier, A. (2013). Endostructural characterization of the *H. heidelbergensis* dental remains from the early Middle Pleistocene site of Tighenif, Algeria. *Comptes Rendus Palevol*, 12 (5), 293-304. Doi: 10.1016/j.crpv.2013.06.004.

Zelditch, M., Swiderski, D. & Sheets, H. (2012). *Geometric morphometrics for biologists: a primer* (2nd ed.). London, UK: Academic Press.

Zollikofer, C. P. E., Ponce de León, M. S., Martin, R. D., & Stucki, P. (1995). Neanderthal computer skulls. *Nature*, 375**,** 283–285. Doi: 10.1038/375283b0.

Zollikofer, C. P. E., Ponce De León, M. S., & Martin, R. D. (1998). Computer-assisted paleoanthropology. *Evolutionary Anthropology: Issues, News, and Reviews*, *6* (2), 41-54.

Zollikofer, C. P. E., & Ponce de Léon, M.S. (2005). *Virtual reconstruction: a primer in computer-assisted paleontology and biomedicine*. Hoboken (NJ): Wiley.

Zollikofer, C. P. E., Ponce de León, M. S., Lieberman, D. E., Guy, F., Pilbeam, D., Likius, A., Mackaye, H. T., Vignaud, P., & Brunet, M. (2005). Virtual cranial reconstruction of Sahelanthropus tchadensis. *Nature*, *434* (7034), 755-759. Doi: 10.1038/nature0339.

Appendix

Study I: Apidima Ectocrania

Apidima Cave fossils provide earliest evidence of *Homo sapiens* in Eurasia

By Katerina Harvati, Carolin Röding, Abel M. Bosman, Fotios A. Karakostis, Rainer Grün, Chris Stringer, Panagiotis Karkanas, Nicholas C. Thomspon, Vassilis Koutoulidis, Lia A. Moulopoulos, Vassilis G. Goroulis and Mirsini Kouloukousssa

Published in *Nature* (2019) 571: 500-504.
Doi: 10.1038/s41586-019-1376-z.

Apidima Cave fossils provide earliest evidence of *Homo sapiens* in Eurasia

Katerina Harvati[1,2,3]*, Carolin Röding[1], Abel M. Bosman[1,2], Fotios A. Karakostis[1], Rainer Grün[4], Chris Stringer[5], Panagiotis Karkanas[6], Nicholas C. Thompson[1,3], Vassilis Koutoulidis[7], Lia A. Moulopoulos[7], Vassilis G. Gorgoulis[8,9,10]* & Mirsini Kouloukoussa[3,8]

Two fossilized human crania (Apidima 1 and Apidima 2) from Apidima Cave, southern Greece, were discovered in the late 1970s but have remained enigmatic owing to their incomplete nature, taphonomic distortion and lack of archaeological context and chronology. Here we virtually reconstruct both crania, provide detailed comparative descriptions and analyses, and date them using U-series radiometric methods. Apidima 2 dates to more than 170 thousand years ago and has a Neanderthal-like morphological pattern. By contrast, Apidima 1 dates to more than 210 thousand years ago and presents a mixture of modern human and primitive features. These results suggest that two late Middle Pleistocene human groups were present at this site—an early *Homo sapiens* population, followed by a Neanderthal population. Our findings support multiple dispersals of early modern humans out of Africa, and highlight the complex demographic processes that characterized Pleistocene human evolution and modern human presence in southeast Europe.

Southeast Europe is considered to be a major dispersal corridor as well as one of the principal European Mediterranean glacial refugia1–3. As such, the human fossil record of this region has previously been proposed to be more diverse than that of more isolated and less hospitable areas of Europe, reflecting the complexities of repeated dispersals, late survivals and admixture of human groups1,3. This hypothesis has been difficult to test, as palaeoanthropological finds from the Balkans are relatively scarce. The two fossilized human crania from Apidima, Mani (southern Greece)4, are among the most important finds from the region, yet remain little known. Here we applied the U-series dating method to elucidate their chronology and depositional history. We virtually reconstructed both specimens, correcting for taphonomic damage, and conducted detailed comparative description and geometric morphometric analyses.

[1]Paleoanthropology, Senckenberg Centre for Human Evolution and Palaeoenvironment, Eberhard Karls University of Tübingen, Tübingen, Germany. [2]DFG Centre of Advanced Studies 'Words, Bones, Genes, Tools', Eberhard Karls University of Tübingen, Tübingen, Germany. [3]Museum of Anthropology, Medical School, National and Kapodistrian University of Athens, Athens, Greece. [4]Australian Research Centre for Human Evolution, Griffith University, Nathan, Queensland, Australia. [5]Centre for Human Evolution Research, Department of Earth Sciences, The Natural History Museum, London, UK. [6]Malcolm H. Wiener Laboratory for Archaeological Science, American School of Classical Studies at Athens, Athens, Greece. [7]First Department of Radiology, National and Kapodistrian University of Athens, Athens, Greece. [8]Department of Histology and Embryology, Medical School, National and Kapodistrian University of Athens, Athens, Greece. [9]Biomedical Research Foundation of the Academy of Athens, Athens, Greece. [10]Division of Cancer Sciences, Faculty of Biology, Medicine and Health, Manchester Academic Health Science Centre, Manchester Cancer Research Centre, NIHR Manchester Biomedical Research Centre, University of Manchester, Manchester, UK. *e-mail: katerina.harvati@ifu.uni-tuebingen.de; vgorg@med.uoa.gr

Chronology

The Apidima specimens were discovered in a block of breccia wedged high between the cave walls of Apidima Cave A2,4–6 (Extended Data Fig. 1), during research by the Museum of Anthropology, School of Medicine, National Kapodistrian University of Athens, which started in 1978. Owing to the lack of associated context, their geological age has been difficult to assess. Attempts to date the site radiometrically proved to be inconclusive7. However, geomorphology indicates a Middle–Late Pleistocene age, and a bracket between 190 and 100 thousand years ago (ka) has been proposed as the most-probable period for the deposition of the 'skull breccia'6,8. Previous work calculated a minimum age of approximately 160 ka by U-series dating of an Apidima 2 bone fragment, which suggests a most-probable time of deposition of around 190 ka (transition between Marine Isotope Stage (MIS) 7 and MIS 6)5. We analysed three samples from the 'skull breccia', selected from fragments produced when cleaning the specimens from the matrix, using the U-series method. These included human bone fragments (subsamples 3720A and B of Apidima 2; and subsamples 3754 and 3755 of Apidima 1) and four unidentified bone subsamples (3757A–C and 3758, see Supplementary Information section 1). Our analyses show that both crania are older than the solidification of the matrix, which occurred around 150 ka. Despite their depositional proximity, Apidima 1 obtained its uranium in a

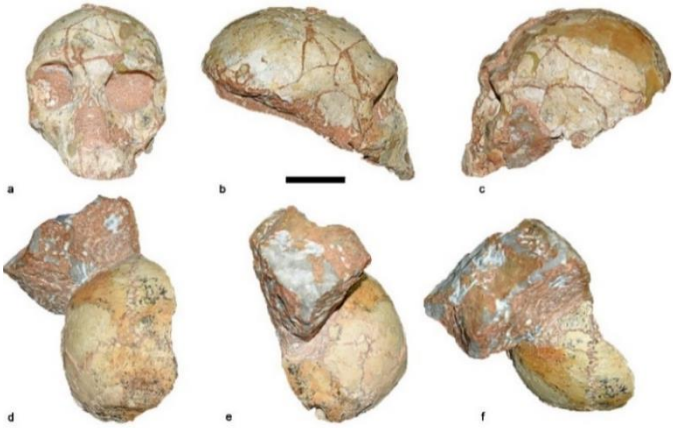

Fig. 1 | The fossil crania of Apidima 2 and Apidima 1. a–c, Apidima 2. **a**, Frontal view. **b**, Right lateral view. **c**, Left lateral view. **d–f**, Apidima 1. **d**, Posterior view. **e**, Lateral view. **f**, Superior view. Scale bar, 5 cm.

considerably different environment than Apidima 2, during an accumulation event in MIS 7 (around 210 ka), whereas the uranium-uptake process of Apidima 2 took place in MIS 6 (around 170 ka) (see Methods 'Depositional context', Supplementary Information section 1). The crania and associated bones were therefore probably trapped on the surface of the talus cone, Apidima 1 around 210 ka and Apidima 2 around 170 ka, and were brought to their final position before the cementation and solidification of the sedimentary matrix around 150 ka (see Methods, 'Depositional context').

Description and comparative analyses

Apidima 2 (Fig. 1a–c and Extended Data Fig. 2) is the more complete and better known of the crania, and has previously been considered to be an early Neanderthal or *Homo heidelbergensis*4–6,9. It preserves an almost complete face and most of the vault (Supplementary Information section 2), but is taphonomically distorted. We produced four virtual manual reconstructions by two observers, following two different criteria, from a computed tomography scan of the original

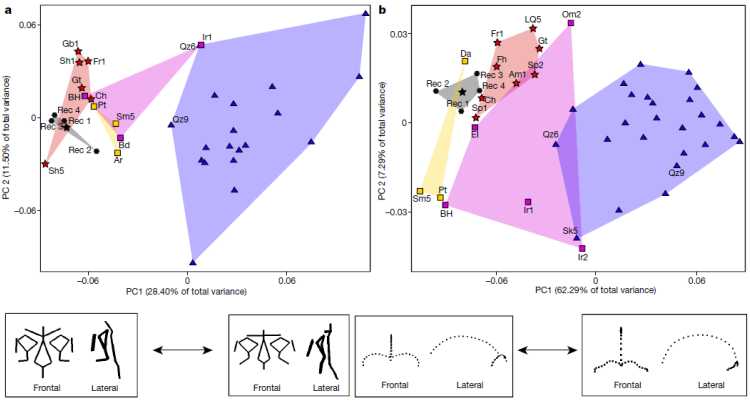

Fig. 2 | Shape analyses of Apidima 2. a, Analysis 1. PCA of Procrustessuperimposed facial landmarks, PC1 compared to PC2. *H. sapiens*, blue triangles (n = 19); Neanderthals, red stars (n = 6); MPE, yellow squares (n = 3); MPA, purple squares (n = 3). **b**, Analysis 2. PCA of Procrustes-superimposed neurocranial landmarks and semilandmarks, PC1 compared to PC2. *H. sapiens* (n = 25), Neanderthals (n = 8), MPE (n = 3), MPA (n = 5); Apidima reconstructions, black polygons, Apidima reconstruction mean configuration, black star. Wireframes below the plots illustrate facial and neurocranial shape changes along the PC1 of each analysis, respectively. Specimen abbreviations can be found in Supplementary Table 9. See Methods for detailed descriptions of analyses 1 and 2.

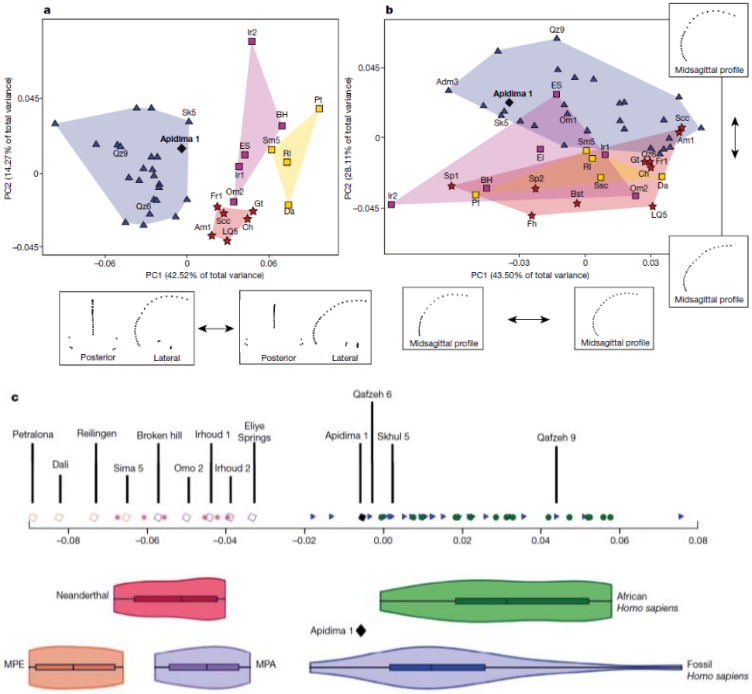

Fig. 3 | Shape analyses of Apidima 1. a, Analysis 3. PCA of Procrustessuperimposed neurocranial landmarks and semilandmarks, PC1 compared to PC2. *H. sapiens* (n = 23), Neanderthals (n = 6), MPE (n = 4), MPA (n = 5). **b**, Analysis 4. PCA of Procrustes-superimposed midsagittal landmarks and semilandmarks, PC1 compared to PC2. *H. sapiens* (n = 27), Neanderthals (n = 10), MPE (n = 5), MPA (n = 6). Wireframes below and next to the plots illustrate neurocranial and midsagittal shape changes along PC1 (analyses 3 and 4), and PC2 (analysis 4). **c**, Neurocranial shape index (analysis 3). Violins show the minimum–maximum range, boxes show the 25–75% quartiles and lines indicate the median. Modern Africans, green dots (n = 15); all other samples and symbols as in **a** and Fig. 2. See Methods for detailed descriptions of analyses 3 and 4.

specimen (Extended Data Figs. 3, 4 and Methods).

Apidima 1 (Fig. 1d–f) preserves the posterior cranium (Supplementary Information section 2). It shows no distortion; its virtual reconstruction therefore consisted of mirror-imaging the better-preserved side (Fig. 1e, Methods and Extended Data Fig. 5). Although no detailed study of

this specimen has been conducted to date, it has been assumed to share the same taxonomic attribution as Apidima 2 (see, for example, a previously published study on the Apidima 2 chronology5). Apidima 2 shows Neanderthal-like features: a continuous, thick and rounded supraorbital torus with no break between the glabellar, orbital and lateral regions; a lack of break in plane between the glabellar and lateral regions in superior view; an anterior position of the nasal root; inflated infraorbital region; bi-level morphology of the inferior nasal margin; and rounded *en bome* cranial profile in posterior view (Fig. 1a–c and Extended Data Figs. 2, 6, 7c, d). Most standard measurements (Supplementary Table 2) align it with Neanderthals. We conducted

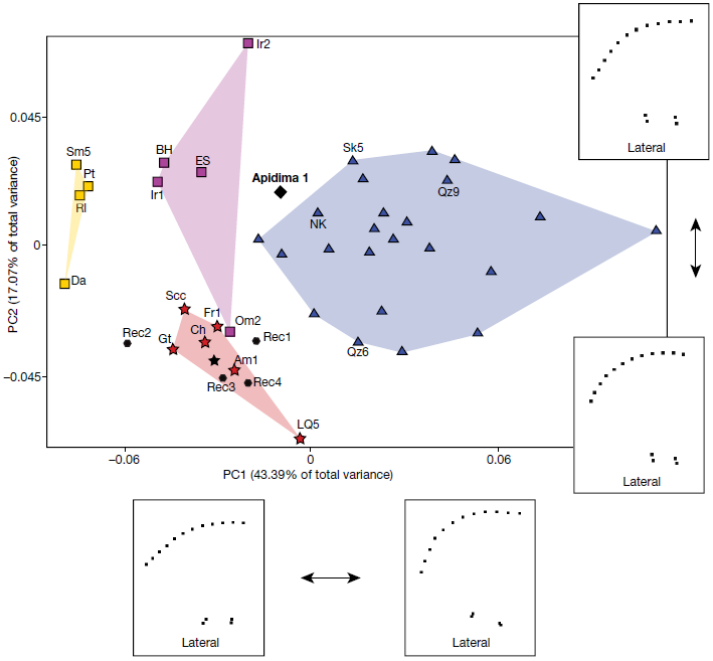

Fig. 4 | Shape analysis of Apidima 1 and Apidima 2. Analysis 5. PCA of Procrustes-superimposed neurocranial landmarks and semilandmarks shared between Apidima 1 and Apidima 2, PC1 compared to PC2. *H. sapiens* (n = 23), Neanderthals (n = 6), MPE (n = 4), MPA (n = 5). Wireframes below and next to the plot illustrate shape changes along PC1 and PC2. Symbols as in Fig. 2.

comparative geometric morphometric analyses of the face and neurocranium (analyses 1 and 2; Methods, Fig. 2, Extended Data Table 1 and Supplementary Tables 4, 5), treating the Apidima 2 reconstructions and their mean configuration as separate individuals, projected into the principal component analysis (PCA). In both PCAs, the reconstructions plotted closest to Neanderthals or between Neanderthals and Middle Pleistocene Eurasians (MPEs). Linear discriminant analyses classified them as Neanderthal (except for reconstruction 2, which was classified as MPE only in analysis 1; Extended Data Table 1). The overall shape of the Apidima 2 reconstruction mean was closest to Gibraltar 1 in Procrustes distance in the face and to Spy 1 in the neurocranium, both of which are Neanderthals.

By contrast, Apidima 1 does not have Neanderthal features; its linear measurements fall mainly in the region of overlap between taxa (Supplementary Information section 2 and Supplementary Table 3). It lacks a Neanderthal-like rounded *en bombe* profile in posterior view (Fig. 1d and Extended Data Fig. 7a, b). The widest part of the cranium is relatively low on the parietal; the parietal walls are nearly parallel and converge only slightly upwards, a plesiomorphic morphology that is common in Middle Pleistocene *Homo*10,11. It does not show the occipital plane convexity and lambdoid flattening associated with Neanderthal occipital 'chignons'. Rather, its midsagittal outline is rounded in lateral view, a feature that is considered derived for modern humans12 (Fig. 1e and Extended Data Fig. 7b). The superior nuchal lines are weak with no external occipital protuberance. In contrast to some Middle Pleistocene specimens, the occipital bone is not steeply angled and lacks a thick occipital torus (Fig. 1d, e and Extended Data Fig. 7a). A small, very faint, depression is found above the inion (length, approximately 12 mm; height, approximately 4.55 mm; Extended Data Fig. 7a). Although suprainiac fossae are considered derived for Neanderthals13, similar depressions occur among modern humans and in some African early *H. sapiens*14. The Apidima 1 depression does not present the typical Neanderthal combination of features. It is far smaller15 and less marked even than the 'incipient' suprainiac fossae of MPE specimens from Swanscombe and Sima de los Huesos, and is closest in size to the small supranuchal depression of the Eliye Springs cranium, a Middle Pleistocene African (MPA)16. Apidima 1 therefore lacks derived Neanderthal morphology, and instead shows a combination of ancestral and derived modern human features.

We conducted a geometric morphometric analysis of the Apidima 1 neurocranium and its midsagittal profile (analyses 3 and 4;

Fig. 3, Extended Data Table 1 and Supplementary Tables 6, 7). In both analyses, Apidima 1 clearly clustered with *H. sapiens* in the PCAs and was classified as *H. sapiens* by the linear discriminant analyses (posterior probability 100% and 93.4% in analyses 3 and 4, respectively; Extended Data Table 1). Its overall shape was closest to Nazlet Khater 2 (analysis 3) and Dolní Věstonice 3 (analysis 4); both of which are modern humans. We calculated a neurocranial shape index based on the dataset from analysis 3 following a previous study17, using our Neanderthal and a modern African sample (n = 15; Methods) and projecting Apidima 1 and all other specimens onto this axis (Fig. 3c). Both fossil and recent *H. sapiens* are clearly separated from all archaic samples in this index. Apidima 1 fell within the range of fossil *H. sapiens* and just outside that of modern Africans, away from Neanderthals and Middle Pleistocene samples. Notably, the MPA crania from Jebel Irhoud, Morocco—which are considered to be early representatives of the *H. sapiens* lineage18— plotted with Neanderthals. The same analysis for the midsagittal profile dataset produced similar results (Extended Data Fig. 8).

We compared the Apidima specimens for their common preserved anatomy. Although broadly similar in bi-auricular breadth, Apidima 2 is larger in its maximum cranial breadth, which reflects its *en bombe*

outline in posterior view (Extended Data Figs. 6, 7c). Apidima 1 is shorter antero-posteriorly and more rounded in lateral view (Extended Data Fig. 9). The analysis of a restricted dataset of shared neurocranial landmarks and semilandmarks (analysis 5; Fig. 4, Extended Data Table 1 and Supplementary Table 8) shows results similar to analyses 1–4. The Apidima 2 reconstructions fell with or close to Neanderthals along principal components 1 and 2 (PC1 and PC2) and were classified as Neanderthal (Extended Data Table 1). Their mean was closest in overall shape to Saccopastore 1, an early Neanderthal. Apidima 1 plotted closest to the *H. sapiens* convex hull, was classified as *H. Sapiens* (posterior probability 92%, Extended Data Table 1) and was closest to Nazlet Khater 2 (a modern human) in Procrustes distance.

Implications for human evolution

Our assessment of the overall features, linear measurements and shape analyses of the face and neurocranium of Apidima 2 support a Neanderthal or early Neanderthal attribution, consistent with its chronological age of approximately 170 thousand years under the 'accretion hypothesis'19. By contrast, Apidima 1 lacks derived Neanderthal features despite postdating the establishment of the distinct Neanderthal morphology19. Instead

it shows a rounded posterior cranium, which is considered derived for modern humans12. This morphology cannot be explained by ontogenetic age, sexual dimorphism or interindividual variability. Although these factors might produce attenuated Neanderthal characteristics, they should not result in a complete lack of Neanderthal occipital features20,21, nor in the presence of derived modern human traits. It might be hypothesized that Apidima 1 represents an early stage of the Neanderthal lineage, when facial morphology was established but derived features of the posterior cranium were not5,10. However, Apidima 1 differs not only from similarly dated early Neanderthals (for example, Saccopastore and Biache-St-Vaast), but also from earlier specimens from Sima de los Huesos, Swanscombe and Reilingen, which exhibit Neanderthal-like occipital features19. It also differs from MPE specimens such as Petralona (Northern Greece) or Ceprano, which show angulated occipitals and thickened tori; features that are absent in Apidima 1. Although the Steinheim MPE specimen appears relatively rounded in lateral view, it is heavily damaged (having suffered multidirectional distortions and erosion), which makes its morphology and taxonomic attribution uncertain14,22.

Apidima 1, therefore, does not fit in the 'accretional' scheme of Neanderthal evolution19, which has been proposed as the main explanatory model of human evolution in Europe. Rather, its combination of ancestral and derived modern human features and overall shape are consistent with a taxonomic attribution to early modern humans. If this interpretation is correct, it documents—to our knowledge—the earliest known presence of *Homo sapiens* in Eurasia, which indicates that early modern humans dispersed out of Africa starting much earlier, and reaching much further, than previously thought. It also suggests that contact with the Neanderthal lineage may also have occurred during the Middle Pleistocene, as postulated from ancient DNA evidence23. Together, the Apidima crania suggest a complex pattern of population dispersal and possible replacement for southern Greece that is not dissimilar to that proposed for the Levant24–26—a potential source area for the population represented by Apidima 1. In such a scenario, early modern humans who were present in the region in the late Middle Pleistocene were replaced by Neanderthals, whose subsequent presence in southern Greece is well-documented27–29. The latter were themselves replaced by Upper Palaeolithic modern humans, whose earliest appearance in the region—as documented by Upper Palaeolithic lithic industries30–32—dates to approximately 40 ka. Our results highlight both the scarcity of our knowledge of the human fossil record

in southeast Europe and the importance of this region in understanding Pleistocene human evolution and modern human dispersals.

As we completed this paper, we noted the publication of a new study33 of the partial crania of Apidima 1 and Apidima 2. The authors of that study conclude that the two crania represent a transitional population between European *Homo erectus* and Neanderthals, a conclusion that is not supported by our more comprehensive analyses.

Online content

Any methods, additional references, Nature Research reporting summaries, source data, extended data, supplementary information, acknowledgements, peer review information; details of author contributions and competing interests; and statements of data and code availability are available at https://doi.org/10.1038/s41586-019-1376-z.

Received: 28 March 2018; Accepted: 14 June 2019;
Published online 10 July 2019

1. Dennell, R. W., Martinón-Torres, M. & Bermúdez de Castro, J. M. Hominin variability, climatic instability and population demography in Middle Pleistocene Europe. *Quat. Sci. Rev.* **30**, 1511–1524 (2011).
2. Tourloukis, V. & Harvati, K. The Palaeolithic record of Greece: a synthesis of the evidence and a research agenda for the future. *Quat. Int.* **466**, 48–65 (2018).
3. Roksandic, M., Radović, P. & Lindal, J. Revising the hypodigm of *Homo heidelbergensis*: a view from the Eastern Mediterranean. *Quat. Int.* **466**, 66–81 (2018).
4. Pitsios, T. K. Paleoanthropological research at the cave site of Apidima and the surrounding region (South Peloponnese, Greece). *Anthropol. Anz.* **57**, 1–11 (1999).
5. Bartsiokas, A., Arsuaga, J. L., Aubert, M. & Grün, R. U-series dating and classification of the Apidima 2 hominin from Mani Peninsula, Southern Greece. *J. Hum. Evol.* **109**, 22–29 (2017).
6. Harvati, K., Stringer, C. & Karkanas, P. Multivariate analysis and classification of the Apidima 2 cranium from Mani, Southern Greece. *J. Hum. Evol.* **60**, 246–250 (2011).
7. Liritzis, Y. & Maniatis, Y. ESR experiments on quaternary calcites and bones for dating purposes. *J. Radioanal. Nucl. Chem.* **129**, 3–21 (1989).
8. Rondoyanni, T., Mettos, A. & Georgiou, C. Geological–morphological observations in the greater Oitilo-Diros area, Mani. *Acta Anthropol.* **1**, 93–102 (1995).
9. Coutselinis, A., Dritsas, C. & Pitsios, T. K. Expertise médico-légale du crane pléistocène LAO1/S2 (Apidima II), Apidima, Laconie, Grèce. *L'Anthropologie* **95**, 401–408 (1991).
10. Arsuaga, J. L. et al. Neandertal roots: cranial and chronological evidence from Sima de los Huesos. *Science* **344**, 1358–1363 (2014).
11. Stringer, C. The origin and evolution of *Homo sapiens*. *Phil. Trans. R. Soc. Lond. B* **371**, 20150237 (2016).
12. Galway-Witham, J. & Stringer, C. How did *Homo sapiens* evolve? *Science* **360**, 1296–1298 (2018).
13. Harvati, K. in *Handbook of Paleoanthropology* (eds Henke, W. & Tattersall, I.) 2243–2279 (Springer, 2015).
14. Balzeau, A. & Rougier, H. Is the suprainiac fossa a Neandertal autapomorphy? A complementary external and internal investigation. *J. Hum. Evol.* **58**, 1–22 (2010).
15. Verna, C., Hublin, J.-J., Debenath, A., Jelinek, A. & Vandermeersch, B. Two new hominin cranial fragments from the Mousterian levels at La Quina (Charente, France). *J. Hum. Evol.* **58**, 273–278 (2010).
16. Bräuer, G. & Leakey, R. L. The ES-11693 cranium from Eliye Springs, West Turkana, Kenya. *J. Hum. Evol.* **15**, 289–312 (1986).
17. Gunz, P. et al. Neandertal introgression sheds light on modern human endocranial globularity. *Curr. Biol.* **29**, 120–127 (2019).
18. Hublin, J.-J. et al. New fossils from Jebel Irhoud, Morocco and the pan-African origin of *Homo sapiens*. *Nature* **546**, 289–292 (2017).
19. Hublin, J.-J. The origin of Neandertals. *Proc. Natl Acad. Sci. USA* **106**, 16022–16027 (2009).

20. Caspari, R. The Krapina occipital bones. *Period. Biol*. **108**, 299–307 (2006).
21. Arsuaga, J. L., Martínez, I., Gracia, A. & Lorenzo, C. The Sima de los Huesos crania (Sierra de Atapuerca, Spain). A comparative study. *J. Hum. Evol.* **33**, 219–281 (1997).
22. Prossinger, H. et al. Electronic removal of encrustations inside the Steinheim cranium reveals paranasal sinus features and deformations, and provides a revised endocranial volume estimate. *Anat. Rec.* **273B**, 132–142 (2003).
23. Posth, C. et al. Deeply divergent archaic mitochondrial genome provides lower time boundary for African gene flow into Neanderthals. *Nat. Commun.* **8**, 16046 (2017).
24. Mercier, N. et al. Thermoluminescence date for the Mousterian burial site of Es-Skhul, Mt. Carmel. *J. Archaeol. Sci*. **20**, 169–174 (1993).
25. Hershkovitz, I. et al. The earliest modern humans outside Africa. *Science* **359**, 456–459 (2018).
26. Stringer, C. & Galway-Witham, J. When did modern humans leave Africa? *Science* **359**, 389–390 (2018).
27. Harvati, K., Panagopoulou, E. & Karkanas, P. First Neanderthal remains from Greece: the evidence from Lakonis. *J. Hum. Evol*. **45**, 465–473 (2003).
28. Harvati, K. et al. New Neanderthal remains from Mani peninsula, Southern Greece: the Kalamakia Middle Paleolithic cave site. *J. Hum. Evol*. **64**, 486–499 (2013).
29. Tourloukis, V. et al. New Middle Paleolithic sites from the Mani peninsula, Southern Greece. *J. Field Archaeol*. **41**, 68–83 (2016).
30. Elefanti, P., Panagopoulou, E. & Karkanas, P. The transition from the Middle to the Upper Paleolithic in the Southern Balkans: the evidence from Lakonis 1 Cave, Greece. *Eurasian Prehistory* **5**, 85–95 (2008).
31. Douka, K., Perlès, C., Valladas, H., Vanhaeren, M. & Hedges, R. E. M. Francthi Cave revisited: the age of the Aurignacian in south-eastern Europe. *Antiquity* **85**, 1131–1150 (2011).
32. Lowe, J. et al. Volcanic ash layers illuminate the resilience of Neanderthals and early modern humans to natural hazards. *Proc. Natl Acad. Sci. USA* **109**, 13532–13537 (2012).
33. De Lumley, M. A. *Les Restes Humains Anténéanderthaliens Apidima 1 et Apidima 2* (CNRS, 2019).

Methods

Depositional context. The crania were encased in a small block of breccia (65 cm × 45 cm × 35 cm)34, discovered in 1978 wedged between the walls and near the ceiling of Apidima Cave A (Extended Data Fig. 1). In a previous study5, the minimum depositional date was calculated to be approximately 160 ka for a bone fragment from Apidima 2 by U-series dating, thus constraining the upper limit of this range, and a most-likely time of deposition around 190 ka was proposed (during the transition between MIS 7 and MIS 6)5. The breccia block is interpreted as a remnant of an eroded steep talus cone that originally fanned out of the cliffs in front and above the cave6 (Extended Data Fig. 1c). The talus had to be graded to a previously existing dryland surface, indicating that the sea level was much lower for most of the time of its formation, most likely during a glacial period.

The U-series results (Supplementary Information section 1) show that both human samples are older than the solidification of the matrix at around 150 ka. This completely concurs with common sense. Apidima 1 accumulated its uranium in a considerably different environment than Apidima 2, during an accumulation event in MIS 7 (around 210 ka), whereas the uranium-uptake process of Apidima 2 took place in MIS 6 (around 170 ka). The crania and associated bones were probably trapped on the surface of the talus

cone, first Apidima 1 around 210 ka and later Apidima 2 at around 170 ka. The two crania were then brought into their final position at a later time, before the cementation and solidification of the sedimentary matrix around 150 ka. Water that preferentially infiltrates along cave walls often produces sediment dissolution and down-washing, and the formation of open spaces between the cave walls and the sedimentary fill. These sedimentary traps are later filled with collapsed material from the overlying sedimentary sequence. The location of the finds—between the walls of Apidima Cave A, wedged near the ceiling—suggest a similar scenario, in which bone material from Apidima 2 could be dislocated in a sedimentary trap from the overlying sequence and could have mixed with Apidima 1 remains, which also entered the trap at a later stage. The bones seem to have been thoroughly mixed, perhaps by a mudflow creeping down the sedimentary trap before consolidating at around 150 ka.

Computed tomography scanning and virtual manual reconstruction. The crania of Apidima 1 and Apidima 2 were scanned at the First Department of Radiology of the National and Kapodistrian University of Athens using a multidetector computed tomography scanner (Philips). The scanning parameters were as follows: tube voltage 120 kV, tube current–time product 599 mAs, 16 × 0.75 collimation, 0.8-mm slice thickness, slice increment 0.4 mm, field of view 249 mm, matrix 768 × 768, pitch 0.44, rotation time 0.75 s, convolution kernel detailed (*D*) and ultra-high focal spot resolution. The computed tomography scans of both individuals show isotropic pixel sizes of 0.31 and 0.32 mm, respectively.

Apidima 1 and Apidima 2 were virtually reconstructed by A.M.B. and C.R. In all cases, the reconstruction was manual and based on the preserved anatomical features. All reconstruction steps were carried out in the software environment of Avizo (Visualization Sciences Group). Before the multiple reconstructions of Apidima 2, each fragment was segmented separately to allow independent movement during the virtual reconstructions (Extended Data Figs. 3, 4). Several thin and tiny fragments could not be segmented in a reproducible way, owing to minimal differences in the grey values of bone and sediment matrix, and were thus excluded from the reconstructions. In total, 66 fragments were segmented. It was possible to segment fragments of the posterior neurocranium with semi-automated processes, as there were sufficient density differences between bone and matrix in this area. Facial fragments were mostly segmented manually slice by slice, owing to small differences in density between bone and matrix, combined with a low thickness of the fragments. Four independent reconstructions of Apidima 2 were carried out by A.M.B. and C.R., each using two different

protocols (for comparison, see a previous study35). Independent of the protocol used, matrix-filled cracks were not closed completely in the reconstructions, to account for possible alterations of the edges of the fragments. No reference cranium was used during the reconstructions of Apidima 2, to exclude the risk of driving the results in the direction of the chosen reference specimen.

A shared feature of vertebrate crania is approximate bilateral symmetry. The first protocol was based on this principle and had the goal to restore this symmetry. The anterior right part of the neurocranium was chosen as a starting point, as it presented a low amount of taphonomic deformation. Fragments of the right neurocranium were reconstructed according to a biologically meaningful position relative to each other. All reconstructed fragments of the right side were duplicated and mirrored along the midsagittal plane onto the left side. This mirrored duplicate was used as reference for the reconstruction of the fragments from the distorted left side of the neurocranium. The reconstructed left side of the brain case was subsequently mirrored to the right side to reconstruct the missing right temporal bone. Following the same procedure, the area close to the midsagittal plane on the right and a part of the supraorbital region on the left were reconstructed (shown as grey areas in Extended Data Figs. 3, 4). For restoring facial symmetry, the midsagittal plane of the neurocranium was used as a reference. The right facial side was reconstructed and mirrored to reconstruct the fragmented left side. The left nasal bone, right maxilla-zygomatic fragment, and the left side of the lower face were duplicated and mirrored to reconstruct missing areas (shown as grey areas in Extended Data Figs. 3, 4).

The second protocol exploited the assumption that the ectocranial surface should follow a smooth curvature, especially in the neurocranium. In this protocol, each fragment is spatially constrained by its neighbouring fragments. The anterior right part of the neurocranium was chosen as a starting point, as several fragments were located in positions relative to each other that almost preserved smooth curvature. After reconstructing the vault, the facial fragments were repositioned relative to each other to match the smoothness criterion. However, mirroring of the right side was necessary to check and correct the fragmented left side. When the position of fragments had to be corrected to deal with taphonomic distortion, smoothness was prioritized over bilateral symmetry. Finally, missing areas—such as the right temporal bone, the right nasal bone and the left maxilla—were reconstructed by duplicating and mirroring their preserved

counterpart (shown as grey areas in Extended Data Figs. 3, 4).

As previously shown36,37, multiple reconstructions of the same specimen will typically show some shape differences and no single reconstruction can be considered to be 'perfect'. As the different reconstructions might be considered equally plausible36, we treated them as separate individuals in all geometric morphometric analyses. Furthermore, we calculated the mean configuration of all four reconstructions and treated this as an additional individual in our analysis. The final Apidima 2 reconstructions retain some distortion with respect to the relationship between the face and the neurocranium. Therefore, these two anatomical regions were analysed separately (see 'Comparative samples').

The reconstruction of Apidima 1 was carried out by first computing a plane through the preserved part of the sagittal suture. The slices of the computed tomography scan were resampled according to this computed plane. Subsequently, preserved parts of the right parietal bone and right side of the occipital bone were cropped out along the computed plane in the original scan volume. This allowed mirroring a duplication of the cropped scan volume along the midsagittal plane. As a result, the reconstruction of Apidima 1 is completely symmetrical (Extended Data Fig. 5). Figures of the reconstructions were produced in Adobe Photoshop.

Comparative samples. The samples used for our analyses included Neanderthals (MIS 8–3), earlier Middle Pleistocene specimens from Africa (MPA) and Eurasia (MPE), *H. sapiens* (including early anatomically modern human specimens and Upper Palaeolithic modern humans) and modern Africans (n = 15) from the University of Witwatersrand Dart Collection. Severely taphonomically distorted and pathological specimens were excluded. The comparative summary statistics of the linear measurements reported in Supplementary Tables 2, 5 were based on data collected by C.S., supplemented by published values and by values collected from the Tübingen palaeoanthropology scan collection by K.H. and C.R. in Avizo (Visualization Sciences Group). The geometric morphometric comparative data were collected by K.H. Linear and three-dimensional measurements on the Apidima reconstructions were collected by K.H. and C.R. in Avizo (Visualization Sciences Group).

Analysis 1: the face of Apidima 2. This analysis comprised 25 facial landmarks: postorbital sulcus, glabella, nasion, infraspinale, prosthion, mid torus superior right and left, mid torus inferior right and left, dacryon right and left, zygoorbitale right and left, frontomalare right and left, infraorbital foramen right and left,

zygomaxillare right and left, alare right and left, jugale right and left, frontomalare posterior right and left (landmark definitions have previously been published38). Comparative samples included 31 individuals: MPE, Arago 21 (as previously reconstructed36), Petralona, Sima de los Huesos 5; MPA, Bodo, Broken Hill, Irhoud 1; Neanderthals, La Chapelle-aux-Saints, Gibraltar 1, Guattari, La Ferrassie 1, Shanidar 1 and 5; *H. sapiens*, Abri Pataud, Chancelade, Cro-Magnon 1, 2, Dolní Věstonice 3, 13, 14, 15 and 16, Grimaldi, Hofmeyr, Mladeč 1, Muierii 1, Oase 2, Předmostí 3 and 4, Qafzeh 6 and 9, Wadi Kubbaniya.

Analysis 2: neurocranium of Apidima 2. This analysis included landmarks and curve semilandmarks outlining the supraorbital torus and midsagittal profile: glabella, bregma, lambda, frontomalare posterior (FMLP) right and left; 26 semilandmarks from glabella to bregma; 18 semilandmarks from FMLP right to FMLP left. Comparative samples included 41 specimens: MPE, Dali, Petralona, Sima de los Huesos 5; MPA, Broken Hill, Elandsfontein, Irhoud 1 and 2, Omo 2; Neanderthals, Amud 1, La Chapelle-aux-Saints, Feldhofer, La Ferrassie 1, Guattari, La Quina 5, Spy 1 and 2; *H. sapiens*, Abri Pataud, Brno, Chancelade, Cioclovina, Cro-Magnon 1, 2 and 3, Dolní Věstonice 3, 13, 15 and 16, Mladeč 1, 2 and 5, Muierii 1, Oase 2, Ohalo 2, Pavlov, Předmostí 3 and 4, Qafzeh 6 and 9, Skhul 5, Zhoukoudian Upper Cave 101 and 103. For Mladeč 2, the FMLP points were reconstructed using the entire sample as reference (see 'Data processing').

Analysis 3: neurocranium of Apidima 1. This analysis comprised 30 neurocranial landmarks and semilandmarks, including bregma, lambda and inion, as well as parietal notch, auriculare and porion bilaterally, and 21 semilandmarks from bregma to inion. Although the parietal of Apidima 1 is nearly complete in the midsagittal plane, the bregma is not preserved and was reconstructed on the basis of the entire fossil sample (see 'Data processing') in this and the next two datasets. The comparative sample comprised 38 fossil individuals: MPE, Dali, Petralona, Reilingen, Sima de los Huesos 5; MPA, Broken Hill, Eliye Springs, Irhoud 1 and 2, Omo 2; Neanderthals, Amud 1, La Chapelle-aux-Saints, La Ferrassie 1, Guattari, La Quina 5, Saccopastore 1; *H. sapiens*, Abri Pataud, Brno, Chancelade, Cioclovina, Cro-Magnon 1 and 2, Dolní Věstonice 3, 13, 15 and 16, Mladeč 1 and 5, Muierii 1, Nazlet Khater 2, Oase 2, Ohalo 2, Pavlov, Předmostí 3 and 4, Qafzeh 6 and 9, Skhul 5, Zhoukoudian Upper Cave 101.

Analysis 4: midsagittal profile of Apidima 1. This analysis comprised 24 landmarks and semilandmarks outlining the midsagittal profile from bregma to inion to analyse the parietal and occipital plane convexity of

Apidima 1. The landmarks bregma, lambda and inion, and 21 semilandmarks from bregma to inion were included. The comparative sample consisted of 48 individuals: MPE, Dali, Petralona, Reilingen, Sima de los Huesos 5, Swanscombe; MPA, Broken Hill, Elandsfontein, Eliye Springs, Irhoud 1, 2, Omo 2; Neanderthals, Amud 1, Biachest-Vaast, La Chapelle-aux-Saints, Feldhofer, La Ferrassie 1, Guattari, La Quina 5, Saccopastore 1, Spy 1 and 2; *H. sapiens*, Aduma, Abri Pataud, Brno, Chancelade, Cioclovina, Cro-Magnon 1, 2 and 3, Dolní Věstonice 3, 13, 15 and 16, Mladeč 1 and 5, Muierii 1, Nazlet Khater 2, Oase 2, Ohalo 2, Omo 1, Pavlov, Předmostí 3 and 4, Qafzeh 6 and 9, Skhul 5, Zhoukoudian Upper Cave 101 and 103.

Analysis 5: shared landmarks and semilandmarks of Apidima 1 and Apidima 2. This analysis included bregma and lambda, as well as parietal notch and auriculare (bilaterally), and 10 semilandmarks from bregma to lambda. The sample was the same as in analysis 3, but additionally comprised the Apidima 2 reconstructions.

Data processing. The fixed landmarks (type I, II and III) and curve semilandmarks (type IV) were collected from the reconstructions in Avizo 9.2.0 Lite (Visualization Sciences Group). The comparative data37,38 were collected by K.H. and processed with the dorsal-ventral-left-right fitting (DVLR) program (http://www.nycep.org/nmg/programs.html). The curve semilandmarks were calculated by resampling each curve as a predetermined number of equally spaced points, using Resample. exe (http://www.nycep.org/nmg/programs.html). As the bregma was not present in Apidima 1, but most of the bregma–lambda curve was preserved, this point was estimated using generalized Procrustes analysis (GPA) mean substitution in Morpheus39. This protocol first performs GPA to align the specimens. Then, grand-mean coordinate values are computed for the missing landmark using the non-missing points. The inverse scale, rotation and translation are subsequently applied to restore the original data. The same procedure was used to reconstruct the frontomalare temporale for Mladeč 2 in analysis 2. For the important, taphonomically deformed specimen Arago 21, the virtual reconstruction that had previously been produced36 was used in the comparative facial analysis of Apidima 2. Minimal reconstruction based on the surrounding anatomy was allowed during data collection, and landmarks that were missing on one side were reconstructed through reflected relabelling40, or by using a function in R41 based on a previously published study42. This function estimates a mirroring plane based on the unilateral landmarks. The missing landmarks are then reflected according to this plane. After the

reconstruction of missing landmarks, the semilandmarks were slid along their respective closed curves using the Morpho package43 in R. Sliding was performed using the minimized bending energy algorithm44. After sliding, the data were exported in Morphologika format for further analysis45.

Data analysis. The compiled datasets were imported in Morphologika45 and superimposed using GPA, which translates the specimen configurations to common origin, scales them for size and rotates them to best fit. Procrustes distances among specimens are a measure of overall shape difference. The superimposed coordinates of the comparative samples, excluding the Apidima specimens, were used as variables in a PCA, performed in the Past 3.04 software46. The resulting eigenvectors (principal component loadings) were used to compute the principal component scores for the Apidima specimens to plot them into the PCA graphs after the latter had been calculated on the basis of the comparative samples only. PCA plots were processed using Adobe Illustrator and extracted as Adobe PDF files. Furthermore, linear discriminant analyses (LDAs) and classification analyses were performed in Past 3.04 using the principal components as variables, in each case treating the reconstructions of Apidima 1 and Apidima 2 as unknown. The number of principal components included in the LDA for each of the 5 analyses included the first 7, 8, 8, 4 and 4 principal components, accounting for 70.72%, 91%, 88.6%, 85.4% and 78.2% of the total variance, respectively. Posterior probabilities were calculated with the SPSS software package (IBM, version 24 for Windows). We investigated whether the datasets used met the LDA assumptions47. We verified that all variables (principal component scores) showed an approximately normal distribution on the basis of both histograms and normal probability plots47. We removed potential outliers from the analysis by excluding pathological or taphonomically distorted specimens. On the basis of *z*-score analyses47, we found that outliers were absent in all variables, except for one case in PC3 of analysis 2: the MPA individual Omo 2, for which the *z*-score was 0.08 points over the maximum acceptable limit47 of 3.29. Given the limited number of well-preserved MPA crania in the fossil record, we decided to maintain this specimen in the analysis to maximize the representation of this group. Finally, the covariance matrices were similar among groups in all analyses, and Box's *M*-tests showed that they were homogeneous for the samples used in analyses 4 and 5 (resulting *P* values were 0.19 and 0.07, respectively)47. However, this assumption could not be tested using Box's *M*-test for most analyses owing to the small sample sizes of certain fossil groups, a common problem in

palaeontology48. Because of these limitations, the results of the LDAs must be approached with caution, and not be interpreted in isolation, but in the context of all analyses presented here.

Visualization. Shape changes along principal component axes were visualized in Morphologika45. To further aid in visualization of shape differences between Apidima 1 and Apidima 2 (Extended Data Fig. 9), we conducted manual superimpositions of their three-dimensional models in the software environment of Avizo 9.2.0 Lite (Visualization Sciences Group). Apidima 2 stayed in its original configuration and manipulations were carried out on Apidima 1. In the first step of superimposition, Apidima 1 was scaled to the biauricular breadth of Apidima 2. The transmeatal axes of both specimens were matched by translating and rotating Apidima 1. In the last step, Apidima 1 was rotated around the transmeatal axis to match the orientations of the external auditory meatus and the supramastoid crest of Apidima 2.

Shape index. The globular shape of the modern human neurocranium is considered derived for modern humans and differentiates them from Neanderthals another archaic *Homo*. It has recently been shown17 that a less-globular cranial shape in modern Europeans is related to the presence of specific Neanderthal alleles in their genome. We calculated the shape index for the posterior neurocranium of Apidima 1, to approximate the globularization index of this previous study17. We calculated an axis between the mean shapes of our Neanderthal sample and a Neanderthal-unadmixed, modern African sample (Zulu, Dart Collection, University of the Witwatersrand, n = 15) and projected all other specimens (Apidima 1, MPE, MPA and fossil *H. sapiens*) onto this axis, to further evaluate the degree of globularity of the Apidima 1 neurocranium (Fig. 3c, Extended Data Fig. 8).

Reporting summary. Further information on research design is available in the Nature Research Reporting Summary linked to this paper.

Data availability

The data that support the findings of this study are available from the correspondingauthors upon reasonable request.

34. Kormasopoulou-Kagalou, L., Protonotariou-Deilaki, E. & Pitsios, T. K. Paleolithic skull burials at the cave of Apidima. *Acta Anthropol.* **1**, 119–124 (1995).
35. Zollikofer, C. P. et al. Virtual cranial reconstruction of *Sahelanthropus tchadensis*. *Nature* **434**, 755–759 (2005).
36. Gunz, P., Mitteroecker, P., Neubauer, S., Weber, G. W. & Bookstein, F. L. Principles for the virtual reconstruction of hominin crania. *J. Hum. Evol.* **57**, 48–62 (2009).
37. Harvati, K., Hublin, J.-J. & Gunz, P. Evolution of middle–late Pleistocene human cranio-facial form: a 3-D approach. *J. Hum. Evol.* **59**, 445–464 (2010).
38. Harvati, K., Gunz, P. & Grigorescu, D. Cioclovina (Romania): affinities of an early modern European. *J. Hum. Evol.* **53**, 732–746 (2007).
39. Slice, D. E. Morpheus et al., Java Edition. http://morphlab.sc.fsu.edu/ (The Florida State University, 2013).

40. Mardia, K. V., Bookstein, F. L. & Moreton, I. J. Statistical assessment of bilateral symmetry of shapes. *Biometrika* **87**, 285–300 (2000).
41. R Development Core Team. R: A Language and Environment for Statistical Computing. http://www.R-project.org/ (R Foundation for Statistical Computing, 2008).
42. Claude, J. *Morphometrics with R* (Springer Science & Business Media, 2008).
43. Schlager, S. in *Statistical Shape and Deformation Analysis* (eds Zheng, G. et al.) 217–256 (Academic, 2017).
44. Bookstein, F. L. Landmark methods for forms without landmarks: morphometrics of group differences in outline shape. *Med. Image Anal.* **1**, 225–243 (1997).
45. O'Higgins, P. & Jones, N. Morphologika: Tools for Shape Analysis. Version 2.2 https://sites.google.com/site/hymsfme/resources (Hull York Medical School, 2006).
46. Hammer, Ø., Harper, D. A. T. & Ryan, P. D. PAST: paleontological statistics software package for education and data analysis. *Palaeontol. Electronica* **4**, 1–9 (2001).
47. Field, A. *Discovering Statistics using SPSS* (Sage, 2013).
48. Brown, P. Nacurrie 1: mark of ancient Java, or a caring mother's hands, I terminal Pleistocene Australia? *J. Hum. Evol.* **59**, 168–187 (2010).

Acknowledgements This research was supported by the European Researc Council (ERC CoG no. 724703) and the German Research Foundation (DF FOR 2237). We thank all curators and their institutions for access to origina specimens or casts used in this study; T. White, B. Asfaw, M. López-Soza V. Tourloukis, D. Giusti, G. Konidaris, C. Fardelas and O. Stolis for their input and assistance; A. Balzeau (Muséum National d'Histoire Naturelle; MNHN), E. Delson (New York Consortium in Evolutionary Primatology; NYCEP), L. Leakey (africanfossils.org) for providing access to three-dimensional models of specimens used in our figures. C.S.'s research is supported by the Calleva Foundation and the Human Origins Research Fund. We are grateful to S. Benazzi, E. Delson and I. Hershkovitz for their comments and suggestions.

Author contributions K.H., M.K. and V.G.G. designed the research; V.K. and L.A.M. carried out the computed tomography scans; C.R. and A.M.B. generated the virtual reconstructions; K.H., C.S. and C.R. collected comparative data; K.H., C.R., A.M.B., F.A.K. and N.C.T. processed and analysed the data; R.G. dated the specimens; P.K. and R.G. provided stratigraphic and geological interpretations; all authors contributed to compiling the manuscript.

Extended Data

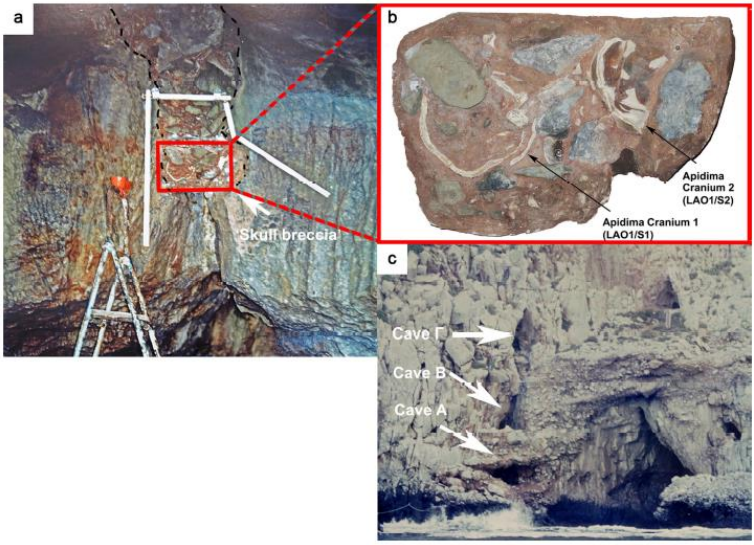

Extended Data Fig. 1 | The depositional setting of the Apidima 1 and Apidima 2 specimens. a, The interior of Apidima Cave A, with the 'skull breccia' (red box) before its removal from the cave, shown wedged between the cave walls and near the ceiling. A cross-section of the Apidima 1 cranium can be seen in the bottom left corner of the red box. Note the bedded appearance of the breccia remnant (black dashed line) consisting of different clast sizes and distribution similar to those seen in the talus cone outside the cave in **c**. **b**, Cast of the 'skull breccia' in the early stages of preparation and cleaning. Apidima 1 is seen on the left, Apidima 2 on the right. **c**, View of the Apidima site from the sea. Images courtesy and copyright of the Museum of Anthropology, Medical School, National Kapodistrian University of Athens.

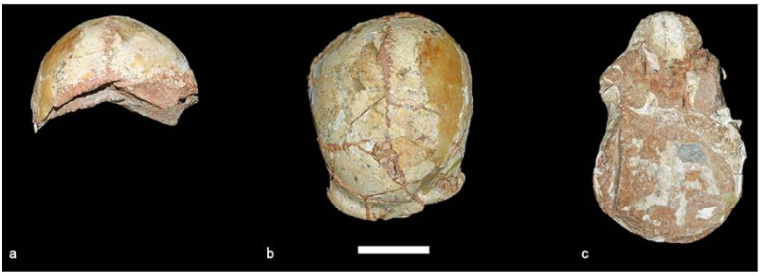

Extended Data Fig. 2 | Additional views of Apidima 2. a, Posterior view. **b**, Superior view. **c**, Inferior view. Scale bar, 5 cm.

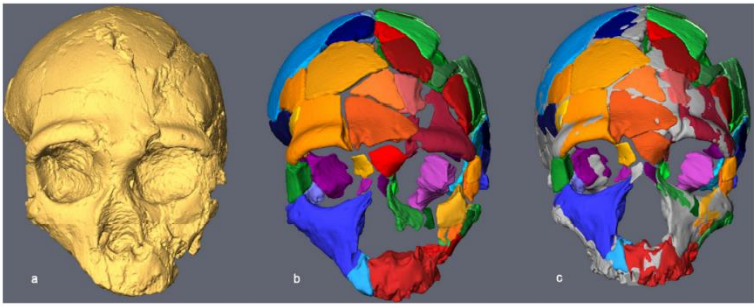

Extended Data Fig. 3 | Main steps of reconstruction of Apidima 2. a–c, Images are the computed surface of the original fossil (**a**), all segmented fragments (**b**) and reconstruction 1 from an anterior-superior view (**c**); segmented fragments are shown in colour and mirrored fragments in grey.

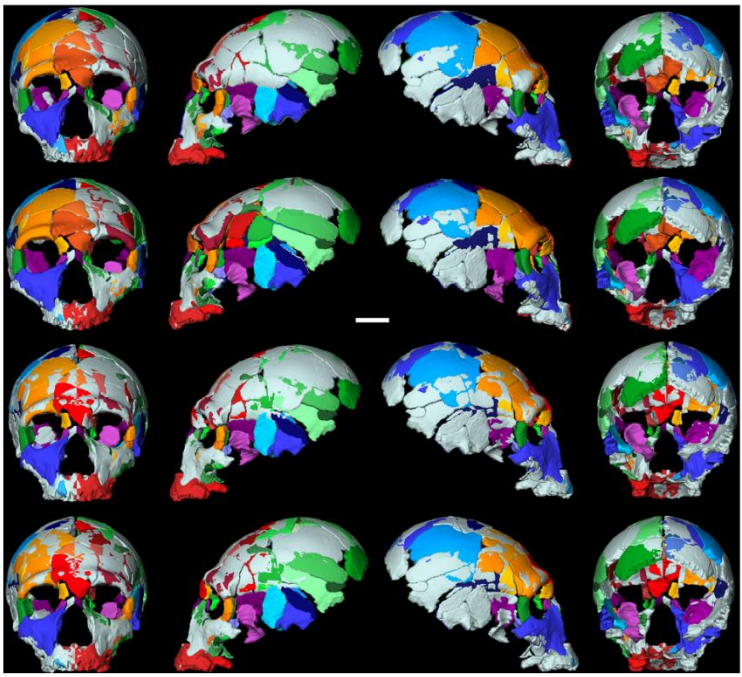

Extended Data Fig. 4 | Four manual reconstructions of Apidima 2. Top row, reconstruction 1 (made by C.R., mirroring criterion). Second row, reconstruction (made by C.R., smoothness criterion). Third row, reconstruction 3 (made by A.B., mirroring criterion). Bottom row, reconstruction 4 (made by A.B., smoothness criterion). Scale bar, 3 cm.

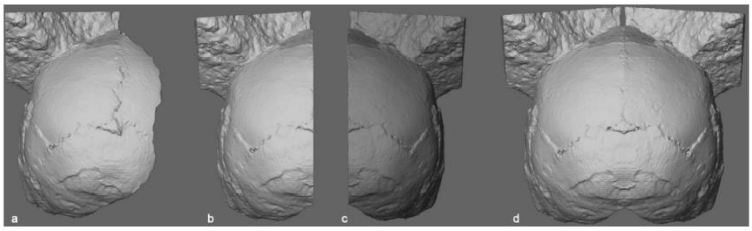

Extended Data Fig. 5 | Main steps of reconstruction of Apidima 1. a–d, Images are the computed surface of the original fossil (**a**), the cropped scan volume (**b**), the duplicated and mirrored scan volume (**c**) and the complete reconstruction (**d**).

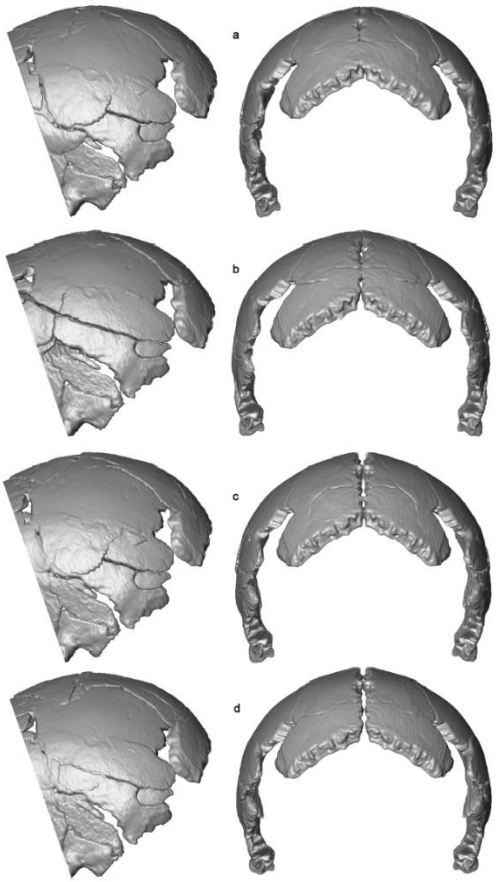

Extended Data Fig. 6 | Lateral and posterior views of the parietal region of the four manual reconstructions of Apidima 2. Images as shown in Extended Data Fig. 4. **a**, Reconstruction 1 (made by C.R., mirroring criterion). **b**, Reconstruction 2 (made by C.R., smoothness criterion). **c**, Reconstruction 3 (made by A.B., mirroring criterion). **d**, Reconstruction 4 (made by A.B., smoothness criterion).

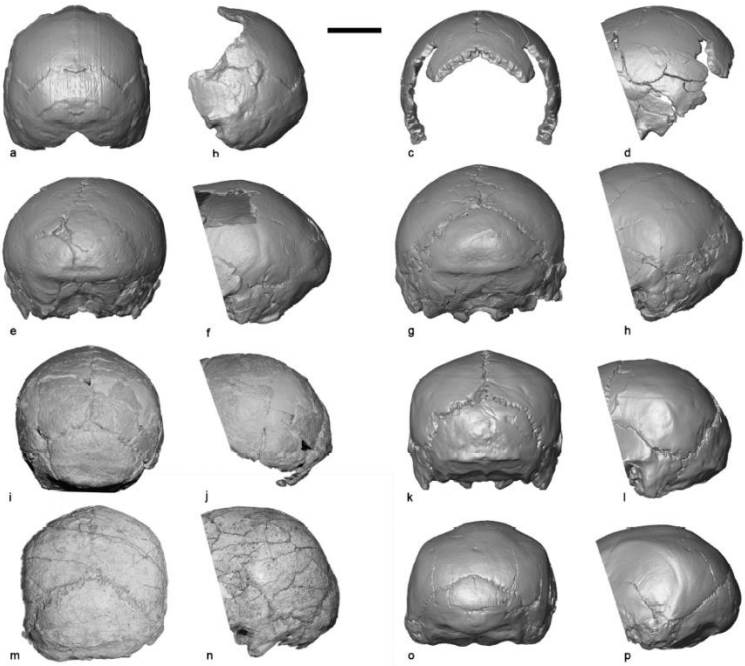

Extended Data Fig. 7 | Posterior cranial morphology. a, **b**, Posterior and lateral views of the Apidima 1 reconstruction. **c**, **d**, Posterior and lateral views of Apidima 2 reconstruction 1. **e**, **f**, Posterior and lateral views of the three-dimensional model of La Chapelle-aux-Saints (Neanderthal). **g**, **h**, Posterior and lateral views of the three-dimensional model of La Ferrassie 1 (Neanderthal). **e**–**h**, Images courtesy of A. Balzeau (MHNH). **i**, **j**, Posterior and lateral views of Elandsfontein (MPA). Images courtesy of C.S. **k**, **l**, Posterior and lateral views of the three-dimensional model of Sima de los Huesos Cranium 5, cast (MPE). Images courtesy of E. Delson (NYCEP). **m**, **n**, Posterior and lateral views of Skhul 5 (*H. sapiens*). Images courtesy of C.S. **o**, **p**, Posterior and lateral views of the three-dimensional model of Eliye Springs (MPA). Images reproduced with permission from https://africanfossils.org/. Scale bar, 5 cm.

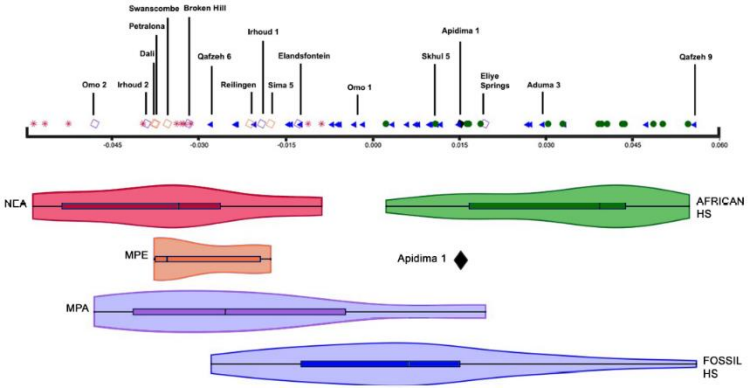

Extended Data Fig. 8 | Midsagittal profile shape index. Values calculated from the dataset used in analysis 4 (midsagittal posterior cranial profile), based on the axis between the mean Neanderthal and mean modern African shape. Apidima 1 and the remaining fossil samples are projected onto this axis. Violins extend from the minimum to the maximum value; boxes show the 25–75% quartiles and lines indicate the median. Samples as in Fig. 3b, symbols as in Fig. 2; modern Africans, green dots (n = 15).

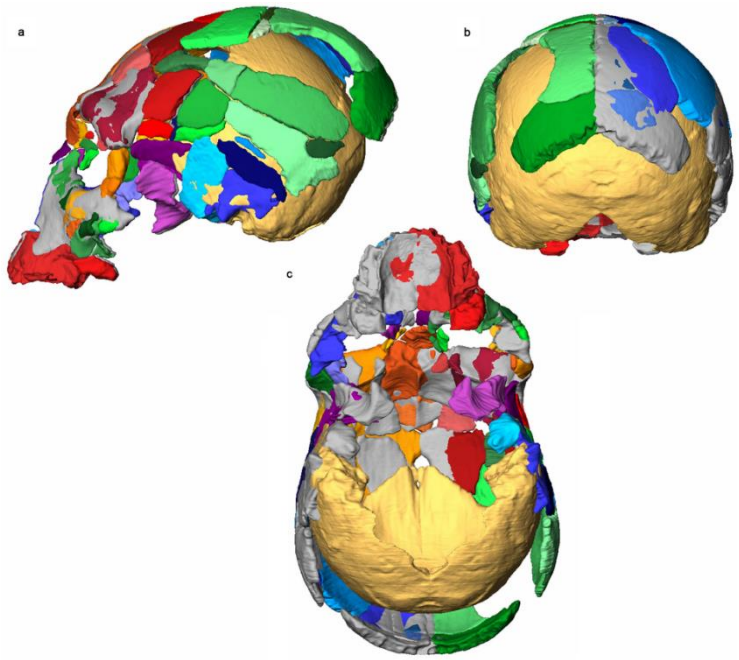

Extended Data Fig. 9 | Apidima 1 reconstruction superimposed manually with Apidima 2 reconstruction 1. Aidima 1 is shown in yellow; Apidima 2 is shown in rainbow. **a**, Lateral view. **b**, Posterior view. **c**, Ventral view.

Extended Data Table 1 | Classification results. Classification of Apidima 1 and Apidima 2 reconstructions and posterior probabilities for analyses 1–5. HS, *H. sapiens*; NEA, Neanderthal.

		Posterior probability of membership in:			
ANALYSIS 1 - APIDIMA 2 FACE	**Classified as:**	**HS**	**MPA**	**MPE**	**NEA**
Apidima 2 Reconstruction 1	**NEA**	0.0000	0.0073	0.2327	**0.7600**
Apidima 2 Reconstruction 2	**MPE**	0.0000	0.0078	**0.6649**	0.3273
Apidima 2 Reconstruction 3	**NEA**	0.0000	0.0106	0.2276	**0.7618**
Apidima 2 Reconstruction 4	**NEA**	0.0000	0.0068	0.1737	**0.8195**
Apidima 2 Reconstruction Mean	**NEA**	0.0000	0.0087	0.3050	**0.6863**
ANALYSIS 2 - APIDIMA 2 NEUROCRANIUM	**Classified as:**	**HS**	**MPA**	**MPE**	**NEA**
Apidima 2 Reconstruction 1	**NEA**	0	0	0.1163	**0.8837**
Apidima 2 Reconstruction 2	**NEA**	0	0.0001	0.3414	**0.6585**
Apidima 2 Reconstruction 3	**NEA**	0	0	0.0366	**0.9634**
Apidima 2 Reconstruction 4	**NEA**	0	0	0.0872	**0.9128**
Apidima 2 Reconstruction Mean	**NEA**	0	0	0.1124	**0.8876**
ANALYSIS 3 - APIDIMA 1 NEUROCRANIUM	**Classified as:**	**HS**	**MPA**	**MPE**	**NEA**
Apidima 1 Reconstruction	**HS**	**1**	0	0	0
ANALYSIS 4 - APIDIMA 1 MIDSAGITTAL	**Classified as:**	**HS**	**MPA**	**MPE**	**NEA**
Apidima 1 Reconstruction	**HS**	**0.9340**	0.0123	0.0480	0.0056
ANALYSIS 5 - COMBINED APIDIMA 1 AND 2	**Classified as:**	**HS**	**MPA**	**MPE**	**NEA**
Apidima 2 Reconstruction 1	**NEA**	0.0304	0.0121	0.0005	**0.9570**
Apidima 2 Reconstruction 2	**NEA**	0	0.001	0.0888	**0.9101**
Apidima 2 Reconstruction 3	**NEA**	0.0001	0.0004	0.0008	**0.9986**
Apidima 2 Reconstruction 4	**NEA**	0.0012	0.0014	0.0002	**0.9972**
Apidima 2 Reconstruction Mean	**NEA**	0.0002	0.0018	0.0017	**0.9963**
Apidima 1 Reconstruction	**HS**	**0.9204**	0.0796	0	0

Supplementary Data

1.Uranium-Series dating

We analyzed samples from the 'skull breccia', selected from fragments produced in the process of cleaning the specimens from the matrix, with the U-series method. These included human bone fragments (subsamples 3720A, B, Apidima 2, and subsamples 3754, 3755, Apidima 1) and four unidentified bone subsamples (3757A-C, 3758, see Supplementary Fig. 1). The Apidima 1 remains have shiny, somewhat translucent and seemingly mineralised surfaces, as had the subsamples3757B and C. The fragments from Apidima 2 have matte, soft surfaces, as had subsamples3757A and 3758.The analyses followed the procedures described in detail in 49. All isotope ratios in this paper are activity ratios. U-series age results on bones are generally regarded as minimum age results. Thus, all individual age estimates reported here are apparent closed system ages. The initial 234U/238U ratio (234U/238Ui) can be used to identify whether the source for the uranium in a bone has remained the same or may have changed, or whether there are different U-sources involved for the various materials analyzed. The earlier analysis of a larger cranial fragment of Apidima 2 was carried out in 2010 and published in 5. The detailed analyses are shown in Supplementary Table 1 and Supplementary Fig. 2.

The two matrix sections 3720A and B show generally low 234U/238U ratios in the range of 1.09 to 1.11 and finite ages of around 150 ka (using a Th correction with an elemental Th/U ratio of 4.25 50, see Supplementary Fig. 2E). This points to a calcification event around this time. The initial average 234U/238U ratios of the two sections are closely similar around 1.18 to 1.19. There are no relationships between measured 234U/238U ratios and age or U-concentrations and age (Supplementary Fig. 2A, B), indicating that no partial leaching or secondary U-overprint has occurred.

For discussing the various U-migration effects in the skeletal material, it is beneficial to start with the bone samples 3757A-C and 3758. The matte samples 3757A and 3758 show age results around 150 to 160 ka (Supplementary Fig. 2C, D). Sample 3758 has relatively low 234U/238U ratios of around 1.14, with 234U/238Ui ratios of ~1.22. 3758 shows no relationships between age and 234U/238U ratios or U-concentration. Sample 3757A has a similarly low measured 234U/238U ratios (~1.14) with 234U/238Ui ratios of ~1.22. However, the range of the 234U/238U ratios and U-concentrations in the individual analysis spots are much wider than for 3758 (Supplementary Fig. 2C, D) and there are also trends between ages and measured 234U/238U ratios or U-concentrations. The ages become younger with lower 234U/238U ratios

as well as lower U-concentrations. The U-source for any secondary U-uptake event after the calcification of the breccia at around 150 ka would be located in the matrix, which has lower 234U/238U ratios than the bones. In other words, overprints with U from the breccia will lead to lower ages and 234U/238U ratios. Secondly, sample 3757 has domains with calcitic fillings (Supplementary Fig. 1, on the left side of the specimen), which have lower U-concentrations. Analysis # 7 has by far the lowest U-concentrations, a lower than average 234U/238U ratio and the youngest age. The lower U-concentration is most likely the result of pores filled with secondary calcite containing uranium derived from the matrix.

The "shiny" samples 3757B and C have generally higher measured 234U/238U ratios than the previous two and significantly older ages. Sample 3757C has 234U/238U ratios of around 1.22, with 234U/238Ui of ~1.43. The apparent ages are around 240 ka. Analyses #1 and #2 show signs of leaching and #10 secondary U-overprint. However, the overprint seems to have taken place before the sample was embedded in the matrix, as this analysis points to an uranium source with a much higher 234U/238U ratio (~1.34) than that of the matrix. Excluding this value from the average has little effect, as the U-concentrations are low. Sample 3757B has 234U/238U ratios of around 1.20, with 234U/238Ui ratios of ~1.38. While there is nearly no relationship between age and measured 234U/238U ratio, there is a clear relationship between age and U-concentration (Supplementary Fig. 2D). This may be explained with secondary fillings, however, with 234U/238Ui ratios significantly higher than the matrix.

The bone samples show that samples of different ages and U-isotope signatures are present in the matrix. The "shiny" samples 3757B and C accumulated their U-signature in a different environment from the breccia, well before the matrix was solidified. The "matte" samples 3757A and 3758 may have accumulated their U from a similar source as the breccia, perhaps while the latter was still uncemented. Only sample, 3757Aseems to have had any direct U-exchange with the matrix.

The results for Apidima 1 and 2 are strikingly different. The previously analyzed specimen from Apidima 2 5 had all finite ages and no relationships between apparent age and U-concentration or measured 234U/238U ratio (Supplementary Fig. 2E, F). The average measured 234U/238U ratio is 1.16 with an average age of 172±11 and a 234U/238Ui of 1.27. The analyses of the bone in 3720A fall well into this range (Supplementary Fig. 2E, F).

In contrast, sample 3754 from Apidima 1 showed mostly leaching effects (230Th/238U » 234U/238U) and sample 3758 showed widely varying results. The U-concentrations in Apidima 1 are significantly lower

than of Apidima 2 and most of the 234U/238U ratios are much higher (SupplementaryFig. 2E, F). The results derived from the analyses #7 to 24 show norelationship between age and Th/U ratio. The average 234U/238U ratio of this section is ~1.30 with an age of 211±16 ka and an 234U/238Ui of 1.54. Analyses #25 to 30 return much lower ages and also lower 234U/238U ratios, which indicates a secondary overprint from a U-source with a much lower 234U/238U ratio. Considering the randomness of the U-results (see analytical results for #21-23, Supplementary Table 1), the variability of analytical results within section #7-24 is likely due to U-micro-migration 51.

Supplementary Table 1: Detailed U-series results. Separate table for each sample.

3754	U (ppm)	Th (ppb)	U/Th	$^{230}Th/^{238}U$	$^{230}Th/^{238}U$ error	$^{234}U/^{238}U$	$^{234}U/^{238}U$ error	Age (ka)	Age error (ka)
1	2.29	2.9	789	1.0944	0.0500	1.2712	0.0326	187.9	25.0
2	2.34	2.3	1000	1.1707	0.0471	1.2425	0.0283	245.1	39.7
3	1.85	2.8	659	1.2487	0.0569	1.2982	0.0410	254.9	51.9
4	1.76	2.6	685	1.4573	0.0566	1.2909	0.0291	leaching	
5	1.83	2.8	656	1.4642	0.0482	1.3330	0.0378	580.9	593.3
6	1.69	3.6	475	1.6054	0.0615	1.3315	0.0331	leaching	
7	1.99	2.2	919	1.6106	0.0690	1.3283	0.0359	leaching	
8	1.84	4.2	437	1.6004	0.0588	1.3310	0.0337	leaching	
9	1.75	3.8	456	1.6577	0.0658	1.3585	0.0249	leaching	
10	1.98	2.7	736	1.7474	0.0458	1.4114	0.0252	leaching	
11	1.70	2.1	800	1.6777	0.0578	1.3428	0.0270	leaching	
12	2.04	4.0	505	1.8493	0.0585	1.3706	0.0287	leaching	
13	1.85	5.0	374	1.7861	0.0566	1.3814	0.0269	leaching	
14	1.29	29.4	44	1.7660	0.0649	1.3676	0.0348	leaching	
15	1.16	19.6	59	1.5507	0.0772	1.3526	0.0306	leaching	
16	1.44	5.9	244	1.7192	0.0644	1.3826	0.0307	leaching	
17	0.87	8.0	109	1.6038	0.0862	1.3518	0.0433	leaching	
18	0.78	6.9	113	1.6023	0.1327	1.3775	0.0380	leaching	
19	1.44	6.6	216	1.6883	0.0621	1.3817	0.0244	leaching	
20	1.40	4.4	319	1.7484	0.0557	1.3748	0.0267	leaching	
21	0.54	8.3	65	1.6018	0.1572	1.3530	0.0545	leaching	
22	1.29	4.6	278	1.6875	0.0688	1.3913	0.0361	leaching	
23	1.34	4.7	285	1.5609	0.0680	1.3486	0.0250	leaching	
24	1.21	28.1	43	1.4721	0.0671	1.3333	0.0325	663.5	1231.1
25	1.03	15.2	68	0.5688	0.0555	1.1809	0.0369	70.2	10.0

3720B	U (ppm)	Th (ppb)	U/Th	$^{230}Th/^{238}U$	$^{230}Th/^{238}U$ error	$^{234}U/^{238}U$	$^{234}U/^{238}U$ error	Age (ka)	Age error (ka)
1	0.48	486	0.99	0.8988	0.0337	1.0663	0.0259	193.9	24.8
2	0.80	1192	1.64	0.8208	0.0337	1.0580	0.0207	159.1	16.7
3	1.73	1292	1.45	0.8085	0.0245	1.0820	0.0149	145.7	10.2
4	0.97	961	0.75	0.7603	0.0259	1.0714	0.0252	132.0	11.0
5	0.58	386	0.60	0.9211	0.0315	1.0931	0.0225	191.0	21.1
6	5.48	919	14.23	0.8860	0.0247	1.1144	0.0107	164.6	11.1
7	3.79	722	4.13	0.8457	0.0162	1.1193	0.0150	147.3	7.4
8	1.70	1604	2.36	0.8371	0.0251	1.0802	0.0187	157.4	12.5
9	0.47	470	0.29	0.9049	0.0378	1.0724	0.0215	193.8	25.0
10	1.34	954	2.86	0.8604	0.0227	1.0780	0.0162	168.3	12.4
11	5.79	995	6.07	0.9295	0.0127	1.1540	0.0092	167.2	6.2
12	4.76	1694	4.78	0.8597	0.0204	1.1103	0.0131	155.5	9.1
13	1.32	1287	0.78	0.8681	0.0221	1.0824	0.0142	169.9	11.9
AVERAGE VALUES									
	initial $^{234}U/^{238}U$	$^{234}U/^{238}Ui$ Error		$^{230}Th/^{238}U$	$^{230}Th/^{238}U$ error	$^{234}U/^{238}U$	$^{234}U/^{238}U$ error	Age (ka)	Age error (ka)
1-13	1.1723	0.0117		0.8705	0.0177	1.1097	0.0085	160.0	7.8
Th/U=4.25 correction	1.1872	0.0122		0.8551	0.0174	1.1228	0.0086	149.6	6.9

3720A	U (ppm)	Th (ppb)	U/Th	$^{230}Th/^{238}U$	$^{230}Th/^{238}U$ error	$^{234}U/^{238}U$	$^{234}U/^{238}U$ error	Age (ka)	Age error (ka)
1	7.20	4	1637	0.9148	0.0133	1.1237	0.0067	173.2	6.6
2	6.15	13	459	0.8863	0.0150	1.1250	0.0063	160.7	6.4
3	7.46	18	421	0.8451	0.0092	1.1266	0.0066	144.9	3.8
4	1.96	1201	1.64	0.7896	0.0185	1.0816	0.0182	139.0	8.4
5	1.66	1519	1.09	0.8126	0.0211	1.0727	0.0125	150.3	9.3
6	1.43	1615	0.89	0.8436	0.0255	1.0763	0.0330	161.6	17.1
7	1.83	1643	1.11	0.8007	0.0227	1.0688	0.0317	147.1	13.6
8	1.65	1674	0.99	0.8607	0.0228	1.0696	0.0278	172.2	16.7
9	4.48	20279	0.22	1.0866	0.0603	1.0734	0.0194	465.7	403.8
10	2.13	3754	0.57	0.8765	0.0233	1.0659	0.0201	181.9	16.0
11	5.16	984	5.24	0.8949	0.0199	1.1224	0.0064	165.1	8.6
AVERAGE VALUES									
	initial $^{234}U/^{238}U$	$^{234}U/^{238}Ui$ Error		$^{230}Th/^{238}U$	$^{230}Th/^{238}U$ error	$^{234}U/^{238}U$	$^{234}U/^{238}U$ error	Age (ka)	Age error (ka)
1-3	1.1958	0.0113		0.8813	0.0177	1.1251	0.0078	158.7	7.4
4-11, not 9	1.1405	0.0139		0.8525	0.0180	1.0894	0.0096	160.3	8.3
Th/U=4.25 correction	1.1824	0.0110		0.8572	0.0167	1.1189	0.0077	151.6	6.7

3755	U (ppm)	Th (ppb)	U/Th	$^{230}Th/^{238}U$	$^{230}Th/^{238}U$ error	$^{234}U/^{238}U$	$^{234}U/^{238}U$ error	Age (ka)	Age error (ka)
1	1.69	189.6	9	1.1798	0.0493	1.2848	0.0309	221.7	32.5
2	1.34	122.8	11	1.4868	0.0835	1.3139	0.0295	0.0	0.0
3	1.16	147.0	8	1.3513	0.1079	1.3134	0.0302	333.5	147.5
4	0.37	112.9	3	0.4089	0.0746	1.1275	0.0499	48.7	11.5
5	0.95	41.9	23	1.7144	0.1096	1.3643	0.0414	0.0	0.0
6	1.11	231.1	5	1.4743	0.0952	1.3021	0.0314	0.0	0.0
7	1.06	78.2	14	1.1760	0.0857	1.2783	0.0393	223.6	53.3
8	1.71	5.6	305	1.3117	0.0894	1.2815	0.0292	334.8	131.9
9	1.46	10.1	144	1.3370	0.0670	1.3431	0.0299	281.6	62.4
10	1.88	7.0	270	1.1421	0.0667	1.3033	0.0411	194.2	33.5
11	0.34	15.0	22	1.1179	0.1501	1.3030	0.0639	184.5	63.9
12	0.91	9.3	97	1.2649	0.0862	1.3029	0.0328	262.6	69.9
13	1.57	55.2	28	1.1765	0.0572	1.2976	0.0324	212.8	33.3
14	2.07	12.3	169	1.1799	0.0607	1.2875	0.0282	220.2	36.4
15	1.45	5.0	287	1.2678	0.0775	1.3580	0.0486	225.8	48.6
16	1.90	6.3	301	1.1022	0.0478	1.2861	0.0312	185.0	22.9
17	1.45	7.2	201	1.1604	0.0865	1.2951	0.0376	206.3	45.0
18	1.61	15.3	105	1.2307	0.0548	1.3091	0.0228	235.3	35.7
19	1.47	19.1	77	1.2467	0.0715	1.3159	0.0291	240.3	47.9
20	1.60	3.5	458	1.0039	0.0631	1.2732	0.0377	154.4	22.6
21	1.53	3.7	416	1.1671	0.0983	1.3106	0.0267	201.9	45.8
22	1.15	2.7	424	1.3505	0.0752	1.3102	0.0346	337.8	116.7
23	2.51	8.0	314	0.9462	0.0504	1.2527	0.0202	142.4	15.6
24	1.95	5.8	338	1.1390	0.0870	1.2984	0.0361	195.1	40.7
25	3.56	9.6	370	0.7076	0.0344	1.2206	0.0155	91.4	7.0
26	2.61	13.9	188	0.6326	0.0568	1.2206	0.0203	77.5	10.1
27	1.77	58.6	30	0.3930	0.0700	1.1955	0.0240	43.0	9.3
28	1.90	64.9	29	0.3982	0.0690	1.1616	0.0328	45.3	9.8
29	2.04	59.7	34	0.3804	0.0664	1.1878	0.0230	41.6	8.8
30	1.47	66.3	22	0.1970	0.0300	1.1546	0.0207	20.3	3.4
AVERAGE VALUES									
	initial $^{234}U/^{238}U$	$^{234}U/^{238}Ui$ Error		$^{230}Th/^{238}U$	$^{230}Th/^{238}U$ error	$^{234}U/^{238}U$	$^{234}U/^{238}U$ error	Age (ka)	Age error (ka)
1-6	1.8631	0.2049		1.3625	0.0463	1.3025	0.0170	371.5	90.8
7-24	1.5400	0.0253		1.1725	0.0295	1.2980	0.0124	210.6	15.8
25-30	1.2305	0.0146		0.4958	0.0278	1.1960	0.0127	57.4	4.3

3757A	U (ppm)	Th (ppb)	U/Th	$^{230}Th/^{238}U$	$^{230}Th/^{238}U$ error	$^{234}U/^{238}U$	$^{234}U/^{238}U$ error	Age (ka)	Age error (ka)
1	4.32	2.1	2085	0.8621	0.0319	1.1330	0.0244	148.9	13.7
2	3.79	1.4	2787	0.8072	0.0381	1.0918	0.0344	142.1	17.0
3	2.99	1.3	2269	0.8044	0.0361	1.1119	0.0216	135.4	13.1
4	3.77	1.4	2627	0.8582	0.0354	1.1317	0.0196	147.9	13.9
5	2.95	0.8	3674	0.8677	0.0354	1.1488	0.0480	146.0	18.6
6	4.24	1.5	2851	0.9103	0.0327	1.1476	0.0177	161.9	14.3
7	0.75	0.4	1901	0.6797	0.0515	1.1091	0.0396	101.3	14.0
8	5.51	1.5	3636	0.9280	0.0358	1.1573	0.0269	165.3	17.4
9	3.79	1.0	3800	0.9549	0.0364	1.1737	0.0162	169.9	16.0
10	2.35	2.4	971	0.8680	0.0591	1.1388	0.0358	149.1	23.7
11	1.52	0.9	1628	0.7889	0.0497	1.1442	0.0251	122.9	14.9
12	3.78	1.0	3774	0.9188	0.0330	1.1648	0.0198	159.1	14.0
13	4.05	1.8	2272	0.8924	0.0350	1.1538	0.0225	153.1	14.5
14	5.09	2.3	2258	0.9026	0.0363	1.1332	0.0193	164.2	16.4
AVERAGE VALUES									
	initial $^{234}U/^{238}U$	$^{234}U/^{238}Ui$ Error		$^{230}Th/^{238}U$	$^{230}Th/^{238}U$ error	$^{234}U/^{238}U$	$^{234}U/^{238}U$ error	Age (ka)	Age error (ka)
1-14	1.2173	0.0154		0.8796	0.0205	1.1413	0.0110	152.5	8.2

3758	U (ppm)	Th (ppb)	U/Th	$^{230}Th/^{238}U$	$^{230}Th/^{238}U$ error	$^{234}U/^{238}U$	$^{234}U/^{238}U$ error	Age (ka)	Age error (ka)
1	6.44	5.7	1134	0.9247	0.0280	1.1435	0.0134	169.3	12.9
2	6.75	0.7	9253	0.9274	0.0254	1.1409	0.0267	171.4	15.4
3	6.35	0.6	11380	0.9259	0.0297	1.1465	0.0247	168.6	15.7
4	5.99	0.1	80040	0.8959	0.0257	1.1275	0.0176	163.6	12.4
5	6.05	-0.3	-17945	0.9008	0.0294	1.1501	0.0139	157.4	12.0
6	5.72	0.0	343113	0.9128	0.0276	1.1505	0.0169	161.8	12.3
7	5.66	-0.4	-14524	0.8966	0.0293	1.1409	0.0211	159.0	13.5
8	5.48	0.5	11876	0.9169	0.0287	1.1460	0.0243	165.1	14.7
9	5.88	-0.1	-73613	0.9103	0.0241	1.1430	0.0142	163.6	11.0
10	5.79	0.3	19177	0.8805	0.0238	1.1259	0.0152	158.1	10.7
11	5.84	-0.3	-22630	0.8851	0.0246	1.1345	0.0153	156.8	10.7
12	4.68	0.8	5952	0.8987	0.0306	1.1328	0.0201	162.7	14.4
13	6.12	0.2	28012	0.9010	0.0294	1.1610	0.0156	153.8	11.7
14	5.74	1.1	5248	0.9068	0.0322	1.1647	0.0127	154.7	12.3
15	5.61	3.1	1822	0.8758	0.0208	1.1349	0.0166	153.2	9.4

AVERAGE VALUES									
	initial $^{234}U/^{238}U$	$^{234}U/^{238}Ui$ Error		$^{230}Th/^{238}U$	$^{230}Th/^{238}U$ error	$^{234}U/^{238}U$	$^{234}U/^{238}U$ error	Age (ka)	Age error (ka)
1-15	1.2255	0.0139		0.9048	0.0196	1.1430	0.0096	161.4	8.4

3757B	U (ppm)	Th (ppb)	U/Th	$^{230}Th/^{238}U$	$^{230}Th/^{238}U$ error	$^{234}U/^{238}U$	$^{234}U/^{238}U$ error	Age (ka)	Age error (ka)
1	5.79	14.0	414	1.0870	0.0353	1.1667	0.0191	247.1	32.7
2	5.59	1.5	3648	1.0879	0.0254	1.1557	0.0189	258.5	29.6
3	5.74	1.8	3173	1.0827	0.0274	1.1517	0.0161	258.0	29.3
4	4.19	1.1	3881	1.0621	0.0281	1.1758	0.0204	222.5	22.7
5	4.14	1.0	3942	1.1373	0.0300	1.2053	0.0247	251.8	32.0
6	3.88	1.5	2602	1.1097	0.0340	1.2298	0.0228	216.0	23.3
7	3.12	1.3	2831	1.0606	0.0369	1.2308	0.0184	190.9	18.6
8	3.15	1.6	2020	1.0495	0.0419	1.2076	0.0307	196.8	25.6
9	2.58	1.0	2561	1.0282	0.0431	1.2062	0.0213	187.6	21.7
10	2.80	3.2	885	1.0274	0.0572	1.2187	0.0421	181.7	29.9
11	4.10	7.7	530	1.1303	0.0430	1.1651	0.0179	289.5	54.4
12	4.22	1.8	2336	1.1755	0.0398	1.2270	0.0200	262.2	37.7
13	3.61	1.7	2105	1.1235	0.0310	1.2242	0.0219	227.7	24.3
14	2.82	1.5	1938	1.1568	0.0533	1.2177	0.0301	255.9	50.2
15	4.36	2.4	1842	1.1457	0.0297	1.2267	0.0255	240.2	28.3
16	2.94	3.4	860	0.9907	0.0394	1.1905	0.0249	177.9	19.7
17	3.08	3.2	958	0.8919	0.0392	1.1405	0.0249	157.3	17.1
18	1.08	28.7	38	0.8778	0.0641	1.1605	0.0410	146.0	24.6
19	3.27	2.8	1187	1.0132	0.0331	1.2038	0.0226	182.0	17.2
20	0.91	3.2	285	0.7754	0.0602	1.1637	0.0326	115.3	16.6
AVERAGE VALUES									
	initial $^{234}U/^{238}U$	$^{234}U/^{238}Ui$ Error		$^{230}Th/^{238}U$	$^{230}Th/^{238}U$ error	$^{234}U/^{238}U$	$^{234}U/^{238}U$ error	Age (ka)	Age error (ka)
1-20	1.3568	0.0186		1.0744	0.0233	1.1923	0.0102	219.0	15.5
1-15	1.3774	0.0210		1.1001	0.0241	1.1956	0.0105	233.0	18.0
16-20	1.2780	0.0213		0.9398	0.0273	1.1754	0.0151	163.3	11.7

3757C	U (ppm)	Th (ppb)	U/Th	$^{230}Th/^{238}U$	$^{230}Th/^{238}U$ error	$^{234}U/^{238}U$	$^{234}U/^{238}U$ error	Age (ka)	Age error (ka)
1	3.44	3.0	1130	1.3484	0.0361	1.2342	0.0199	leaching	
2	3.86	1.8	2086	1.2763	0.0526	1.2060	0.0205	507.9	368.5
3	4.63	1.3	3498	1.1594	0.0397	1.2312	0.0209	246.2	33.0
4	3.50	1.6	2212	1.1546	0.0363	1.2326	0.0244	241.8	31.3
5	2.83	2.5	1112	1.1506	0.0414	1.2191	0.0340	249.9	42.6
6	2.79	3.2	872	1.1245	0.0529	1.2298	0.0243	224.5	35.3
7	2.67	2.9	921	1.0918	0.0438	1.2020	0.0315	223.1	34.1
8	2.40	1.8	1301	1.0997	0.0329	1.1832	0.0295	242.5	34.7
9	2.60	3.4	766	1.1413	0.1722	1.2079	0.0617	252.7	144.8
10	1.96	4.1	479	1.0576	0.0550	1.3446	0.1984	151.3	52.9
AVERAGE VALUES									
	initial $^{234}U/^{238}U$	$^{234}U/^{238}U$i Error		$^{230}Th/^{238}U$	$^{230}Th/^{238}U$ error	$^{234}U/^{238}U$	$^{234}U/^{238}U$ error	Age (ka)	Age error (ka)
1-10	1.4754	0.0405		1.1809	0.0317	1.2182	0.0132	275.8	32.9
3-9	1.4289	0.0324		1.1355	0.0341	1.2178	0.0151	240.1	26.3

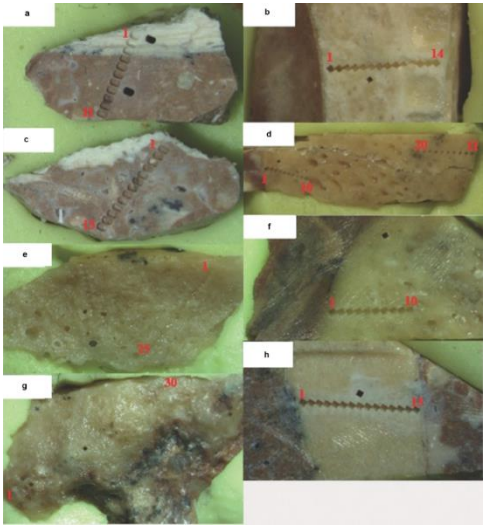

Supplementary Figure 1: Position of laser spots for U-series analyses: a, c, Breccia samples with remains of Apidima 2. e, g, Small sections of Apidima 1. b, d, f, h, Bone cross sections embedded in the breccia.

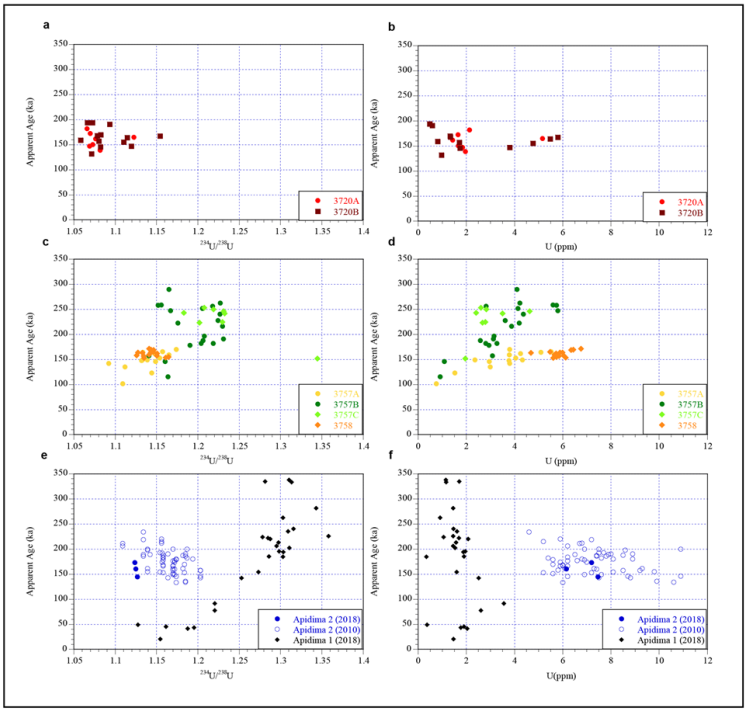

Supplementary Figure 2: Results of U-series analyses. a, c, e, measured $^{234}U/^{238}U$ ratios vs age. **b, d, f,** U-concentration vs age for breccia (A, B), faunal bones (C, D) and hominid samples (E, F).

2. Overall morphologyand linear measurements of the Apidima crania

Apidima 2 (Fig 1a-c, Extended Data Fig. 2) is the more complete and better known of the Apidima specimens. It preserves an almost complete face and most of the vault, but lacks the occipital bone and most of the cranial base and shows taphonomic distortions. Most of the temporal bone on the left side, and part of the right temporal squama, as well as the greater wings of the sphenoid on either side, are present, while the parietals are nearly complete but laterally fragmented. The thickness of its cranial bones (at bregma = 8 mm; at lambda = 8.3 mm), falling near the upper limit and close to the mean of the adult Neanderthal ranges, respectively52,53, its well-developed supraorbital torus (thickness at mid orbit = 11.9 mm, within the Neanderthal range10), and its overall dimensions indicate that Apidima 2 is adult.

Apidima 1 (Fig. 1d-f) preserves most of the left parietal and temporal bones, part of the left occipitomastoid region, broken anteriorly and inferiorly; the posterior part of the left temporal squama; a fragment of the right parietal along the sagittal suture; and a large portion of the occipital, mainly on the left. A large stone is attached to it anteriorly on the left. It is probably also adult: its bone thickness (at inion = 9.3 mm; at lambda = 7.9 mm) is well within the reported adult Neanderthal ranges53,54. In its linear measurements (Supplementary Table 3), the Apidima 1 specimen falls mainly in the region of overlap among taxa. However its maximum cranial breadth is relatively small, overlapping only with our H. Sapiens sample. Its bi-auricular breadth overlaps with the ranges of all comparative samples except Middle Pleistocene Europeans. The height of the occipital plane(lambda-inion) is small, an ancestral feature most similar here to the Middle Pleistocene samples.

Supplementary Table 2. Linear measurements (in mm)*, Apidima 2 reconstructions

Variable name (Howells's)[1]	Apidima 2 (recon-structed)[2]		Middle Pleistocene Eurasians	Middle Pleistocene Africans	Neanderthals	*H. sapiens*
Maximum cranial breadth (XCB)	**147.0 ± 2.65**	**Mean ± s.d.**	147.87 ± 8.52	145.35 ± 5.63	148.21 ± 6.18	140.93 ± 7.22
		Range	164.00-136.00	154.45-137.75	158.50-138.00	155.00-126.00
		N	7	7	12	34
Maximum frontal breadth (XFB)	**124.42 ± 2.49**	**Mean ± s.d.**	119.00 ± 3.04	117.43 ± 2.51	120.80 ± 5.51	119.41 ± 4.27
		Range	126.00-115.00	120.00-113.00	128.00-110.00	128.00-112.00
		N	9	7	15	27
Biauricular breadth (AUB)	**129.68 ± 4.33**	**Mean ± s.d.**	146.26 ± 6.76	136.09 ± 10.75	133.08 ± 10.58	128.13 ± 7.08
		Range	152.95-139.00	148.00-122.99	155.00-118.00	139.00-113.00
		N	4	6	13	29
Nasion-prosthion height (NPH)	**82.07 ± 0.93**	**Mean ± s.d.**	89.50 ± 6.36	84.97 ± 8.63	85.32 ± 5.86	69.28 ± 6.21
		Range	94.00-85.00	90.00-75.00	94.00-75.20	79.00-58.00
		N	2	3	10	27
Nasal height (NLH)	**65.70 ± 1.52**	**Mean ± s.d.**	57.33 ± 8.15	53.73 ± 8.21	62.05 ± 2.83	51.32 ± 3.90
		Range	65.50-49.20	62.00-43.50	68.50-58.00	60.20-42.70
		N	3	4	10	26
Orbit height (OBH)	**38.91 ± 0.77**	**Mean ± s.d.**	34.75 ± 1.26	36.75 ± 2.36	36.54 ± 1.07	31.41 ± 2.30
		Range	36.00-33.00	38.50-33.50	38.00-34.00	36.00-27.00
		N	4	4	11	29
Orbit breadth (OBB)	**49.68 ± 1.81**	**Mean ± s.d.**	43.62 ± 3.40	46.20 ± 2.48	44.07 ± 2.19	41.62 ± 2.72
		Range	48.00-39.40	48.50-43.30	47.00-39.50	47.00-37.00
		N	5	4	11	28
Nasal breadth (NLB)	**39.60 ± 1.13**	**Mean ± s.d.**	36.17 ± 2.25	33.52 ± 5.48	32.31 ± 3.34	26.57 ± 2.99
		Range	38.50-34.00	42.50-28.00	38.50-27.50	32.00-21.40
		N	3	5	10	26

Supplementary Table 2 continued.

Variable name (Howells's)[1]	Apidima 2 (recon-structed)[2]		Middle Pleistocene Eurasians	Middle Pleistocene Africans	Neanderthals	*H. sapiens*
External palate breadth (MAB)	**71.31 ± 1.57**	**Mean ± s.d.**	79.6 ± 7.23	78.25 ± 2.82	74.48 ± 4.97	65.62 ± 4.85
		Range	88.00-75.00	82.00-75.20	81.50-64.00	75.50-54.70
		N	3	4	12	26
Bimaxillary breadth (ZMB)	**114.53 ± 7.25**	**Mean ± s.d.**	110.60 ± 12.15	116.50 ± 12.01	11.54 ± 6.65	100.39 ± 6.68
		Range	119.00-93.00	130.00-107.00	120.00-100.00	114.00-88.00
		N	4	3	13	23
Zygomaxillary subtense (SSS)	**45.03 ± 0.75**	**Mean ± s.d.**	30.50 ± 6.36	32.67 ± 2.52	35,45 ± 3.86	24.34 ± 3.26
		Range	35.00-26.00	35.00-30.00	44.00-30.00	32.00-19.00
		N	2	3	11	21
Bifrontal breadth (FMB)	**112.99 ± 4.16**	**Mean ± s.d.**	113.75 ± 7.89	119.25 ± 7.24	114.16 ± 5.99	105.08 ± 7.00
		Range	126.00-103.50	130.00-110.00	125.00-100.00	120.00-90.00
		N	6	6	18	32
Nasio-frontal subtense (NAS)	**24.67 ± 1.33**	**Mean ± s.d.**	20.00 ± 2.53	20.50 ± 4.36	23.21 ± 3.96	16.73 ± 2.79
		Range	22.00-16.00	26.00-17.00	30.00-16.00	23.00-12.00
		N	6	4	14	30
Biorbital breadth (EKB)	**111.07 ± 2.12**	**Mean ± s.d.**	111.80 ± 9.47	119.75 ± 5.56	109.50 ± 6.69	104.72 ± 7.21
		Range	125.00-100.00	128.00-116.00	118.00-95.00	126.00-92.00
		N	5	4	12	25
Interorbital breadth (DKB)	**26.22 ± 1.80**	**Mean ± s.d.**	31.40 ± 5.59	32.40 ± 3.65	28.25 ± 4.50	23.29 ± 3.33
		Range	37.00-25.00	38.00-29.00	37.00-23.00	31.00-19.00
		N	5	5	12	21
Nasion-bregma chord (FRC)	**103.38 ± 2.56**	**Mean ± s.d.**	110.43 ± 6.35	114.25 ± 4.71	112.14 ± 7.03	114.24 ± 6.99
		Range	115.00-98.00	121.00-107.00	122.00-102.00	131.00-103.00
		N	7	8	14	33

Supplementary Table 2 continued.

Variable name (Howells's)[1]	Apidima 2 (recon-structed)[2]		Middle Pleistocene Eurasians	Middle Pleistocene Africans	Neanderthals	*H. sapiens*
Nasio-bregma subtense (FRS)	**12.27 ± 0.85**	**Mean ± s.d.**	24.00 ± 2.65	21.25 ± 3.54	19.93 ± 2.79	26.97 ± 2.43
		Range	26.00-29.00	26.00-16.00	24.00-15.00	33.00-23.00
		N	3	8	14	32
Bregma-lambda chord (PAC)	**108.51 ± 3.19**	**Mean ± s.d.**	105.70 ± 7.20	116.71 ± 4.50	108.08 ± 3.66	120.45 ± 5.30
		Range	119.00-95.00	122.00-109.00	113.00-103.00	129.00-107.00
		N	10	7	13	33
Bregma-lambda subtense (PAS)	**18.76 ± 1.04**	**Mean ± s.d.**	16.50 ± 2.08	18.71 ± 2.63	18.00 ± 2.65	24.5 ± 3.21
		Range	19.00-14.00	23.00-15.00	23.00-13.00	33.00-19.00
		N	4	7	13	32

1See Howells55.
2For each variable, this column presents the mean and standard deviation among the four reconstructions of Apidima 2 (see Materials and Methods).
*Data from CS and from Arsuaga et al.22, Ascenzi et al.56, White et al.57, Grine et al.58, Creveceur et al.59, Daura et al.60

Supplementary Table 3. Linear measurements (in mm)*, Apidima 1 reconstruction

Variable name (Howells's)[1]	Apidima 1		Middle Pleistocene Eurasians	Middle Pleistocene Africans	Neanderthals	*H. sapiens*
Maximum cranial breadth (XCB)	**134.85**	**Mean ± s.d.**	147.87 ± 8.52	145.35 ± 5.63	148.21 ± 6.18	140.9 ± 7.22
		Range	164.00-136.00	154.45-137.75	158.50-138.00	155.00-126.00
		N	7	7	12	34
Biauricular breadth (AUB)	**132.24**	**Mean ± s.d.**	146.26 ± 6.76	136.09 ± 10.75	133.08 ± 10.58	128.13 ± 7.08
		Range	152.95-139.00	148.00-122.99	155.00-118.00	139.00-113.00
		N	4	6	13	29
Biasteronic breadth (ASB)	**114.99**	**Mean ± s.d.**	120.26 ± 5.26	121.27 ± 4.49	120.29 ± 6.17	113.44 ± 6.85
		Range	132.00-113.50	129.00-116.43	131.00-110.00	132.00-99.70
		N	11	6	9	32
Lambda-Inion chord	**49.71**	**Mean ± s.d.**	59.68 ± 9.30	60.16 ± 3.73	60.94	61.99 ± 3.70
		Range	71.27-49.80	67.07-53.33	-	68.03-57.33
		N	5	8	20	6
Lambda-Inion arc	**53.19**	**Mean ± s.d.**	61.94 ± 8.64	63.57 ± 6.08	61.57	63.78 ± 4.01
		Range	73.36-53.00	71.56-54.86	-	68.32-57.72
		N	5	5	17	5
Lambda-Inion subtense	**6.78**	**Mean ± s.d.**	8.62 ± 3.72	10.55 ± 3.25	13.56	8.15 ± 0.73
		Range	11.64-4.46	13.93-5.50	-	9.11-7.36
		N	3	5	16	4

Supplementary Table 3 continued.

Variable name (Howells's)[1]	Apidima 1		Middle Pleistocene Eurasians	Middle Pleistocene Africans	Neanderthals	*H. sapiens*
Lambda-Inion chord / Lambda-Inion arc (%)	93.46	Mean ± s.d.	96.28 ± 2.47	94.91 ± 2.19	88.48	*96.61 ± 2.87*
		Range	99.92-94.00	97.21-91.81	-	*99.58-92.73*
		N	5	5	17	*5*
Lambda-Inion subtense / Lambda-Inion chord (%)	13.64	Mean ± s.d.	12.88 ± 5.00	17.31 ± 4.60	22.09	*13.12 ± 1.27*
		Range	16.33-7.15	22.94-10.31	-	*14.69-11.63*
		N	3	5	16	*4*

1see Howells55.

*Data from CS and from Hublin61, Wolpoff62, Arsuaga et al.22, Ascenzi et al.56, Verna et al.16, Rightmire63

3. Results of the classification analysis

Supplementary Table 4. Classification, Dataset 1 (Apidima 2 face). Jackknifed classification matrix, PC1-7 (70.72% of total variance). Overall jackknifed classification success: 80.65 %. Abbreviations: Neanderthals (NEA), H. sapiens (HS) Middle Pleistocene Africans (MPA), Middle Pleistocene Eurasians (MPE).

	MPA	MPE	NEA	HS	Total
MPA	2	1	0	0	3
MPE	1	2	0	0	3
NEA	0	2	4	0	6
HS	0	1	1	17	19
Total	3	6	5	17	31

Supplementary Table 5. Classification, Dataset 2 (Apidima 2 neurocranium). Jackknifed classification matrix, PC1-8 (90.95 % of total variance). Overall jackknifed classification success: 78.05 %. Abbreviations: Neanderthals (NEA), H. sapiens (HS) Middle Pleistocene Africans (MPA), Middle Pleistocene Eurasians (MPE).

	HS	NEA	MPE	MPA	Total
HS	24	1	0	0	25
NEA	1	6	1	0	8
MPE	0	2	1	0	3
MPA	1	1	2	1	5
Total	26	10	4	1	41

Supplementary Table 6. Classification, Dataset 3 (Apidima 1 neurocranium). Jackknifed classification matrix, PC1-8 (88.58% of total variance). Overall jackknifed classification success: 89.47 %. Abbreviations: Neanderthals (NEA), H. sapiens (HS) Middle Pleistocene Africans (MPA), Middle Pleistocene Eurasians (MPE).

	HS	NEA	MPE	MPA	Total
HS	22	0	0	1	23
NEA	0	5	1	0	6
MPE	0	0	4	0	4
MPA	0	1	1	3	5
Total	22	6	6	4	38

Supplementary Table 7. Classification, Dataset 4 (Apidima 1 midsagittal profile). Jackknifed classification matrix, PC1-4(85.43% of total variance). Overall jackknifed classification success: 70.83 %. Abbreviations: Neanderthals (NEA), H. sapiens (HS) Middle Pleistocene Africans (MPA), Middle Pleistocene Eurasians (MPE).

	HS	NEA	MPE	MPA	Total
HS	23	2	1	1	27
NEA	0	8	2	0	10
MPE	0	3	1	1	5
MPA	1	0	3	2	6
Total	24	13	7	4	48

Supplementary Table 8. Classification, Dataset 5 (combined Apidima 1 -Apidima 2 dataset). Jackknifed classification matrix, PC1-4(78.24% of total variance). Overall jackknifed classification success: 92.11%. Abbreviations: Neanderthals (NEA), H. sapiens (HS) Middle Pleistocene Africans (MPA), Middle Pleistocene Eurasians (MPE).

	HS	NEA	MPE	MPA	Total
HS	22	1	0	0	23
NEA	0	6	0	0	6
MPE	0	0	4	0	4
MPA	1	1	0	3	5
Total	23	8	4	3	38

4. Specimen abbreviations

Supplementary Table 9. Specimen abbreviations used in the plots.

Specimen	Abbreviation
Aduma 3	Adm3
Amud 1	Am1
Arago	Ar
Bodo	Bd
Broken Hill	BH
Biache St. Vaast	Bst
La Chapelle-aux-Saints 1	Ch
Dali	Da
Dolni Vestonice 3	DV3
Elandsfontein	El
Eliye Springs	ES
Feldhofer	Fh
La Ferrassie 1	Fr1
Gibraltar 1	Gb1
Guattari 1	Gt
Irhoud 1	Ir1
Irhoud 2	Ir2
La Quina 5	LQ5
Omo 1	Om1
Omo 2	Om2
Nazlet Khater 2	NK
Petralona	Pt
Qafzeh 6	Qz6
Qafzeh 9	Qz9
Reilingen	Rl
Saccopastore 1	Scc
Shanidar 1	Sh1
Shanidar 5	Sh5
Skhul 5	Sk5
Sima de los Huesos 5	Sm5
Spy 1	Sp1
Spy 2	Sp2
Swanscombe	Ssc

Supplementary References

49. Grün, R., Eggins, S., Kinsley, L., Mosely, H., Sambridge, M. Laser ablation U-series analysis of fossil bones and teeth. Palaeogeography, Palaeoclimatology, Palaeoecology416, 150-167 (2014).

50. Paul, D., White, W.M., and D. L. Turcotte, D.L. Constraints on the 232Th/238U ratio (k) of the continental crust. Geochem. Geophys. Geosyst. 4(12), 1102, 1-17 (2003) doi:10.1029/2002GC000497.

51. Duval, M., Aubert, M., Hellstrom, J., Grün, R. High resolution, LA-ICP-MS mapping of U and Th isotopes in an Early Pleistocene equid tooth from Fuente Nueva-3 (Orce, Andalusia, Spain). Quaternary Geochronology6, 458-467 (2011).

52. Hershkovitz, I. et al. Levantine cranium from Manot cave (Israel) foreshadows the first European modern humans. Nature520, 216–219 (2015).

53. Quam, R., Martinez, I. & Arsuaga, J. L. New Observations on the Human Fossils from Petit-Puymoyen (Charente). PaleoAnthropology2011, 95–105 (2011).

54. Bastir, M. et al. Comparative morphology and morphometric assessment of the Neandertal occipital remains from the El Sidrón site (Asturias, Spain: years 2000–2008). J. Hum. Evol.58, 68–78 (2010).

55. Howells,W. W.Cranial variation in Man. A study by multivariate analysis of patterns of differences among recent human populations. Pap. Peabody Mus. Archaeol. Ethnol. Harvard Univ.67, 1–259 (1973).

56. Ascenzi,A., Mallegni,F., Manzi,G., Segre,A. G., Naldini,E. S.A re-appraisal of 24Ceprano calvaria affinities with Homo erectus, after the new reconstruction. J. Hum Evol.39, 443–450 (2000).

57. White,T. D. et al.Pleistocene Homo sapiens from Middle Awash, Ethiopia. Nature423, 742–747 (2003).

58. Grine, F. E. et al. Late Pleistocene Human skull from Hofmeyr, South Africa, and Modern Human Origins. Science315, 226–229 (2007).

59. Crevecoeur,I., Rougier,H., Grine,F. & Froment,A.Modern human cranial diversity in the Late Pleistocene of Africa and Eurasia: Evidence from Nazlet Khater, Pestera cu Oase, and Hofmeyr. Am. J. Phys. Anthropol.140, 347–358 (2009).

60 .Daura,J.et al.New Middle Pleistocene hominin cranium from Gruta de Aroeira (Portugal). Proc. Natl. Acad. Sci. U. S. A.114, 3397–3402 (2017).

61. Hublin,J. –J. Le torus occipital transverse et les structures associées. Evolution dans le genre Homo(1978).

62. Wolpoff,M. H.Cranial remains of Middle Pleistocene European Hominids. J. Hum. Evol. 9, 339–358 (1980).

63. Rightmire,G. P.Homo erectusand Middle Pleistocene hominins: brain size, skull form and species recognition. J. Hum. Evol.65, 223–252 (2013).

Study II: Megalopolis Molar

Crown outline analyses of the hominin upper third molar from the Megalopolis basin, Peloponnese, Greece.

By Carolin Röding, Julia Zastrow, Heike Scherf, Constantin Doukas and Katerina Harvati.

Published as chapter in *Ancient Connections in Eurasia* (2021), ed. by H. Reyes-Centeno and K. Harvati, pp. 13-36. Tübingen: Kerns Verlag.
ISBN: 978-3-935751-37-7.
Doi: 10.51315/9783935751377.001.

The following version is based on the authors formatting of the manuscript and figures from the open access book chapter.

Crown outline analysis of the hominin upper third molar from the Megalopolis Basin, Peloponnese, Greece

Carolin Röding[1], Julia Zastrow[2], Heike Scherf[1], Constantin Doukas[3] and Katerina Harvati[1,2,4]

1 Paleoanthropology, Senckenberg Centre for Human Evolution and Palaeoenvironment, Eberhard Karls University of Tübingen, Germany.
2 DFG Centre of Advanced Studies 'Words, Bones, Genes, Tools', Eberhard Karls University of Tübingen, Germany.
3 Faculty of Geology and Geoenvironment, National and Kapodistrian University of Athens, Greece.
4 Museum of Anthropology, Medical School, National and Kapodistrian University of Athens, Greece.

Cite this article: Röding, C., J. Zastrow, H. Scherf, C. Doukas, and K. Harvati. 2021. Crown outline analysis of the hominin upper third molar from the Megalopolis Basin, Peloponnese, Greece. In Ancient Connections in Eurasia, ed. by H. Reyes-Centeno and K. Harvati, pp. 13-36. Tübingen: Kerns Verlag. ISBN: 978-3-935751-37-7. Doi: 10.51315/9783935751377.001.

Abstract

The left upper third molar from the Megalopolis Basin is enigmatic due to its problematic preservation and context. The Megalopolis molar is the only possible human fossil known to date from the Megalopolis Basin. It was found on the surface during geological surveys in 1962-63. Based on the faunal assemblage collected during the same survey, it was proposed to be of Middle Pleistocene age and possibly one of the oldest human fossils in Europe. However, its actual geological age is unknown. In the past, dental crown outline analysis has been successfully used to differentiate between hominin species and populations. We applied the method to upper third molars, attempting to shed light on the affinities of the Megalopolis specimen. Principal component analysis (PCA) of the crown outline shape grouped the Megalopolis molar with our *Homo sapiens* sample; however, the PCA in form space, including shape plus size, as well as Procrustes distances based on overall shape, grouped it with our Neanderthal comparative sample. We conclude that its most likely identification is as a member of the Neanderthal lineage. However, we urge further analyses with an increased fossil comparative sample to include representatives of *Homo heidelbergensis*, which is underrepresented in our study. The Megalopolis molar contributes to the scarce Pleistocene human fossil record of Greece and highlights the potential of the Megalopolis Basin for yielding further paleoanthropological finds.

INTRODUCTION

The Megalopolis Basin, Peloponnese, Greece, is well-known for its fossil fauna (e.g., Skouphos 1905; Melentis 1961; Sickenberg 1976; Athanassiou 2018; Athanassiou et al. 2018) and more recently for its Middle Pleistocene archaeological sites (e.g., Panagopoulou et al. 2015; Giusti et al. 2018; Thompson et al. 2018; Konidaris et al. 2019). The most important of these, Marathousa 1, has yielded a stratified lithic as well as faunal assemblage including elephant remains showing signs of butchery (e.g., Tourloukis et al. 2018a; Konidaris et al. 2018). The site has been dated to 400-500 ka (Blackwell et al. 2018; Jacobs et al. 2018), testifying to an early human presence in the region. In contrast to

these recently discovered sites, many of the earlier paleontological finds from the Megalopolis Basin are non-stratified surface finds. Surface finds can be transported and can originate from varying exposed surfaces in the proximity of the find spot, which complicates their dating (Wandsnider 2004). In the case of the Megalopolis area, exposed surfaces span a wide geological age range (Siavalas et al. 2009; Vinken 1965). In 1962-63 an isolated human tooth was found on the surface in the basin and recovered together with Pleistocene fossil faunal remains (Sickenberg 1976; Marinos 1975). This putative fossil human specimen is a left upper third molar, hereafter referred to as the Megalopolis molar (Fig. 1). Its geological age and species attribution are unknown because of its problematic context as surface find, as well as its state of preservation.

The Megalopolis molar was first described during the analysis of the faunal remains collected at the same time (Marinos 1975). It was proposed that the Megalopolis molar has a similar age as the fauna. The faunal assemblage was assigned to the "Biharium" (Sickenberg 1976), which roughly translates to the lower half of the Middle Pleistocene and the Early Pleistocene (Koenigswald and Heinrich 2007). If Sickenberg's assessment was correct, the Megalopolis molar would be one of the oldest hominin fossils known in Europe at the time of its discovery. In some cases, ESR and U-series dating enable direct dating of teeth (e.g., Duval et al. 2012). In the case of the Megalopolis molar, direct dating has not been attempted due to previous chemical treatment (Xirotiris et al. 1979) but also because of the destructive nature of these dating methods. Because of its status as a surface find without datable surrounding context, its fossil status is uncertain, as it could potentially derive from a recent, modern human skeleton (Marinos 1975).

Xirotiris et al. (1979) analyzed the enamel prism structure via scanning electron microscopy (SEM) with the aim to classify the Megalopolis molar. For this purpose, a part of the crown was cleaned with acid to remove the enamel surface layer, which does not show a prism structure (Xirotiris et al. 1979). The SEM method

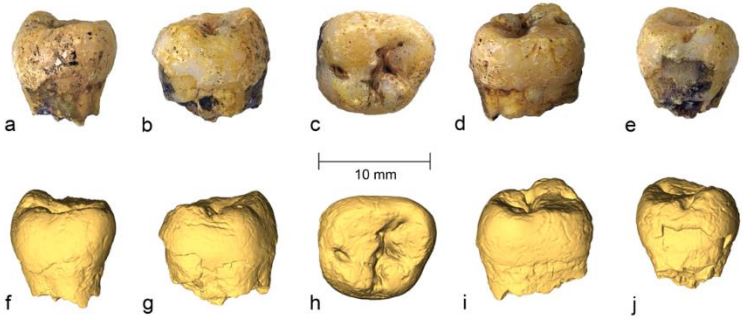

Fig. 1. Left upper third molar from the Megalopolis Basin. Shown as pictures of the original (a-e) and surface model from a CT scan (f-j). Displayed in buccal view (a,f), distal view (b,g), occlusal view with the mesial side being oriented towards the top (c,h), mesial view (d,i) and lingual view (e,j).

usually requires a thin gold or platinum coating of the sample to improve contrast and the signal-to-noise ratio (Carter and Shieh 2015: 117–144). Remnants of the gold coating are still visible on the fossil (Fig. 1 a-e). It is assumed that the gold coating was at least partly removed by acid due to the concomitant removal of labelling on the crown (cf. Fig. 1, Xirotiris et al. 1979: 118), which resulted in the obliteration of its crown features. The authors of that study did not reach a species attribution due to the limited comparative sample of fossil human enamel prism structures and an overlap in the linear crown measurements of the Megalopolis molar with several *Homo* species (Xirotiris et al. 1979).

The preservation of the Megalopolis molar is problematic for most standard methods used to assess external morphology. The absence of its roots and the eroded condition of its occlusal surface limit analysis to internal structures and overall shape of the tooth crown. Dental outline analysis provides a framework in which teeth can be analyzed independent of their absolute size, presence of the dental root and to a certain degree occlusal wear (see, e.g., Benazzi et al. 2011a, 2012). On other tooth types the cervical and crown outline analyses were successfully used to distinguish between Neanderthals and *Homo sapiens* as well as between fossil *Homo sapiens* and recent populations (e.g., Benazzi et al. 2011a, 2011b;

Harvati et al. 2015). For the analysis of the cervical outline, the preservation of the Megalopolis molar would require reconstruction to avoid introducing a possible source of error because parts of this outline are missing. In contrast, an analysis of the crown outline is possible without reconstruction. In this chapter, we show that the method of crown outline analysis can be applied on upper third molars and thereby help shed light on the taxonomic status of the Megalopolis molar.

MATERIAL AND METHODS

Crown outline analysis on upper third molars

Tooth outlines can be analyzed by direct extraction of diameters, diagonals, and area or by geometric morphometric analysis of landmark data collected on the outline. We analyzed landmark data collected on the crown outline of the Megalopolis molar to allow the consideration of its shape as well as its form (defined as shape considered together with size). It is important to note that landmark data collected on outlines do not strictly fall into the classical concepts of fixed landmarks and semi-landmarks because of the lack of homologous fixed points and start or end points of the outline curve, respectively (for discussion of landmark types see, e.g., Bookstein 1991; Gunz et al. 2005). Therefore, the required removal of orientation, location and absolute size from the landmark coordinates cannot be achieved by a Generalized Procrustes analysis (GPA) alone. A geometric morphometric analysis of a dental outline requires additional specific steps during data collection to remove orientation and ensure homology between landmark configurations (Bauer et al. 2018; Harvati et al. 2015).

Prior to the data collection, consistent orientation was identified as possible source of error due to the high intraspecific variation of third molars (e.g., Gómez-Robles et al. 2012; Schneider et al. 2014). We used only upper third molars (M^3) with a mesial contact facet to the second molar or with a very distinct crown that immediately allowed the identification of the mesial side to minimize this source of error. Landmark data of the crown outline were collected by two observers (C.R.; J.Z.) on 39 µCT scans from

Table 1. Sample of µCT of original specimens in detail.

Species / Population		Individuals / Collection numbers	Right or Left Side	scan resolution (µm)	Scanner	Collection / Repository	Used in analysis
Homo sapiens	Neolithic from Egypt	1290	left	36.3	µCT GE Phoenix v|tome|x s240 at the University of Tübingen, Germany	osteological collection University of Tübingen, Germany	all
		1299		24.5			
		1306		28.9			
	Bronze Age from Tunisia	83, 84, 85	left	23.4			
		80, 81, 82, 86	right				
	Recent from Oceania	4249, 4265, 4300	left	20.9			
		4258, 4262		23.7			
		4259	right				
		4260		22.6			
	Recent from Europe	13156, 13162, 13253, 13266	left	25.6			
		13181, 13231, 13273	right				
	fossil	La Rochette	left	10.3			
Homo neanderthalensis		Feldhofer Grotte (Fe)	left	10.3	not further specified µCT scanner	NESPOS online database	all
		Krapina (Kr) d97		16.2			
		Kr d173		32.5			
		Kr d180		20			
		Kr: d58, d163	right	31.2			
		Kr d109		18.7			
		Kr d162		27.5			
		Kr: d170, d178		25			
Homo erectus		Sangiran (Sa): NG0802.1 (Zanolli 2013, 2015)	left	20.9	µCT X8050-16 from Viscom AG at the University of Poitiers, France	Balai Pelestarian Situs Manusia Purba of Sangiran, Java	all
		Sangiran (Sa): 7-17	right	17	µCT GE Phoenix v|tome|x s240 at the University of Tübingen, Germany	Senckenberg Institute Frankfurt, Germany	
Homo heidelbergensis		Steinheim	left	25.6	µCT BIR SN001 ACTIS5 at the MPI EVA, Leipzig, Germany	Staatliches Museum für Naturkunde Stuttgart, Germany	
		Megalopolis	left	24.3	µCT GE Phoenix v|tome|x, Phoenix Service Center in Stuttgart, Germany	Museum of Palaeontology and Geology, Athens, Greece	projected into PCA

Table 2. Sample of µCT of dental casts in detail.

Species / Population		Individuals / Collection numbers	Right or Left Side	scan resolution (µm)	Scanner[1]	Collection / Repository	Used in analysis
Homo sapiens	Recent from Europe	13156	left	> 50	Artec Space Spider handheld 3D surface scanner	osteological collection University of Tübingen, Germany	only error calculations
				75.9	µCT GE Phoenix v|tome|x s240		
	Fossil	Brno 1 (Br); Ohalo 2 (Oh)	right		µCT GE Phoenix v|tome|x s240	dental cast collection from Dr. Sireen El Zaatari	all
		Qafzeh 9 (Qa)	left				
Homo neanderthalensis		Amud 1 (Am)	left				
		Le Petit-Puymoyen 2 (Pe)		50.3			
		Saint Césaire 1 (Sc)	right	75.9			
		Spy 1 (Sp)		77.6			

1 All specimens were scanned at the Paleoanthropology High-Resolution Computing Tomography Laboratory, University of Tübingen, Germany.

original specimens with their resolution ranging from 10.3 to 36.3 µm (Table 1). The M^3 landmark data showed a very high interspecific homogeneity. Almost all individuals exhibit differences of less than 0.05 mm in their centroid size (CS) corrected landmark coordinates. In addition, one modern human specimen (Tunisia 80) was digitized five times each by two observers (C.R.; J.Z.) over the period of six months in order to evaluate intra- as well as interobserver error.

Dental casts are a source of information often neglected in geometric morphometric studies of dentition. Especially in cases when the access to CT scans is restricted, casts can provide a valuable addition to the comparative sample. Landmark data were collected by one observer (C.R.) on seven µCT scans of high resolution dental casts from fossil individuals (resolution ranging from 50.3 to 77.6 µm; Table 2). Only casts with clearly visible cervical lines were scanned and included in our analysis. To evaluate inter-method error, a high resolution dental cast of one modern human individual from the µCT scan sample (Vaihingen

13156) was created. Subsequently the cast was both µCT scanned and surface scanned. Landmark data were collected five times each from the µCT scan of the original tooth, the µCT of the cast and from the surface scan of the cast over a period of six months by one observer (C.R.).

The following protocol includes all data collection steps necessary for geometric morphometric analysis of the crown outline (Fig. 2). All teeth from the right side were mirror-imaged and treated as teeth from the left side in all subsequent steps. Mirroring of anatomical antimeres is often used to expand sample size (e.g., Bauer et al. 2018; Harvati et al. 2015). It has to be noted that combining right and left teeth might increase noise, since fluctuating asymmetry is the norm in dentition (e.g., Scott et al. 2018; Sprowls et al. 2008). An orientation system based on the cervical line ensured repeatability of the spatial positioning and orientation (Benazzi et al. 2009). A best-fit plane along the cervical line was calculated and the tooth virtually sectioned along this plane. The best-fit cervical plane was translated to the x-y plane of a coordinate system to establish a relationship between the measured crown outline and the cervical plane. In addition, this enabled a consistent orientation of the teeth. Each tooth was rotated until the mesio-distal axis was parallel to the x-axis with the mesial side pointing towards higher values along the x-axis. A standardized occlusal view with a 90° angle to the x-y plane was used to project the crown outline onto the x-y plane (Benazzi et al. 2011a, 2012). The projected outline's area centroid was calculated and translated to a predetermined point, here 10,10,0. Sixteen radii were digitized at an angle of 22.5° to each other outgoing from the centroid (Bauer et al. 2018; Benazzi et al. 2012). The points of interception between the radii and the crown outline created a set of 16 two-dimensional landmarks per tooth. The landmark set was statistically analyzed after scaling it to centroid size (CS) and removing location from the scaled landmark data. The CS is calculated as the square root of the summed squared of each landmark-centroid distance (Zelditch et al. 2012). A partial GPA with inhibited rotation was performed to remove scale and location at the same time. All steps of data collection were carried out in the software environments of Avizo 9.2 (FEI Visualization Sciences Group) and Rhinoceros 6 (Robert McNeel and Associates,

Seattle, WA). Statistical analyses were carried out in R (R Development Core Team 2011) using published and freely available code (GPA: Morpho package; following error calculations: Morpho, geomorph, and stats packages).

The relative reproducibility of individual landmarks was assessed by calculating the error in percent of the Euclidean distance (ED) between the configuration centroid and repeat measures of each landmark in the configuration (Fig. 3a; Singleton 2002). The EDs were calculated based on the raw, not scaled landmark configurations. For each observation the configuration's centroid and the 16 ED's between the centroid and each landmark were computed. Percentage error was calculated for each landmark, and within and between observers the average deviation was determined. The measured error was below five percent in all cases, which is commonly seen as the maximum of acceptable deviation between repeated measurements. The two landmark positions with the smallest ED to the configuration's centroid showed the highest error percentages in all cases, inter-method, intraobserver as well as interobserver error. This is considered a side effect when the configuration deviates from a circular or spherical shape and of small landmark configurations (von Cramon-Taubadel et al. 2007).

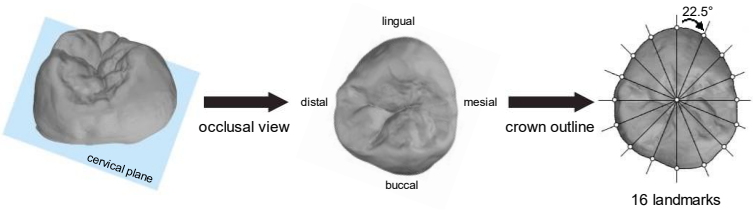

Fig. 2. Illustration of the method used. From left to right: virtual surfaces were sectioned along a best-fit plane of the cervical line; the created cervical plane of the crown was translated to the x-y plane of a coordinate, the crown was rotated until in occlusal view the mesio-distal axis was parallel to the x-axis, the crown outline was projected onto the x-y plane and outgoing from the outline's centroid cut by 16 radii in a 22.5° angle to each other, the points of interception between the radii and the crown outline created 16 landmarks. Illustration created in Photoshop CS 5 based on virtual surface models from Rhinoceros 6.

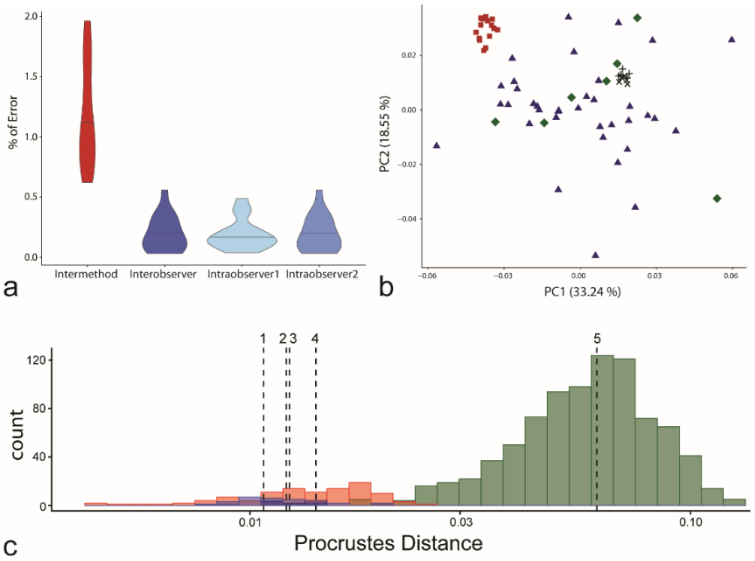

Fig. 3. Illustrations for the error calculations. A) Error in Euclidean distance (ED) per landmark between repeated measurements. The 16 ED's are summarized for the intermethod error in red (mean = 1.173, max = 1.964), interobserver error in dark blue (mean = 0.198, max = 0.558), intraobserver error 1 in light blue (mean = 0.190, max = 0.487), and intraobserver error 2 in medium blue (mean = 0.198, max = 0.557). B) Projection of PCA of the crown outline in shape space. PCA calculated based on CT scans of original specimens; repeated measurements and data from casts later projected into the plot. CT scans shown as blue triangles, dental casts as green diamonds, intermethod error as red squares and the intraobserver error as black + and X, respectively. C) Histogram of pairwise Procrustes distances (PD). PDs along x-axis logarithmized and dotted lines showing the means. Pairwise PDs between intraobserver measurements shown in light blue ($mean_1$ = 0.011, $mean_2$ = 0.012), between the interobserver measurements in dark blue ($mean_4$ = 0.012), between the intermethod measurements in red ($mean_3$ = 0.014), and between individuals in the comparative sample shown in green ($mean_5$ = 0.061). Graphic created in R and processed in Adobe Illustrator CS5.

The effects of inter- and intraobserver as well as inter-method error were explored in a comparative sample composed of the above mentioned sample of µCT scans (Fig. 3b-c). Pairwise Procrustes distances (PD) between multiple measurements of the same individual were compared to interindividual distances

assuming that specimen affinity is not influenced when the largest PD between repeated measurements of the same individuals is smaller than the smallest PD between different specimens (Neubauer et al. 2009). The PDs were calculated based on the scaled and GPA superimposed landmark configurations. Due to the very homogenous sample, the interobserver and inter-method error overlapped with the smallest distances between individuals (Fig. 3c). The highest PDs between repeated inter-method measurements were found in surface scans. Pairwise PDs between measurements on surface scans and the comparative sample were smaller than PDs to other inter-method measurements on CT scans. In contrast, all inter- as well as intraobserver measurements showed smaller PDs to each other than to other individuals. Both intraobserver errors showed values smaller than the smallest interindividual PD. All mean errors were more than four times smaller than the interindividual distance mean.

When projecting the repeated interobserver measurements into a Principal Component Analysis (PCA) in shape space the measurements clustered together (Fig. 3b). No other individual plotted into the space between the repeated interobserver measurements. Likewise, the inter-method measurements clustered together (Fig. 3b). The higher error in surface scans was reflected by some measurements being more scattered. A possible explanation is the less secure identification of the cervical line on the surface scans due to problems in capturing the lower part of the crown during the surface scanning. Therefore, surface scans of dental casts were excluded from further analysis due to their potential influence on the results.

Crown outline analysis of the Megalopolis molar

The cervical line on the Megalopolis molar shows damage especially on the lingual and distal sides (Fig. 1). Contrary to the illustrated surface model, the µCT scan showed the original boundary between dentin and enamel on the majority of the tooth. A best-fit cervical plane was therefore computed based on this visible part of the original and not the damaged enamel-dentin boundary.

The crown outline of the Megalopolis molar was compared to a sample of modern as well as fossil *Homo sapiens*, Neanderthals, two *Homo erectus* individuals from Sangiran and the *Homo heidelbergensis* individual from Steinheim (Tables 1, 2). The majority of the comparative sample consisted of CT scans of the original specimens with the addition of seven µCT scans of high resolution dental casts.

Multivariate Statistics

All following multivariate statistics were calculated in R (R Development Core Team 2011, packages: Morpho, geomorph, stats, MASS). The PCA is a method to reduce high-dimensional space to interpret large-scale trends of data and is subject to mathematical assumptions (Abdi and Williams 2010). For the shape PCA only the scaled and superimposed landmark coordinates were used, whereas for the form PCA, CS was added as variable. The most important assumption of this method is that the dataset does not contain outliers or influential individuals. This assumption was tested on the comparative sample (the Megalopolis molar was not used to calculate the PCAs but was projected into the plots). Cook's distance was estimated for each individual and influential individuals were identified by using the cut-off values recommended by Bollen and Jackman (1985). One individual, Qafzeh 9, reached the sensitive cut-off of 4/N, here $N = 45$ and $\alpha = 0.05$, in shape space as well as form space. An omission did not alter the pattern of results and the individual was not excluded from the analyses so as not to further limit our already small fossil *Homo sapiens* sample. In addition, the PC scores, including those of Qafzeh 9, did not show any outliers when using the ± 3 standard deviations criterion.

Shape changes along the PCs (Figs. 4, 5) were visualized as landmark configurations at ± 2 standard deviations (sd). The landmark configurations were calculated by rotating and translating PC-scores derived from shape data back into configuration space. Therefore, the coefficients of the PC, which express the relationship between the PC and the original variables, were used to predict a hypothetical landmark configuration outgoing from a PC score ± 2 sd from the PC mean. PC-scores were converted to landmark coordinates in R (R Development Core

Team 2011, packages: Morpho). Convex hulls were calculated around the extreme points of each defined group and contain no information about confidence intervals.

To further explore the relationship between shape and size in our sample, a linear regression between shape and logarithmized CS was calculated. Due to its influential Cock's distance, Qafzeh 9 was excluded for this analysis. To maximize sample size, all superimposed landmark coordinates from *Homo sapiens* and Neanderthals were pooled (N = 41). The regression was calculated in R with a function that performs statistical assessment based on Procrustes distances among specimens, rather than explained covariance matrices among variables (Adams et al. 2020: proc.lm function).

RESULTS

The first two shape PCs explained 55.19 % of variance and their combination showed no clear separation between groups (Fig. 4), a pattern which is repeated by all higher PC's. PC1 explained 35.23 % of variance and summarized shape changes ranging from a bucco-lingual elongated oval outline with parallel mesial and distal sides (positive values) to a bucco-lingual compressed rounder outline with an outward bulging of the distal side (negative values). Teeth expressing a more positive value showed a reduction of the distal cusps on the occlusal surface compared to teeth with more negative values that showed four well developed cusps. PC2 explained 19.96 % of variance and described shape changes from an outline with bulging on the lingual part of the distal side (negative values) to an outline with bulging on the buccal part of the lingual side (positive values). A reduction of the hypocone relative to the metacone was expressed by teeth showing positive values. In contrast, a reduction of the metacone relative to the hypocone was expressed by teeth showing negative values. When projecting the Megalopolis molar into the PCA plot, it plotted among the negative values of both PC1 and PC2, reflecting its four developed cusps with a slight reduction of the metacone. The Megalopolis molar plotted into the modern *Homo sapiens* convex hull and close to the fossil *Homo sapiens* from Ohalo II.

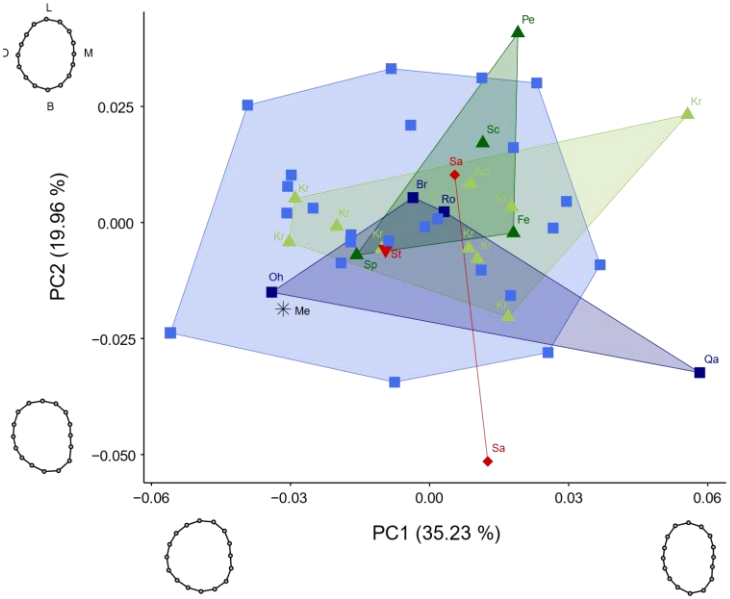

Fig. 4. PCA of the crown outline with PC1 and PC2 projected into shape space. Modern *Homo sapiens* shown as light blue squares (N = 24), fossil *Homo sapiens* as dark blue squares (N = 4), *Homo neanderthalensis* from the Near East and the Balkan as light green triangles (N = 10), *Homo neanderthalensis* from Central Europe as dark green triangles (N = 4), *Homo erectus* as red diamonds (N = 2) and *Homo heidelbergensis* as red inverted triangle (N = 1). Megalopolis molar, shown as black star, was projected into the plot calculated based on the comparative sample. Shape changes along PCs illustrated as landmark configurations at ± 2 sd. Abbreviations of all fossil individuals listed in Tables 1, 2. Graphic created in R and processed in Adobe Illustrator CS5.

The form PCA combines the scaled, superimposed landmark data with the variable of CS (Fig. 5). PC1 explained 82.94 % of variance and was highly positively correlated with CS. PC2 explained 6.08 % of variance and summarized shape changes ranging from a bucco-lingual elongated oval outline with parallel mesial and distal sides (negative values) to a bucco-lingual compressed rounder outline with an outward bulging of the distal side especially disto-lingual (positive values). Teeth expressing more negative values showed the reduction of both distal cusps

while more positive values showed four well developed cusps with a slightly more pronounced hypocone relative to the metacone.

On the one hand, PC1 in form space reflected a high interspecific homogeneity by explaining 82.94 % of variation. On the other hand, PC1 separated most of the Neanderthals individuals with positive values from the modern *Homo sapiens* with rather negative values. Overall, the PCA plot showed varying degrees of overlap between all groups and large intraspecific

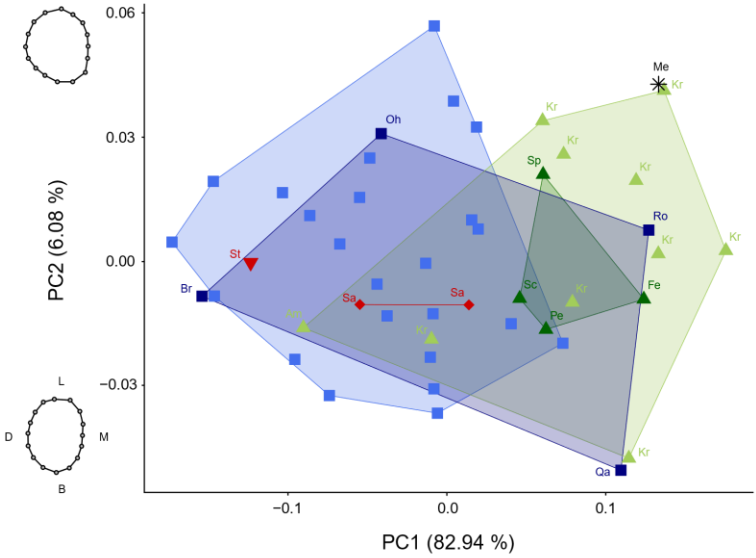

Fig. 5. PCA of the crown outline with PC1 and PC2 projected into form space. Modern *Homo sapiens* shown as light blue squares (N = 24), fossil *Homo sapiens* as dark blue squares (N = 4), *Homo neanderthalensis* from the Near East and the Balkan as light green triangles (N = 10), *Homo neanderthalensis* from Central Europe as dark green triangles (N = 4), *Homo erectus* as red diamonds (N = 2) and *Homo heidelbergensis* as red inverted triangle (N = 1). Megalopolis molar, shown as black star, was projected into the plot calculated based on the comparative sample. PC1 negatively correlated with logarithmic centroid size. Shape changes along PC2 illustrated as landmark configurations at ± 2 sd. Abbreviations of all fossil individuals listed in Tables 1, 2. Graphic created in R and processed in Adobe Illustrator CS5.

variation. Two fossil *Homo sapiens*, La Rochette and Qafzeh 9, showed the most positive values along PC1 for all *Homo sapiens* and thereby, plotted closer to Neanderthals than other *Homo sapiens*. The Neanderthal individuals Amud 1 and Krapina d097 plotted within the modern *Homo sapiens*. The chronologically older individuals from Steinheim and Sangiran plotted into the modern *Homo sapiens* variation. When projecting the Megalopolis molar into the PCA plot, it plotted in the positive values of PC1 and PC2, and thereby away from the *Homo sapiens* convex hulls. Krapina d178 plotted closest to the Megalopolis molar and showed the greatest resemblance in overall shape based on PD. Their pairwise PD was in a similar order of magnitude as the reported mean interobserver error. The Megalopolis molar would still plot outside of the *Homo sapiens* convex hulls and closest to Neanderthals from Krapina when assuming a circular error range with the plotted distance to Krapina d178 as radius.

CS in our sample ranges from 17.71 to 25.08 (Table 3), with Neanderthals on average showing higher values (mean: 22.45 ± 1.49) than *Homo sapiens* (mean: 20.63 ± 1.52). Megalopolis showed a CS of 24.08. No statistically significant relationship between shape and size was found ($F = 1.14$, $Dof = 1$, $R^2 = 0.03$, $p = 0.29$; $\alpha = 0.05$).

DISCUSSION

A high degree of variability in distal maxillary molars in both fossil as well as recent populations is repeatedly reported in the literature (e.g., Bailey 2002; Macho and Moggi-Cecchi 1992; Martinón-Torres 2006). This observation was reflected in the high intraspecific variation in shape space (Fig. 4). Nevertheless, the size corrected superimposed landmark coordinates of many individuals showed differences of less than 0.05 mm. On the one hand, it implies that the crown outline alone does not capture certain aspects of the crown morphology, e.g., the position of fissures and cusps. On the other hand, it implies that even these subtle differences can potentially be informative and therefore error measurements should not be purely based on Euclidean distances (ED). The traditionally accepted error range for EDs is up to five percent. In case, of M^3s five percent deviation between repeated

measurements could be up to four times higher than the difference between individuals at this one landmark position.

Besides high intraspecific variability, an expanded fossil sample spanning Australopithecines to recent *Homo sapiens* showed that a hypocone reduction in M^3s characterizes later *Homo*, like *Homo*

Table 3. Centroid sizes of all *Homo sapiens* (N = 28) and Neanderthals (N = 14).

Species	Individuals / Collection numbers	Centroid Size[1,2]	Mean[2]	Standard deviation[2]
Homo sapiens	13273	17.71	20.63	1.52
	Brno 1	18.04		
	84	18.19		
	85	18.21		
	13181	19.02		
	13162	19.08		
	1290	19.32		
	13231	19.50		
	4300	19.66		
	83	19.94		
	81	20.11		
	4259	20.14		
	1299	20.23		
	Ohalo 2	20.25		
	4262	20.77		
	1306	20.77		
	4265	20.83		
	13266	20.84		
	13253	20.85		
	4249	20.94		
	13156	21.20		
	82	21.39		
	4260	21.48		
	86	21.50		
	80	21.88		
	4258	22.60		
	Qafzeh 9	23.39		
	La Rochettte	23.87		

Table 3 continued.

Species	Individuals / Collection numbers	Centroid Size[1,2]	Mean[2]	Standard deviation[2]
Homo neanderthalensis	Amud 1	19.21	22.45	1.49
	Krapina d097	20.81		
	Saint Césaire	22.02		
	Spy 1	22.37		
	Le Petit-Puymoyen 2	22.39		
	Krapina d173	22.39		
	Krapina d162	22.68		
	Krapina d170	22.73		
	Krapina d178	23.50		
	Krapina d163	23.72		
	Feldhofer Grotte	23.80		
	Krapina d058	24.02		
	Krapina d180	24.17		
	Krapina d109	25.08		
	Megalopolis	24.08		

1 sorted from minimum to maximum centroid size within each species.
2 values rounded to two decimals.

sapiens and Neanderthals (Gómez-Robles et al. 2012). In addition, Gómez-Robles et al. (2012) found a higher level of metacone reduction in *Homo sapiens* than in Neanderthals. We could not analyze hypocone reduction to the same level of resolution, as our sample almost exclusively consists of later *Homo*. The PCA in shape space (Fig. 4) showed varying degrees of hypocone and metacone reduction for all groups. In our sample, only six *Homo sapiens*, Sangiran 7-17, and Krapina d170, as well as Megalopolis, show signs of metacone reduction. Ohalo II, Krapina d170 and Megalopolis express almost identical values along PC2, which described the metacone reduction. It has to be noted that Gómez-Robles et al. (2012) analyzed a different landmark set which provided additional information about the occlusal surface that is absent in our analyses. Further differences in methodology include the data acquisition from photographs and the use of sliding curve semi-landmarks by Gómez-Robles et al. (2012). A curve requires a homologous point, which provides the start for a predefined

number of equidistantly spaced semi-landmarks on the curve (e.g., Gunz et al. 2005). Identification of the homologous start point is highly dependent on the orientation, here the position of the tooth during photographing, as well as preservation and occlusal wear. However, the preservation of the Megalopolis molar does not allow a secure identification of the landmarks on the occlusal surface nor a homologous start point for a curve of semi-landmarks.

Beyond shape differences, dental size, and especially linear measurements are commonly used to discriminate between both fossil and recent populations (e.g., Harvati et al. 2003, 2013; Smith et al. 2015; Xing et al. 2014). Xirotiris et al. (1979) reported a mesio-distal breadth 9.1 mm and a bucco-lingual length of 10.3 mm for the Megalopolis molar, which was at the lower end of their measurements for Neanderthals and *Homo sapiens*. In contrast, when using CS as a measure of size, the Megalopolis molar falls slightly outside the range of variation of our *Homo sapiens* comparative sample and at the upper end of the Neanderthal range (Table 3). The difference is that CS is based on multiple aspects (landmark coordinates) of the tooth while a linear measurement captures a single aspect of the tooth. For example, mesio-distal and bucco-lingual measurements hardly take into account reductions of one distal cusp. Nevertheless, both linear measurements and CS show the same trend that, on average, Neanderthals have larger M^3s than *Homo sapiens* (e.g., Harvati et al. 2013; Xirotiris et al. 1979).

Macho and Moggi-Cecchi (1992) suggested that simplification in M^3 morphology is partially caused by a reduction in size. The PCA in form space (Fig. 5) showed no relationship between shape and size in our sample of M^3s. Larger teeth (PC1 positive values) varied in their morphology from completely reduced distal cusps to four well-developed cusps with only a slight reduction of the metacone. This reflects a common issue regarding allometric relationships in the hominin dentition. On the one hand, some studies have assumed or established no clear allometric effects in hominin dentition (e.g., Wood et al. 1983; Bailey and Lynch 2005). On the other hand, additional studies have suggested small but significant allometric relationships (e.g., Martinón-Torres et al. 2006; Gómez-Robles et al. 2008). It can be assumed that allometric

effects do not explain morphological changes over an evolutionary time span, but might have some impact on patterns of intraspecific morphological variation (Gómez-Robles et al. 2012).

The process of dental development is multifactorial and thereby dental morphology is influenced by genetic, epigenetic and environmental factors (Brook et al. 2014a, 2014b). Genetic admixture might partially explain the observed overlap between *Homo sapiens* and Neanderthals in form space (Fig. 5). The two fossil *Homo sapiens*, La Rochette and Qafzeh 9, plotted closer to Neanderthals than other *Homo sapiens* while the Neanderthal individuals Amud 1 and Krapina d097 plotted within the modern *Homo sapiens*. Genetic evidence suggests admixture between Neanderthals and *Homo sapiens* in the Middle and Late Pleistocene (e.g., Green et al. 2010; Posth et al. 2017; Sankararaman et al. 2012). Therefore, admixture cannot be ruled out entirely as a possible explanation for the observed morphology of La Rochette, Qafzeh 9, Krapina d097 and Amud 1. Admixture and genetics are based on the heritability of traits. Biological distance studies commonly use dental traits and often assume equal and additive inheritance of traits (e.g., Macchiarelli et al. 2008; Vargiu et al. 2009). However, non-additive genetic variation might preserve certain dental traits over time (Edgar and Ousley 2016). The chronologically older individuals from Steinheim and Sangiran plotted into the modern *Homo sapiens* variation or express an even more extreme metacone reduction (Figs. 4, 5). On the one hand, this might imply that some aspects of the crown outline in *Homo sapiens* are conserved and resemble the primitive state found in chronologically older groups. On the other hand, this might be an artifact of the high intraspecific variation in combination with the underrepresentation of *Homo heidelbergensis* and *Homo erectus* in our sample.

All in all, the two main components of the crown outline shape of the Megalopolis molar matched the variation found in the Holocene comparative sample. In contrast, outline form and overall shape did not match the Holocene sample. The form PCA, the Procrustes distances based on overall shape, as well as its centroid size, grouped the Megalopolis molar with the Neanderthal comparative sample. Although our samples were small, we cautiously interpret these results as indicating that the Megalopolis

specimen likely dates to the Pleistocene and has affinities with the Neanderthal lineage.

It is important to note that our comparative sample lacked important individuals from the Middle Pleistocene of Europe (e.g., Petralona and Sima de los Huesos) and Africa (e.g., Broken Hill and Herto) and also many Neanderthal specimens. These were not possible to include due to a lack of access to dental casts or CT scans. A secure classification of the Megalopolis molar would require a more comprehensive sampling framework for the taxonomic interpretation and must be tested with further analyses and with an expanded comparative fossil sample.

The number of Neanderthal and pre-Neanderthal fossils from Greece has remained small even while the number of archaeological sites from the Middle and Lower Paleolithic has increased over recent years (e.g., Harvati 2016; Tourloukis and Harvati 2018). The oldest, radiometrically dated, Pleistocene site in Greece known to date, Marathousa 1, is located within the Megalopolis Basin. Marathousa 1 was dated to 400-500 ka (Blackwell et al. 2018; Jacobs et al. 2018) and provides a rich lithic as well as faunal assemblage (e.g., Tourloukis et al. 2018a; Konidaris et al. 2018). In contrast, the oldest human fossil, Petralona, commonly attributed to *Homo heidelbergensis*, or pre-Neanderthal, is not well dated (Dean et al. 1998; Hublin 1998, 2009). A Neanderthal presence in Greece was demonstrated by several Middle Paleolithic find spots and sites (Tourloukis and Harvati 2018), especially in the Mani Peninsula, Southern Peloponnese, where human fossils have also been recovered (e.g., Elefanti et al. 2008; Tourloukis et al. 2016). Three sites in Mani yielded Neanderthal remains: Lakonis (Harvati et al. 2003), Kalamakia (Harvati et al. 2013) and Apidima (Pitsios 1999; Harvati et al. 2019), dated to ca. 40 ka, between 100 and 40 ka, and to ca. 170 ka, respectively.

Although a direct or indirect dating is not available for the Megalopolis molar, the geology of the Megalopolis Basin suggests a Middle Pleistocene geological age, under the assumption that the molar is a fossil and not a modern intrusion. The Megalopolis Basin is a tectonic half-graben and filled with Neogene to Holocene sediments (Vinken 1965). Geological mapping showed that the

surrounding hills consist of pre-Pliocene basement while the majority of the basin encompasses sediments of Pleistocene, especially Middle Pleistocene, origin (Siavalas et al. 2009). The Middle Pleistocene sediments can be divided into the Megalopolis member of the Choremi formation, which consists of fluvial deposits, and the Marathousa member, which consists of fossil-rich lacustrine deposits (Löhnert and Nowak 1965; Vinken 1965). On the grounds of paleomagnetic, cyclostratigraphic, biochronological and palynological data, the lacustrine sequence has been chronologically bracketed between ca. 950-350 ka (van Vugt et al. 2000; Okuda et al. 2001), or ca. 800-300 ka (Tourloukis et al. 2018b), with its upper age-limit being poorly constrained at around 300 or 200 ka (see also Jacobs et al. 2018; Blackwell et al. 2018). Recent multiproxy paleoenvironmental reconstruction (Bludau et al. 2021) has highlighted the role of the Megalopolis Basin as a potential glacial refugium for Pleistocene humans due to its ability to retain freshwater bodies during glacial periods. The Megalopolis molar was part of a surface collection, in which many of the collected fossils were found still embedded in blocks of lacustrine sediments and derived from deposits of the Marathousa Member (Sickenberg 1976: 26). Therefore, we hypothesize that the Megalopolis molar dates to the Middle Pleistocene and derives from the Marathousa Member of the Choremi Formation.

Future work should focus on expanding the comparative sample, especially the fossil sample of Neanderthals in order to span their entire spatial and temporal range, as well as representatives of *Homo heidelbergensis*, which are underrepresented in our study. Methods based on segmentation, e.g., analyses of the enamel dentine junction (EDJ), are limited by the state of preservation of the Megalopolis molar, which complicate the differentiation between enamel and dentine. Future improvements in CT scanning techniques might enable the latter and provide a more complete picture of the taxonomic affinities of the Megalopolis molar.

CONCLUSION

The case study of the Megalopolis molar demonstrates the necessity of analytical tools that allow the study of incomplete

specimens. The method of crown outline analysis was applied to M^3s and allowed the first quantitative study of the Megalopolis molar. On the basis of our results, we conclude that the Megalopolis molar most likely represents a Pleistocene specimen with Neanderthal lineage affinities. The importance of the Megalopolis molar is threefold. First, it contributes to the Pleistocene human fossil record of Greece. Every new individual is valuable in adding to our understanding of human evolution in this relatively understudied region (see, e.g., Harvati 2016; Tourloukis and Harvati 2018). Second, the Megalopolis molar was found in the Megalopolis Basin, where the Middle Pleistocene site Marathousa 1 is also located. Both this specimen and the site highlight the potential of this region for yielding precious paleoanthropological finds. Furthermore, the present study adds to the examples of methodological improvements enabling new insights from known material, which could not be studied at the time of discovery due to its fragmentary status or taphonomic distortion.

ACKNOWLEDGMENTS

We would like to thank Catherine C. Bauer and Vangelis Tourloukis for their useful comments and remarks about the methodology and geology of the Megalopolis Basin, respectively. We are grateful to Sireen El Zaatari for access to her collection of high resolution dental casts and her valuable comments, and to Panagiotis Karkanas for assistance with photographing the specimen. For access to the Megalopolis molar, we thank the Faculty of Geology and Geoenvironment and the Museum of Paleontology and Geology, National and Kapodistrian University of Athens, as well as Vassilis Karakitsios, George Lyras, Hara Drinia and the late Nikolaos Symeonidis. We would like to acknowledge all institutions and researchers that provided CT scans for this research: NESPOS online database; the Staatliches Museum für Naturkunde Stuttgart for access to the Steinheim material; the Senckenberg Research Institute in Frankfurt am Main and Friedemann Schrenk for access to Sangiran 7-17; the Balai Pelestarian Situs Manusia Purba of Sangiran, Java, as well as

Arnaud Mazurier, Clément Zanolli, Roberto Macchiarelli, Harry Widianto, Dominique Grimaud-Hervé and Françoise Sémah for access to Sangiran NG0802.1. In addition, we would like to acknowledge the assistance of the Paleoanthropology High Resolution Computing Tomography Laboratory at the Eberhard-Karls University of Tübingen, supported by the DFG INST 37/706-1, in scanning the dental casts and all used individuals from the osteological collection of the University of Tübingen. This research was supported by the European Research Council (ERC CoG no. 724703). We are grateful to the reviewers, Mirjana Roksandic and Hugo Reyes-Centeno, for their comments and suggestions.

REFERENCES

Abdi, H., and L. Williams. 2010. Principal component analysis. *Willey Interdisciplinary Reviews: Computational Statistics* 2: 433-459. doi:10.1002/wics.101.

Adams, D., M. Collyer, and A. Kaliontzopoulou. 2020. Geomorph: Software for geometric morphometric analyses. Version 3.2.1. https://cran.r-project.org/package=geomorph.

Athanassiou, A. 2018. Pleistocene vertebrates from the Kyparíssia lignite mine, Megalopolis Basin, S. Greece: Rodentia, Carnivora, Proboscidea, Perissodactyla, Ruminantia. Quaternary International 497: 198-221. doi:10.1016/j.quaint.2018.06.042.

Athanassiou, A., D. Michailidis, E. Vlachos, V. Tourloukis, N. Thompson, and K. Harvati. 2018. Pleistocene vertebrates from the Kyparíssia lignite mine, Megalopolis Basin, S. Greece: Testudines, Aves, Suiformes. *Quaternary International* 497: 178–197. doi:10.1016/j.quaint.2018.06.030.

Bailey, S. E. 2002. Neandertal dental morphology: Implications for modern human origins. Ph.D. Dissertation, Arizona State University.

Bailey, S. E., and J. M. Lynch. 2005. Diagnostic differences in mandibular P4 shape between Neandertals and anatomically modern humans. *American Journal of Physical Anthropology* 126: 268e277.

Bauer, C. C., S. Benazzi, A. Darlas, and K. Harvati. 2018. Geometric morphometric analysis and internal structure measurements of the Neanderthal lower fourth Premolars from Kalamakia, Greece. *Quaternary International* 497: 14–21. doi:10.1016/j.quaint.2018.01.035.

Benazzi, S., M. Fantini, F. De Crescenzio, F. Persiani, and G. Gruppioni. 2009. Improving the spatial orientation of human teeth using a virtual 3D approach. *Journal of Human Evolution* 56: 286–293. doi:10.1016/j.jhevol.2008.07.006.

Benazzi, S., M. Coquerelle, L. Fiorenza, F. Bookstein, S. Katina, and O. Kullmer. 2011a. Comparison of dental measurement

systems for taxonomic assignment of first molars. *American Journal of Physical Anthropology* 144: 342–54. doi:10.1002/ajpa.21409.

Benazzi, S., K. Douka, C. Fornai, C. C. Bauer, O. Kullmer, J. Svoboda, I. Pap, F. Mallegni, P. Bayle, and M. Coquerelle. 2011b. Early dispersal of modern humans in Europe and implications for Neanderthal behavior. *Nature* 479: 525–529. doi:10.1038/nature10617.

Benazzi, S., C. Fornai, L. Buti, M. Toussaint, F. Mallegni, S. Ricci, G. Gruppioni, G. W. Weber, G. W., Condemi, and A. Ronchitelli. 2012. Cervical and crown outline analysis of worn Neanderthal and modern human lower second deciduous molars. *American Journal of Physical Anthropology* 149: 537–546. doi:10.1002/ajpa.22155.

Blackwell, B. A. B., N. Sakhrani, I. K. Singh, K. K. Gopalkrishna, V. Tourloukis, E. Panagopoulou, P. Karkanas, J. I. B. Blickstein, A. R. Skinner, J. A. Florentin, and K. Harvati. 2018. ESR Dating Ungulate Teeth and Molluscs from the Paleolithic Site Marathousa 1, Megalopolis Basin, Greece. *Quaternary* 1: 22. doi:10.3390/quat1030022.

Bludau, I. J. E., P. Papadopoulou, G. Iliopoulos, M. Weiss, E. Schnabel, N. Thompson, V. Tourloukis, C. Zachow, S. Kyrikou, G. E. Konidaris, P. Karkanas, E. Panagopoulou, K. Harvati, and A. Junginger. 2021. Lake-level changes and their paleo-climatic implications at the MIS12 Lower Paleolithic (Middle Pleistocene) site Marathousa 1, Greece. *Frontiers in Earth Science* 9: 668445. doi: 10.3389/feart.2021.668445.

Bollen, K. A., and R. Jackman. 1985. Regression diagnostics: An expository treatment of outliers and influential cases. *Sociological Methods and Research* 13: 510–542. doi:10.1177/0049124185013004004.

Bookstein, F. L. 1991. *Morphometric Tools for Landmark Data: Geometry and Biology*. New York: Cambridge University Press, Cambridge (UK).

Brook, A. H., M. B. O'Donnell, A. Hone, E. Hart, T. E. Hughes, R. N. Smith, and G. C. Townsend. 2014a. General and craniofacial development are complex adaptive processes influenced by diversity. *Australian Dental Journal* 59: 13–22. doi:10.1111/adj.12158.

Brook, A. H., J. Jernvall, R. N. Smith, T. R. Hughes, and G. C. Townsend. 2014b. The dentition: The outcomes of morphogenesis leading to variations of tooth number, size and shape. *Australian Dental Journal* 59: 131–142. doi:10.1111/adj.12160.

Carter, M., and J. Shieh. 2015. *Guide to Research Techniques in Neuroscience*, pp. 117–144. Amsterdam, Boston: Elsevier Academic Press. doi:10.1016/B978-0-12-800511-8.00005-8.

Dean, D., J. J. Hublin, R. Holloway, and R. Ziegler. 1998. On the phylogenetic position of the pre-Neandertal specimen from Reilingen, Germany. *Journal of Human Evolution* 34: 485–508. doi:10.1006/jhev.1998.0214.

Duval, M., C. Falguères, and J. J. Bahain. 2012. Age of the oldest hominin settlements in Spain: Contribution of the combined U-series/ESR dating

method applied to fossil teeth. *Quaternary Geochronology* 10: 412–417. doi:10.1016/j.quageo.2012.02.025.

Edgar, H. J., and S. D. Ousley. 2016. Dominance in dental morphological traits: Implications for biological distance studies. In *Biological Distance Analysis: Forensic and Bioarchaeological Perspectives*, ed. by M. A. Pilloud and J. T. Hefner, pp. 317–332. Amsterdam, Boston: Elsevier Academic Press. doi:10.1016/B978-0-12-801966-5.00017-2.

Elefanti, P., E. Panagopoulou, and P. Karkanas. 2008. The transition from the Middle to the Upper Paleolithic in the Southern Balakans: The evidence from the Lakonis 1 Cave, Greece. *Eurasian Prehistory* 5: 85–95.

Giusti, D., V. Tourloukis, G. E. Konidaris, N. Thompson, P. Karkanas, E. Panagopoulou, and K. Harvati. 2018. Beyond maps: Patterns of formation processes at the Middle Pleistocene open-air site of Marathousa 1, Megalopolis Basin, Greece. *Quaternary International* 497: 137–153. doi:10.1016/j.quaint.2018.01.041.

Gómez-Robles, A., M. Martinón-Torres, J. M. B. de Castro, L Prado, S. Sarmiento, and J. L. Arsuaga. 2008. Geometric morphometric analysis of the crown morphology of the lower first premolar of hominins, with special attention to Pleistocene *Homo. Journal of Human Evolution* 55: 627e638.

Gómez-Robles, A., J. M. B. de Castro, M. Martinón-Torres, L. Prado-Simón, and J. L. Arsuaga. 2012. A geometric morphometric analysis of hominin upper second and third molars, with particular emphasis on European Pleistocene populations. *Journal of Human Evolution* 63: 512-526. doi:10.1016/j.jhevol.2012.06.002.

Gunz, P., P. Mitteroecker, F. L. Bookstein. 2005. Semilandmarks in three dimensions. In *Modern Morphometrics in Physical Anthropology*, ed. by D. E. Slice, pp. 73–98. Boston: Springer. doi:10.1007/0-387-27614-9_3.

Green, R. E., J. Krause, A. W. Briggs, T. Maricic, U. Stenzel, M. Kircher, N. Patterson, H. Li, W. Zhai, M. H.-Y. Fritz, et al. 2010. A draft sequence of the Neandertal genome. *Science* 328:710–722. doi:10.1126/science.1188021.

Harvati, K., E. Panagopoulou, and P. Karkanas. 2003. First Neanderthal remains from Greece: The evidence from Lakonis. *Journal of Human Evolution* 45: 465–473. doi:10.1016/j.jhevol.2003.09.005.

Harvati, K., A. Darlas, S. E. Bailey, T. R. Rein, S. El Zaatari, L. Fiorenza, L., O. Kullmer, and E. Psathi. 2013. New Neanderthal remains from Mani Peninsula, Southern Greece: The Kalamakia Middle Paleolithic cave site. *Journal of Human Evolution* 64: 486–499. doi:10.1016/j.jhevol.2013.02.002.

Harvati, K., C. C. Bauer, F. E. Grine, S. Benazzi, R. R. Ackermann, K. L. van Niekerk, and C. S. Henshilwood. 2015. A human deciduous molar from the Middle Stone Age (Howiesons Poort) of Klipdrift Shelter, South Africa. *Journal of Human Evolution* 82: 190–196. doi:10.1016/j.jhevol.2015.03.001.

Harvati, K. 2016. Paleoanthropology in Greece: Recent findings and interpretations. In *Paleoanthropology of the Balkans and Anatolia: Human Evolution and Its Context*, ed. by K. Harvati and M. Roksandic, pp. 3–14. Dordrecht: Springer. doi:10.1007/978-94-024-0874-4_1.

Harvati, K., C. Röding, A. M. Bosman, A. F. Karakostis, R. Grün, C. Stringer, P. Karkanas, N. C. Thompson, V. Koutoulidis, L. A. Moulopoulos, V. G. Gorgoulis, and M. Kouloukoussa. 2019. Apidima Cave fossil provides earliest evidence of *Homo sapiens* in Eurasia. *Nature*. doi:10.1038/s41586-019-1376-z.

Hublin, J. J..1998. Climatic changes, paleogeography, and the evolution of the Neandertals. In *Neandertals and Modern Humans in Western Asia*, ed. by T. Akazawa, K. Aoki and O. Bar-Yosef, pp. 295–310. New York: Plenum Press. doi:10.1007/0-306-47153-1_18.

Hublin, J.-J. 2009. The origin of Neandertals. *Proceedings of the National Academy of Sciences* 106: 16022–16027. doi:10.1073/pnas.0904119106.

Jacobs, Z., B. Li, P. Karkanas, V. Tourloukis, N. Thompson, E. Panagopoulou, and K. Harvati. 2018. Optical dating of K-feldspar grains from Middle Pleistocene lacustrine sediment at Marathousa 1 (Greece). *Quaternary International* 497: 170–177. doi:10.1016/j.quaint.2018.06.029.

Koenigswald, W. V., and W. D. Heinrich. 2007. Biostratigraphische Begriffe aus der Säugetierpaläontologie für das Pliozän und Pleistozän Deutschlands. *Eiszeitalter und Gegenwart Quaternary Science Journal* 56: 96–115.

Konidaris, G. E., A. Athanassiou, V. Tourloukis, N. Thompson, D. Giusti, E. Panagopoulou, and K. Harvati. 2018. The skeleton of a straight-tusked elephant (Palaeoloxodon antiquus) and other large mammals from the Middle Pleistocene butchering locality Marathousa 1 (Megalopolis Basin, Greece): Preliminary results. *Quaternary International* 497: 65–84. doi:10.1016/j.quaint.2017.12.001.

Konidaris, G. E., V. Tourloukis, A. Athanassiou, D. Giusti, N. Thompson, E. Panagopoulou, P. Karkanas, and K. Harvati. 2019. Marathousa 2: A new Middle Pleistocene locality in Megalopolis Basin (Greece) with evidence of human modifications on faunal remains. *PESHE* 8: 82.

Landis, J., and G. Koch. 1977. The measurement of observer agreement for categorical data. *Biometrics* 33:159–174. doi:10.2307/2529310.

Löhnert, E., and H. Nowack. 1965. Die Braunkohlenlagerstätte von Khoremi im Becken von Megalopolis/Peloponnes. *Geologisches Jahrbuch* 82: 847–868.

Macchiarelli, R., L. Bondioli, and A. Mazurier. 2008. Virtual dentitions: Touching the hidden evidence. In *Technique and Application in Dental Anthropology*, ed. by J. D. Irish and G. C. Nelson, Cambridge Studies in Biological and Evolutionary Anthropology 53, pp. 426–448. Cambridge: Cambridge University Press. doi:10.1017/CBO9780511542442.018.

Macho, G. A., and J. Moggi-Cecchi. 1992. Reduction of maxillary molars in *Homo sapiens sapiens*: a different perspective. *American Journal of Physical Anthropology* 87: 151e159.

Marinos, G. 1975. Über einen menschlichen Zahn unter den Säugetier-Resten biharischen Alters von Megalopolis. *Annales Géologiques des Pays Helléniques* 27: 64–65.

Martinón-Torres, M., M. Bastir, J. M. B. de Castro, A. Gómez, S. Sarmiento, A. Muela, J. L. Arsuaga. 2006. Hominin lower second premolar morphology: Evolutionary inferences through geometric morphometric analysis. *Journal of Human Evolution* 50: 523e533.

Melentis, J. K. 1961. Die Dentition der Pleistozänen Proboscidier des Beckens von Megalopolis im Peloponnes (Griechenland). *Annales Géologiques des Pays Helléniques* 12: 153–262.

Neubauer, S., P. Gunz, and J. J. Hublin. 2009. The pattern of endocranial ontogenetic shape changes in Humans. *Journal of Anatomy* 215: 240–255. doi:10.1111/j.1469-7580.2009.01106.x.

Okuda, M., N. van Vugt, T. Nakagawa, M. Ikeya, A. Hayashida, Y. Yasuda, and T. Setoguchi. 2002. Palynological evidence for the astronomical origin of lignite–detritus sequence in the Middle Pleistocene Marathousa member, Megalopolis, SW Greece. *Earth and Planetary Science Letters* 201: 143–157. doi:10.1016/S0012-821X(02)00706-9.

Panagopoulou, E., V. Tourloukis, N. Thompson, A. Athanassiou, G. Tsartsidou, G. E. Konidaris, D. Giusti, P. Karkanas, and K. Harvati. 2015. Marathousa 1: A new Middle Pleistocene archaeological site from Greece. *Antiquity* 89: Project Gallery. doi:10.15496/publikation-5878.

Pitsios, T. K. 1999. Paleoanthropological research at the cave site of Apidima and the surrounding region (South Peloponnese, Greece). *Anthropologischer Anzeiger* 57: 1–11.

Posth, C., C. Weißling, K. Kitagawa, L. Pagani, L. Van Holstein, F. Racimo, N. J. Conard, C. J. Kind, H. Bocherens, and J. Krause. 2017. Deeply divergent archaic mitochondrial genome provides lower time boundary for African gene flow into Neanderthals. *Nature Communications* 8: 16046. doi:10.1038/ncomms16046.

R Development Core Team. 2011. *R: A language and Environment for Statistical Computing*. R Foundation for Statistical Computing, Vienna, Austria. ISBN 3-900051-07-0.

Sankararaman, S., N. Patterson, H. Li, S. Pääbo, D. Reich. 2012. The date of interbreeding between Neanderthals and modern humans. *PLOS Genetics* 8: e1002947. doi:10.1371/journal.pgen.1002947.

Schneider, T., K. Filo, A. L. Kruse, M. Locher, K. W. Grätz, and H. T. Lübbers. 2014. Variations in the anatomical positioning of impacted mandibular wisdom teeth and their practical implications. *Swiss Dental Journal* 124: 520-538.

Scott, G., C. Turner II, G. Townsend, G., and M. Martinón-Torres. 2018. *The Anthropology of Modern Human Teeth: Dental Morphology and its Variation in Recent and Fossil Homo sapiens*. Cambridge Studies in Biological and Evolutionary Anthropology 79. Cambridge: Cambridge University Press. doi:10.1017/9781316795859.

Siavalas, G., M. Linou, A. Chatziapostolou, S. Kalaitzidis, H. Papaefthymiou, and K. Christanis. 2009. Palaeoenvironment of Seam I in the marathousa

lignite mine, Megalopolis Basin (Southern Greece). *International Journal of Coal Geology* 78: 233–248. doi:10.1016/j.coal.2009.03.003.

Sickenberg, O. 1976. Eine Säugetierfauna des tieferen Bihariums aus dem Becken von Megalopolis (Peloponnes, Griechenland). *Annales Géologiques des Pays Helléniques* 27: 25–63.

Singleton, M. 2002. Patterns of cranial shape variation in the Papionini (Primates: Cercopithecinae). *Journal of Human Evolution* 42:547–578. doi:10.1006/jhev.2001.0539.

Skouphos, T. G. 1905. Über die palaeontologischen Ausgrabungen in Griechenland in Beziehung auf das Vorhandensein des Menschen. In *Comptes Rendus du Congrès International d'Archéologie*, pp. 231–236. Athènes.

Smith, P., J. S. Brink, J. W. Hoffman, L. C. Bam, R. Nshimirimana, and F.C. de Beer. 2015. The late Middle Pleistocene upper third molar from Florisbad: Metrics and morphology. *Transactions of the Royal Society of South Africa* 70: 233–244. doi:10.1080/0035919X.2015.1065930.

Sprowls, M. W., R. E. Ward, P. L. Jamison, and J. K. Hartsfield. 2008. Dental arch asymmetry, fluctuating dental asymmetry, and dental crowding: A comparison of tooth position and tooth size between antimeres. *Seminars in Orthodontics* 14: 157–165. doi:10.1053/j.sodo.2008.02.006.

Thompson, N., V. Tourloukis, E. Panagopoulou, and K. Harvati. 2018. In search of Pleistocene remains at the gates of Europe: Directed surface survey of the Megalopolis Basin (Greece). *Quaternary international* 497: 22–32. doi:10.1016/j.quaint.2018.03.036.

Tourloukis, V., N. Thompson, C. Garefalakis, P. Karkanas, G. E. Konidaris, E. Panagopoulou, and K. Harvati. 2016. New Middle Palaeolithic sites from the Mani Peninsula, Southern Greece. *Journal of Field Archaeology* 41: 68–83. doi:10.1080/00934690.2015.1125223.

Tourloukis, V., N. Thompson, E. Panagopoulou, D. Giusti, G. E. Konidaris, P. Karkanas, and K. Harvati. 2018a. Lithic artifacts and bone tools from the Lower Palaeolithic Site Marathousa 1, Megalopolis, Greece: Preliminary results. *Quaternary International* 497: 47–64. doi:org/10.1016/j.quaint.2018.05.043.

Tourloukis, V., G. Muttoni, P. Karkanas, E. Monesi, G. Scardia, E. Panagopoulou, and K. Harvati. 2018b. Magnetostratigraphic and chronostratigraphic constraints on the Marathousa 1 Lower Palaeolithic site and the Middle Pleistocene deposits of the Megalopolis Basin, Greece. *Quaternary International* 497: 154–169. doi:10.1016/j.quaint.2018.03.043.

Tourloukis, V., and K. Harvati. 2018. The Palaeolithic record of Greece: A synthesis of the evidence and a research agenda for the future. *Quaternary International* 466: 48–65. doi:10.1016/j.quaint.2017.04.020.

White, S., J. A. J. Gowlett, and M. Grove. 2014. The place of the Neanderthals in hominin phylogeny. J*ournal of Anthropological Archaeology* 35: 32–50.

Wood, B., S. A. Abbott, and S. H. Graham. 1983. Analysis of the dental morphology of Plio-Pleistocene hominids II: Mandibular molars - study of cusp areas, fissure pattern and cross sectional shape of the crown. *Journal of Anatomy* 137: 287e314.

Van Vugt, N., H. de Bruijn, T. van Kolfschoten, and C. G. Langereis. 2000. Magneto- and cyclostratigraphy and mammal-fauna's of the Pleistocene lacustrine Megalopolis Basin, Peloponnesos, Greece. *Geological Ultrajectina* 189: 69–92.

Vargiu, R., A. Cucina, and A. Coppa. 2009. Italian populations during the Copper Age: Assessment of biological affinities through morphological dental traits. *Human Biology* 81: 479–494. doi:10.3378/027.081.0406.

Venables, W. N., and B. D. Ripley. 2002. *Modern Applied Statistics with S*. 4th edition. New York: Springer. doi:10.1007/978-0-387-21706-2.

Vinken, R. 1965. Stratigraphie und Tektonik des Beckens von Megalopolis (Peloponnes, Griechenland). *Geologisches Jahrbuch* 83: 97-148.

von Cramon-Taubadel, N., B. C. Franzier, and M. Marizón Lahr. 2007. The problem of assessing landmark error in geometric morphometrics: Theory, methods, and modifications. *American Journal of Physical Anthropology* 134: 24–35. doi:10.1002/ajpa.20616.

Wandsnider, L. 2004. Solving the puzzle of the archaeological labyrinth: Time perspectivism in Mediterranean surface archaeology. In *Side-by-Side Survey: Comparative Regional Studies in the Mediterranean World*, ed. by S. Alcock and J. F. Cherry, pp. 49–62. Anthropology Faculty Publications 75. Oxford: Oxbow Press.

Xing, S., M. Martinón-Torres, J. M. B. de Castro, Y. Zhang, X. Fan, L. Zheng, W. Huang, and W. Liu. 2014. Middle Pleistocene hominin teeth from Longtan Cave, Hexian, China. *PloS one* 9: e114265. doi:10.1371/journal.pone.0114265.

Xirotiris, N., W. Henke, and N. Symeonidis. 1979. Der M^3 von Megalopolis – ein Beitrag zu seiner Morphologischen Kennzeichnung. *Zeitschrift für Morphologie und Anthropologie* 70: 117–122.

Zanolli, C. 2013. Additional evidence for morpho-dimensional tooth crown variation in a new Indonesian *H. erectus* sample from the Sangiran Dome (Central Java). *PLoS ONE* 8: e67233. doi:10.1371/journal.pone.0067233.

Zanolli, C. 2015. Molar Crown Inner Structural Organization in Javanese *Homo erectus*. *American Journal of Physical Anthropology* 156: 148–157. doi:10.1002/ajpa.22611.

Zelditch, M., D. Swiderski, and H. Sheets. 2012. *Geometric Morphometrics for Biologists: A Primer*. 2nd Edition. San Diego: Elsevier Academic Press.

Study III: Mugharet el'Aliya Maxilla

Mugharet el'Aliya: affinities of an enigmatic North African Aterian maxillary fragment

By Carolin Röding, Chris Stringer, Rodrigo S. Lacruz and Katerina Harvati

Manuscript ready for submission[1].

[1]The final submitted and accepted manuscript may deviate from the version included in this thesis.

Mugharet el'Aliya: affinities of an enigmatic North African Aterian maxillary fragment

Carolin Röding[1]*, Chris Stringer[2], Rodrigo S. Lacruz[3] and Katerina Harvati[1,4]

[1]Paleoanthropology, Senckenberg Centre for Human Evolution and Palaeoenvironment, Eberhard Karls University of Tübingen, Tübingen, Germany.
[2] Centre for Human Evolution Research, Department of Earth Sciences, The Natural History Museum, London, UK
[3]Department of Molecular Pathobiology, New York University College of Dentistry, New York, NY, USA.
[4]DFG Centre of Advanced Studies 'Words, Bones, Genes, Tools', Eberhard Karls University of Tübingen, Tübingen, Germany.

Objectives. This study uses a virtual framework to examine the left maxillary fragment of the Mugharet el'Aliya juvenile fossil, Morocco, found in association with an Aterian lithic industry. Previously this fossil has been ascribed to modern humans or to the Neanderthal lineage based on its 'archaic' / 'Neanderthal-like' features and apparent large size. Here, we conducted a novel 3D shape comparative analysis of the maxillary fragment to clarify its taxonomic affinities with regard to its size and ontogeny.

Materials and Methods. 80 Computed Tomography and surface scans representing ontogenetic samples of *Homo sapiens* and *Homo neanderthalensis* were used to capture species-specific differences. The toolkit of geometric morphometrics in combination with surface registration and an elastic iterative closest point algorithm were used to create a dataset of meshes with an identical number of corresponding vertices for the maxillae. Multivariate statistics were applied to Procrustes superimposed coordinates derived from the vertices of this dataset.

Results. Our analysis showed affinities of the Mugharet el'Aliya individual with our *Homo sapiens* sample, especially with a subadult individual from Qafzeh. No size-independent affinities with Neanderthals of comparable dental age could be identified.

Discussion. Our results add to the evidence connecting fossils from western Asia, especially Qafzeh and Skhul, and the North African Aterian. Furthermore, Mugharet el'Aliya adds to our knowledge of the ontogenetic development of adult morphology that is frequently used to characterize hominin groups, e.g., Neanderthals and modern humans.

Introduction

North Africa, long considered a peripheral geographical region in comparison with eastern or southern Africa (e.g., Balter, 2011), has recently gained renewed importance in modern human origins research. Renewed work at the site of Jebel Irhoud, Morocco, pushed back the appearance of *Homo sapiens* remains associated with an early Middle Stone Age (MSA) to ca. 300 ka (Richter et al., 2017; Hublin et al., 2017), the earliest date known for our lineage. This discovery contributed greatly to the formulation of the pan-African model for modern human origins (e.g., review in Henn, Steele & Weaver, 2018; references therein) and highlights the complexity of the evolutionary processes that led to the appearance of our lineage.

The later Moroccan human fossil record, associated with the Aterian lithic industry, has garnered less attention despite its relevance to modern human evolution. While some researchers have considered Aterian fossils to represent the oldest anatomically modern humans in Northern Africa (Hublin, 1993; references therein), their geological age, and therefore relevance to human origins, has been unclear. Redating of Aterian sites points to an earlier chronology than previously considered, and to a possible overlap with a lithic industry attributed to the early MSA (historically referred to as 'African Mousterian') during MIS5-6, underlining the potential evolutionary significance of these remains (e.g., Barton, Bouzouggar, Collcutt, Schwenninger & Clark-Balzan, 2009; Mercier, Wengler, Vallda, Joron, Froget & Reyss, 2007; Richter, Moser, Nami, Eiwanger & Mikdad, 2010; Jacobs, Meyer, Roberts, Aldeias, Dibble & El Harjraoui, 2011; Hublin et al., 2012). Human fossils associated with the Aterian industry remain poorly understood, being described as showing a mixture of primitive and derived traits with robust jaws and high levels of megadonty, particularly in the post-canine dentition (e.g., Ferembach, 1976; Hublin & Tillier, 1981; Smith et al., 2007; Hublin et al., 2012). Especially during the first half of the 20th century, this combination of features often led to the attribution of such fossils (e.g., Şenyürek, 1940; McBurney, Trevor & Wells, 1953) - as well as the specimens from Jebel Irhoud (Ennouchi, 1962) - to the Neanderthal lineage. Although these are now generally recognized as early *H. sapiens* with some similarities to individuals from Skhul and Qafzeh, Israel (e.g., Harvati & Hublin,

2012; Hublin et al., 2012; Hublin & Tillier, 1988; Freidline et al., 2021), the origin of their archaic morphology remains unclear and is an important topic of investigation for understanding evolutionary processes underlying modern human origins in the region. This is especially true in light of paleogenetic evidence of repeated interbreeding among human lineages, both in Eurasia and in Africa, in the Pleistocene (e.g., Posth et al., 2017; Meyer et al., 2016; Dannemann & Racimo, 2018; Durvasula & Sankararaman, 2020; Hsieh et al., 2016; Lachance et al., 2012); of fossil evidence pointing to considerable geographic dispersals of early human populations (Hershkovitch et al. 2018; Harvati et al. 2019); and of the geographic position of North Africa at the southern rim of the Mediterranean Basin as a potential dispersal corridor and contact zone for early human groups (e.g., Green et al., 2010; Lazaridis et al., 2016; Prüfer et al., 2014; Osbourne et al., 2008; Bae, Douka & Petraglia, 2017). It is increasingly clear that the origin of *H. sapiens* was a more complicated process than previously thought, and the Aterian human fossil record can help shed light on this complexity.

Here, we aim to contribute to this discussion by examining the fragmentary left maxilla from Mugharet el'Aliya in the framework of virtual anthropology. Our goal is to help clarify the phylogenetic and taxonomic affinities of this enigmatic specimen and to analyze its archaic, 'Neanderthal-like' features in the context of size and ontogeny.

Mugharet el'Aliya: background and previous studies. A left maxillary fragment of a juvenile hominin with three unerupted teeth (see below) was recovered in 1939 from the cave site of Mugharet el'Aliya (Coon in Şenyürek, 1940). The site is part of the Caves of Hercules, a cave complex on the Moroccan Atlantic coast at Cap Ashakar, now located 18 m above sea level (35°45´N, 5°56´W; Wrinn & Rink, 2003). It was known at the time for yielding archeological material mainly attributed to the Neolithic and Later Stone Age (LSA) (Bouzouggar, Kozłowski & Otte, 2002). Layers underlying the LSA were first excavated in 1939 and ascribed to the Aterian (Coon, 1957a; Bouzzouggar et al., 2002). The maxillary fragment was presumably recovered during sieving of unmixed sand from the lowest and oldest layer that had yielded the Aterian tools (Coon in Şenyürek, 1940; Coon, 1957a; Howe, 1967; Bouzouggar et al., 2002; Wrinn & Rink, 2003). The cave is now almost completely emptied of its sediments, preventing the

assessment of the exact provenance of the fossil, whose geological age therefore remains uncertain (Bouzouggar et al., 2002; Wrinn & Rink, 2003). The original provenance of the fossil reported by Coon was later questioned, suggesting that the discovery was a surface find within a trench (Coon, 1957b). Moreover, fluorine analyses performed using samples extracted from the maxilla did not match the dates of the layer originally associated with the fossil (Coon, 1957b; Minugh-Purvis, 1993). Dating of faunal remains showed Aterian occupations between 35-60 ka at Mugharet el'Aliya (Wrinn & Rink, 2003), thus providing a broad chronological framework. However, because the proposed layers that yielded the maxilla include both the youngest and oldest Aterian layers, its age cannot be narrowed down further. In addition to the maxillary fragment, an isolated permanent second molar was recovered in 1939 (Şenyürek, 1940) and two additional teeth were reported in 1947, which remain undescribed (Hublin, 1993). The presences of at least two fossil individuals at Mugharet el'Aliya is indicated by the combination of heavy dental wear on the permanent molar and subadult status of the maxillary fragment (Şenyürek, 1940).

Mugharet el'Aliya maxilla: The maxillary fragment was originally described by Şenyürek, (1940). Since then, some aspects of the external anatomy have been modified or lost. The unerupted left upper third premolar and left upper canine were removed after the initial description by opening the crypts with a dentist drill (Şenyürek, 1940). Moreover, samples for fluorine and nitrogen analysis were removed from the maxilla (although the location of the samples collected was not recorded) and the anterior nasal spine was damaged at some point after the excavation (Minugh-Purvis, 1993). The fragment comprises the left maxilla from approximately the midline to the anterior border of the crypt of the permanent second molar and includes the almost complete zygomatic process, left nasal opening and facies frontalis inferior to the infraorbital foramen (Figure 1; Şenyürek, 1940; Minugh-Purvis, 1993). Based on the dental developmental status, this juvenile individual is considered to have been ca. 9 years old at the time of death, with an age range of ± 2 years (Şenyürek, 1940; Minugh-Purvis, 1993).

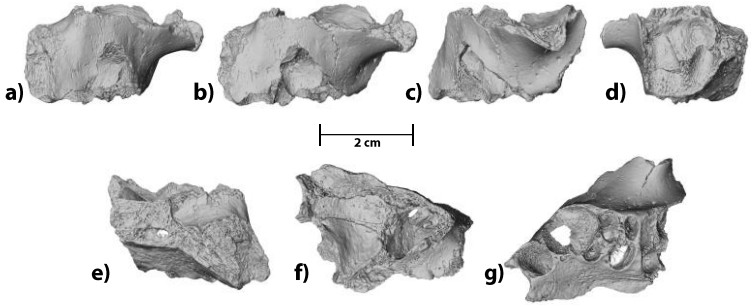

Figure 1: Virtual reconstruction of the left maxillary fragment of Mugharet el'Aliya. Shown in a) anterior, b) antero-lateral, c) lateral, d) posterior, e) medial, f) superior and g) inferior view.

The maxilla is large in absolute size and has thick bone walls (Şenyürek, 1940). The preserved external anatomy lacks a deep and distinct canine fossa, and the root of the zygomatic process is placed anterior to the first permanent molar, originating at the deciduous second molar (Şenyürek, 1940; Minugh-Purvis, 1993). These two features deviate from the typical adult modern human maxillary anatomy, whose ontogenetic manifestation remains in part elusive (cf. e.g., Minugh-Puris, 1993; Lieberman, McBratney & Krovitz, 2002; Schuh et al., 2020). Additionally, several modern human traits are not clearly identified in the Mugharet el'Aliya maxilla, including an angle of about 90 degrees between the anterior surface of the zygomatic bone to the midline, the inferior border of the zygoma being either vertically below the superior border or being retracted, and the inferior border of the zygoma reaching the alveolar process in a sharp inflexion with a malar notch (Lacruz et al., 2019). However, a clear presence of an *'incurvatio inframalaris frontalis'* in the Mugharet el'Aliya maxilla was reported (Hublin, 1993, 2000; Minugh-Purvis 1993). Such a curvature at the inferior zygomatic margin (IZM; also called zygomaticoalveolar crest) is considered to be a marked feature in modern humans and weak or absent in Neanderthals (e.g., Sergi, 1947; Pope, 1991; Weber & Krenn, 2017; Lacruz et al., 2019). In all, the preserved anatomy of the Mugharet el'Aliya maxilla has been described as showing modern human-like, unclear or 'archaic' / 'Neanderthal-like' features.

Materials & Methods

Sample. We evaluated the external morphology of the maxillary fragment through a set of 80 CT and surface scans (Table 1; Supplementary Table S1). Individuals from the comparative sample were assigned to one of three groups: Neanderthals (Roc the Marsal, Pech de l'Azé, La Quina H18, Teshik Tash, Amud, Shanidar 1, La Ferrassie 1, Forbes' Quarry 1, Saccopastore 2), *H. sapiens* (Grotte des Enfants 6, Nazlet Khater 2, Abri Pataud, Mladec 1, Predmosti 3, Liujiang, Holocene sample), and early *H. sapiens* (Qafzeh 10, Qafzeh 6, Skhul V, Jebel Irhoud 1, Omo 1). In addition, the dataset was divided into developmental age groups (see below).

Age estimation. Developmental age groups were based on dental eruption stages (e.g., Smith, 1989; Zihlman, Bolter & Boesch, 2004; Robson & Wood, 2008; Mori & Harvati, 2019; Freidline, Gunz, Harvati & Hublin, 2012). We used the eruption status of the permanent maxillary dentition to assign each individual to one of four dental age groups: (3) complete deciduous dentition, (4) erupted first molar, (5) erupted second molar, and (6) adult with erupted third molar. Modern humans with an erupted second molar and a closed spheno-basilar synchondrosis (SBS) were treated as adult due to the highly variable eruption time of the third molar (Carter & Worthington, 2015). We did not include age groups 1 and 2, i.e., individuals with no or incomplete deciduous dentition, so as to target comparable age groups for Mugharet el'Aliya; age group 6 was included to cover the adult inter-specific variation.

Measurement protocol. Attempts to analyze the microanatomy of the maxilla to determine its predominant pattern of facial growth and remodeling were unsuccessful due to a thick layer of preservative on the fossil. Thus, we focused our analysis on geometric morphometric methods. The Mugharet el'Aliya maxilla preserves only a limited number of diagnostic features, restricting the use of common linear measurements employed in classical comparative analyses of fossils. In addition, insufficient homologous points and structures are preserved for a comprehensive study using the standard toolkit of geometric morphometrics, which captures shape as a configuration of landmarks. Landmarks are homologous points covering

Table 1: Sample used in the dataset. Individuals are grouped in four dental age groups (3: complete deciduous dentition; 4: M^1 > ¾ erupted; 5: M^2 > ¾ erupted; 6: M^3 > ¾ erupted & SBS fused). [†]for Holocene non-fossil individuals only the number of used individuals provided.

Dental Age Group	Geological Age Groups	Country of Origin	Individuals[†]	Abbreviation for Fossil Individuals
3	*H. sapiens* Holocene	Tunisia	1	
		Germany	3	
		South Africa	6	
	H. neanderthalensis Late Pleistocene	France	Roc de Marsal	RdM
			Pech de l'Azé	PdA
4	Late Pleistocene	Morocco	Mugharet el'Aliya	El'Aliya
	H. sapiens Holocene	Tunisia	2	
		Egypt	1	
		Germany	9	
		South Africa	9	
	Late Pleistocene	Israel	Qafzeh 10	QA10
	H. neanderthalensis Late Pleistocene	France	La Quina H18	LQ18
	Middle / Late Pleistocene	Uzbekistan	Teshik Tash	TT
5	*H. sapiens* Holocene	Germany	11	
		South Africa	1	
	Late Pleistocene	Italy	Grotte des Enfants 6	GdE6
6	*H. sapiens* Holocene	Germany	5	
		Tanzania	5	
		South Africa	6	
	Late Pleistocene	Egypt	Nazlet Khater 2	NK2
		France	Abri Pataud	AP
		Czech Republic	Mladec 1	ML1
			Predmosti 3	PR3
		China	Liujiang	LI
		Israel	Qafzeh 6	QA6
			Skhul V	SK5
	Middle Pleistocene	Morocco	Jebel Irhoud 1	IR1
		Ethiopia	Omo 1	OM1
	H. neanderthalensis Late Pleistocene	Israel	Amud	AM
			Shanidar 1	SH1
		France	La Ferrassie 1	LF
		Gibraltar	Forbes' Quarry 1	FQ
	Middle / Late Pleistocene	Italy	Saccopastore 2	SA2

recognizable bony structures that can be extended by semi-landmarks on curves and surfaces (for discussion see e.g., Zelditch, Swiderski & Sheets, 2012; Slice, 2007; Bookstein, 1997; Mitteroecker & Gunz, 2009; Gunz, Mitteroecker & Bookstein, 2005). To maximize the analysis of the preserved external morphology of Mugharet el'Aliya we followed a recently described protocol for surface registration (cf. Schlager & Rüdell, 2013; Figure 2). To our knowledge, this study is among the first using surface registration in a fossil context. It offers a unique opportunity for the study of the fragmentary Mugharet el'Aliya specimen, despite some shortcomings that the use of this method entails (cf. Error calculations, Discussion).

The goal of the surface registration protocol is to deform a reference mesh to best match a target mesh by using Gaussian smoothed displacement vectors (Moshfeghi, Ranganath & Nawyn, 1994). By deforming the reference to match several target meshes, a sample of triangular meshes with the identical number of corresponding vertices is created. These vertices can be extracted and used as coordinates during analyses. Here, Mugharet el'Aliya was the reference and all other individuals were considered the targets.

In a first step, we extracted the external maxillary surface from each scan through either semi-automated segmentation of CT scans or manipulation of meshes generated via surface scanning. Creation of single-layered triangular meshes and mesh cleaning

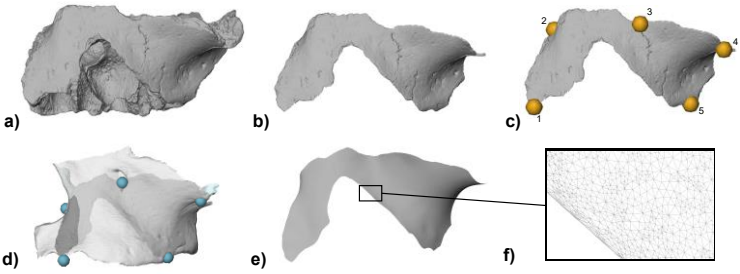

Figure 2: Visualization of the main steps for the method of surface registration. A) original maxillary fragment; b) extracted external maxillary surface as single-layered triangular mesh; c) landmark placement (see Table 2 for definitions); d) initial landmark-based TPS registration of reference onto each target mesh; e) elastic ICP-matching of surfaces from d, resulting in new single-layered triangular meshes; f) extraction of the vertices as coordinates for further analysis.

Table 2: Definitions for the landmarks used in the initial step of registration. †depending on dental age group as the sample includes complete deciduous, mixed and complete permanent dentition

Number in Figure 2c	Landmark Definition
1	Interalveolar septa between the first and second incisor (here either deciduous or permanent dentition)†
2	Point of maximum curvature between Alare (lateral-most point of the nasal aperture) and inferior-most margin of nasal aperture
3	Infero-medial foramen infraorbitale
4	Posterior-most point on the processus zygomaticus maxillae before the zygomaxillary suture
5	Anterior inter-alveolar septa of the first permanent molar (here either between UP^4/M^1 or dm^2/M^1)†

are essential in avoiding distortions in the following steps. Extracted surfaces from the right side were mirrored to the left side and their vertex orientation was inverted. In the next step, an initial landmark-based registration between the reference and each target was carried out by using the thin-plate spline (TPS) algorithm (Figure 2c, d; Table 2; Zelditch et al., 2012). After the initial registration, an iterative closest point algorithm was used to best match the reference onto the target (also called ICP-matching). The ICP-matching was coupled with an elastic component based on Gaussian displacement vectors (Moshfeghi et al., 1994) and was run with 40 iterations. Each iteration contained the four following steps (cf. Schlager & Rüdell, 2013): 1) each vertex of the reference mesh was projected onto the target mesh; 2) this was followed by discarding all displacement vectors for closest points that point to the wrong direction or where the angle between the normal and the displacement vector exceeded 45°; 3) the resulting displacement vectors were smoothed by applying Gaussian smoothing based on the neighborhood of each vertex; and 4) the resulting surface was smoothed to prevent mesh folding (Vollmer, Mencl & Müller, 1999).

In a final step, the coordinates underlying the vertices were extracted and Generalized Procrustes analysis (GPA) was used to superimpose the coordinates of all individuals to allow a statistical analysis of the resulting Procrustes shape coordinates. During GPA, information about orientation and location is removed and the landmark configurations are scaled to centroid size (CS),

calculated as the square root of the summed squared of each landmark-centroid distance (e.g., Zelditch et al., 2012).

Error calculations. Multiple measurements of the same individual were carried out by two observers (C.R.; J.Z.). Distances between repeated measures of landmarks placed for initial registration as well as between resulting surfaces were calculated (Supplementary Figures S1, S2). Out of all vertex combinations of the error measurements (N = 1,574,730) less than 0.001 % (N = 51) exceed a displacement of 1 mm, all of which were located at the edges of the meshes and can be explained by observer error during landmark placement. Additionally, the error introduced by the method itself was assessed by comparing each mesh created via surface registration with the corresponding original. For well-preserved, complete individuals distance heat maps show almost no displacement within the surface area (Supplementary Figure S3 a-c). For individuals with taphonomic damage or showing structures not present in the reference mesh (e.g., additional foramen), the displacement can locally exceed 1 mm and creates a smoothed mesh surface (Supplementary Figure S3 d-e; cf. Discussion). Smoothing restricted to small locally confined surface areas while preserving the vast majority of the original surface does not significantly affect the analyses (cf. Veneziano, Landi & Profico. 2018). However, individuals where surface registration resulted in large smoothed areas were excluded from the sample, to avoid artifacts and potential influence on the analyses (cf. Profico, Veneziano, Lanteri, Piras, Sansalone & Manzi, 2016).

Analyses. Patterns of shape variation were investigated by performing principal component analysis (PCA) of the Procrustes shape variables. Mugharet el'Aliya and all early *H. sapiens* fossils were not used to calculate the PCAs but were instead projected into the plots, following established procedure (see, e.g., Harvati et al., 2019; Mori, Profico, Reyes-Centeno & Harvati, 2020; Bosman, Reyes-Centeno & Harvati, 2020; Röding, Zastrow, Scherf, Doukas & Harvati, 2021). Shape changes occurring along each plotted principal component (PC) were illustrated as direct visualization of the vertices of each PC extreme. Dental age groups and species attribution were not part of the calculation of the PCA, which is independent of group membership, but were shown post facto in the form of convex hulls in the corresponding PCA plots. Convex hulls were calculated around the extreme points of each defined group and contain no information about confidence intervals. In

addition, log centroid size (CS) and PC1 were plotted against each other to visualize their allometric relationship and their correlation was tested via Pearson correlation tests. Ontogenetic trends were further explored as illustration of consecutive dental age group mean shapes and by computation of the common allometric component (CAC). The CAC is a scaled vector of slopes from a pooled regression calculated based on PC scores, which were corrected for their group-specific means based on size (Mitteroecker, Gunz, Bernhard, Schaefer & Bookstein, 2004).

The correlation between the main PCs and CAC was tested via Pearson correlation tests and CAC scores and log CS were plotted against each other to visualize their relationship. Overall shapes between individuals were compared based on Procrustes Distances (PD) of the entire shape captured in the dataset (e.g., Harvati, 2009; Mori & Harvati, 2020). Summary statistics were performed for sample mean, standard deviation (s.d.), minimum and maximum for CS and for mean and s.d. for PD. Statistical tests were considered significant at $\alpha \leq 0.05$.

Software. All steps of the measurement protocols and the following analyses were carried out in a combination of two different software environments. Avizo 9.2 Lite (Visualization Science Group) was used to create meshes and to obtain fixed landmarks. All other steps were carried out in R (R Developmental Core Team, 2020) by using freely available R packages, mainly geomorph, mesheR, Morpho, Rvcg, shapes. Graphics were created in R and processed in Adobe Illustrator CS5.

Results

As expected, size in form of CS shows an overall trend of maxillary size increase from younger dental age groups to the adults (Figure 3; Supplementary Tables S3, S4). On average, all early *H. sapiens* and Neanderthal dental age groups show larger CS than comparable recent modern humans, with Neanderthals showing the largest adult CS values. Mugharet el'Aliya and Qafzeh 10 fall within the Neanderthal variation of their corresponding dental age group 4 and within adult modern human variation. The only fossil subadult that falls outside the range of adult modern human CS is the youngest Neanderthal, Pech de l'Azé.

A set of vertices resulting from surface registration was analyzed in a PCA (cf. Methods; Figures 4, 5). The first PC explains 60.15 % of the total variance and summarizes shape changes related to width and height, as well as the relative position of the root of the zygomatic process in relation to the dentition. Individuals with positive PC1 scores show a relatively wide and low maxilla, with a rather anteriorly placed root of the zygomatic process. Individuals with negative PC1 scores show a relatively narrow and tall maxilla with a rather posteriorly placed root of the zygomatic process.

These shape changes are highly negatively correlated with CS as well as dental age group (Supplementary Figure S4) with Pearson correlation coefficients of -0.714 for shape summarized in PC1 and CS (T = -9.008, DoF = 78, p = <0.01) and of -0.834 for PC1 and dental age groups (T = -13.315, DoF = 78, p < 0.01). Thereby, PC1 separates partially consecutive age groups of Neanderthals and

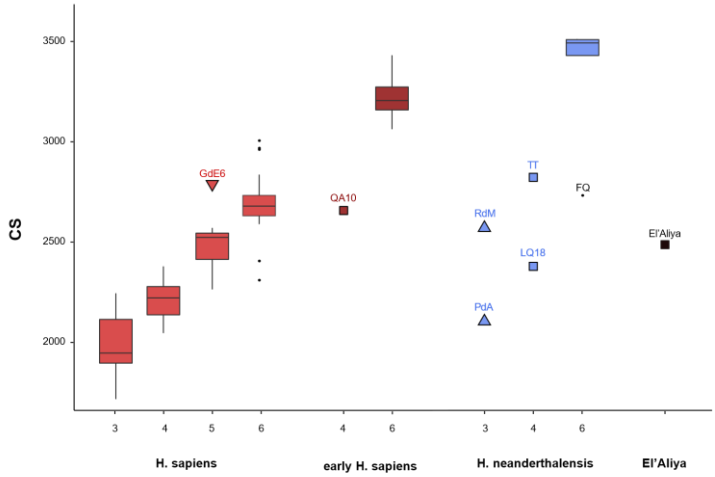

Figure 3: Box-Whisker plots as illustration of Centroid Size (CS) distribution per dental age group within the *H. sapiens* (red), early *H. sapiens* (dark red) and Neanderthal (blue) samples as well as Mugharet el'Aliya (black). Subadult fossil individuals assigned to dental age group 3 are shown as triangles, age group 4 as squares and age group 5 as inverted triangles. Dental age groups, abbreviations and CS of all individuals listed in Table 1 & Supplementary Tables S3, S4, respectively.

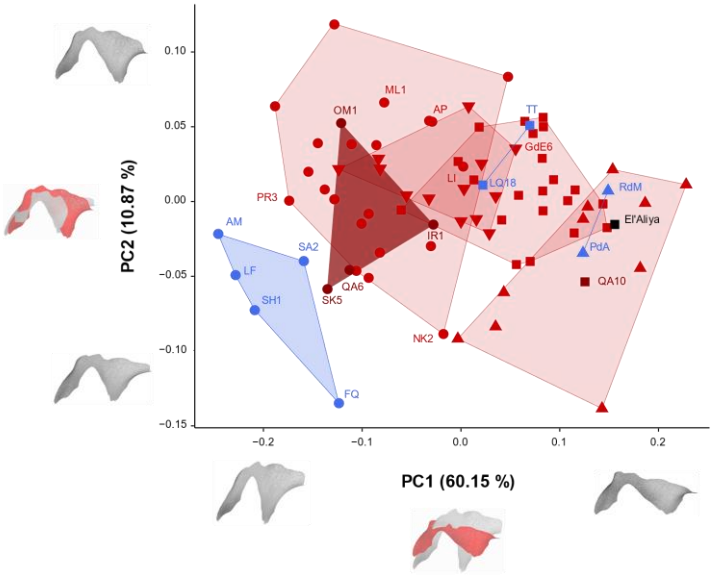

Figure 4: Maxillary shape PCA, PC1 plotted against PC2. *H. sapiens* shown in light red (N = 65), early *H. sapiens* samples in darker red (N = 5), and *H. neanderthalensis* in blue (N = 9). Individuals assigned to dental age group 3 are shown as triangles, age group 4 as squares, age group 5 as inverted triangles and age group 6 as dots. Mugharet el'Aliya is shown as a black square. Shape changes along PCs illustrated as surfaces at ± 2 sd and direct comparison of extreme surfaces at maximum (red) and minimum (grey). Dental age groups of all individuals and abbreviations of all fossil individuals listed in Table 1.

H. sapiens, as well as adult Neanderthals from the adult modern human sample. All subadult fossils of both species, including Mugharet el'Aliya, plot within the PC1 variation of subadult modern humans and, with the exception of Pech de l'Azé, show CS within recent adult variation (Figure 3; Supplementary Tables S3, S4).

PC2 and PC3 capture some inter-specific and mostly intra-specific variation but are not significantly correlated to CS or dental age groups. PC2 explains 10.87 % of total variance and summarizes shape changes from an anteriorly oriented zygoma, concave anterior maxillary surface and narrow nasal area (more positive PC2 scores); to a receding zygoma, relatively flat anterior maxillary surface and wide nasal area leading to a medial displacement of

the anterior dentition relative to the lateral boarder of the nasal apparatus (more negative PC2 scores). PC3 captures 6.32 % of total variance and summarizes shape changes from a maxilla with the anterior dentition being anterior to the lower part of the nasal apparatus and an arched IZM (more positive PC3 scores); to a maxilla with anterior dentition being on the same plane as the lower part of the nasal apparatus and relatively straight IZM (more negative PC3 scores).

When combining PC1 and PC2, the maxillae from Mugharet el'Aliya and Qafzeh 10 plot into the convex hull of a younger modern human age group than their own dental status would suggest (Figure 4). In contrast, the subadult Neanderthals plot into the corresponding modern human convex hulls of their dental age groups. Neanderthal adults are fully separated from *H. sapiens* by combination of PC1 and PC2 as well as PC1 and PC3, while the adult early *H. sapiens* sample overlaps almost completely with the variation observed in later adult modern humans (Figures 4, 5).

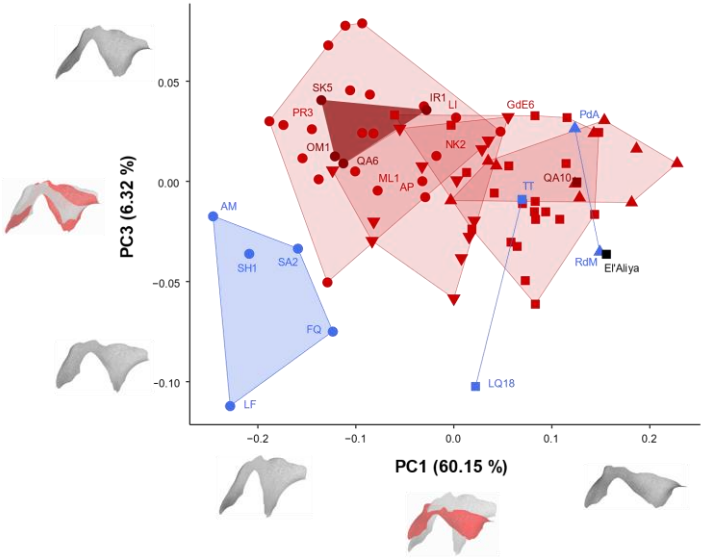

Figure 5: Maxillary shape PCA, PC1 plotted against PC3. Symbols, colors, and abbreviations as in Figure 4 and Table 1.

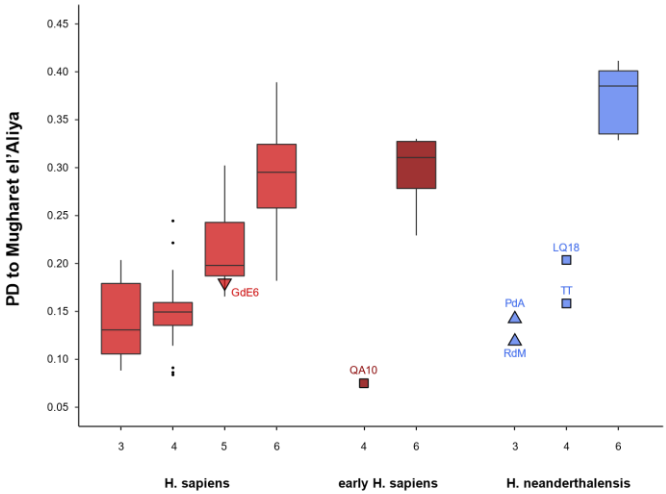

Figure 6: Box-Whisker plots as illustration of the distribution of pairwise Procrustes distances (PD) to Mugharet el'Aliya per dental age group within the *H. sapiens*, early *H. sapiens* and Neanderthal samples. PD of all individuals listed in Supplementary Tables S2. Symbols, colors, and abbreviations as in Figure 3 and Table 1.

The Procrustes Distances (PD) calculated for the dataset show that Mugharet el'Aliya is most similar in its overall shape to the Qafzeh 10 individual (Figure 6; Supplementary Table S2; cf. Figure 7). The Neanderthals closest in overall shape are Roc de Marsal and Pech de l'Azé which belong to a younger age group than Mugharet el'Aliya. The two Neanderthals of comparable dental age show a greater pairwise PD to Mugharet el'Aliya than almost all modern human individuals from age group 3 and 4, which is reflected in the mean pairwise PDs per dental age group (Figure 6; Supplementary Table S2).

A CAC was calculated based on the previously obtained PC scores and plotted against log CS to further examine the allometric relationship of the PCs, especially PC1 (Figure 7). The CAC scores are highly negatively correlated with the PC1 scores with a Pearson correlation coefficient of -0.952 ($T = -27.495$, $DoF = 78$, $p = <0.01$). The other PCs show no significant correlation with the CAC. The calculation based on scores from all PCs does not allow for a direct

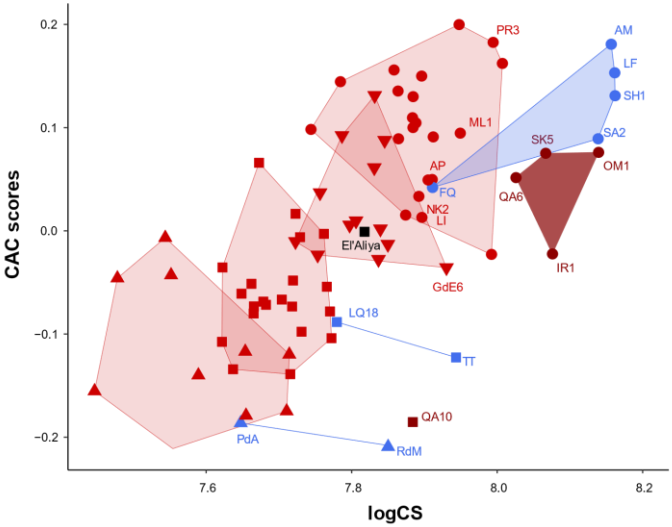

Figure 7: Common Allometric Component (CAC) scores plotted against log CS. Symbols, colors, and abbreviations as in Figure 4 and Table 1.

visualization of the shape changes along the CAC but the high correlation with PC1 suggests similar shape changes (Supplementary Figure S5). The CAC more clearly separates *H. sapiens*, early *H. sapiens* and Neanderthals when plotted against log CS compared to PC1 (cf. Figure 8 & Supplementary Figure S4). These differences do not significantly affect the slopes of each group's ontogenetic allometric trend (Supplementary Table S5), while the intercept with the x-axis, here log CS, between groups differs (cf. Figure 3). Mugharet el'Aliya plots within the *H. sapiens* variation for CAC versus log CS, while it plots outside modern variation and closer to the younger Neanderthal from Roc de Marsal in case of PC1 versus log CS. Qafzeh 10 on the other hand plots in both cases closest to Roc de Marsal and outside the modern variation.

Dental age group mean shapes calculated from the Procrustes coordinates of each individual for each group illustrate overall shape differences between groups as well as between consecutive age groups (Figure 8). For *H. sapiens,* ontogenetic changes include

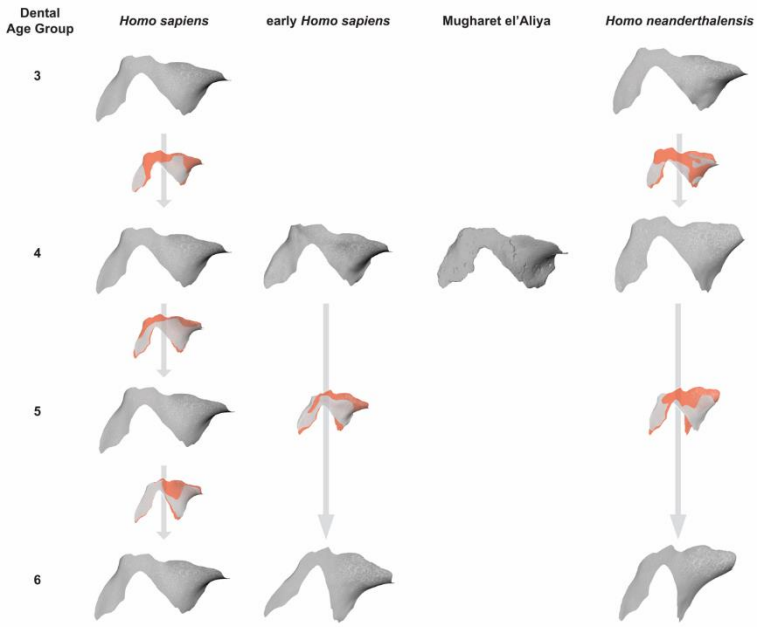

Figure 8: Illustration of maxillary ontogenetic shape changes. Shapes shown as group mean shapes per dental age group. Direct comparison of surfaces from consecutive mean shapes with the younger dental age group in grey and the older in red. Dental age groups of all individuals listed in Table 1

increasing concavity of the anterior maxillary surface, slight posterior shift of the relative position of the root of the zygomatic process in relation to the dentition, slight increase in height relative to width, and until age group 5 a reduction of the alveolar prognathism; whereas the arched IZM and relative nasal width show little change. For early *H. sapiens* the most prominent ontogenetic shape changes between the one subadult and the adult individuals in our sample include a widening of the nasal area, a posterior shift of the relative position of the root of the zygomatic process in relation to the dentition, a slight increase of the concavity of the anterior maxillary surface, and an increase in height relative to width; while the alveolar prognathism and arched IZM show little change. In contrast, the most prominent ontogenetic changes for Neanderthals include a pronounced

increase in height relative to width particularly in the lateral aspect, a pronounced posterior shift of the relative position of the root of the zygomatic process in relation to the dentition, a slight widening of the nasal area, a pronounced widening of the arch at the IZM between age groups 3 and 4, and an increase in midfacial prognathism; while the concavity of the anterior maxillary surface shows little change. Thereby, early *H. sapiens* deviates in some respects from later *H. sapiens* but overall shows an ontogenetic trajectory more similar to later *H. sapiens* than to Neanderthals.

Discussion

Maxillary morphology. The previous attribution of Mugharet el'Aliya to the Neanderthal lineage was based on its absolute size, particularly in the dentition, and on maxillary features such as the absence of a distinct canine fossa and a receding zygomatic arch (cf. Şenyürek, 1940). Our analysis confirmed the large overall size of this specimen in relation to our comparative sample (Figure 3; Supplementary Tables S3, S4). Its CS falls within the range of our modern human adults but above the modern variation of its own dental age group. This is shared with all fossil subadults, with the exception of the youngest Neanderthal in our sample Pech de l'Azé. However, our analysis of maxillary morphology could not clearly differentiate between early and later *H. sapiens* and Neanderthal subadults along the main PCs (Figures 4, 5). Plotting the CAC against log CS showed less overlap between groups with this separation being mostly explained by a shift in size between the groups (Figure 8; Supplementary Table S5). The early *H. sapiens* sample follows this pattern by plotting closer to the similarly sized Neanderthals than relatively smaller later *H. sapiens*, while Mugharet el'Aliya deviates and falls within modern variation despite its large size (cf. Supplementary Figure 5). In addition, overall shape based on PD, age group mean shapes and the zygomatic root position showed affinities of the subadult Mugharet el'Aliya individual to modern humans, especially to a subadult individual from Qafzeh, Israel (Figures 4, 6, 8; Supplementary Table S2).

The state of preservation of Mugharet el'Aliya remains a major limiting factor to its analysis. For example, we could not fully evaluate its canine fossa morphology, as postmortem damage, both taphonomic and incurred during the extraction of the

unerupted teeth, has resulted in considerable damage to this region. Moreover, the maxillary fragment is not preserved up to the midline, which is commonly used as reference plane to define a receding zygoma. When comparing only the preserved morphology (c.f. Measurement Protocol), adult Neanderthal facial characteristics include mid-facial prognathism, 'inflated' morphology of the infra-orbital plate lacking a distinct canine fossa, receding zygomatic arches without an arched IZM and wide nasal apertures, as well as a larger facial size overall (cf. Figures 3, 8; e.g., Harvati, 2015; Clement, Hillwon & Aiello, 2012; Harvati, Hublin & Gunz, 2010; Trinkaus, 1987; Hublin, 1998; Bermúdez de Castro, Arsuaga, Carbonell, Rosas, Martinez & Mosquera, 1997). Most of these traits are not exclusive to Neanderthals individually, but their combination helps define them as a distinct group (Clement et al., 2012; Harvati et al., 2010). Our data set successfully captured these features, as reflected in our PCA results which clearly separate adult Neanderthals from our adult *H. sapiens* sample on PCs 1-3 and PC2-3 (Figures 4, 5). In contrast, no combination of the main PCs can separate the adult early *H. sapiens* sample from later *H. sapiens*, despite early *H. sapiens* on average showing more pronounced alveolar prognathism, a slightly more receding but still arched IZM (Figures 4, 5, 8). Only the greater maxillary size in early *H. sapiens* allows a separation within adult *H. sapiens* (Figures 3, 7; Supplementary Figure 4).

It must be noted that our subadult comparative samples of Neanderthals and especially early *H. sapiens* are limited and may not be representative. Nevertheless, the absence of a deep, expanded and distinct canine fossa and the presence of a slightly receding zygoma are shared between Mugharet el'Aliya and several subadult individuals, both modern human and Neanderthal, especially those of comparable dental age to the Mugharet el'Aliya fossil (dental age group 4) (cf. Figures 4 PC2, 8). Therefore, these features should be treated with caution when evaluating the taxonomic status of fossil subadult maxillae. After the eruption of the first permanent molar (age group 4), mid-facial prognathism and curvature of the IZM appear to differentiate *H. sapiens* from Neanderthals more clearly (cf. Figures 5 PC3, 8). Neanderthals show an ontogenetic trend from slight alveolar prognathism and weak curvature at the IZM towards mid-facial prognathism and a rather straight IZM reflecting increased levels of remodeling and

bone deposition in the nasal area during ontogeny, potentially leading to their adult mid-facial prognathism (Lacruz et al., 2015). In contrast, the majority of the *H. sapiens* sample shows alveolar prognathism and arched IZM with both features present during ontogeny, while in early *H. sapiens* the alveolar prognathism increases (cf. Figures 5 PC3, 8). Some Holocene subadult and adult modern humans from Central Europe lack clear alveolar prognathism and thereby show an anterior dentition almost on the same level as the lower part of the nasal opening (cf. Figure 5 PC3). The differences within our modern human sample might be linked to population-specific differences in the ontogenetic remodeling of the maxilla (Schuh, Gunz, Villa, Kupczik, Hublin & Freidline, 2020; Freidline et al., 2012). It has been suggested that such differences in bone remodeling patterns are maintained throughout ontogeny in several *H. sapiens* populations (Schuh et al., 2020). The absence of a clear alveolar prognathism in Mugharet el'Aliya may reflect such differences in the remodeling of the maxilla. Our attempts to reveal growth remodeling pattern in this fossil were unsuccessful due to its curation with a thick layer of preservative (cf. Measurement protocol).

One aspect shared between ontogenetic trends in early and later *H. sapiens* as well as Neanderthals is a shift in the relative position of the root of the zygomatic process in relation to the dentition (Figures 4 PC1, 7, 8; Supplementary Figure S4). With increasing age, the root of the zygomatic process moves to a more posterior position, with adult Neanderthals showing more posterior zygomatic root positions than adult *H. sapiens*. A relatively posterior zygomatic root position is considered a Neanderthal derived feature (e.g., Weber & Krenn, 2017; Trinkaus, 1987). The Mugharet el'Aliya specimen shows a more anterior zygomatic root position, as expected for its dental age group (Minugh-Purvis, 1993). This is reflected by it plotting towards the younger dental age group 3 than its own dental age group 4 (Figure 4 PC1). In our sample this tendency is shared with the subadult *H. sapiens* individual Qafzeh 10, which is also closest in overall shape based on PD to Mugharet el'Aliya (Supplementary Table S2). Additionally, some adult *H. sapiens* individuals in our sample show relatively anterior placed zygomatic roots, including Nazlet Khater 2 (Egypt), for which this feature has been described previously (Crevecoeur, 2012), and most distinctly a Holocene individual from Tanzania (Figure 4 PC1). In contrast, the subadult Neanderthals in our

sample plot into the corresponding modern human dental age groups or even closer to the overlap with older age groups, and thereby mirror the adult condition of relatively more posterior zygomatic roots in Neanderthals.

Placing Mugharet el'Aliya and the Aterian in a broader context. The initial description of Mugharet el'Aliya in 1940 and its attribution to the Neanderthal lineage were carried out in the context of a much more limited knowledge of the human fossil record. Today's understanding of human evolution and the relationship between modern humans and Neanderthals has been drastically reshaped by recent discoveries and methodological advances (e.g., Harvati et al., 2019; Hublin et al., 2017; Reich et al., 2010; Berger et al., 2010; Villanea & Schraiber, 2019). In this framework, the absolute dental and facial size, which were among the principal features used to group Mugharet el'Aliya with the Neanderthal lineage, are now known to be variable features and therefore are inadequate as sole phylogenetic indicators (e.g., Bernal, Perez, Gonzalez & Diniz-Filho, 2010). Megadonty, especially in mesio-distal dimensions, is associated with a relative size increase of the corresponding jaw. In contrast, particularly in recent *H. sapiens* jaw and facial size might be reduced due to the potential absence of wisdom teeth (Oeschger, Kanavakis, Halazonetis & Gkantidis, 2020).

Nevertheless, the factors potentially underlying such a great robustness and megadonty in Aterian populations, a group of modern humans associated with lithics that may be as recent as 20 ka before present (Richter, Moser & Nami, 2012; Doerschner et al., 2016), should be investigated. Other studies of the Aterian fossil record have reported a mosaic of derived modern and ancestral traits, including general robusticity and relatively large size, shared with Middle Pleistocene African fossils (Ferembach, 1976; Hublin & Tillier, 1981; Hublin, 2000; Hublin et al., 2012). The rather clear shape affiliation of Aterian fossils with *H. sapiens* combined with archaic traits such as large size might indicate previous hybridization with surviving archaic lineages or reflect retention of ancestral traits (Ackermann, 2011). The overall maxillary dental pattern of Aterian fossils from the Témara region showed similarities to Peştera cu Oase 2, Romania (Hublin et al., 2012). Hybridization between modern humans and Neanderthals was suggested for the individuals from Oase and could be confirmed by paleogenetic analyses (Rougier et al., 2007;

Trinkaus, Constantin & Zilhão, 2013; Fu et al., 2015; Siska, 2019). Evidence from genetics indicates not only admixture between modern humans with Neanderthals, but also suggests introgression from ghost populations into the modern human African gene pool (e.g., Durvasula & Sankararaman, 2020; Hsieh et al., 2016; Lachance et al., 2012). Additionally, unusually large size of admixed individuals is a commonly described effect of hybridization (e.g., Ackermann 2011; Harvati et al. 2009; Harvati & Roksandic, 2016). However, this hypothesis cannot be tested for the Aterian without further genetic evidence and additional fossils providing a more complete picture of the morphological variation associated with the Aterian.

Recent re-evaluation of the Aterian fossil record supports the hypothesis of retained archaic traits due to regional continuity, which would be in accordance to a re-evaluation of dates and lithic assemblages associated with the Aterian. Historically, the Aterian was dated to 40-20 ka based on radiocarbon dates (Debénath, 2000; Wengler, 1997). Employing additional dating methods including ESR or Uranium/Thorium pushed back the beginning of the Aterian to MIS6 around 145 ka (Barton et al., 2009; Richter et al., 2010). The Aterian apparently overlaps with an early MSA industry by up to 85 ka in the region of today's Morocco and Algeria (Dibble et al., 2013). Several sites show Aterian layers below layers with supposedly earlier MSA assemblages in a stratified context (Nami & Moser, 2010; Richter et al., 2010; Aouadi-Abdeljaouad & Belhouchet, 2008). Thereby, a distinction of the Northwest African MSA into multiple industries has been questioned (Richter, Moser & Nami, 2012; Linstädter, Eiwanger, Mikdad & Weniger, 2012; Scerri et al., 2017, 2019). The Aterian was often recognized by the presence of the so-called 'tanged' pieces. Although additional characteristics were identified, some researchers claim that the similarities between the industries are too great to separate them (Richter et al., 2012; Dibble et al., 2013, Scerri et al., 2017). This would suggest a degree of regional continuity within North African MSA industries. A similar hypothesis of a regional continuity was proposed for the Northwest African MSA associated hominin fossil record (Hublin, 2000; Hublin et al., 2017; Nespoulet et al., 2008). The hominin fossils from late Middle Pleistocene and Late Pleistocene associated with Northwest African MSA technology show anatomical similarities, whereas later populations in the region associated with the LSA

differ morphologically (Scerri, 2017; Hublin, 2000; Hublin et al., 2017; Nespoulet et al., 2008; Harvati & Hublin, 2012). MSA individuals from Jebel Irhoud and the Aterian show a comparable combination of the same primitive retentions, including large overall size and megadonty, and modern features as well as similarities with the samples from Qafzeh and Skhul (Hublin et al., 2012; Harvati & Hublin, 2012; Hublin & Tillier, 1988, Freidline et al., 2021; Ferembach, 1976; Hublin & Tillier, 1981; Hublin et al., 2017). Large facial and dental size relative to recent *H. sapiens* are frequent traits in many late Middle and early Late Pleistocene African fossils, e.g., Herto, Rabat-Kébibat, Kabwe and some individuals from Haua Fteah and Klasies River Mouth (e.g., McBurney, Trevor & Wells, 1953; Rightmire & Deacon, 1991; White et al., 2003; Bräuer, 2012; Hublin et al., 2012; Hublin et al., 2017; Oujaa et al., 2017). In contrast, in the second half of the Late Pleistocene such extremes are rare outside the northwestern African fossil record due to facial reduction in *H. sapiens* (e.g., Liebermann, McBratney & Krovitz, 2002; Trinkaus, 2003; Bastir & Rosas, 2016).

However, the majority of human fossils associated with the Aterian and earlier Northwest African MSA have been found in Morocco, often along the Atlantic coast (Hublin et al., 2012; Freidline et al., 2021). These fossils span a long period, from ca. 300 ka represented by Jebel Irhoud, to potentially as recent as 35 ka as represented by Mugharet el'Aliya (Richter et al., 2017; Hublin et al., 2017; Wrinn & Rink, 2003). Dating of archaeological sites roughly coincides with wet periods in MIS5 for both lithic industries and MIS3 for the Aterian in today's Sahara, Morocco, and Algeria whereas the gaps in the fossil record seem to reflect dry periods in MIS4 (Jacobs, Roberts, Nespoulet, El Hajraoui & Debénath, 2012; Drake & Breeze, 2016). Wet periods were characterized by megalakes and river channels in today's Sahara Desert (Armitage et al., 2007; Osborne, Vance, Rohling, Barton, Rogerson & Fello, 2008) and thereby, presenting a scenario of connected Aterian sites across North Africa from the Moroccan Atlantic coast to the Nile valley. Nevertheless, the known morphology and dated lithic assemblages within the Aterian are snapshots, which complicates their comparison with the earlier Northwest African MSA and other sites associated with early *H. sapiens*. Comparing Mugharet el'Aliya with the earlier MSA subadult fossil maxilla such as the Contrebandiers fossil (Balter,

2011; Freidline et al., 2021; Jacobs et al., 2011) would be relevant to address questions on the hypothesis of regional continuity throughout the Moroccan MSA.

Methodological considerations. The Aterian fossil record is partially unpublished or poorly described (cf. Hublin et al., 2012). The lack of suitable methods available at the time of their discovery and the fragmented nature of the fossil remains may have contributed to their limited exposure in human evolution research. The surface registration method implemented here has the potential to be a robust research alternative to analyze fragmentary specimens, common in the fossil record, that do no preserve enough linear measurements or homologous landmarks for a conventional linear analysis or typical geometric morphometric study. It can potentially enable the investigation of the entire preserved morphology of specimens that were hitherto impossible to analyze quantitatively. To our knowledge, the present study is among the first using surface registration in an archaeological context.

The process of surface registration is sensitive to missing data, and the measurement protocol described here necessitates the exclusion of all individuals with large areas of missing data or missing data in crucial parts of the surface of interest. Only individuals with relatively small locally confined damage, i.e., cracks, porosities, or additional foramen, can still be included. In these cases, the matched surface can differ locally more than 1 mm from the original and is smoothed during the ICP-matching (Supplementary Figure S3 d-f). Furthermore, the amount of data produced by the surface registration method can be enormous. The geometric complexity of the anatomical structure under study determines the mesh resolution and, in turn, the number of vertices and variables used during analyses. On the one hand, in complex geometric structures a reduction in mesh resolution might lead to systematic artifacts during the ICP-matching (Supplementary Figure S6). On the other hand, a high mesh resolution can render the calculation of some commonly used analyses almost impossible, e.g., in our data set the calculation of a canonical variate analysis based on Procrustes coordinates would require an integer that lays beyond the codomain supported by R. Further research is needed to adjust the method of surface registration to the field of paleoanthropology, for example in combination with data reduction techniques and statistical shape

models, which are already used for reconstruction of damaged skeletal areas in computer assisted surgery (e.g., Semper-Hogg et al., 2017).

Conclusion

Mugharet el'Aliya adds to the growing number of subadult hominins recovered from sites across Africa enabling a better understanding of facial ontogeny in the fossil record. Yet the fragmentary nature of the maxilla highlights the necessity to develop new analytical tools to study incomplete specimens. Surface registration allowed the placement of this fossil in a quantitative comparative framework based on most of its surviving external morphology. Based on our results, we conclude that the preserved facial anatomy of the juvenile fossil from Mugharet el'Aliya closely aligns with that of Late Pleistocene *H. sapiens* individuals and we found no clear affinities to the Neanderthal lineage. Previous associations of this specimen with the Neanderthal lineage were likely due to its large absolute size and to features such as its shallow canine fossa, which are ontogenetically variable among modern humans, and therefore not necessarily informative on phylogenetic relationships. Whether these observed features are primitive retentions or may reflect admixture between early *H. sapiens* and archaic lineages is unclear.

The striking similarities between Mugharet el'Aliya and an early *H. sapiens* individual from the Levant add to the evidence connecting fossils from western Asia, especially Qafzeh and Skhul, and the North African Late Pleistocene human fossil record (see e.g., Harvati & Hublin, 2012; Freidline et al., 2021; Shea & Bar-Yosef, 2005). The extent and phylogenetic relevance of such similarities, and the implications on possible connections across populations dated from ~300 ka to ca. 20 ka from the Moroccan Atlantic Coast to the Levant, remains an important area of research in human evolution.

Acknowledgements

This research was supported by the European Research Council (ERC CoG no. 724703) and the German Research Foundation (DFG FOR 2237). C.S.'s research is supported by the Calleva Foundation and the Human Origins Research Fund and R.S.L.'s research was supported the MA003 funding from New York University (NYU). We thank S. Schlager (University of Freiburg) for his extensive help in regard to the method of surface registration. In addition, we would like to thank J. Zastrow and H. Rathmann for their valuable input and assistance. We are thankful to Loring Burgess and the staff at the Peabody Museum, Harvard University, for granting access to the study of the Mugharet el'Aliya fossil and for providing its CT scans. We thank all curators and their institutions for access to original specimens or CT scans used in the comparative sample, especially: A. Balzeau and D. Grimaud-Hervé (Muséum National d'Histoire Naturelle; MNHN); E. Delson (New York Consortium in Evolutionary Primatology; NYCEP); G. Manzi (Università 'La Sapienza', Rome). Furthermore, the bones of Nazlet Khater 2 were scanned thanks to the Agence Nationale de la Recherche (ANR) project 'Big Dry' (ANR-14-CE31) and we thank the coordinator F. Bon and the partners I. Crevecoeur, D. Pleurdeau, J. Lesur, and C. Tribolo for granting us access to the material of Nazlet Khater 2.

Author contribution

All authors contributed to the research design; C.R. collected virtual comparative data, processed and analysed the data; all authors contributed to compiling the manuscript.

References Main text

Ackermann, R. R. (2011). Phenotypic Traits of Primate Hybrids: Recognizing Admixture in the Fossil Record. *Evolutionary Anthropology*, 19 (6), 258-270. Doi: 10.1002/evan.20288.

Aouadi-Abdeljaouad, N., & Belhouchet, L. (2008). Recent prehistoric field research in Central Tunisia: prehistoric occupations in the Meknassy Basin. *African Archaeological Review*, 25, 75-85. Doi: 10.1007/s10437-008-9027-z.

Armitage, S. J., Drake, N. A., Stokes, S., El-Hawat, A., Salem, M. J., White, K., Turner, P., & McLaren, S. J. (2007). Multiple phases of North African humidity recorded in lacustrine sediments from the Fazzan Basin, Libyan Sahara. *Quaternary Geochronology*, 2, 181-186. Doi: 10.1016/j.quageo.2006.05.019.

Bae, C. J., Douka, K., & Petraglia, M. D. (2017). On the origin of modern humans: Asian perspectives. Science, 358, 1269. Doi: 10.1126/science.aai9067.

Balter, M. (2011). Was North Africa the Launch Pad for Modern Human Migrations? *Science*, 331, 20-23. Doi: 10.1126/science.331.6013.20.

Bastir, M., & Rosas, A. (2016). Cranial base topology and basic trends in the facial evolution of Homo. *Journal of Human Evolution*, *91*, 26-35. Doi: 10.1016/j.jhevol.2015.11.001.

Barton, R. N. E., Bouzouggar, A., Collcutt, S. N., Schwenninger, J.-L., & Clark-Balzan, L. (2009). OSL dating of the Aterian levels at Dar es-Soltan I (Rabar, Morocco) and implications for the dispersal of modern Homo sapiens. *Quaternary Science Reviews*, 28, 1914-1931. Doi: 10.1016/j.quascirev.2009.03.010.

Berger, L. R., de Ruiter, D. J., Churchill, S. E., Schmid, P., Carlson, K. J., Dirks, P. H. G. M., & Kibii, J. M. (2010). Australopithecus sediba: a New Species of Homo-like Australopith from South Africa. *Science*, 328, 195-204. Doi: 10.1126/science.1184944.

Bermúdez de Castro, J. M., Arsuaga, J. L., Carbonell, E., Rosas, A., Martinez, I., & Mosquera, M. (1997). A hominid from the Lower Pleistocene of Atapuerca, Spain: possible ancestor to Neandertals and modern humans. *Science*, 276, 1392-1395. Doi: 10.1126/science.276.5317.1392.

Bernal, V., Perez, S. I., Gonzalez, P. N., & Diniz-Filho, J. A. F. (2010). Ecological and evolutionary factors in dental morphological diversification among modern human populations from southern South America. *Proceedings of the Royal Society B*, 277, 1107-1112. Doi: 10.1098/rspb.2009.1823.

Bookstein, F. L. (1997). *Morphometric tools for landmark data: geometry and biology*. Cambridge, UK: Cambridge University Press.

Bosman, A. M., Reyes-Centeno, H., & Harvati, K. (2020). A virtual assessment of the supraniac depression on Eyasi I (Tanzania) and Aduma ADU-VP-1/3 (Ethiopia) Pleistocene hominin crania. Journal of Human Evolution, 145, 102815. Doi: 10.1016/j.jhevol.2020.102815.

Bouzouggar, A., Kozłowski, J. K., & Otte, M. (2002). Étude des ensembles lithiques atériens de la grotte d'El Aliya à Tanger (Maroc). *L'Anthropologie*, 106, 207-248. Doi: 10.1016/S0003-5521(02)01090-7.

Bräuer, G. (2012). Middle Pleistocene diversity in Africa and the origin of modern humans. In J.-J. Hublin, & S. P. McPherron (Eds.), *Modern Origins: A North African Perspective* (pp. 221-240). Vertebrate Paleobiology and Paleoanthropology. Berlin, Germany: Springer. Doi: 10.1007/978-94-007-2929-2_15.

Carter, K. & Worthington, S. (2015). Morphologic and demographic predictors of third molar agenesis: a systematic review and meta-analysis. *Journal of Dental Research*, 94 (7), 886–894. Doi: 10.1177/0022034515581644.

Clement, A. F., Hillwon, S. W., & Aiello, L. C. (2012). Tooth wear, Neanderthal facial morphology and the anterior dental loading hypothesis. *Journal of Human Evolution*, 62 (3), 367-376. Doi: 10.1016/j.jhevol.2011.11.014.

Coon, C.S. (1957a). *The Seven Caves*. New York: published by Alfred A. Knopf.

Coon, C.S. (1957b). Correspondence, dated 25 May, 1957 to Dr. Hugh Hencken. Harvard University, Peabody Museum Archives.

Crevecoeur, I. (2012). The Upper Paleolithic human remains of Nazlet Khater 2 (Egypt) and past modern human diversity. In J.-J. Hublin, & S. P. McPherron (Eds.), *Modern Origins: A North African Perspective* (pp. 205-219). Vertebrate Paleobiology and Paleoanthropology. Berlin, Germany: Springer. Doi: 10.1007/978-94-007-2929-2_14.

Dannemann, M., & Racimo, F. (2018). Something old, something borrowed: admixture and adaptation in human evolution. *Current Opinion in Genetics & Development*, 53, 1-8. Doi: 10.1016/j.gde.2018.05.009.

Debénath, A. (2000). Le peuplement préhistorique du Maroc: données récentes et problems. *L'Anthropologie*, 104 (1), 131-145. Doi: 10.1016/S0003-5521(00)90006-2.

Dibble, H. L., Aldeias, V., Jacobs, Z., Olszewski, D. I., Rezek, Z., Lin, S. C., Alvarez-Fernández, E., Barshay-Szmidt, C. C., Hallett-Desguez, E., Reed, D., Reed, K., Richter, D., Steele, T. E., Skinner, A., Blackwell, B., Doronicheva, E., & El-Hajraoui, M. (2013). On the industrial attributions of the Aterian and Mousterian of the Maghreb. *Journal of Human Evolution*, 64 (3), 194-210. Doi: 10.1016/j.jhevol.2012.10.010.

Doerschner, N., Fitzsimmons, K. E., Ditchfield, P., McLaren, S. J., Steele, T. E., Zielhofer, C., McPherron, S. P., Bouzouggar, A., & Hublin, J.-J. (2016). A new Chronology for Rhafas, Northeast Morroco, Spanning the North African Middle Stone Age through to the Neolithic. *PloS one*, 11 (9), e0162280. Doi: 10.1371/journal.pone.0162280.

Drake, N., & Breeze, P. (2016). Climate change and modern human occupation of the Sahara from MIS 6-2. In S. C. Jones & B. A. Steward (Eds.), *Africa from MIS 6-2: Population Dynamics and Paleoenvironments* (pp.103-122). Vertebrate Paleobiology and Paleoanthropology. Berlin, Germany: Springer. Doi: 10.1007/978-94-017-7520-5_6.

Durvasula, A., & Sankararaman, S. (2020). Recovering signals of ghost archaic introgression in African populations. *Science Advances*, 6 (7), eaax5097. Doi: 10.1126/sciadv.aax5097.

Ennouchi, E. (1962) Un neandertalien: l'homme du Jebel Irhoud (Maroc) *L'Anthropologie*, 66: 279–299.

Ferembach, D. (1976). Les restes humains de la Grotte de Dar-es-Soltane II (Maroc). Campagne 1975. *Bulletines et Mémoires de la Société*

d'anthropologie de Paris, XIII, 183-193. Doi: 10.3406/bmsap.1976.1849.

Freidline, S. E., Gunz, P., Harvati, K., & Hublin, J.-J. (2012). Middle Pleistocene human facial morphology in an evolutionary and developmental context. *Journal of Human Evolution*, 63 (5), 723-740. Doi: 10.1016/j.jhevol.2012.08.002.

Freidline, S. E., Schuh, A., Gunz, P., Alichane, H., Oujaa, A., El Hajaroui, M., & Hublin, J.-J. (2021). The undescribed juvenile maxilla from Grotte des Contrebandies, Morocco – a study on Aterian facial growth. PaleoAnthropology, 2021:1, p. 180.

Fu, Q., Hajdinjak, M., Moldovan, O. T, Constantin, S., Mallick, S., Skoglund, P., Patterson, N., Rohland, N., Lazaridis, I., Nickel, B., Viola, B., Prüfer, K., Meyer, M., Kelso, J., Reich, D., & Pääbo, S. (2015). An early modern human from Romania with a recent Neanderthal ancestor. *Nature*, 524, 216–219. Doi: 10.1038/nature14558.

Green, R. E., Krause, J., Briggs, A. W., Maricic, T., Stenzel, U., Kircher, M., Patterson, N., Li, H., Zhai, W., Fritz, M. H., Hansen, N. F., Durand, E. Y., Malaspinas, A.-S., Jensen, J. D., Marques-Bonet, T., Alkan, C., Prüfer, K., Meyer, M., Burbano, H. A., Good, J. M., Schultz, R., Aximu-Petri, A., Butthof, A., Höber, B., Höffner, B., Siegemund, M., Weihmann, A., Nusbaum, C., Lander, E. S., Russ, C., Novod, N., Affourtit, J., Egholm, M., Verna, C., Rudan, P., Brajkovic, D., Kucan, Ž., Gušic, I., Doronichev, V. B., Golovanova, L. V., Lalueza-Fox, C., de la Rasilla, M., Fortea, J., Rosas, A., Schmitz, R. W., Johnson, P. L. F., Eichler, E. E., Falush, D., Birney, E., Mullikin, J. C., Slatkin, M., Nielsen, R., Kelso, J., Lachmann, M., Reich, D., & Pääbo, S. (2010). A draft sequence of the Neandertal genome. *Science*, 328, 710–722. Doi: 10.1126/science.1188021.

Gunz, P., Mitteroecker, P., & Bookstein, F. (2005). Semilandmarks in Three Dimensions. In: D. E. Slice (Eds.), *Modern Morphometrics in Physical Anthropology* (pp. 73-98). New York: Kluwer Academic/Plenum Publisher.

Harvati, K. (2009). Into Eurasia: A geometric morphometric re-assessment of the Upper Cave (Zhoukoudian) specimen. *Journal of Human Evolution*, 57 (6), 751-762. Doi: 10.1016/j.jhevol.2009.07.008.

Harvati, K., Hublin, J.-J., & Gunz, P. (2010). Evolution of middle-late Pleistocene human cranio-facial form: a 3-D approach. *Journal of Human Evolution*, 59 (5), 445-464. Doi: 10.1016/j.jhevol.2010.06.005.

Harvati, K., & Hublin, J.-J. (2012). Morphological continuity of the face in the Late Middle and Late Pleistocene Hominins from Northwestern Africa: a 3D geometric morphometric analysis. In J.-J. Hublin, & S. P. McPherron (Eds.), *Modern Origins: A North African Perspective* (pp. 179-188). Vertebrate Paleobiology and Paleoanthropology. Berlin, Germany: Springer. Doi: 10.1007/978-94-007-2929-2_12.

Harvati, K. (2015). Neanderthals and Their Contemporaries. In: W. Henke & I. Tattersall (Eds.), *Handbook of Paleoanthropolog* (pp. 2243-2280). Berlin, Germany: Springer. https://doi.org/10.1007/978-3-642-39979-4_56

Harvati, K., & Roksandic, M. (2016). The Human Fossil Record from Romania: Early Upper Paleolithic Mandibles and Neanderthal Admixture. In: K. Harvati & M. Roksandic (Eds.), *Paleoanthropology of the Balkans and Anatolia: Human Evolution and its Context* (pp. 51-68).

Vertebrate Paleobiology and Paleoanthropology Series. Dordrecht: Springer. Doi: 10.1007/978-94-024-0874-4_4.

Harvati, K., Röding, C., Bosman, A. M., Karakostis, F. A., Grün, R., Stringer, C., Karkanas, P., Thompson, N. C., Koutoulidis, V., Moulopoulos, L. A., Gorgoulis, V. G., & Kouloukoussa, M. (2019). Apidima Cave fossils provide earliest evidence of Homo sapiens in Eurasia. *Nature*, 571, 500-504. Doi: 10.1038/s41586-019-1376-z.

Henn, B. M., Steele, T. E., & Weaver, T. D. (2018). Clarifying distinct models of modern human origins in Africa. Current Opinion in Genetics & Development, 53, 148-156. Doi: 10.1016/j.gde.2018.10.003.

Hershkovitz, I., Weber, G. W., Quam, R., Duval, M., Grün, R., Kinsley, L., Ayalon, A., Bar-Matthews, M., Valladas, H., Mercier, N., Arsuaga, J. L., Martinón-Torres, M., Bermúdez de Castro, J. M., Fornai, C., Martín-Francés, L., Sarig, R., May, H., Krenn, V. A., Slon, V., Rodríguez, L., García, R., Lorenzo, C., Carretero, J. M., Frumkin, A., Shahack-Gross, R., Bar-Yosef Mayer, D. E., Cui, Y., Wu, X., Peled, N., Groman-Yaroslavski, I., Weissbrod, L., Yeshurun, R., Tsatskin, A., Zaidner, Y., & Weinstein-Evron, M. (2018). The earliest modern humans outside Africa. *Science*, 359, 456-459. Doi: 10.1126/science.aap8369.

Howe, B. (1967). The Palaeolithic of Tangier, Morocco. *American School of Prehistoric Research Bulletin*, 22, 1–200.

Hsieh, P. H., Woerner, A. E., Wall, J. D., Lachance, J., Tishkoff, S. A., Gutenkunst, R. N., & Hammer, M. F. (2016). Model-based analyses of whole-genome data reveal a complex evolutionary history involving archaic introgression in Central African Pygmies. *Genome Research*, 26, 291–300. Doi: 10.1101/gr.196634.115.

Hublin, J. J., and Tillier, A. M. (1981). The Mousterian juvenile mandible from Irhoud (Morocco): a phylogenetic interpretation. In C. B. Stringer (Eds.), *Aspects of Human Evolution* (pp. 167–185). London, UK: Taylor and Francis.

Hublin, J.-J., Tillier, A.-M. (1988). Les enfants moustériens de Jebel Irhoud (Maroc), comparaison avec les Néandertaliens juveniles d'Europe. *Bulletins es Mémoires de la Société d'anthropologie de Paris*, XIV (4), 237-246. Doi: 10.3406/bmsap.1988.1680.

Hublin, J.-J. (1993). Recent Human Evolution in Northwestern Africa. In M. J. Aitken, C. B. Stringer & P. A. Mellars (Eds.), *The Origin of Modern Humans and the Impact of Chronometric Dating* (pp. 118-131). Princeton, New Jersey: Princeton University Press. Doi: 10.1515/9781400851553.118.

Hublin, J.-J. (1998). Climatic changes, paleogeography and the evolution of Neanderthals. In: T. Akazawa, K. Aoki & O. Bar-Yosef (Eds.), *Neanderthals and Modern Humans in Western Asia* (pp. 295-310). Boston, MA: Springer. Doi: 10.1007/0-306-47153-1_18.

Hublin, J.-J. (2000). Modern-nonmodern hominid interactions: a Mediterranean perspective. In O. Bar-Yosef & D. R. Pilbeam (Eds.), *The geography of Neandertals and modern humans in Europe and the Greater Mediterranean* (157-182). Peabody Museum Bulletins. Cambridge, Massachusetts: Harvard University Press.

Hublin, J.-J., Verna, C., Bailey, S., Smith, T., Olejniczak, A., Sbihi-Alaoui, F. Z., & Zouak, M. (2012). Dental Evidence from the Aterian Human Populations of Morocco. In J.-J. Hublin, & S. P. McPherron (Eds.), *Modern Origins: A North African Perspective* (pp. 189-204). Vertebrate

Paleobiology and Paleoanthropology. Berlin, Germany: Springer. Doi: 10.1007/978-94-007-2929-2_13.

Hublin, J.-J., Ben-Ncer, A., Bailey, S. E., Freidline, S. E., Neubauer, S., Skinner, M. M., Bergmann, I., Le Cabec, A., Benazzi, S., Harvati, K., & Gunz, P. (2017). New fossils from Jebel Irhoud, Morocco and the pan-African origin of Homo sapiens. *Nature*, 546, 289-292. Doi: 10.1038/nature22336.

Jacobs, Z., Meyer, M. C., Roberts, R. G., Aldeias, V., Dibble, H., & El Hajraoui, M. A. (2011). Single-grain OSL dating at La Grotte des Contrebandiers ('Smugglers' Cave'), Morocco: improved age constraints for the Middle Paleolithic levels. *Journal of Archaeological Science*, 38 (12), 3631–3643. Doi: 10.1016/j.jas.2011.08.033.

Jacobs, Z., Roberts, R. G., Nespoulet, R., El Hajraoui, M. A., & Debénath, A. (2012). Single-grain OSL chronologies for Middle Palaeolithic deposits at El Mnasra and El Harhoura 2, Morocco: Implications for Late Pleistocene human-environment interactions along the Atlantic coast of northwest Africa. *Journal of Human Evolution*, 62 (3), 377-394. Doi: 10.1016/j.jhevol.2011.12.001.

Lachance, J., Vernot, B., Elbers, C. C., Ferwerda, B., Froment, A., Bodo, J.-M., Lema, G., Fu, W., Nyambo, T. B., Rebbeck, T. R., Zhang, K., Akey, J. M., & Tishkoff, S. A. (2012). Evolutionary history and adaptation from high-coverage whole-genome sequences of diverse African hunter-gatherers. *Cell*, 150 (3), 457-469. Doi: 10.1016/j.cell.2012.07.009.

Lacruz, R. S., Bromage, T. G., O'Higgins, P., Arsuaga, J.-L., Stringer, C., Godinho, R. M., Washaw, J., Martínez, I., Gracia-Tellez, A., Bermúdez de Castro, J. M., & Carbonell, E. (2015). Ontogeny of the maxilla in Neanderthals and their ancestors. *Nature Communications*, 6, 8996. Doi: 10.1038/ncomms9996

Lacruz, R. S., Stringer, C. B., Kimbel, W. H., Wood, B., Harvati, K., O'Higgins, P., Bromage, T. G., & Arsuaga, J.-L. (2019). The evolutionary history of the human face. *Nature Ecology & Evolution*, 3, 726–736. Doi: 10.1038/s41559-019-0865-7.

Lazaridis, I., Nadel, D., Rollefson G., Merrett, D. C., Rohland, N., Mallick, S., Fernandes, D., Novak, M., Gamarra, B., Sirak, K., Connell, S., Stewardson, K., Harney, E., Fu, Q., Gonzalez-Fortes, G., Jones, E. R., Roodenberg, S. A., Mizrahi, A.-S., Meiklejohn, C., Gerritsen, F., Bejenaru, L., Blüher, M., Campbell, A., Cavalleri, G., Comas, D., Froguel, P., Gilbert, E., Kerr, S. M., Kovacs, P., Krause, J., McGettigan, D., Merrigan, M.,, Merriwether, D. A., O'Reilly, S., Richards, M. B.,, Semino, O., Shamoon-Pour, M., Stefanescu, G., Stumvoll, M., Tönjey, A., Torroni, A., Wilson, J. F., Yengo, L., Hovhannisyan, N. A., Patterson, N., Pinhasi, R., & Reich, D. (2016). Genomic insights into the origin of farming in the ancient Near East. Nature, 536, 419-44. Doi: 10.1038/nature19310.

Lieberman, D. E., McBratney, B. M., & Krovitz, G. (2002). The evolution and development of cranial form in Homo sapiens. *PNAS*, *99* (3), 1134-1139. Doi: 10.1073/pnas.022440799.

Linstädter, J., Eiwanger, J., Mikdad, A., Weniger, G.-C. (2012). Human occupation of Northwest Africa: A review of Middle Palaeolithic to Epipalaeolithic sites in Morocco. *Quaternary International*, 274, 158-174. Doi: 10.1016/j.quaint.2012.02.017.

McBurney, C. B. M., Trevor, J. C., & Wells, L. H. (1953). The Haua Fteah Fossil Jaw. *The Journal of the Royal Anthropological Institute of Great Britain and Ireland*, 83 (1), 71-85.

Mercier, N., Wengler, L., Vallada, H., Joron, J.-L., Froget, L., & Reyss, J.-L. (2007). The Rhafas Cave (Morocco): Chronology of the Mousterian and Aterian archaeological occupations and their implications for Quaternary geochronology based on luminescence (TL/OSL) age determinations. *Quaternary Geochronology*, 2, 309-313. Doi: 10.1016/j.quageo.2006.03.010.

Meyer, M., Arsuaga, J.-L., de Filippo, C., Nagel, S., Aximu-Petri, A., Nickel, B., Martínez, I., Gracia, A., Bermúdez de Castro, J. M., Carbonell, E., Viola, B., Kelso, J., Prüfer, K., & Pääbo, S. (2016). Nuclear DNA sequences from the Middle Pleistocene Sima de los Huesos hominins. *Nature*, 531, 504–507. Doi:10.1038/nature17405.

Minugh-Purvis, N. (1993). Reexamination of the Immature Hominid Maxilla from Tangier, Morocco. American *Journal of Physical Anthropology*, 92 (4), 449-461. Doi: 10.1002/ajpa.1330920404.

Mitteroecker, P., Gunz, P., Bernhard, M., Schaefer, K., & Bookstein, F. L. (2004). Comparison of cranial ontogenetic trajectories among great apes and humans. Journal of Human Evolution, 46 (6), 679-698. Doi: 10.1016/j.jhevol.2004.03.006.

Mitteroecker, P., & Gunz, P. (2009). Advances in Geometric Morphometrics. *Evolutionary Biology*, 36, 235-247.

Mori, T., & Harvati, K. (2019). Basicranial ontogeny comparison in Pan troglodytes and Homo sapiens and its use for developmental stage definition of KNM-ER 42700. *American Journal of Physical Anthropology*, 170 (4), 579-594. Doi: 10.1002/ajpa.23926.

Mori, T., Profico, A., Reyes-Centeno, H., & Harvati, K. (2020). Frontal bone virtual reconstruction and geometric morphometric analysis of the mid-Pleistocene hominin KNM-OG 45500 (Olorgesailie, Kenya). *Journal of Anthropological Sciences*, 98, 49-72. Doi: 10.4436/jass.98022

Moshfeghi, M., Ranganath, S., & Nawyn, K. (1994). Three-Dimensional Elastic Matching of Volumes. IEEE Transactions on Image Processing, 3 (2), 128-138. Doi: 10.1109/83.277895.

Nami, M., & Moser, J. (2010). *La grotte d'Ifri n'Ammar; Tome 2: Le Paléolithique Moyen*. Forschungen zur Archäologie Außereuropäischer Kulturen (FAAK) Vol. 9. Wiesbaden, Germany: Reichert Verlag.

Nespoulet, R., El Hajraoui, M. A., Amani, F., Ben-Ncer, A., Debénath, A., El Idrissi, A., Lacombe, J.-P., Michel, P., Oujaa, A., & Stoetzel, E. (2008). Paleolithic and Neolithic Occupations in the Témara region (Rabat, Morocco): Recent data on Hominin Contexts and Behaviour. *African Archaeological Review*, 25, 21-39. Doi: 10.1007/s10437-008-9025-1.

Oeschger, E. S., Kanavakis, G., Halazonetis, D. J., & Gkantidis, N. (2020). Number of teeth is associated with facial size in humans. *Scientific Reports*, 10, 1820. Doi: 10.1038/s41598-020-58565-8.

Oujaa, A., Arnaud, J., Bardey-Vaillant, M., & Grimaud-Hervé, D. (2017). The Fossil Human from Rabat-Kébibat (Morocco): Comparative Study of the Cranial and Mandibular Fragments. *African Archaeological Review*, *34* (4), 511-523. Doi: 10.1007/s10437-017-9278-7.

Osborne, A. H., Vance, D., Rohling, E. J., Barton, N., Rogerson M., & Fello, N. (2008). A humid corridor across the Sahara for the migration of early

modern humans out of Africa 120,000 years ago. *PNAS*, 105 (43), 16444-16447. Doi: 10.1073/pnas.0804472105.

Plavcan, J. M., & Daegling, D. J. (2006). Interspecific and intraspecific relationships between tooth size and jaw size in primates. *Journal of Human Evolution*, *51* (2), 171-184. Doi: 10.1016/j.jhevol.2006.02.005.

Pope, G. G. (1991). Evolution of the zygomaticomaxillary region in the genus Homo and its relevance to the origin of modern humans. *Journal of Human Evolution*, 21, 189-213. Doi: 10.1016/0047-2484(91)90061-Y.

Posth, C., Wißling, C., Kitagawa, K., Pagani, L., von Holstein, L., Racimo, F., Wehrberger, K., Conard, N. J., Kind, C. J., Bocherens, H., & Krause, J. (2017). Deeply divergent archaic mitochondrial genome provides lower time boundary for African gene flow into Neanderthals. *Nature Communications*, 8, 16046. Doi: 10.1038/ncomms16046.

Profico, A., Veneziano, A., Lanteri, A., Piras, P., Sansalone, G., & Manzi, G. (2016). Tuning Geometric Morphometrics: an R tool to reduce information loss caused by surface smoothing. *Methods in Ecology and Evolution*, 7 (10), 1195-1200. Doi: 10.1111/2041-210X.12576.

Prüfer, K., Racimo, F., Patterson, N., Jay, F., Sankararaman, S., Sawyer, S., Heinze, A., Renaud, G., Sudmant, P. H., de Filippo, C., Li, H., Mallick, S., Dannemann, M., Fu, Q., Kircher, M., Kuhlwilm, M., Lachmann, M., Meyer, M., Ongyerth, M., Siebauer, M., Theunert, C., Tandon, A., Moorjani, P., Pickrell, J., Mullikin, J. C., Vohr, S. H., Green, R. E., Hellmann, I., Johnson, P. L. F., Blanche, H., Cann, H., Kitzman, J. O., Shendure, J., Eichler, E. E., Lein, E. S., Bakken, T., Golovanova, L. V., Doronichev, V. B., Shunkov, M. V., Derevianko, A. P., Viola, B., Slatkin, M., Reich, D., Kelso, J., & Pääbo, S. (2014). The complete genome sequence of a Neanderthal from the Altai Mountains. *Nature*, 505, 43-49. Doi: 10.1038/nature12886.

R Development Core Team (2020). R: a language and environment for statistical computing; version 3.4.1. *R Foundation for Statistical Computing*: http://www.R-project.org.

Reich, D., Green, R. E., Kircher, M., Krause, J., Patterson, N., Durand, E. Y., Viola, B., Briggs, A. W., Stenzel, U., Johnson, P. L. F., Maricic, T., Good, J. M., Marques-Bonet, T., Alkan, C., Fu, Q., Mallick, S., Li, H., Meyer, M., Eichler, E. E., Stoneking, M., Richards, M., Talamo, S., Shunkov, M. V., Derevianko, A. P., Hublin, J.-J., Kelso, J., Slatkin, M., & Pääbo, S. (2010). Genetic history of an archaic hominin group from Denisova Cave in Siberia. *Nature*, 468, 1053-1060. Doi: 10.1038/nature09710.

Richter, D., Moser, J., Nami, M., Eiwanger, J., & Mikdad, A. (2010). New chronometric data from Ifri n'Ammar (Morocco) and the chronostratigraphy of the Middle Palaeolithic in the Western Maghreb. *Journal of Human Evolution*, 59 (6), 672–679. Doi: 10.1016/j.jhevol.2010.07.024.

Richter, D., Moser, J., & Nami, M. (2012). New Data from the Site of Ifri n'Ammar (Morocco) and some remarks on the chronometric status of the Middle Paleolithic in the Maghreb. In J.-J. Hublin, & S. P. McPherron (Eds.), *Modern Origins: A North African Perspective* (pp. 61-78). Vertebrate Paleobiology and Paleoanthropology. Berlin, Germany: Springer. Doi: 10.1007/978-94-007-2929-2_5.

Richter, D., Grün, R., Joannes-Boyau, R., Steele, T. E., Amani, F., Rué, M., Fernandes, P., Raynal, J.-P., Geraads, D., Ben-Ncer, A., Hublin, J.-J.,

& McPharron, S. (2017). The age of the hominin fossils from Jebel Irhoud, Morocco, and the origins of the Middle Stone Age. *Nature*, 546, 293-296. Doi: 10.1038/nature22335.

Rightmire, G. P., & Deacon, H. J. (1991). Comparative studies of late Pleistocene human remains from Klasies River mouth, South Africa. *Journal of Human Evolution*, 20 (2), 131-156. Doi: 10.1016/0047-2484(91)90054-Y.

Robson, S. L. & Wood, B. (2008). Hominin life history: reconstruction and evolution. *Journal of Anatomy*, 212 (4), 394-425. Doi: 10.1111/j.1469-7580.2008.00867.x.

Röding, C., Zastrow, J., Scherf, H., Doukas, C. & Harvati, K. (2021). Crown outline analysis of the hominin upper third molar from the Megalopolis Basin, Peloponnese, Greece. In: H. Reyes-Centeno & K. Harvati (Eds.), *Ancient Connections in Eurasia* (pp. 13-36). Tübingen: Kerns Verlag. Doi: 10.51315/9783935751377.001.

Rougier, H., Milota S., Rodrigo, R., Gherase, M., Sarcina, L., Moldovan, O., Zilhão, J., Constantin, S., Franciscus, R. G., Zollikofer, C. P. E., Ponce de León, M., & Trinkaus, E. (2007). Peştera cu Oase 2 and the cranial morphology of early modern Europeans. *PNAS*, 104 (4), 1165-1170. Doi: 10.1073/pnas.0610538104.

Scerri, E. M. L. (2017). The North African Middle Stone Age and its place in recent human evolution. Evolutionary Anthropology, 26 (3), 119-135. Doi: 10.1002/evan.21527.

Scerri, E. M., & Spinapolica, E. E. (2019). Lithics of the North African Middle Stone Age: assumptions, evidence and future directions. *Journal of Anthropological Sciences*, *97*, 9-43. Doi: *10.4436/jass.97002.*

Schlager, S., & Rüdell, A. (2013). Shape analysis of the human zygomatic bone – surface registration. American Journal of Physical Anthropology, 150, 243. doi:10.1002/ajpa.22247 (Poster: https://www.researchgate.net/profile/Stefan-Schlager/publication/260135091_Zygomatic_Surface_Registration_AAPA_2013/links/0f31752fb6cc76c40e000000/Zygomatic-Surface-Registration-AAPA-2013.pdf).

Schuh, A., Gunz, P., Villa, C., Kupczik, K., Hublin, J.-J., & Freidline, S. E. (2020). Intraspecific variability in human maxillary bone modeling patterns during ontogeny. *American Journal of Physical Anthropology*, 173, 655-670. Doi: 10.1002/ajpa.24153.

Semper-Hogg, W., Fuessinger, M. A., Schwarz, S., Ellis, E., Cornelius, C.-P., Probst, F., Metzger, M. C., & Schalger, S. (2017). Virtual reconstruction of midface defects using statistical shape models. *Journal of Cranio-Maxillo-Facial Surgery*, 45 (4), 461-466. Doi: 10.1016/j.jcms.2016.12.020.

Şenyürek, M. S. (1940). Fossil Man in Tangier. In *Papers of the Peabody Museum of American Archaeology and Ethnology*, Vol. 16, No. 3. Cambridge, Massachusetts: Harvard University Press.

Sergi (1947). Sulla morfologia della »facies anterior corporis maxillae« nei Paleantropi di Saccopastore e del Monte Circeo. *Rivista di Anthropologia*, 35, 401-408.

Shea, J. J., & Bar-Yosef, O. (2005). Who were the Skhul/Qafzeh people? An archaeological perspective on Eurasia's oldest modern

humans. *Mitekufat Haeven: Journal of the Israel Prehistoric Society*, 35, 451-468.

Siska, V. (2019). *Human population history and its interplay with natural selection* (Doctoral thesis). University of Cambridge, Cambridge, UK. Doi: 10.17863/CAM.31536.

Slice, D. E. (2007). Geometric morphometrics. *Annual Review of Anthropology, 36*, 261-281. Doi: 10.1146/annurev.anthro.34.081804.120613.

Smith, B. H. (1989). Dental development as a measure of life history in primates. *Evolution*, 43 (3), 683-688.

Smith, T. M., Tafforeau, P., Reid, D. J., Grün, R., Eggins, S., Boutakiout, M., & Hublin, J.-J. (2007). Earliest evidence of modern human life history in North African early Homo sapiens. *PNAS*, 104 (15), 6128-6133. Doi: 10.1073pnas.0700747104.

Trinkaus, E. (1987). The Neandertal face: evolutionary and functional perspectives on a recent hominid face. *Journal of Human Evolution*, 16 (5), 429-443. Doi: 10.1016/0047-2484(87)90071-6.

Trinkaus, E. (2003). Neandertal faces were not long; modern human faces are short. *PNAS*, 100, 8142-8145. Doi: 10.1073/pnas.1433023100.

Trinkaus, E., Constantin, S., & Zilhão, J. (2013). *Life and death at the Peştera cu Oase: A setting for modern human emergence in Europe*. Oxford, UK: Oxford University Press.

Veneziano, A., Landi, F., & Profico, A. (2018). Surface smoothing, decimation, and their effects on 3D biological specimens. American Journal of Physical Anthropology, 166 (2), 473-480. Doi: 10.1002/ajpa.23431.

Villanea, F. A., & Schraiber, J. G. (2019). Multiple episodes of interbreeding between Neanderthal and modern humans. *Nature Ecology and Evolution*, 3, 39-44. Doi: 10.1038/s41559-018-0735-8.

Vollmer, J., Mencl, R., & Muller, H. (1999). Improved Laplacian Smoothing of Noisy Surface Meshes. *Computer Graphics Forum*, 18 (3), 131-138. Doi: 10.1111/1467-8659.00334.

Weber, G. W., & Krenn, V. A. (2017). Zygomatic root position in recent and fossil hominids. *The Anatomical Record*, 300 (1), 160-170. Doi: 10.1002/ar.23490.

Wengler, L. (1997). La transition du Moustérien à l'Atérien. *L'Anthropologie*, 101 (3), 448-481.

White, T., Asfaw, B., DeGusta, D., Gilbert, H., Richards, G. D., Suwa, G., & Howell, F. C. (2003). Pleistocene *Homo sapiens* from Middle Awash, Ethiopia. *Nature*, 423, 742–747. Doi: 10.1038/nature01669.

Wrinn, P. J., & Rink, W. J. (2003) ESR Dating of Tooth Enamel from Aterian Levels at Mugharet el'Aliya (Tangier, Morocco). *Journal of Archaeological Science*, 30 (1), 123-133. Doi: 10.1006/jasc.2002.0813.

Zelditch, M., Swiderski, D. & Sheets, H. (2012). *Geometric morphometrics for biologists: a primer* (2nd ed.). London, UK: Academic Press.

Zihlman, A., Bolter, D. & Boesch, C. (2004). Wild chimpanzee dentition and its implications for assessing life history in immature hominin fossils. *PNAS*, 101 (29), 10541-10543. Doi: 10.1073/pnas.0402635101.

Supplementary Data

Supplementary Table S1: Complete sample list with detailed information about people and institutions providing material for this study.

Collection / Repository	Data Type	N. of Individuals	Fossil Individuals	Citation or Person / Institution to thank
Peabody Museum, Harvard, USA	CT	1	El'Aliya	L. Burgess; the Peabody Museum, Harvard University
osteological collection University of Tübingen	CT	37		H. Rathmann
South African Museum, Cape Town, South Africa	CT	22		
ESRF heritage database	CT	2	La Quina 18; Qafzeh 10	Smith et al. 2010
Muséum national d'histoire naturelle (MNHN) Paris, France	CT	2	Abri Pataud; Pech de l'Azé	A. Balzeau; D. Grimaud-Hervé
Museo di Antropologia 'G. Sergi', Dipartimento di Biologia Animale e dell'Uomo; Rome, Italy	CT	1	Saccopastore 2	G. Manzi
NESPOS database	CT	1	Roc de Marsal	
	surface	1	Teshik Tash	
The Egyptian Museum, Cairo, Egypt	surface	1	Nazlet Khater 2	I. Crevecoeur; F. Bon; D. Pleurdeau; J. Lesur; C. Tribolo; ANR project 'Big Dry' (ANR-14-CE31)
American Museum of Natural History, NY, USA	surfaces	12	Mladec 1; Predmosti 3; Liujiang; Skhul V; Jebel Irhoud 1; Omo 1; Amud; Shanidar 1; La Ferrassie 1; Forbes' Quarry 1; Qafzeh 6; Grotte des Enfants 6	E. Delson

Supplementary Table S2: Complete list of pairwise PD between the comparative sample and Mugharet el'Aliya. Individuals ordered by ascending pairwise PD.

	ID	PD	Group	Dental age group
1	Qafzeh 10	0.0751	early *Homo sapiens*	
2	UCT-423	0.0839		4
3	UCT-149	0.0863		
4	SAM-AP-4635	0.0883		3
5	UCT-173	0.0911	*Homo sapiens*	4
6	UCT-151	0.1001		
7	SAM-AP-6340	0.1054		3
8	Hs_1069	0.1062		
9	Roc de Marsal	0.1129	*Homo neanderthalensis*	
10	SAM-AP-1448	0.1142		4
11	SAM-AP-5044	0.1196		
12	SAM-AP-6315	0.1243		3
13	CH_TUN_82K?T11P1	0.1354		4
14	Hs_1070	0.1371	*Homo sapiens*	3
15	EGY_NEOL_1317	0.1376		
16	CH_TUN_82K18T10P2	0.1393		4
17	Hs_1081	0.1404		
18	Pech de l'Azé	0.1453	*Homo neanderthalensis*	3
19	Hs_13190	0.1479		
20	Hs_1080	0.1494		
21	UCT-51	0.1504		
22	Hs_1083	0.1511	*Homo sapiens*	
23	Hs_13078	0.1522		4
24	Hs_1074	0.1553		
25	Teshik Tash	0.1576	*Homo neanderthalensis*	
26	UCT-150	0.1593		
27	Hs_1072	0.1642		
28	Hs_1085	0.1656		5
29	SAM-AP-6263	0.1711		4
30	SAM-AP-5087	0.1758		3
31	Hs_1088	0.1799	*Homo sapiens*	5
32	Hs_1066	0.1803		3
33	Grotte des Enfants 6	0.1818		5
34	Masai 3	0.1820		6
35	Hs_1089	0.1870		5
36	Hs_1087	0.1895		

Supplementary Table S2 continued.

	ID	PD	Group	Dental age group
37	Hs_1082	0.1933		4
38	Hs_1092	0.1943		
39	Hs_13136	0.1980	*Homo sapiens*	5
40	CH_TUN_81K5T6P2	0.1987		3
41	Hs_1091	0.1993		5
42	La Quina H18	0.2025	*Homo neanderthalensis*	4
43	UCT-437	0.2036		3
44	Liujiang	0.2143	*Homo sapiens*	6
45	Hs_13080	0.2215		4
46	Hs_1086	0.2227		5
47	Jebel Irhoud 1	0.2293	early *Homo sapiens*	
48	Nazlet Khater 2	0.2311		6
49	Abri Pataud	0.2345		
50	Masai 6	0.2369		
51	SAM-AP-6348a	0.2429		5
52	SAM-AP-3737a	0.2444		4
53	Hs_857	0.2579	*Homo sapiens*	
54	Mladec 1	0.2706		6
55	SAM-4312	0.2716		
56	Hs_13131	0.2756		5
57	Hs_1099	0.2767		
58	Fish Hoek	0.2786		
59	Masai 10	0.2833		
60	Qafzeh 6	0.2946	early *Homo sapiens*	6
61	Masai 1	0.2952		
62	SAM-27	0.2954		
63	Hs_1100	0.3023		5
64	SAM-1268	0.3039	*Homo sapiens*	
65	Masai 9	0.3068		
66	SAM-26	0.3112		
67	SAM-4790	0.3244		6
68	Omo 1	0.3265	early *Homo sapiens*	
69	Hs_856	0.3276	*Homo sapiens*	
70	Saccopastore 2	0.3287	*Homo neanderthalensis*	
71	Hs_813	0.3291	*Homo sapiens*	

Supplementary Table S2 continued.

	ID	PD	Group	Dental age group
72	Skhul 5	0.3300	early *Homo sapiens*	6
73	Forbes' Quarry 1	0.3352	*Homo neanderthalensis*	
74	Hs_780	0.3411	*Homo sapiens*	
75	Predmosti 3	0.3561		
76	Shanidar 1	0.3852	*Homo neanderthalensis*	
77	Hs_507	0.3891	*Homo sapiens*	
78	La Ferrassie 1	0.4010	*Homo neanderthalensis*	
79	Amud	0.4115		

Supplementary Table S3: Complete list of CS for all *H. neanderthalensis* individuals.

Dental age group	Individual	CS
3	Pech de l'Azé	2101.289
	Roc de Marsal	2568.419
4	La Quina H18	2398.174
	Teshik Tash	2825.027
6	Forbes' Quarry 1	2734.890
	Saccopastore 2	3433.875
	Amud	3496.567
	La Ferrassie 1	3513.282
	Shanidar 1	3515.154

Supplementary Table S4: Complete list of CS for all *H. sapiens* individuals.

Group	Dental age group	Individual	CS
Aterian	4	Mugharet el'Aliya	2491.126
Homo sapiens	3	SAM-AP-5087	1718.831
		Hs_1066	1773.641
		UCT-437	1894.299
		CH_TUN_81K5T6P2	1909.460
		SAM-AP-6315	1914.121
		UCT-151	1982.498
		Hs_1069	2114.416
		SAM-AP-4635	2116.671
		SAM-AP-6340	2238.279
		Hs_1070	2246.418
	4	UCT-149	2047.805
		UCT-150	2049.246
		UCT-423	2079.229
		Hs_13190	2103.514
		Hs_1072	2132.396
		SAM-AP-1448	2138.931
		UCT-51	2139.785
		SAM-AP-3737a	2154.980
		Hs_1081	2167.722
		Hs_1083	2175.594
		Hs_13078	2223.312
		UCT-173	2249.437
		Hs_1074	2255.018
		Hs_1080	2257.861
		Hs_13080	2265.718
		Hs_1082	2279.793
		CH_TUN_82K?T11P1	2284.486
		SAM-AP-6263	2355.794
		EGY_NEOL_1317	2365.249
		SAM-AP-5044	2375.567
		CH_TUN_82K18T10P2	2380.552
	5	Hs_1092	2265.576
		Hs_1085	2335.805
		Hs_1086	2343.391
		Hs_1091	2440.629
		Hs_1099	2415.101
		Hs_13136	2462.177

Supplementary Table S4 continued.

Group	Dental age group	Individual	CS
Homo sapiens	5	SAM-AP-6348a	2524.834
		Hs_1100	2526.212
		Hs_1087	2539.375
		Hs_1089	2546.144
		Hs_13131	2560.995
		Hs_1088	2572.369
		Grotte des Enfants 6	2788.104
	6	SAM-4312	2313.941
		SAM-26	2409.815
		Hs_780	2594.107
		SAM-4790	2608.006
		SAM-27	2609.692
		Nazlet Khater 2	2635.497
		SAM-1268	2660.937
		Masai 1	2662.297
		Masai 9	2663.061
		Fish Hoek	2673.108
		Masai 6	2684.001
		Hs_856	2694.491
		Liujiang	2695.353
		Hs_857	2718.232
		Abri Pataud	2733.517
		Masai 10	2737.443
		Hs_507	2836.681
		Mladec 1	2841.064
		Masai 3	2965.772
		Predmosti 3	2972.556
		Hs_813	3010.826
early *Homo sapiens*	4	Qafzeh 10	2662.034
	6	Qafzeh 6	3067.313
		Skhul 5	3195.456
		Jebel Irhoud 1	3224.993
		Omo 1	3436.112

Supplementary Table S5: Tukey's range test for slope differences in the regression of CAC scores and log CS between *H. sapiens*, early *H. sapiens* and Neanderthals.

Group 1	Group 2	Estimate	Standard Error	Degrees of Freedom	t ratio	p-value
early *Homo sapiens*	*Homo neanderthalensis*	-0.368	0.455	73	-0.809	0.699
early *Homo sapiens*	*Homo sapiens*	-0.156	0.420	73	-0.371	0.927
Homo neanderthalensis	*Homo sapiens*	0.213	0.237	73	0.895	0.645

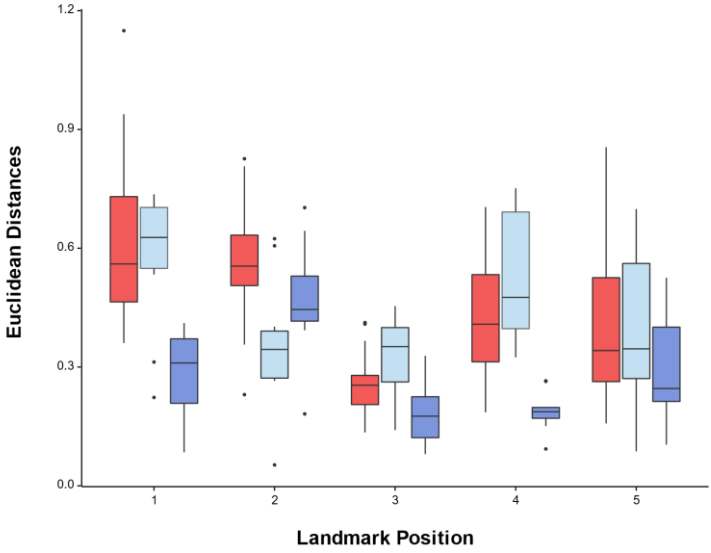

Supplementary Figure S1: Boxplots of pairwise Euclidean Distances in mm as illustration for the intra- and inter-observer error in placing the fixed landmarks for initial registration. Pairwise Euclidean Distances between intra-observer measurements 1 (C.R.) shown in light blue, between intra-observer measurements 2 (J.Z.) in dark blue and between the inter-observer measurements in red.

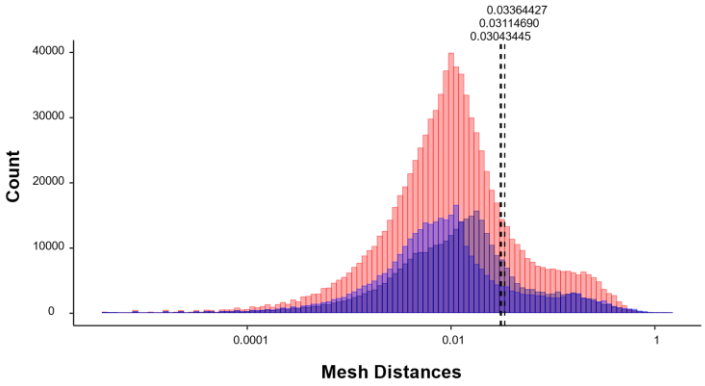

Supplementary Figure S2: Histogram of distances in mm between meshes as illustration for the error calculations for the dataset. Mesh distances between intra-observer measurements shown in blue (mean1 = 0.030 (C.R.), mean2 = 0.031 (J.Z.)), and between the inter-observer measurements in red (mean3 = 0.034). Distances are shown log-transformed on the x-axis and dotted lines indicating the means.

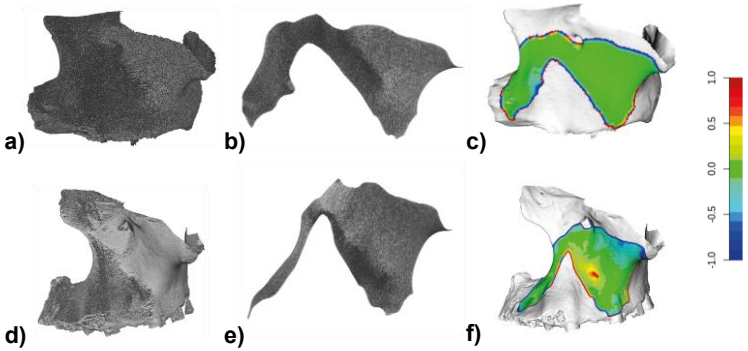

Supplementary Figure S3: Illustrations for the error introduced by the surface registration method for the dataset. a-c) example of a good and d-f) a bad match between surfaces from the original and those created via surface registration. a,d) original surface meshes, b,e) meshes generated via surface generation, and c,f) distance heat maps of surfaces from the original and created via surface registration. Distances in mm translated to colour code ranging from no difference in green to ≥ 1 mm difference in dark red and to ≥ -1 mm difference in dark blue.

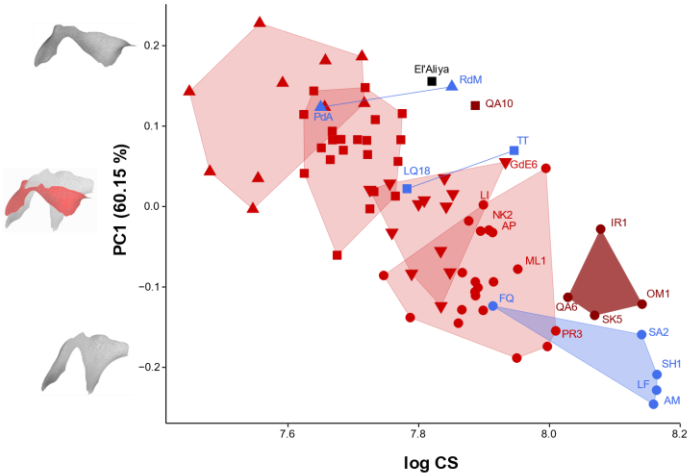

Supplementary Figure S4: PC1 plotted against log CS. Symbols, colors and abbreviations as in Figure 4 and Table 1.

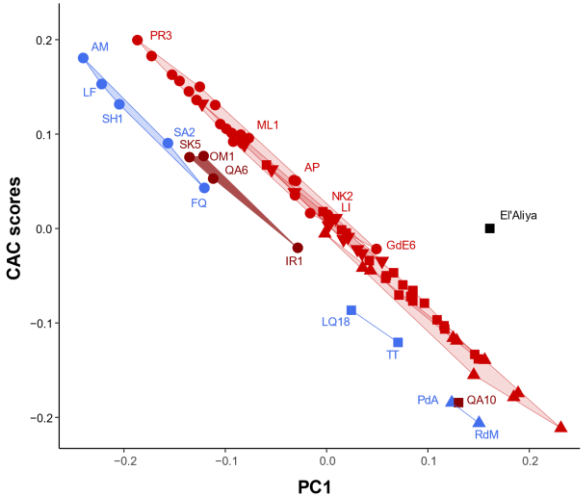

Supplementary Figure S5: CAC scores plotted against PC1. Symbols, colors and abbreviations as in Figure 4 and Table 1.

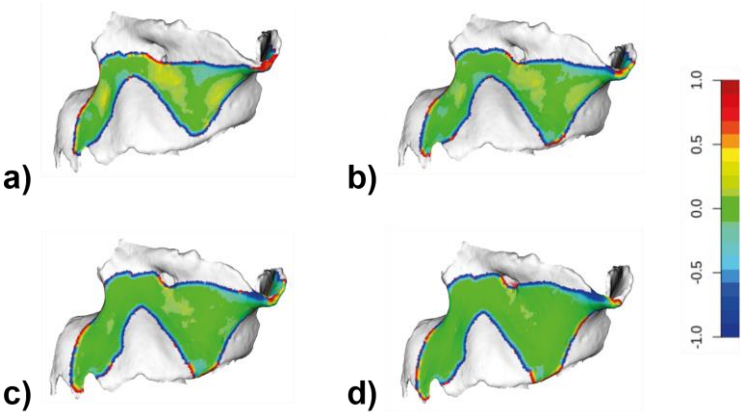

Supplementary Figure S6: Illustrations for the error introduced by reduction of the mesh resolution for the surface registration method. Match between surfaces from the original and those created via surface registration at a mesh resolution of a) ca. 3k vertices, b) ca. 5.6k, c) ca. 16k and d) the resolution of the here used dataset with ca. 35k vertices. Distances in mm translated to colour code ranging from no difference in green to ≥ 1 mm difference in dark red and to ≥ -1 mm difference in dark blue.

References Supplemental Material

Smith, T. M., Tafforeau, P., Reid, D. J., Pouech, J., Lazzari, V., Zermeno, J. P., Guatelli-Steinberg, D., Olejniczack, A., Hoffman, A., Radovcic, J., Makaremi, M., Toussaint, M., Stringer, C., & Hublin, J.-J. (2010). Dental evidence for ontogenetic differences between modern humans and Neanderthals. *PNAS*, 107 (49), 20923–20928. Doi: 10.1073/pnas.1010906107.

EBERHARD KARLS
UNIVERSITÄT
TÜBINGEN